Evaluation of polarisation parameters as predictor of morphology of nickel electrodeposits produced from sulfate electrolyte

By

Liezl Schoeman

A thesis submitted in partial fulfillment of the requirements of the degree of

PhD: Metallurgy

In the

Faculty of Engineering, Built Environment and Information Technology,

University of Pretoria,

Pretoria

Study leader: Dr. Kathryn C. Sole

May 2018

I, Liezl Schoeman, hereby declare that this thesis is my own account of my research and contains as its main content work that has not been previously submitted for a degree at any tertiary education institution.

Liezl Schoeman

08 May 2018

Acknowledgments

To my family for their love, understanding and endless support

My colleagues at IMMRI for encouragement and numerous rewarding discussions

To Dr. Sole for her time, positivity, commitment and passion

Anglo American Platinum Rustenburg Base Metals Refiners for samples, suggestions and support

To Karen Voogt, for information, samples and valuable discussions

To the examiners, for their time, valuable comments and suggestions

To God for infinite blessings

Publications and conference presentations

Chiyangwa, E., Sandenbergh, R.F., Schoeman, L. (2014). Development and evaluation of polarization parameters as quality predictors for zinc electroplated from acid sulphate electrolytes. Proceedings of the 7th International Symposium, Hydrometallurgy, Vancouver, Canada, Volume II, Canadian Institute of Mining, Metallurgy and Petroleum, Montreal, (pp.141–151).

Schoeman, L. and Sole, K.C. (2017). Accurate measurement of polarization potentials during electrodeposition of nickel metal from sulfate electrolyte. Proceedings of the 3rd Young Professionals Conference, South African Institute of Mining and Metallurgy, Innovation Hub, Pretoria, 9–10 March 2017, Southern African Institute of Mining and Metallurgy, Johannesburg,.(pp. 169 – 177).

Schoeman, L. and Sole, K.C. (2017). Accurate measurement of polarization potentials during electrodeposition of nickel metal from sulfate electrolyte. Journal of the Southern African Institute of Mining and Metallurgy, Volume 117, (pp. 624 – 628).

Schoeman, L. and Sole, K.C. (2017). Prediction of morphology development from nucleation and plating overpotentials in nickel electrodeposition. Canadian Metallurgical Quarterly, Volume 56, No. 4, (pp. 393 – 400).

Table of contents

List of tables

List of figures

List of symbols and terms

BR	Base-oriented reproduction
C_{Me}	Metal ion concentration in the bulk solution
E	Overpotential
E_c	Crystallisation overpotential
E_d	Diffusion overpotential
E_n	Nucleation overpotential
E_p	Plating overpotential
E_r	Reaction overpotential
E_t	Charge-transfer potential
E_Ω	Resistance overpotential
Rs	Electrolyte solution resistance
E^0	Standard potential
FI	Field-oriented isolated crystals
FT	Field-oriented texture
ΔG	Gibbs free energy of formation
J	Current density
N	Number of adatoms
ΔS	Supersaturation
UD	Un-oriented dispersion
δ	Cluster mean surface specific energy
$\phi(N)$	Excess free energy
z	Number of electrons

Abstract

Industrial electrowinning of nickel requires specific control and optimisation of the electrolyte composition, the presence of impurities, the addition of additives (to achieve particular deposit properties) and the operating parameters (such as pH and temperature) in order to produce electroplated nickel of high quality and desirable morphological characteristics. Without understanding and strict control of the electrocrystallisation process, nickel can delaminate due to internal strain, frequent pitting of the deposit can occur, current efficiency can decrease significantly or dendritic growth can cause short circuits. Prediction of the effect of the electrolyte composition and operating parameters on the structure and morphology of the plated metal in the early stages of electrodeposition could be paramount to controlling and/or eliminating such problems during the later stages of electrowinning. Such prediction remains an enormous challenge.

The use of polarisation measurements to investigate the electrocrystallisation process and predict the outcome of the resulting deposit quality and morphology was used with variable success in early investigations. Some of the main problems with techniques such as cyclic voltammetry and the later-developed continuous monitoring techniques are inaccuracy and unreliability of the results. The aim of the present work was to develop a galvanodynamic polarisation technique to investigate the electrocrystallisation process of nickel metal from sulfate electrolyte in order to examine the effect of electrolyte composition, operating parameters and the presence of impurities or additives. This could then be used to optimise these factors and thereby predict the outcome of the quality and morphological characteristics of the produced nickel deposit. The idea was that a relatively easy and concise method needed to be developed that could be implemented industrially to monitor and detect problems in the early stages of electrowinning in order to take control and rapid corrective action if needed.

A two-step galvanodynamic method was developed to measure plating and nucleation potentials accurately and repeatably. It was shown that the relationship between the two potentials could be used as an indication of the effect of electrolyte composition and operating parameters on the composition and morphological characteristics of the produced nickel electrodeposits. This

method, together with studies on the buffering capabilities of electrolyte solutions, can be used to investigate the influence of additives and impurities industrially introduced during the process in the electrolytes. Typical variations in commercial electrolytes and nickel electrodeposits were evaluated using this developed technique and results compared with those obtained from synthetic electrolyte. The insights gained from this work can be useful to predict and manipulate the electrodeposition process in order to optimise electrocrystallisation and the production of high quality nickel deposits.

Chapter 1
Introduction

1.1. Introduction and problem statement

Nickel electrowinning from sulfate electrolyte proceeds as potential is applied between a cathode and anode that polarises the electrodes sufficiently such that stable nickel nuclei are formed, reduced and deposited on the cathode surface. This nickel reduction onto the cathode occurs simultaneously with the oxidation of water at the anode, which releases electrons for further nickel reduction. A typical side reaction during nickel electrowinning is the reduction of hydrogen ions to hydrogen gas. These gas bubbles can interfere with the nickel deposition process and the produced hydrogen ions change the pH. It is therefore common practice to separate the anode and cathode by means of an ion-permeable membrane. Typical nickel electrowinning processes from sulfate electrolyte are carried out at relatively high temperatures (around 60 ºC), at low pH values (2 – 4), in the presence of a boric acid buffer (typically at concentrations of approximately 10 g/L) and at applied current densities in the range of 200 – 220 A/m^2 (Crundwell *et al*., 2011).

Understanding and control of the electrolyte composition and operating parameters during electrowinning of nickel from sulfate electrolyte is crucial to producing electrodeposits of high quality and desirable morphological characteristics. The most important factors that need to be controlled and optimised include: the type and preparation of the electrodes, the nickel concentration, pH, temperature, buffer type and concentration, sodium sulfate concentration, additives and impurities, surface tension, conductivity and current density (Amblard *et al*., 1983; Holm and O'Keefe, 2000; Kittelty, 2002).

A critical factor that needs to be controlled is the relationship between the initial nucleation of nickel clusters on the electrode surface and further growth as more and more nickel nuclei are deposited and incorporated into the developing crystal lattice (Abyaneh *et al*., 1982; Bockris, 2000). Each new phase forming requires energy for nucleation to occur. After this initial nucleation process, growth of the nuclei typically requires less energy. This can be attributed to the increased energy released by the bonding of the atoms in the nucleus relative to that required for the creation of new surface area due to the addition of atoms as the

nucleus becomes larger (Winand, 1991; Budevski *et al*., 2000). Energy is supplied by an external source of applied overpotential, i.e., the potential relative to the reversible potential of the electrode. Nucleation overpotential refers to the overpotential at which the formation of new metal nuclei on the electrode surface becomes sustainable (Van den Brande *et al*., 1994).

Manipulation of the electrodeposition process can be achieved by changing the applied overpotential of the electrode in such a way that charge transfer is promoted and the metal species (nickel cations) in solution is most favourable to electroplate. At applied overpotential values of large magnitude, such as in industrial electrowinning processes, nucleation also occurs at energetically less favourable sites. The electrocrystallisation process is then determined by the rate of cluster formation and surface diffusion of the nickel clusters. Growth in the form of protrusions perpendicular to the surface is also favoured by the potential gradient between the electrodes and can be countered by the choice of overpotential and the use of additives to render such processes relatively less attractive. Therefore, if the overpotential can be monitored and controlled such that both nucleation and growth occur simultaneously, the product outcome can be controlled. Nickel electrodeposits of specific desired quality and characteristics can therefore be produced (Winand, 1991; Bockris, 2000; Budevski *et al*., 2000).

1.2. Research approach and project objectives

Nickel electrowinning has been studied extensively and much information regarding the process, mechanism and factors that affect the process is readily available. The importance of optimisation of the parameters and conditions has been established. Impurities and contaminants have been shown to have a definite effect on the actual process and electrocrystallisation mechanism as well as on the deposit properties and the morphology (Budevski *et al*., 2000, Kittelty, 2002). The influence of internal strain on deposit quality has been researched and methods for monitoring and control of stress have been proposed. There are still, however, many uncertainties associated with nickel electrowinning and development and improvement of the process are still desired.

The main aim in this research was to develop a method to measure nucleation and plating overpotentials accurately in order to use these to classify nucleation and growth. These measured parameters were then investigated for application to optimise the electrolyte composition and operating conditions, to classify the effect of impurities and additives more definitively and to predict the outcome of a specific nickel electrowinning process.

The approach was to investigate the reliability of galvanodynamic polarisation techniques compared with potential-controlled techniques, and to develop such a galvanodynamic measuring method to measure both nucleation and plating potentials. The effects of parameter and condition changes of the electrolyte on the measured potential values were investigated. The effect of the presence of impurities and additives on the potential values was established. The relationship between the nucleation and plating overpotentials was correlated with morphological changes observed in the nickel deposit microstructure.

A reliable, repeatable method was developed for the measurement of both nucleation and plating overpotentials of nickel electrodeposition processes from various sulfate electrolytes differing in composition, pH and temperature, and in the presence and absence of impurities and additives. These measured polarisation parameters were successfully correlated with the quality, general morphology and internal strain of the resulting nickel electrodeposits. The mechanistic working and buffer capabilities of such typical sulfate electrolytes for nickel electrodeposition were further investigated. It was found that boric acid, as well as impurities and additives, play a crucial role in the transport, inhibition and buffering of electrolytes and, ultimately, also on the morphological outcome of the produced nickel electrodeposit.

It is proposed that the use of the developed techniques may be useful during industrial electrowinning processes to investigate and monitor the electrocrystallisation process under various changes in the conditions and parameters and to predict the general characteristics of nickel deposits that will be produced during the early stages of the electrodeposition process.

1.3. Presentation of the work

Chapter 2 provides background information and an overview of nickel electrowinning, the process and principles, the effect of electrolyte composition and operating parameters and the influence of impurities and certain additives. The electrocrystallisation process during nickel electrodeposition is described as well as the most important considerations that must be kept in mind to achieve a specific quality and morphology of the deposit. Previously developed techniques are then discussed in the context of the development of a new galvanodynamic polarisation technique.

In Chapter 3, the experimental setup, methods and procedures that were followed are fully described. The development of a two-step galvanodynamic scanning technique, correlation of the polarisation parameters with deposit morphology and investigations of the buffer capacity

of various electrolyte solutions are detailed and discussed. The experimental method, parameters and other necessary considerations are explained.

Development of a reliable, repeatable galvanodynamic measurement technique is presented in Chapter 4.

Results for the variation of polarisation parameters with changes in electrolyte conditions and composition as well as the morphology and strain characteristics of thick deposits are presented in Chapter 5.

Results for prediction of the morphological outcome of nickel electrodeposits are discussed in Chapter 6.

Results for investigation of the applicability of the technique to an industrial electrolyte are presented in Chapter 7.

Final conclusions and possible future work are discussed in Chapter 8.

Chapter 2
Literature survey

2.1. Introduction to nickel recovery and production

2.1.1. Natural sources and characteristics of nickel

Nickel comprises approximately 0.008 % of the Earth crust's total mass and is mainly found in either sulfide or laterite ore, commonly in association with cobalt and manganese (Moskalyk and Alfantazi, 2002a; Moskalyk and Alfantazi, 2002b). Nickel has many useful metallurgical properties, including high melting point, ferromagnetic characteristics, catalytic capabilities, relative ease of electroplating, alloying properties, corrosion resistance and ductility (Kittelty, 2002; Moskalyk and Alfantazi, 2002b). These characteristics allow nickel to be employed in various industries, such as telecommunications, infrastructure, chemical production, environmental protection, energy supply, water treatment, food preparation, consumer electronics and transportation (Fornari and Abbruzzese, 1999; Moskalyk and Alfantazi, 2002a; Di Bari, 2010).

Approximately 12 % (Di Bari, 2010) of produced nickel is consumed by electroplating and electrodeposition processes, which are used for decorative, engineering and electroforming applications. Modern decorative applications are improved by the addition of organic additives to produce bright and level nickel deposits. In engineering processes, nickel deposits are used for improved corrosion or wear resistance, to enhance magnetic properties, as a preparative layer for other applications and as diffusion barriers in electronic applications. During electroforming, nickel is loosely deposited onto a mould that provides for later removal of the then formed electrodeposit. This process is used in the textile, aerospace, communication, electronic, automotive, photocopying and entertainment industries (Di Bari, 2010).

2.1.1.1. Nickel from sulfide-bearing ores

Sulfide-containing ores are the source of approximately 30 % of global base and noble metals. The main nonferrous metals recovered from these ores include nickel, copper and cobalt

(Agatzini-Leonardou *et al*., 2009). The mining of sulfide ores normally requires underground operations. Some open pit operations are in use, but it is generally found that higher nickel and other metal contents are present at greater depths (Park *et al*., 2006; Crundwell *et al*., 2011). Approximately 55 % of mined nickel (from nickel sulfide ore) is contained in pentlandite ($(Fe,Ni)_9S_8$). Iron- and copper-containing pyrrhotite ($Fe_{1-x}S$ (where x ranges from 0.0 to 0.2)) and chalcopyrite ($CuFeS_2$) are also contained in pentlandite ($(Fe,Ni)_9S_8$). Millerite (NiS) and heazlewoodite (Ni_3S_2) have the highest nickel contents but are only present in small quantities (Moskalyk and Alfantazi, 2002a).

2.1.1.2. Nickel from laterite sources

Mining of nickel from laterites is becoming increasingly important as nickel from sulfide sources is progressively depleted. Laterites contain approximately 70 % of the world's nickel resources and nickel can nowadays be successfully recovered (Moskalyk and Alfantazi, 2002b). Laterite ore is found in tropical regions that were sub-tropical in past geologic epochs. These occur in close proximity to the surface (0 – 40 m) in layers that contain an iron cap consisting of goethite (FeO(OH)), an iron shot overburden, limolitic overburden, limonite ($FeO(OH)\cdot nH_2O$) ore, a transition zone, saponite ($Ca_{0.25}(Mg,Fe)_3((Si,Al)_4O_{10})(OH)\cdot n(H_2O)$) and boulders, and peridotite. Nickel–magnesium silicate is present in mixtures of serpentine ($(Mg,Fe,Ni,Al,Zn,Mn)_{2-3}(Si,Al,Fe)_2O_5(OH)_4$), saponite ($Ca_{0.25}(Mg,Fe)_3((Si,Al)_4O_{10})(OH)$ $n(H_2O)$) and deweylite. Nickelferrous components are present in limonite that also contains goethite. Laterite mines are generally open pit mines and therefore are less costly operations compared with sulfide ore processes. Other metals such as cobalt, zinc and copper are produced as by-products (Moskalyk and Alfantazi, 2002b; Agatzini-Leonardou *et al*., 2009; Crundwell *et al*., 2011).

2.1.2. Nickel recovery and production processes

After mineral processing of the nickel-containing ore, further processing depends on the characteristics of the specific ore, energy costs and environmental constraints. Pyrometallurgical or hydrometallurgical routes can be followed, after which electrometallurgical steps are incorporated to obtain a pure nickel product (Kittelty, 2002; Crundwell *et al*., 2011).

2.1.2.1. Pyrometallurgical processes

For ores that contain nickel together with magnesium and silica, pyrometallurgical processing is preferred. The pyrometallurgical processing route for nickel sulfide-type ore involves roasting to fully oxidise the iron present, with the evolution of all sulfur as SO_2 gas as by-product. The oxidised iron is then removed by melting the product with a siliceous flux. The iron forms a liquid silicate that is separated from a molten sulfide phase. The remainder of the sulfur is then oxidised and removed from the melt while iron still present is oxidised and the silicate is removed in converters (Kittelty, 2002; Crundwell *et al*., 2011).

Nickel oxide ore is treated in an arc furnace, which produces a matte. The matte product is roasted to an oxide product, from which nickel metal is then recovered. In some cases, the product can be treated with chloride or sulfate reagents to produce water-soluble products that are further treated hydrometallurgically. The nickel can also be recovered by electrorefining processes (Fornari and Abbruzzese, 1999; Whittington and Muir, 2000). There are some environmental constraints, as well as energy cost issues, that make pyrometallurgical processes non-ideal in some cases. The SO_2 gas that is emitted during these processes is monitored and controlled as it is dangerous to the environment. Costly and time-consuming procedures such as pre-concentration of the ore are also generally necessary before pyrometallurgical processing to make it effective and viable. Therefore, hydrometallurgy is also employed to process ore further as well as recover nickel successfully from nickel-bearing ore, especially in new plants all over the world (Kittelty, 2002; Crundwell *et al*., 2011).

2.1.2.2. Hydrometallurgical processes

Ore that contains nickel with a high iron or cobalt content is normally processed hydrometallurgically. Hydrometallurgical processes generally aim to selectively leach an ore to recover only certain specific elements. It is carried out in acid or base media at elevated temperatures and pressures to improve kinetics. A commonly used hydrometallurgical leaching procedure for sulfide ore is the Sherritt–Gordon process, which is carried out in aqueous ammonia. Impurities and unwanted metals are removed and nickel and cobalt are recovered by hydrogen reduction (Kittelty, 2002).

More often than not, a combination of pyro- and hydrometallurgical processes is employed for nickel oxide ore. In some cases, specifically in laterite ore processing, the leach product contains nickel and cobalt sulfides, which are processed by the Caron process. This process consists of several steps, including: drying and grinding of high-limonitic ore, reduction roasting, leaching with ammonia–ammonium carbonate to dissolve the nickel and cobalt as amine complexes and, lastly, the recovery of the base metal from the solution as a nickel oxide product (Moskalyk and Alfantazi, 2002a). Nickel and cobalt are reduced to form alloys with iron at temperatures of around 700 °C. Calcine is then removed by leaching (selectively for nickel and cobalt) in ammonia–ammonium carbonate solution. The ammonia is then removed by boiling and the product is nickel carbonate, which is calcined at 1200 °C to form nickel oxide. This type of process is often costly, energy consumption is high and nickel recovery is only moderate while cobalt recovery is low (Kittelty, 2002).

The developed pressure acid leaching (PAL) process is nowadays often used. Leaching is carried out in a sulfate- or chloride-containing medium followed by solvent extraction and then electrolytic recovery by means of electrowinning processes. The PAL system involves several centrifugal, diaphragm pumping and heat recovery stages. The leach product contains nickel, cobalt and metallic impurities. Some metallic impurities, such as iron, may then be precipitated by pH adjustment. Sulfide precipitation, re-leach, hydrogen reduction or solvent extraction procedures may then follow, before electrowinning or electrorefining. This PAL method is generally more environmentally friendly, reduces cost and has a better nickel recovery compared with the Caron process (Crundwell *et al*., 2011).

2.1.2.3. Electrometallurgical recovery

The electrochemical deposition or similar electrometallurgical processes of metals such as zinc, copper and nickel is widely used in the final step of hydrometallurgical or pyrometallurgical processes to recover a desired metal product from aqueous solution or melt (Popov *et al*., 2002). Approximately 45 % of the nickel produced annually in the world makes use of electrorefining and electrowinning processes (Moskalyk and Alfantazi, 2002a). Most nickel-containing solutions produced after hydrometallurgical or pyrometallurgical processes contain residual impurities even after complex solvent extraction procedures have been carried out. Some of these are organic in nature and come from the leach processes. Others are metallic impurities inherent to

the ore. These impurities are often dealt with by adjustment of the parameters and additives to obtain desired plate cathodes, metal powders and mixed sulfides (Küzeci and Kammel, 1994; Wu *et al*., 2003; Crundwell *et al*., 2011).

Electrometallurgy refers to the electrochemical deposition of metals during electrowinning, electroplating, electrorefining and electroforming. During electrowinning, metals are extracted from aqueous solution or molten salts by electrodeposition. Electrowinning refers to the reduction of metal compounds from the electrolyte (or solution after leaching and purification) onto a metal cathode. Electrorefining refers to processes of purification of metals by means of electrolysis. An impure metal anode is dissolved electrolytically and metal of higher purity is plated onto the cathode. The aim of both electrowinning and electrorefining is to produce compact, pure metal deposits at relatively low current densities and low energy consumption. Electroplating is an electrolytic process where a bare surface metal is coated by cathodic metal deposition to change the surface properties of the metal while keeping the bulk properties constant (Popov *et al*., 2002). This application is extensively used in the electronics industry or in engineering applications to improve, for instance, corrosion properties or abrasion sensitivity. Electroforming is used for the manufacturing of articles by electrodepositing a metal onto a mandrel or master template. The deposited metal must then be smooth and level, and easily removed from the template (Malevich *et al*., 2008).

Electrowinning of nickel specifically can be performed in chloride- or sulfate-based medium or a combination of the two. In a sulfate-based medium, oxygen is produced as by-product while in chloride medium, chlorine gas is produced. The sulfate routes are today used to electrowin nickel successfully from laterite ores after solvent–extraction procedures (Alfantazi and Shakshouki, 2002; Wu *et al*., 2003). The highest purity nickel commercially available produced via this route is referred to as London Metal Exchange (LME) grade nickel, which is approximately 99.80 % pure nickel. Impurities include Bi, C, Ca, Co, Fe, Mn, Pb, S, Sb, Si, Sn and Zn (Kittelty, 2002).

2.2. Parametric effects in nickel electrowinning from sulfate electrolyte

2.2.1. Reactions at the anode and cathode

In order to evaluate nickel electrodeposition, it is imperative to understand the reactions taking place in the electrolyte. Conditions should be conducive to promoting the main nickel deposition reaction while limiting unwanted or side reactions that could hinder or interfere with the main deposition reaction. The process of nickel electrodeposition from sulfate electrolyte involves the passing of a direct current between two electrodes immersed in a sufficiently conductive solution of nickel sulfate salt. Nickel cations are reduced to nickel metal at the cathode (Reaction [1]) while oxidation of water at the anode (Reaction [2]) releases the required electrons. The nickel ions consumed at the cathode are replenished from the nickel ions in the electrolyte. All standard potentials are given relative to the standard hydrogen electrode (SHE) at 25 °C (Holm and O'Keefe, 2000; Crundwell *et al*., 2011):

At the cathode: $Ni^{2+} + 2e^- \rightarrow Ni$ $\quad E^0 = -0.250$ V [1]

At the anode: $2H_2O \rightarrow O_2 + 4H^+ + 4e^-$ $\quad E^0 = 1.229$ V [2]

Nett reaction: $2NiSO_4 + 2H_2O \rightarrow 2Ni + 2H_2SO_4 + O_2$ $\quad E^0 = 1.479$ V [3]

The reduction of species other than that of the sought metal should be avoided because this will reduce the current efficiency of the nickel metal plating process and interfere with the nature and purity of the plated metal. In the case of nickel specifically, the nickel ions are thermodynamically more stable in aqueous solutions than hydrogen ions. Therefore, the reduction of hydrogen to hydrogen gas (Reaction [4]) is thermodynamically more favourable and will occur simultaneously with the reduction of nickel cations (Holm and O'Keefe, 2000; Kittelty, 2002; Di Bari, 2010; Crundwell *et al*., 2011):

$2H^+ + 2e^- \rightarrow H_2$ $\quad E^0 = 0.000$ V [4]

This reaction needs to be controlled or minimised in such a way that nickel cation reduction is optimally promoted. One such precaution to eliminate the interference of hydrogen bubbles is used almost exclusively, in which the anode and cathode are separated by an ion-permeable membrane. The electrolyte ions can freely move through these permeable membranes, the acid and pH is controlled in the catholyte and gas bubbles are trapped on the anolyte side where they

are produced. The pH at the catholyte is more regulated and controlled as the acid flows from the anolyte through the membrane to the catholyte. Membranes or cathode bags are commonly made from a material such as polyethylene or polyester (Crundwell *et al*., 2011).

Another factor that needs to be kept in mind is that, although the stoichiometry and thermodynamics are accurately described by the reactions given above, the simultaneous transfer of more than one electron in an electrochemical process is unlikely to occur (Wiart, 1990). There are many proposed mechanisms for the nickel reduction process, most of which assume that electrocrystallisation occurs in two steps of electron transfer involving an adsorbed intermediate species (Reactions [5] and [6]) (Aaboudi *et al*., 2001; Kittelty, 2002; Di Bari, 2010, Crundwell *et al*., 2011):

First step: $Ni^{2+} + e^- \rightarrow Ni^+_{ads}$ [5]

Second step: $Ni^+_{ads} + e^- \rightarrow Ni$ [6]

Even though there are many proposed ligands, the most common and simplest to consider is the hydroxide ion that originates from the water present in the electrolyte solution. Hydroxides easily coordinate to the nickel ions according to the proposed reactions in Reactions [7] to [10] (Muñoz *et al*., 2003; Di Bari, 2010). The charge-transfer reaction responsible for the formation of the $Ni(OH)_{ads}$ complex (Reaction [8]) is typically considered as the rate-determining step (Di Bari, 2010). The $Ni(OH)_{ads}$ complex is believed to act either as a catalyst for the reduction of the metal ion or as an intermediate that is consumed to form the reduced metal species, as shown in Reactions [9] and [10] (Muñoz *et al*., 2003; Di Bari, 2010):

$$Ni^{2+} + H_2O \rightarrow Ni(OH)^+ + H^+ \quad [7]$$

$$Ni(OH)^+ + e^- \rightarrow Ni(OH)_{ads} \quad [8]$$

$$Ni(OH)_{ads} + Ni^{2+} + 2e^- \rightarrow Ni + Ni(OH)_{ads} \quad [9]$$

$$Ni(OH)_{ads} + e^- \rightarrow Ni + OH^- \quad [10]$$

2.2.2. Effect of electrolyte parameter changes on polarisation parameters and nickel deposit morphology

Crucial parameters specific to nickel electrowinning are pH and temperature of the electrolyte. These are important to measure, monitor and control during the electrocrystallisation process and it is imperative to remember that changes in the one can induce changes in the other. Temperature and pH are interrelated and optimisation of these parameters should be done by considering both parameters simultaneously. The possible effects of changes in pH and temperature on polarisation parameters and morphology of the nickel deposit are discussed in this section.

2.2.2.1. pH

As nickel electrodeposition proceeds, hydrogen ions are readily produced (Reactions [2] and [7]) and the pH decreases. As hydrogen ions combine to form hydrogen gas (Reaction [4]) the H^+ ion concentration at the cathode surface rapidly decreases, causing the pH near the cathode to increase compared with the pH of the bulk electrolyte. If the pH increases significantly to about 5 or 6, insoluble $Ni(OH)_2$ precipitates are likely to form (Reaction [11]) and deposit onto the substrate which decrease the purity and quality of the nickel deposit itself (Amblard *et al*., 1983; Ji and Cooper, 1996; Nicol and Kittelty, 2001; Kittelty, 2002).

$$Ni^{2+} + 2OH^- \rightarrow Ni(OH)_2 \qquad [11]$$

The produced hydrogen bubbles may also co-deposit or interfere with depositing nickel ions, directly influencing the purity and morphology as the nickel deposit forms. If bubbles co-deposit with nickel ions, highly pitted or pin-holed deposits readily form. Therefore, changes in pH can directly influence the way in which nickel ions approach and deposit onto the substrate surface (Amblard *et al*., 1983; Ji and Cooper, 1996; Nicol and Kittelty, 2001; Kittelty, 2002).

The current efficiency is strongly affected by the electrolyte pH. At very low pH values, hydrogen ions are in excess and the hydrogen evolution (Reaction [2]) occurs readily, consuming part of the available current, thereby decreasing current efficiency of nickel deposition. If the pH is high enough for nickel hydroxide precipitates to form (Reaction [11]), the current efficiency is

also decreased in the same way (Amblard *et al*., 1983; Armyanov and Sotirova-Chakarove, 1992; Ji and Cooper, 1996; Lantelme and Seghiouer, 1998; Kittelty, 2002).

The effect of changes in pH of the electrolyte solution on the current efficiency is illustrated in Figure 2.1.

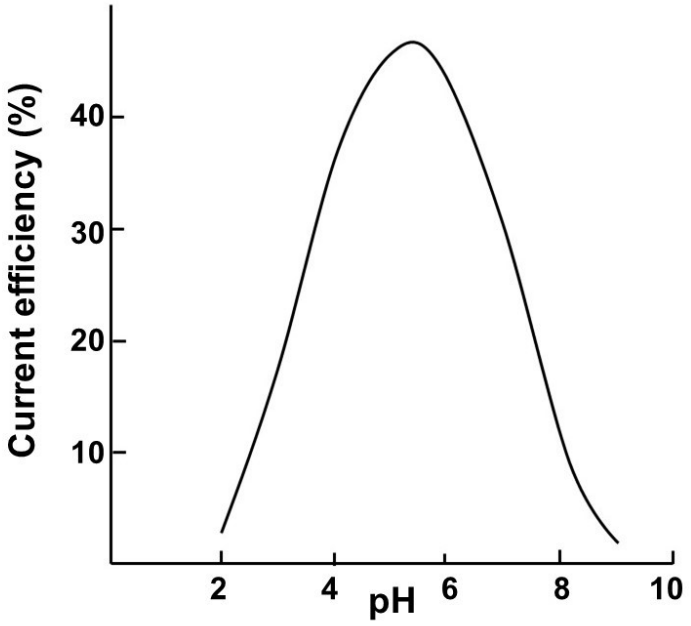

Figure 2.1. Graphical representation indicating the effect of electrolyte pH changes on the current efficiency of nickel electrowinning (after Njau and Janssen, 1995).

At electrolyte pH of 3 or lower, the nickel electrodeposits are ductile, flat, smooth and of required quality. At higher pH values (approximately pH 5 and higher), cracking and curling occurs, and degraded, brittle deposits are easily formed. Changes in pH seem to influence the building morphology of nickel deposits by interfering or altering the frequency of nucleation of nickel ions, therefore directly influencing inhibition and inhibition intensity. Even an increase from pH 2 to 3 shows increased inhibition and the nucleation overpotential increases (Amblard *et al*., 1983; Armyanov and Sotirova-Chakarove, 1992; Ji and Cooper, 1996; Lantelme *et al*., 1998; Kittelty, 2002).

2.2.2.2. Temperature

The temperature of the electrolyte during nickel electrodeposition is one of the fundamental parameters to monitor and control. At temperatures higher than 60 °C the conductivity and solubility increase and therefore diffusivity and transport of nickel ions towards the cathode surface are much more effective. Better mobility and transport of ions in solution cause a significant increase in the ease and rate at which the critical electrochemical reactions take place. At temperatures above 60 °C, the current efficiency increases to approximately 98 % and above, which in turn reduces power consumption of the overall process, even though energy is needed to heat the system initially (Kuhn, 1971; Ji, 1994; Lantelme and Seghiouer, 1998; Holm and O'Keefe, 2000; Kittelty, 2002; Lupi *et al*., 2006).

Changes in the developing morphology can also be related in part to changes in temperature. At temperatures lower than 60 °C, growth proceeds in an outward manner and high internal stress is observed in the deposit. Deposit grains are larger and more loosely packed and brittle deposits are frequently formed. At temperatures above 60 °C, surface diffusion of adsorbed nickel increases and general morphology and ductility of deposits are improved. Deposits are flat, level, smooth and ductile. Rounder, finer, sharply faceted grains are more readily produced and more frequent nucleation takes place. The coherency of deposits to the substrate surface improves and internal strain decreases (Kuhn, 1971; Ji, 1994; Lantelme and Seghiouer, 1998; Holm and O'Keefe, 2000; Kittelty, 2002; Lupi *et al*., 2006).

An interesting study by Ji (1994) investigated the change in surface pH of the cathode at various electrolyte temperatures during nickel deposition from nickel chloride solutions. The pH was measured with a specialised micro-pH meter placed as close as possible to the cathode surface without interfering with the deposition reaction. Three electrolytes of varying temperatures (25, 40 and 60 °C) were investigated. The effect of pH as a function of current density of the three electrolytes is shown in Figure 2.2.

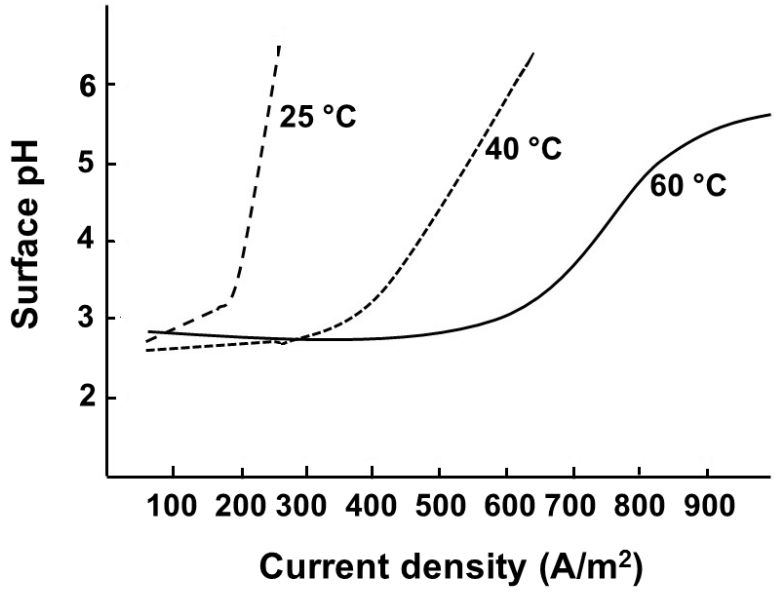

Figure 2.2. Graphical representation of the relationship between surface pH and current density at varying electrolyte temperatures (after Ji, 1994). The $NiCl_2$ concentration was kept constant at 0.937 M. The electrolyte temperatures were 25, 40 and 60 °C.

It is known that surface pH increases with increasing current density as electrodeposition proceeds (Amblard *et al*., 1983). This was observed for all three cases, irrespective of the temperature of the electrolyte. It was, however, observed that the pH increased at a much slower rate for the electrolyte at 60 °C compared with the 40 and 25 °C electrolytes. This effect, therefore, was much less pronounced at higher electrolyte temperatures. Increases in temperature from 25 to 60 °C appeared to counter changes in pH on the electrode surface to some extent. It can therefore be assumed that changes in temperature might have a stronger influence on the electrodeposition process compared with changes in pH (Ji, 1994).

2.2.3. Sulfate electrolyte composition and effect thereof on polarisation parameters and deposit morphology

This section explores the effect of variation in nickel concentration, sodium sulfate concentration, additives and impurities present in the electrolyte on the potential measurements and the characteristics and morphology of the produced nickel electrodeposit under these conditions. A summary is given here in order to understand and predict what the expected

observations should be for such changes in this particular study. It is important to set expectations of relationships and correlations between polarisation changes and morphological changes with varying composition of the electrolyte. It should be mentioned that none of the factors that influence changes in polarisation behaviour and morphological shifts function totally independently and that specific combinations of electrolyte conditions, parameters and composition concentrations would have specific effects. This should always be kept in mind.

It should also be mentioned that most of the work done on nickel electrowinning to date is cyclic voltammetry-based. Therefore, conclusions made regarding overpotential measurements were based on trends in polarisation behaviour and not on accurately measured potential values.

One of the major benefits of using sulfate electrolyte instead of chloride based-electrolyte is the fact that the sulfate system is more environmentally friendly (chlorine gas is not produced as a by-product) and nickel deposits are generally better quality and less strained (Kittelty, 2002; Jing *et al*., 2010). The sulfate system is, however, highly pH dependent and the unwanted hydrogen reduction reaction decreases current efficiency and causes pitting (Amblard *et al*., 1983; Ji and Cooper, 1996; Kittelty, 2002) if the H_2 bubbles are not effectively removed from the substrate surface. The sulfate electrolyte also has poor wettability, which causes the adsorbed hydrogen to stay on the cathode surface (Jing *et al*., 2010). The major components that need to be considered are nickel concentration, sulfate concentration, boric acid concentration and additives and impurities present in the electrolyte. These are discussed in the following sections.

2.2.3.1. Nickel concentration

As nickel concentration increases, the electrolyte characteristics change. The electrolyte density increases and the conductivity changes due to presence of the additional sulfate and nickel ions (Abyaneh and Hashemi-Pour, 1994; Holm and O'Keefe, 2000). Typically, the best conditions for electrodeposition are low density and high conductivity of the electrolyte. Under such conditions, the mobility of nickel ions towards the substrate is more effective, the wettability of the electrolyte increases and the power and energy requirements for the process decrease (Abyaneh and Hashemi-Pour, 1994; Ji and Cooper, 1996; Nicol and Kittelty, 2001; Kittelty, 2002; Di Bari, 2010). Ideal conditions are typically obtained at relatively high nickel(II) concentrations. Increasing nickel(II) concentrations cause lower substrate surface pH, which, in turn, limits the

formation and precipitation of $Ni(OH)_2$, which typically occurs at a pH of around 5 and above (Ji and Cooper, 1996; Holm and O'Keefe, 2000; Kittelty, 2002; Wu *et al*., 2003).

An increase in the nickel(II) concentration normally improves morphology, quality and current efficiency of the deposit. Ductile, flat, compact deposits are generally obtained at nickel(II) concentrations of at least 60 g/L (Holm and O'Keefe, 2000;Di Bari, 2010). Grains are found to be tightly packed and the growth mechanism seems to be more regular (Abyaneh and Hashemi-Pour, 1994; Nicol and Kittelty, 2001; Kittelty, 2002; Di Bari, 2010). Lower internal stress is also observed at higher nickel(II) concentrations – much less peeling, cracking and delamination are observed. At low nickel(II) concentrations, very low three-dimensional (3D) nucleation rates are observed and formed crystals might even stop depositing and growing, leaving a very irregular structure (Abyaneh and Hashemi-Pour, 1994; Ji and Cooper, 1996; Wu *et al*., 2003).

Changes in the nickel(II) concentration and the effect thereof on polarisation parameters are very pH dependent (Di Bari, 2010). If the pH is maintained between 2 and 3, an increase in nickel(II) concentration causes better morphology and higher current efficiency (Ji and Cooper, 1996; Kittelty, 2002). According to changes in morphology that are observed as the nickel(II) concentration increases, it appears that nucleation rate is not severely influenced but the growth rate changes. Larger, tightly packed, fast-growing crystals are mostly observed at higher concentrations (Holm and O'Keefe, 2000; Kittelty, 2002).

At higher nickel concentrations, the surface pH is also more easily maintained throughout the electrodeposition process. This is illustrated in Figure 2.3. This particular study was conducted by Ji (1994) in a nickel chloride electrolyte at various concentrations of nickel chloride.

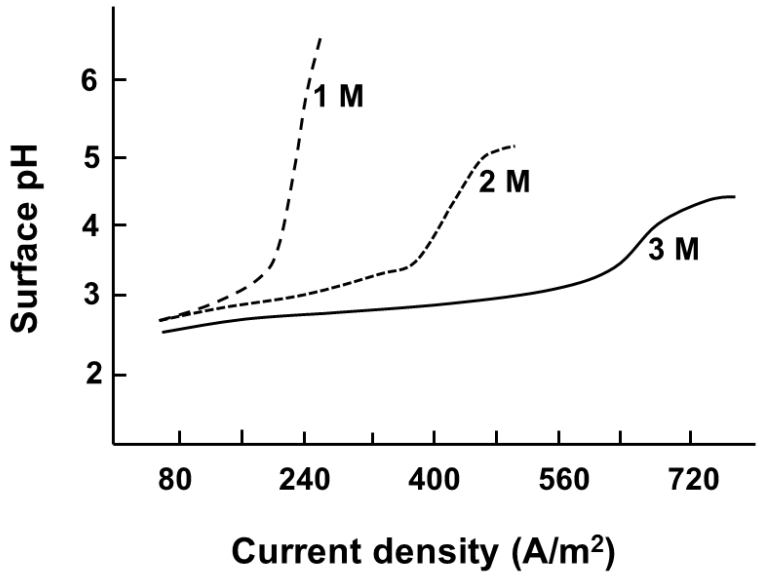

Figure 2.3. Indication of variation of surface pH and current density with changing nickel concentration ([$NiCl_2$] of 1 M, 2 M and 3 M) in the electrolyte solution (after Ji, 1994).

2.2.3.2. Sodium sulfate concentration

Sodium sulfate is typically added to the electrolyte to increase the conductivity in order to reduce the energy and power requirements for the process. Better quality deposits with more desirable morphology are obtained at higher sulfate concentrations. An increase in sulfate concentration should lower the substrate surface pH (Ji, 1994) and therefore decrease the probability of $Ni(OH)_2$ formation and precipitation.

If sulfate is added in large excess (greater than 180 g/L), however, the viscosity of the electrolyte increases (Abyaneh and Hashemi-Pour, 1994), which negatively influences the activity and mobility of nickel ions in the solution towards the substrate. More nodular growth and decreased growth rates are observed in such cases (Abyaneh and Hashemi-Pour, 1994; Di Bari, 2010). At very high sodium sulfate concentrations, the ionic strength of the electrolyte changes and low outward and lateral growth rates are observed as a result of complex formation between the nickel and sulfate ions ($NiSO_4(aq)$) (Abyaneh and Hashemi-Pour, 1994).

At high sulfate concentration combined with low nickel(II) concentration, very little 3D nucleation can occur. The sodium ions in solution do not have an effect on growth rates. A sodium sulfate concentration of 80 g/L to 100 g/L is generally maintained to obtain deposits of desirable quality (Holm and O'Keefe, 2000; Nicol and Kittelty, 2001; Kittelty, 2002; Wu *et al*., 2003).

2.2.3.3. Boric acid concentration

As mentioned, the production of hydrogen gas bubbles at the cathode decreases the hydrogen ion concentration at the cathode surface. The pH on the surface therefore increases with time to higher values than that of the bulk of the electrolyte solution. As electrodeposition progresses and the hydrogen ion concentration reaches very low levels, the undesirable formation of nickel hydroxides precipitates is promoted (Holm and O'Keefe, 2000; Kittelty, 2002).

The hydrogen evolution reaction can occur by means of one of two possible mechanisms (Holm and O'Keefe, 2000). During the first step in both possible mechanisms, an electron-transfer reaction occurs (Reaction [12]) to produce an adsorbed metal (M) intermediate:

$$M + H^+ + e^- \rightarrow M{-}H_{ads} \qquad [12]$$

The second step involves either a discharge–recombination reaction (Reaction [13])) or a discharge–electrochemical desorption reaction (Reaction [14]).

$$M{-}H_{ads} + M{-}H_{ads} \rightarrow H_2 + M \qquad [13]$$

$$M{-}H_{ads} + H^+ + e^- \rightarrow H_2 + M \qquad [14]$$

Most of the adsorbed hydrogen reacts according to one of these mechanisms, but a portion of the hydrogen may also get absorbed into the metallic crystal lattice (Reaction [15]):

$$M{-}H_{ads} \rightarrow M(H_{ads}) \qquad [15]$$

On the one hand, the inclusion of hydrogen bubbles into the deposit can cause poor morphological characteristics and directly influence the electrocrystallisation of the nickel. On the other hand, H^+ discharge is the instigator for the formation of many complex species responsible for desirable inhibition during electrocrystallisation (Holm and O'Keefe, 2000). If

hydrogen bubbles adhere to the substrate surface and the nickel metal electrocrystallisation occurs around the bubbles, severe pitting of the deposit is observed. This is probably due to screening of the surface from the anode such that re-dissolution of the plated metal occurs (Armyanov and Sotirova-Chakarove, 1992). Both H^+ and OH^- ions in the electrolyte are proposed to directly interact with the Ni^{2+} ions to form ligand complexes necessary for electrocrystallisation (Holm and O'Keefe, 2000).

An important fact to consider is that there are various proton-donating pH buffers present in the electrolyte (Ji and Cooper, 1996). Possible reactions are shown in Reactions [16], [17] and [18].

$$HSO_4^- \rightarrow SO_4^{2-} + H^+ \quad [16]$$

$$Ni^{2+} + H_2O \rightarrow NiOH^+ + H^+ \quad [17]$$

$$4Ni^{2+} + 4H_2O \rightarrow Ni_4(OH)_4^{4+} + 4H^+ \quad [18]$$

These dissociation reactions do, however, not necessarily occur at a rate that is quick enough to counter the pH rise at the cathode surface and therefore boric acid is normally added to the solution. The dissociation reactions associated with boric acid are given in Reactions [19] and [20] (Ji and Cooper, 1996):

$$H_3BO_3 + H_2O \rightarrow B(OH)_4^- + H^+ \quad p\mathit{K}a = 9.2 \quad [19]$$

$$3H_3BO_3 \rightarrow B_3O_3(OH)_4^- + H^+ + 2H_2O \quad p\mathit{K}a = 6.8 \quad [20]$$

Boric acid may also rather undergo successive ionisation reactions because it is a tri-protonated acid. Possible reactions are given in Reactions [21] to [23] (Ji and Cooper, 1996).

$$B(OH)_3 \rightarrow BO(OH)_2^- + H^+ \quad p\mathit{K}a_1 = 9.2 \quad [21]$$

$$BO(OH)_2^- \rightarrow BO_2(OH)^{2-} + H^+ \quad p\mathit{K}a_2 = 12.4 \quad [22]$$

$$BO_2(OH)^{2-} \rightarrow BO_3^{3-} + H^+ \quad p\mathit{K}a_3 = 13.3 \quad [23]$$

The addition of boric acid to the sulfate electrolyte has been shown to limit the bulk pH rise to a maximum of approximately 5 (Ji and Cooper, 1996; Kittelty, 2002). If the p*K*a values for the dissociation reactions of boric acid (Reactions [19] to [23]) are considered, however, it is highly

unlikely that these boric acid species could be responsible for maintaining the bath pH at values lower than 5. Other studies suggested that buffering of the electrolyte might rather be due to the formation weak of nickel–borate complexes (Reaction [24] and [25]) (Gadad and Harris, 1998).

$$B(OH)_3 + Ni^{2+} + H_2O \rightarrow Ni[B(OH)_4]^+ + H^+ \quad [24]$$

$$H_3BO_3 + Ni^{2+} \rightarrow Ni(H_2BO_3)^+ + H^+ \quad [25]$$

The mechanism of action of boric acid is still a subject of debate and conflicting results have been reported. Generally, it is observed that an increase in boric acid concentration produces brighter, good quality nickel deposits with deposits formed at higher crystal growth rates. Boric acid is believed to influence the overpotential for both the hydrogen evolution and nickel electrodeposition reactions in such a way that nickel can be deposited more effectively without hydrogen evolution occurring (Abyaneh and Hashemi-Pour, 1994; Ji and Cooper, 1996, Tripathy *et al*., 2001).

If boric acid is added to the electrolyte, the cathode surface pH tends to increase less significantly and also at a slower rate compared with unbuffered electrolyte. Therefore, the possibility of formation of nickel hydroxide precipitates is significantly reduced in the presence of a suitable buffer. Passivation of the cathode surface is also decreased, therefore boric acid or its complexes seem to act as a surface agent to form a selective layer promoting nickel electro-reduction (Yin and Lin, 1996; Gadad and Harris, 1998; Lupi *et al*., 2006). Without boric acid, $Ni(OH)_2$ precipitates on the surface at high potentials due to an increase in the surface pH caused by hydrogen evolution. This precipitated $Ni(OH)_2$ passivates the electrode surface and decreases the desired nickel deposition reaction (Yin and Lin, 1996; Lupi *et al*., 2006).

2.2.3.3.1. Citric acid buffers

Alternative buffers with p*K*a values in the same range as the working pH for nickel electrodeposits from sulfate electrolyte have been proposed. One such possible buffer comprises citric acid and citrate ions. Citric acid is a tri-protonated acid and has p*K*a values of 2.9, 4.3 and 5.2.

It is also proposed that citric acid itself, as well as nickel–citrate complexes, might be responsible for buffering of the electrolyte solution. The complexes adsorb onto the cathode surface, thereby

contributing to the nickel electrocrystallisation reaction. The adsorption is also believed to inhibit the hydrogen evolution reaction and thereby promote nickel deposition. A study by Chao-qun *et al*. (2007) found that the addition of citric acid caused an increase in buffering capacity at high current efficiencies. The nickel deposits were of high quality and desirable morphological characteristics under optimum conditions of pH, temperature and nickel concentration. The deposits were generally fine-grained and compact.

2.2.3.4. Effect of specific additives to the electrolyte

Additives are typically organic molecules added to the electrolyte before or during the electrodeposition process to achieve specific characteristics of the electrodeposited nickel. The type and concentration of additive and the combined effects of various additives are some of the most important aspects to consider (Oniciu and Muresan, 1991; Küzeci and Kammel, 1994). One of the difficult considerations is that the exact mechanism by which additives interact with the nickel ions in solution and the substrate surface is not fully understood and classified (Mackinnon *et al*., 1979a). This makes it difficult to predict the exact effect of an additive and laborious experiments often are needed to determine the concentration range and operating parameters at which the additive is beneficial in the morphological outcome of the electrodeposition process (Rashkov *et al*., 1990; Wiart *et al*., 1990; Muresan *et al*., 1996; Mohanty *et al*., 2009).

Many different theories have been proposed to explain the experimentally observed effects of specific impurities and additives in nickel electrowinning. Proposed mechanisms of interaction or reaction of additives in electrodeposition include: blocking of the substrate surface, changes in polarisation potential, complexation and induced adsorption, ion pairing, changes in interfacial tension of electrodes, hydrogen evolution induction, hydrogen adsorption, anomalous co-deposition and specific effects of intermediates (Franklin, 1987; Rashkov *et al.*, 1990; Wiart *et al.*, 1990; Mohanty *et al*., 2009).

Many commonly used additives cause an increase or a decrease in the polarisation of the cathode. When additives cause an increase in polarisation of the cathode, a decrease in current density at a specific electrode potential is observed (Oniciu and Muresan, 1991). In most cases, this effect is directly dependent on the concentration of the additive in solution (Küzeci and

Kammel, 1994). A maximum plateau of cathode potential is reached at a specific concentration of additive and thereafter any increase in the additive concentration has little effect or an opposite effect on the cathode potential. An increase in agitation rate and temperature in the presence of the same additive may also cause a decrease in cathode polarisation. As additive species adhere and cover sections of the cathode, the effective current density increases, the overvoltage increases and the current efficiency decreases (Oniciu and Muresan, 1991; Küzeci and Kammel, 1994).

Because the additive is typically consumed during the electrodeposition process, the concentration of the additive must be monitored and corrected as it is depleted from the electrolyte (Oniciu and Muresan, 1991). Either direct (radiotracer or mass spectrometry) or indirect methods (determination of bulk concentration or deposit resistivity) are used to monitor the concentration in solution. The additives can co-deposit with the metal in their original form or can undergo reduction at the cathode. If the reduced products are more soluble, they will rather redistribute to the bulk electrolyte solution (Oniciu and Muresan, 1991; Küzeci and Kammel, 1994).

Three specific additives were investigated in this particular study. These are saccharin (SAC), sodium laurel sulfate (SLS) and pyridine (PYR). A short overview of the effects of each of these additives is given in the following sections.

2.2.3.4.1. Saccharin

SAC is an aromatic organic compound that can be added to nickel electroplating electrolytes to improve ductility, brightness and grain size (Rashidi and Amadeh, 2009). The addition of SAC to the electrolyte causes grain refinement, increases microhardness and improves overall quality of the nickel deposits (Xuetao *et al*., 2008). These effects are shown in Figures 2.4 and 2.5.

The mechanism of SAC as an additive in nickel electrowinning is still not fully understood but many possibilities have been proposed (Ciszewski *et al*., 2004; Mohanty *et al*., 2005; Xuetao *et al*., 2008; Rashidi and Amadeh, 2009). The most accepted idea is that the reactive ethylene sulfonyl groups of SAC are able to donate a lone pair of electrons to the 3d orbital of a nickel cation in order to form a stable coordinate bond (Ciszewski *et al*., 2004; Rashidi and Amadeh, 2009). This coordination reaction takes place on the substrate surface, which, in turn, decreases

the rate of discharge of Ni^{2+}. The effect thereof is that overpotential of nickel electrodeposition increases, which promotes the constant formation of new crystal nuclei and thereby increases grain refinement (Ciszewski *et al*., 2004; Rashidi and Amadeh, 2009).

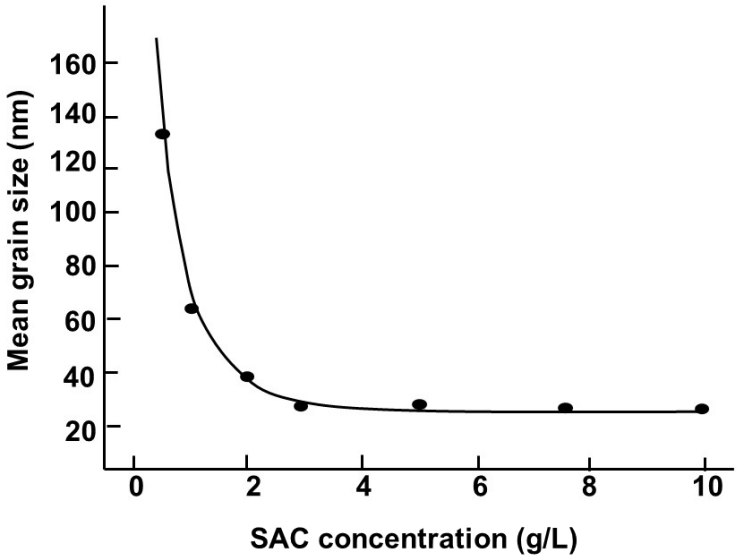

Figure 2.4. Experimental data showing the effect of increasing SAC concentration on grain size of nickel electrodeposits (after Rashidi and Amadeh, 2009).

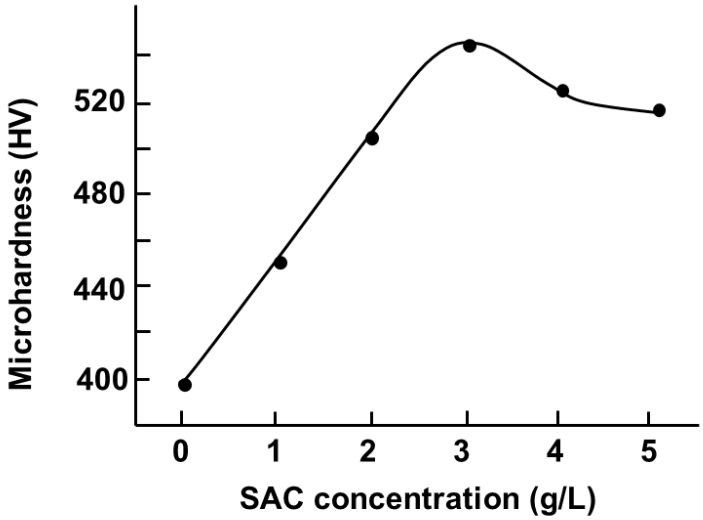

Figure 2.5. Experimental data showing the effect of increasing SAC concentration on microhardness of the nickel electrodeposits (after Xuetao *et al*., 2008).

Another possibility is that the complexes block or inhibit the substrate surface, which causes an increase in nucleation and decreases surface diffusion of the nickel ions (Ciszewski *et al*., 2004). Whatever the exact mechanism, it is expected from these observations and theories that an increase in SAC should cause inhibition and therefore a more cathodic nucleation overpotential (E_n). The effect thereof is expected to manifest as an increase in grain refinement of the nickel deposits (Ciszewski *et al*., 2004; Xuetao *et al*., 2008; Rashidi and Amadeh, 2009).

Two other considerations with the addition of most additives are that operating parameters such as temperature influence transport and activity of the additives and nickel cations, and that the effect of an additive is also expected to be seen up to a certain concentration, presumably due to saturation of adsorption sites (Ciszewski *et al*., 2004; Xuetao *et al*., 2008; Rashidi and Amadeh, 2009).

2.2.3.4.2. Sodium lauryl sulfate

SLS is an anionic surfactant widely used in nickel electroplating to increase the wettability of the electrolyte. Surfactants reduce the surface tension of the electrolyte, which directly affects the ability of hydrogen bubbles to leave the substrate surface. As electrodeposition progresses, the hydrogen produced adheres to the cathode surface. The lower the surface tension (or the higher the wettability) of the electrolyte, the more easily the hydrogen bubbles are removed from the substrate, thereby decreasing pitting of the produced electrodeposit (Kittelty and Nicol, 2003; Mohanty *et al*., 2009; Jing *et al*., 2010).

SLS molecules adsorb onto the cathode surface, which increases the energy barrier that the nickel ions need to overcome in order to deposit onto the substrate. This becomes the rate–controlling step as the concentration of SLS increases (Mohanty *et al*., 2009). As the cathodic overpotential is inhibited to more negative values, nickel reduction is promoted. It is therefore expected that an increase in SLS concentration in the electrolyte should cause a shift in overpotential to more negative values. Therefore, some grain refinement is also expected with an increase in SLS concentration – the more negative the overpotential, the more frequently nucleation takes place (Mohanty *et al*., 2009; Jing *et al*., 2010). It should, however, be noted that these observations were made using cyclic voltammetry techniques and therefore no definite

effect of SLS can be specifically predicted on either E_n or E_p. The effect of SLS on overpotential is shown in Figure 2.6.

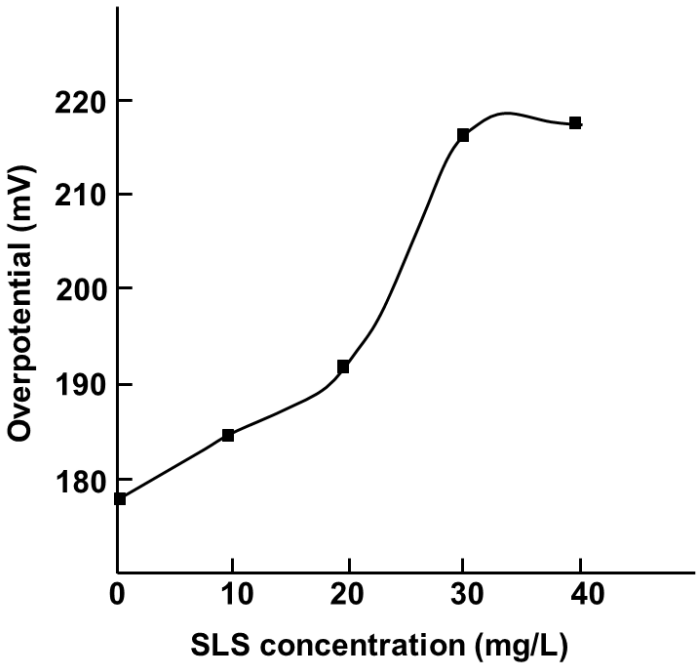

Figure 2.6. Effect of SLS concentration on the overpotential during nickel electrodeposition from sulfate electrolyte (after Mohanty *et al*., 2009).

The addition of SLS does not seem to have a large effect on current efficiency. This was proposed (Mohanty *et al*., 2009; Jing *et al*., 2010) to be due to the repulsion of the large surfactant anions by the negative charge on the electrode surface. Overall, the addition of SLS to the electrolyte should decrease pitting, promote grain refinement and promote the production of smooth, ductile, low-strained nickel deposits.

2.2.3.4.3. Pyridine

The addition of PYR to the electrolyte has a marked effect on the quality and characteristics of the produced nickel electrodeposits. In the presence of PYR, the deposits are generally smooth, bright, level and uniform and the morphology seems to improve with increasing PYR concentration. An increase in PYR concentration causes an increase in E_n due to strong adsorption of the additive onto the substrate surface, causing an increase in the reduction

potential of Ni^{2+} (Mohanty *et al*., 2001; Mohanty *et al*., 2005). Changes in potential and current density with increasing PYR concentration are shown in Figure 2.7.

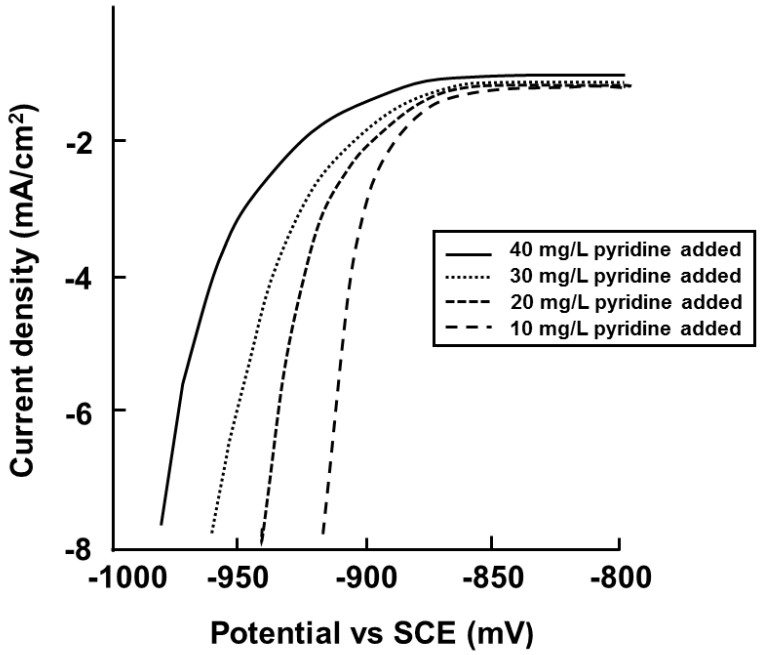

Figure 2.7. Effect of PYR concentration on measured potential illustrated by a typical voltammogram (after Mohanty *et al.*, 2001). PYR concentration was increased from 10 mg/L to 40 mg/L during nickel electrodeposition from acidic sulfate electrolyte.

At the low operating pH values typical of nickel electrolyte solutions, pyridines exist in protonated form. Once migration towards the substrate surface is complete, deprotonation of these groups can easily occur and the conjugate PYR adsorbs onto the surface as a free base (Mohanty *et al*., 2001). As PYR molecules adsorb onto the cathode surface, inhibition increases, which causes an overall polarisation of the cathode surface (Mohanty *et al*., 2001; Mohanty *et al*., 2005).

2.2.3.5. Effect of specific metallic impurities common to nickel electrowinning processes

Impurities in electrowinning operations include inorganic cations and anions, as well as organic substances that may be unintentionally present in the electrolyte. The crystal shape and orientation, grain size, strain and morphology, the degree of hydrogen pitting and discoloration

of the deposit are some of the major characteristics influenced by the presence of impurities (Mackinnon *et al*., 1979b; Wiart *et al*., 1990; Plieth, 2011). Impurities affect the transport of metal ions in solution towards the substrate, can act as carrier molecules, increase inhibition by adhering to the substrate surface during the process and may also be incorporated into the electrodeposit itself (Rashkov *et al*., 1990; Wiart *et al*., 1990; Küzeci and Kammel, 1994; Kittelty and Nicol, 2003; Plieth, 2011).

This study focused on four specific metallic impurities that are industrially relevant to nickel electrowinning from sulfate electrolyte: cobalt, copper, aluminium and amphoterics (selenite and selenate). Cationic impurities influence the quality, purity and morphological characteristics of the produced deposit and the electrocrystallisation process and modes of growth during electrocrystallisation (Mackinnon *et al*., 1979a; Mackinnon *et al*., 1979b; Kittelty, 2002). The idea is to set the framework here of what is expected to be observed for the polarisation and morphological changes during nickel deposition in the presence of certain metallic impurities.

The standard reduction potentials for nickel and those of the investigated impurities and the generally accepted concentration intolerance limits are indicated in Table 2.1 (Gogia and Das, 1988; Gogia and Das, 1991). Nickel was electrodeposited from typical sulfate electrolyte (containing 60 g/L Ni^{2+} and 12 g/L boric acid) onto stainless steel cathodes at a current density of 400 A/m^2. Impurity concentrations were varied from 100 mg/L to 2000 mg/L for Co^{2+}, 100 mg/L to 1000 mg/L for Cu^{2+} (Gogia and Das, 1991) and 5 mg/L to 100 mg/L for Al^{3+} (Gogia and Das, 1988).

Table 2.1. Tolerance limits (with respect to 98% nickel purity) and standard electrode potentials of certain impurities during nickel electrowinning (adapted from Gogia and Das, 1988 and Gogia and Das, 1991).

Metal impurity	Tolerance limit (mg/L)	Standard electrode potential (V) vs. SHE	Electrode reaction
Ni^{2+}	NA	−0.250	$Ni^{2+} + 2e^- \rightarrow Ni$
Co^{2+}	500	−0.277	$Co^{2+} + 2e^- \rightarrow Co$
Cu^{2+}	100 to 250	+0.33	$Cu^{2+} + 2e^- \rightarrow Cu$
Al^{3+}	5 to 10	−1.66	$Al^{3+} + 3e^- \rightarrow Al$

2.2.3.5.1. Cobalt

The standard reduction potential for cobalt (−0.277 V) is only slightly more negative than that of nickel (−0.250 V) (Gogia and Das, 1991). Therefore, co-deposition of cobalt during nickel electrodeposition is a definite possibility, especially because cobalt reduces easily to its own metallic state in simple acid solutions at a lower deposition potential than nickel (Gogia and Das, 1991). The first observation, therefore, is that cobalt–nickel alloys can form should cobalt impurities be present in the electrolyte solution (Kittelty, 2002; Kittelty and Nicol, 2003). The degree of contamination is also expected to increase with increasing cobalt concentration. The current efficiency of nickel electrodeposition would therefore also decrease as cobalt co-deposits (Gogia and Das, 1991; Kittelty, 2002).

Below the tolerance concentration of around 500 mg/L (Gogia and Das, 1991), no definite morphological or quality characteristics changes are observed. If the cobalt concentration is high, deposits are generally cracked, peeled and more spongy. This is probably caused by an increase in internal stress during the electrocrystallisation process because cobalt is also incorporated into the crystal lattice during co-deposition (Kittelty, 2002).

At low cobalt concentrations (below the tolerance concentration limit), the polarisation of nickel is shifted to less negative values (less noble). This can possibly be explained by co-deposition of cobalt and a decrease in free energy of formation of the Co−Ni solid solution. At high concentrations of cobalt in the electrolyte, the polarisation curve for nickel deposition is shifted to more negative values. This may be due to changes in the crystal orientation during the electrodeposition process (Gogia and Das, 1991; Kittelty, 2002; Kittelty and Nicol, 2003).

2.2.3.5.2. Copper

Copper is more noble than nickel (Table 2.1) and is therefore expected to co-deposit with nickel. The current efficiency is therefore also expected to decrease in the presence of copper. The tolerance concentration limit for copper is around 200 mg/L (Gogia and Das, 1991) and the effect of copper on the morphology and polarisation characteristics increases with increasing copper concentration in the electrolyte (Dennis and Fuggle, 1968; Kittelty, 2002; Kittelty and Nicol, 2003).

If copper is present as an impurity, nickel electrodeposits are discoloured, nodular and strained (Gogia and Das, 1991). Larger crystallites that are located in large colonies are observed at lower copper concentrations, but the morphology appears to be completely different if the copper concentration is above the tolerance limit. Some previous studies (Dennis and Fuggle, 1968; Gogia and Das, 1991) have shown that no differences in the polarisation of nickel were observed in the presence of copper even though definite changes were observed in physical appearance, purity, orientation and morphology.

2.2.3.5.3. Aluminium

It has been shown that the tolerance limit for aluminium is much lower in nickel electrowinning compared with that of other metallic impurities. It is reported that deposit morphology is severely influenced from as little as 5 to 10 mg/L of Al^{3+} in solution (Gogia and Das, 1988; Zhou and O'Keefe, 1997; Holm and O'Keefe, 2000). Deposits are cracked, curled, peeled, brittle and highly pitted in the presence of aluminium up to concentrations of approximately 2000 mg/L Al^{3+} (Küzeci and Kammel, 1994; Holm and O'Keefe, 2000). It seems that the effect on the morphology increases with increasing aluminium concentration (Kittelty, 2002). At concentrations of 5 mg/L, the deposits consist mainly of closely packed grains with non-uniform shapes. At 10 mg/L, the crystallites are coarser and exist in larger colonies (Gogia and Das, 1988; Zhou and O'Keefe, 1997; Holm and O'Keefe, 2000). The current efficiency also decreases in the presence of low concentrations of Al^{3+} due to disruption of nickel growth (Gogia and Das, 1988). An increase in oxygen in the composition of these deposits is found and it therefore is most likely that aluminium as $Al(OH)_3$ is co-deposited during nickel electrodeposition (Kittelty, 2002, Kittelty and Nicol, 2003).

The presence of aluminium also affects the polarisation parameters. The polarisation potential for nickel electrodeposition is shifted to more negative values if aluminium is present in the electrolyte. This polarisation effect also increases with increasing concentration of aluminium (Gogia and Das, 1988; Küzeci and Kammel, 1994; Holm and O'Keefe, 2000; Kittelty, 2002).

A particular study by Kittelty (2002), however, showed that in the presence of concentrations higher than 2000 mg/L aluminium, the nickel deposit quality and morphology was either unaffected or improved. Deposits obtained at a concentration of 2700 mg/L aluminium in the

electrolyte were smooth, crack-free, no dendrites were formed and the internal stress was comparable with that of nickel deposits obtained under optimum conditions without impurities in the solution. The reason for this and the possible mechanism were further investigated and Kittelty (2002) proposed that the most probable explanation could be the influence of aluminium on the buffering characteristics of the electrolyte.

The effect of aluminium on the buffering capacity of boric acid was investigated by titration of 50 mL of electrolyte solution (with varying aluminium and boric acid concentrations) with 0.5 M NaOH solution (Kittelty, 2002) The effect of increasing NaOH volume on the pH is shown in Figure 2.8.

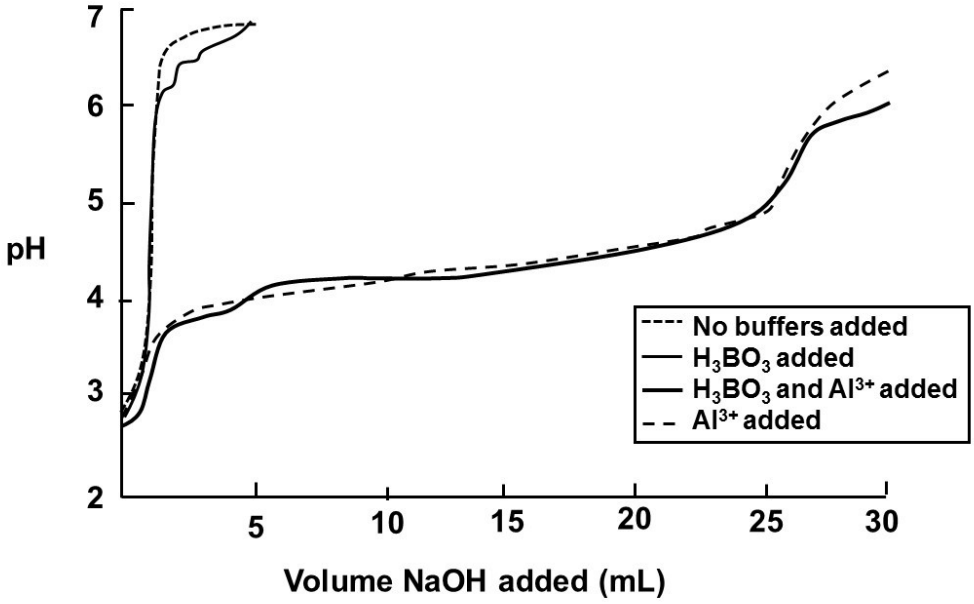

Figure 2.8. Titration curves of various electrolytes (with or without boric acid (4 g/L) and aluminium (2700 mg/L)) with NaOH showing the effect of increasing NaOH on the pH of the electrolyte (after Kittelty, 2002).

If the aluminium concentration is low (less than approximately 2000 mg/L) and the pH of the bulk solution rises to around 4 as electrodeposition proceeds, the aluminium is most likely to exist as $Al(OH)_3$ (Kittelty, 2002; Kittelty and Nicol, 2003). This manifests as an increase in the oxygen content of the produced deposits. Should the concentration of aluminium in the

electrolyte be much higher (approximately at least 2700 mg/L), the formation of other complexes, such as $Al_2(OH)_2^{4+}$ and $Al(OH)_2^{+}$, are probable (Holm and O'Keefe, 2000; Kittelty, 2002). It is probable that these complexes may be able to more effectively buffer the electrolyte below a pH of 6, at which $Ni(OH)_2$ precipitates and is incorporated into the crystal structure, compared with $Al(OH)_3$ which is itself co-deposited with nickel (Holm and O'Keefe, 2000; Kittelty, 2002).

The electrolytes that did not contain aluminium showed an increase in pH to around 6, at which the nickel hydroxide complexes formed and precipitated. The addition of boric acid showed better buffering of the electrolyte and more NaOH was needed to reach pH 6. This could be due to the formation of the $Ni(H_2BO_3)_2$ buffering complex (Ji and Cooper, 1996; Gadad and Harris, 1998). The solutions containing high concentrations of aluminium, however, showed the best buffering of the electrolyte – even better than the standard electrolyte solution containing the optimum boric acid concentration. Much more NaOH needed to be added to the electrolyte to increase the pH to around 6 (Kittelty, 2002).

These observations were made based upon morphological changes observed with changing aluminium concentration. The current study therefore included various concentrations of aluminium impurities in order to determine whether more accurate polarisation measurements and further buffer capacity studies could shed more light on the mechanism not only of aluminium in the electrolyte, but also the efficiencies of boric acid and citric acid on the buffering of the electrolyte.

A study by Nsiengani (2017) particularly focussed on internal strain and yield stress in nickel electrodeposits in the presence of aluminium impurities. Low strain was measured for deposits from electrolytes containing 2500 mg/L aluminium impurities. High strain was obtained for deposits from electrolytes containing 10, 20 or 300 mg/L aluminium. The deposits were visually examined and were compact and smooth without significant strain or cracks in the presence of 2500 mg/L aluminium. Aluminium impurity concentration included within the nickel electrodeposit was also measured and it was found that the nickel deposits contained insignificant amounts of aluminium at concentrations of 2500 mg/L aluminium in the electrolyte.

2.2.3.5.4. Selenium

Selenium as selenite (Se(IV)) and selenate (Se(VI)) impurities is unfavourable in copper electrowinning because these species co-deposit with copper during the electrodeposition process (Crundwell *et al.,* 2011). The quality and purity of the copper deposits are therefore severely influenced: both selenite and selenate are generally removed before copper electrowinning to levels below 1 mg/L for selenite and 10 mg/L for selenate (Crundwell *et al*., 2011).

In nickel electrowinning, the effects of Se(IV) and Se(VI) in industrial electrolyte on stress development and delamination was recently evaluated (Voogt *et al*., 2017). It was evident that selenium, and specifically Se(VI), caused severe cracking and delamination of nickel deposits from optimised industrial electrolyte, even at concentrations as low as 10 mg/L. The effect of selenium in the electrolyte was more severe than those of cobalt and copper impurities. The concentration limit to avoid complete delamination was determined as 15 mg/L (Voogt *et al*., 2017). The effects of Se(IV) and Se(VI) on stress are illustrated in Figure 2.9. Stress measurements were performed with a bent strip.

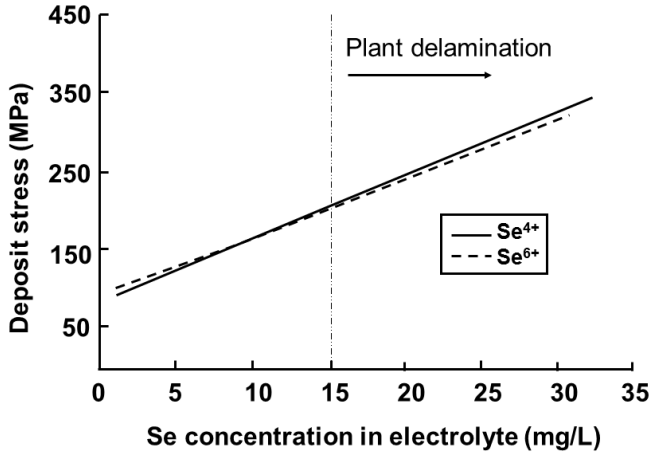

Figure 2.9. Stress development and delamination with increasing Se(IV) and Se(VI) concentration measured during electrodeposition of nickel from optimised industrial electrolyte (after Voogt *et al*., 2017).

2.3. Fundamental aspects of electrocrystallisation – nucleation and growth of electrodeposits

2.3.1. Introductory overview

Electrocrystallisation refers to the process during which a solid metal is deposited onto a substrate surface (cathode) in an electrolytic cell. It involves electrodeposition by reduction of metal ions in solution under an applied electric field over an electrode/electrolyte interface. Metal cation species in solution are complexed to water (hydrated) or other anionic species (ligands) in the electrolyte solution. As potential is applied, these complexes move toward the cathode surface where dissociation and reduction onto the cathode surface will occur (Budevski *et al*., 2000; Kolb, 2001).

Dissociation occurs at the electrochemical double layer where metal cations dissociate from ligands before reduction can occur. The first step in the reduction mechanism of these metallic ions occurs as the complexes reach the electrochemical double layer of capacitance (Budevski *et al*., 2000; Kolb, 2001). Here, partial and/or full dehydration (de-complexation) of the metal ions occurs to form partially or fully charged metallic species known as adions. The adions need to form stable complexes during deposition onto the substrate surface (Amblard *et al*., 1982). The extent of supersaturation mainly determines the number of such nuclei that is needed to form a stable cluster (Amblard *et al*., 1982; Budevski *et al*., 2000). Adatoms (fully reduced metal species) also diffuse on the substrate surface until the most energetically stable position in the growing crystal lattice is reached; nucleation of the adatoms onto the substrate then follows. Newly reduced adatoms can deposit either onto open planes or previously deposited clusters in the developing crystal (Amblard *et al*., 1982; Budevski *et al*., 2000).

The relationship between these nucleation and growth processes is extremely important because it determines how and where in the lattice the clusters will be incorporated and ultimately determines the outcome of characteristics and morphology of the deposit. Typically, a balance between the two processes must be maintained to obtain a deposit of desirable properties (Budevski *et al*., 2000; Adcock *et al*, 2002). Another factor that should be considered is the influence of other species in solution, such as additives or impurities, that can inhibit occupation

of the substrate surface and thereby decrease the available surface area for metal deposition (Adcock *et al*., 2004).

The electrocrystallisation mechanism is influenced by various complex factors, including conditions and parameters of the electrolytic cell and the concentrations of ions in solution. If this fundamental electrocrystallisation process is understood, controlled, predicted and manipulated, especially in the first stages of electrodeposition, the morphological characteristics of the metal deposit could be fine-tuned to produce deposits of a specific quality or desired characteristic (Budevski *et al*., 2000; Adcock *et al*., 2002; Kittelty, 2002; Adcock *et al*., 2004).

It should be mentioned that the some of the results discussed in the these sections were obtained by means of potentiodynamic techniques such as cyclic voltammetry. The results in many instances, such as the studies by Budevski *et al*. (2000) and Amblard *et al*. (1982), were obtained under conditions of controlled potential. Therefore, observations made regarding nucleation, plating and overpotential can only be indicative of processes taking place during deposition and not as absolute conclusions applicable to results obtained by galvanodynamic methods.

2.3.2. Transfer of metal ions from the bulk electrolyte to the substrate surface

The electrochemical double layer is the link between the cathode surface and electrolyte solution and at which dissociation and electron transfer occur. Metal cation species in solution are coordinated to water or anionic ligands in the general form $M(ligand)_n^{x+}$. As the coordinated metal ion species is mass transported from the bulk solution towards the substrate, it reaches the electrochemical double layer shown in Figure 2.10 (Kolb, 2001).

At the electrochemical double layer, dissociation and electron transfer occur. At the outer Helmholtz plane (OHP), the metal ion starts to dissociate from its coordinating ligand(s), is then reduced (electron transfer) to form an adion (partially reduced) or adatom (fully reduced), which is then adsorbed into the inner Helmholtz plane (IHP) of the electrochemical double layer (Kolb, 2001; Adcock *et al*., 2002). The solvated metal ions at the OHP are attracted electrostatically to the metal substrate surface and are non-specifically adsorbed (Amblard *et al*., 1982). As

dissociation occurs, the solvation shell of the adsorbed metal ion is weakened and the metal ion specifically adsorbs onto the substrate surface by a chemical bond in the IHP and electron transfer can readily occur (Amblard *et al*., 1982; Kolb, 2001).

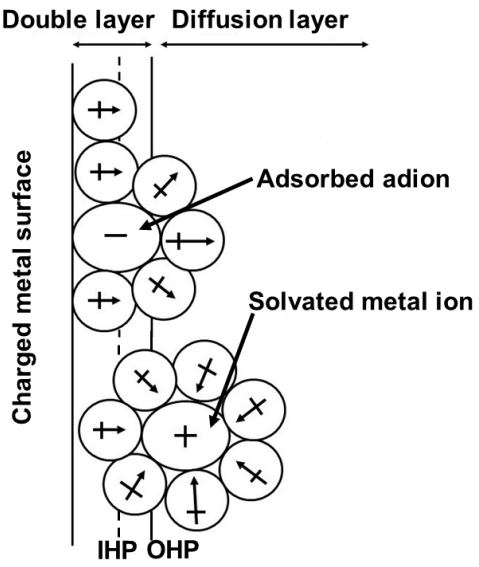

Figure 2.10. Generic layer model showing adsorption of ions onto the substrate surface thereby becoming adions. The inner- (IHP) and outer- (OHP) Helmholtz planes are indicated (after Kolb, 2001).

2.3.3. Surface diffusion and incorporation of adatoms into the growing crystal lattice

Newly formed metal adatoms are preferentially incorporated into the developing crystal lattice in such a way that high stability and low energy requirements are met. The most energetically favourable sites for incorporation of newly deposited adatoms are kinks, holes or edge vacancies, where the newly incorporated adatom would be surrounded by the highest possible number of neighbouring adatoms (specifically a position such as that marked “8”, as illustrated in Figure 2.11) (Winand, 1991; Budevski *et al*., 2000).

Direct incorporation at such sites is not always possible because sites on the plane of the substrate would occur far more frequently compared with kinks or holes (Winand, 1991). This challenge can be overcome by surface diffusion of the metal adatoms. This process takes place along the substrate surface to the closest most energetically favourable site, where the new adatoms interact with other adatoms and get incorporated into the crystal lattice (3D arrangement

of atoms) of the substrate, as illustrated in Figure 2.12 (Winand, 1991; Paunovic and Schlesinger, 2006).

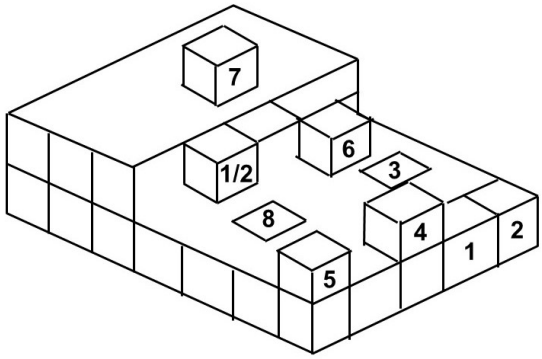

Figure 2.11. Diagrammatic representation of the typical sites available on the substrate surface for metal adatom precipitation (after Winand, 1991).

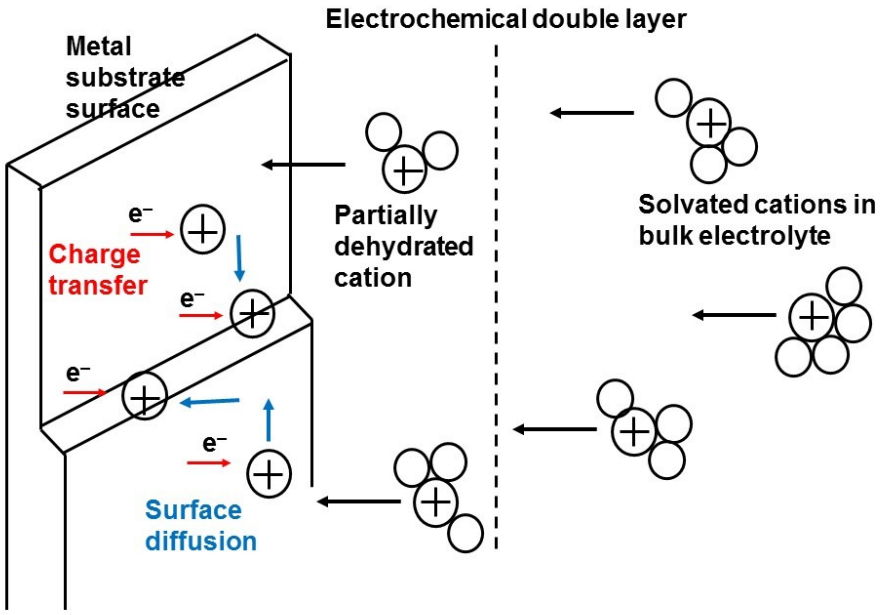

Figure 2.12. Diagrammatic representation of the steps involved in electrocrystallisation showing dehydration of the metal species and substrate surface diffusion (after Paunovic and Schlesinger, 2006).

Surface diffusion is therefore of great importance to ensure that adatoms are incorporated at the lowest energy sites − and not necessarily the most accessible sites − in the growing crystal lattice. This ensures that lattice defects are able to serve as low-energy growth points from which further growth can proceed (Winand, 1991; Budevski *et al*., 2000; Paunovic and Schlesinger, 2006).

The balance between energy available and energy required is of critical importance when a new phase is formed during the early stages of electrocrystallisation on a foreign substrate (Van den Brande *et al*., 1994; Budevski *et al*., 2000). The available electrical energy during this process is supplied by the externally applied potential while the energy needed for incorporation of adatoms and the formation of two-dimensional (2D) or 3D adatom clusters on a crystal incorporation site refers to the Gibbs free energy of formation (ΔG) (Van den Brande *et al*., 1994; Bockris *et al*., 2000). The Gibbs free energy of formation is defined in terms of the number of adatoms (N) that are transferred from the bulk electrolyte to the substrate surface under conditions of applied overpotential (E). This is illustrated in Equation [26] (Budevski *et al*., 2000). The $\phi(N)$ term refers to excess free energy, z to the number of electrons exchanged and e to the electron charge.

$$\Delta G(N) \rightarrow -Nze|E| + \phi(N) \qquad [26]$$

For various cluster shapes, it follows that those with the lowest ΔG will have the highest rate of formation. If external energy is low, the number of atoms required for formation of a stable 3D cluster is higher. If energy is applied by an external source, such as a potentiostat (typically at high overpotentials) by polarisation of the electrode, electrical energy is more freely available for deposition of the adatoms and the number of adatoms required to form a stable 3D cluster decreases (Bockris *et al*., 2000; Budevski *et al*., 2000). The rate of nucleation increases and a large number of smaller nuclei is formed, which promotes 3D cluster formation and causes grain refinement. This implies that there will be a critical size of adatom cluster that will be the most energetically favourable under specific conditions during any electrocrystallisation process (Bockris *et al*., 2000; Popov *et al*., 2002).

2.3.4. Nucleation and growth

Electrodeposit growth is proposed to occur during different, distinct stages during which the preferred orientation of the deposit is developed. The first stage is initial nucleation and growth on the substrate. During this stage, the most important factors influencing nucleation and growth are the substrate surface and its characteristics. During the following transition step, the structure is less dependent on the characteristics of the substrate but still influenced by it (Abyaneh, 1982; Van den Brande *et al*., 1994, Bockris *et al*., 2000). Thereafter, nucleation and growth are influenced by external factors related to the electrolyte, such as components of the electrolyte, current density, agitation, temperature, pH, additives and impurities (Abyaneh, 1982; Ebrahimi and Ahmed., 2003; Muñoz *et al*., 2003).

During the early stages of electrocrystallisation, 3D nucleation is required for the development of new crystals. If a foreign substrate is used, available kinks and steps are already present for growth. If not, growth sites need to be created through the formation of atoms or nuclei from which further growth can proceed (Winand, 1991). The formation of such nuclei is not favoured and therefore a degree of supersaturation is required (Van den Brande *et al*., 1994; Bockris, 2000).

The nucleation step is directly influenced by the interfacial tension and the supersaturation. If the supersaturation is high, 3D nucleation increases because various crystal planes are able to grow simultaneously, grain size of the deposit decreases and the number of critical nuclei required to form a stable nuclei cluster is reduced. If supersaturation is lower, formation of new layers or planes on a particular crystal face (2D) is rather promoted. Supersaturation (ΔS) is a function of cathodic overpotential (E) (Equation [27]), where E_{non} is the chemical potential of the non-equilibrium phase and E_e refers to the potential of the equilibrium bulk metallic phase (as cited by Winand (1991).

$$\Delta S_n = E_e - E_{non} = zeE \qquad [27]$$

The critical cluster size is proportional to $\delta^3/\Delta S^3$, where δ represents the cluster mean surface specific energy. The higher the supersaturation, the smaller the critical size that is needed for stability to form a cluster (Van den Brande *et al*., 1994). Statistically, the concept of a critical nucleus or cluster size refers to the critical size of a specific nucleus to initiate and promote

constant growth. If the nuclei formed are smaller than the critical nucleus size or the critical nucleus is formed too slowly, re-dissolution occurs more readily (Budevski *et al*., 2000; Ebrahimi and Ahmed, 2003). Electrocrystallisation, and ultimately electrodeposition, therefore requires the formation of appropriately sized nuclei under the appropriate degree of inhibition in conjunction with the appropriate structure of the substrate surface (Muñoz *et al*., 2003). Phase boundaries, dislocation and other distortions directly influence nucleus formation and the nucleation process (Popov *et al*., 2002; Plieth, 2011).

It is well known that the electrodeposit will preferably continue the structure of the cathodic substrate during the initial stages of the deposition process, i.e., the initial growth is epitaxial in nature. Epitaxial growth on a foreign substrate includes the formation of isolated 3D islands on top of pre-deposited monolayers and growth occurs according to the crystallographic substrate deposit misfit orientation (Winand, 1991; Bockris, 2000; Budevski *et al*., 2000). After the preferred crystallographic orientation has been established and epitaxial growth has been completed, a particular crystal direction undergoes growth normal to the substrate and parallel to the direction of the applied current. Normally, a one-directional axis of growth is preferred. The substrate structure thus becomes almost insignificant and the structure of the deposit is then mostly determined by the bath composition and the plating conditions (Van den Brande *et al*., 1994; Winand, 1994). The deposit crystals adopt a preferred orientation due to differing rates of growth of specific crystal faces. This is known as the formation of texture: it occurs as a result of nucleation and growth of competing crystal faces due to differing relative surface energies. The texture that requires the least energy is preferentially promoted (Ebrahimi and Ahmed, 2003, Plieth, 2011). The presence of additives, impurities and organic inhibitors influences the rates of growth of specific crystal faces. These substances may increase the overpotential on specific crystallographic faces, which causes an increase in nucleation rate (Budevski *et al*., 2000, Kittelty, 2002).

The relationship between nucleation and growth can therefore be described as a series of reactions in constant competition, which in turn determines how electrocrystallisation occurs and how the electrodeposit forms (Budevski *et al*., 2000). This ultimately influences the texture, granularity and morphological properties of the electrodeposit (Plieth, 2011). If nucleation occurs more frequently compared with growth, 3D nucleation is prevalent and the resulting

deposit grains are generally finer. Growth can either be perpendicular or parallel to the substrate surface depending on the 2D nucleation frequency. The crystalline shape and orientation are directly determined by the most frequent growth mode. It is therefore clear that the relationship between nucleation and growth is a critical factor to determining the outcome of the electrocrystallisation process and electrodeposit properties: if this relationship can be manipulated, the deposit characteristics can possibly be fine-tuned (Oniciu and Muresan, 1991; Winand, 1991; Bockris, 2000; Adcock *et al*., 2002; Plieth, 2011).

2.3.5. Inhibition intensity and morphological changes during electrocrystallisation

Inhibition occurs as a consequence of certain species (organic or inorganic) present on or near the cathode surface that either obstruct or hinder the metal species approaching the substrate or are reduced with the approaching adions and incorporated into the metal deposit. Inhibitors can either be classified according to types of ions or according to mode of inhibition (Winand, 1991; Plieth, 2011). Inorganic cat- or anions can change the electrical structure of the double layer, thereby directly influencing the charge-transfer reactions, causing negative catalysis of the reduction reaction. Organic inhibitors generally adsorb to the metal itself on active growing sites, which inevitably causes reduction of the inhibitor with the metal species and its incorporation into the metal deposit (Rasmussen *et al*., 2006; Plieth, 2011). The blocking of active growing sites by occupying inhibitors therefore directly influences the crystallographic structure and morphology of the developing metal lattice. If inhibitors are present, the electrocrystallisation reaction, overvoltages, deposit structure, morphology and texture are directly altered. Inhibition intensity (or the degree of inhibition) is obviously a very intricate concept and is not only related to the type of inhibitory species but also to the concentration of inhibitory, metallic and any other species present in the electrolyte (Winand, 1991; Winand, 1994).

Winand (1991) proposed that the microstructure of any electrodeposit can be related to two main parameters, provided that the hydrodynamics of electrolyte flow are constant. The first parameter is the ratio of the current density (*J)* to the concentration of the metal ion in the bulk solution (C_{Me}), given that the exchange current density (J_0) at a given degree of inhibition is not influenced by the mass-transfer boundary-layer thickness (δ). If δ is not constant, the first parameter should rather be the ratio of the current density *(J)* to the diffusion-limiting current density (J_d). The second parameter is the inhibition intensity or degree of inhibition.

The well-known Winand diagram (Winand, 1994) refers to the morphology of polycrystalline metal deposits in terms of the degree of inhibition as a function of availability of the reacting metal ion (the ratio J/C_{Me} or J/J_d) at the electrochemical interface (Winand, 1994; Adcock *et al*., 2002). Four predominant morphology types were identified (Figure 2.13).

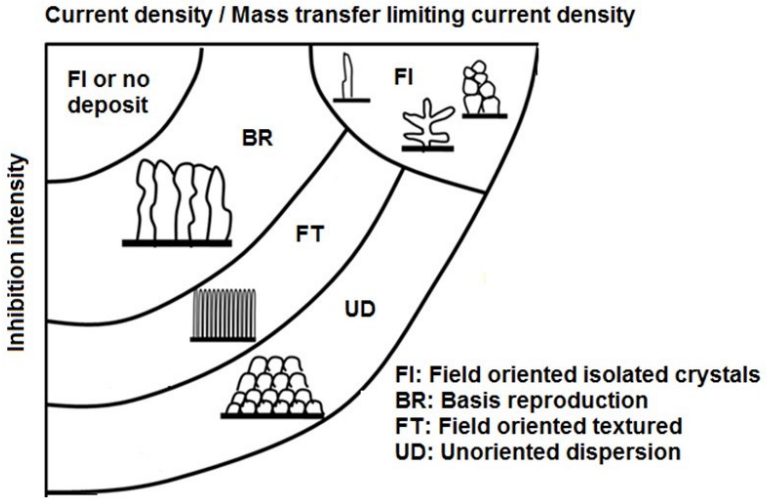

Figure 2.13. Diagram developed by Winand (1994) depicts crystallographic structure of the deposit in relation to inhibition intensity and current density. The labels are as follows: field-oriented isolated crystals (FI), base-oriented reproduction (BR), field-oriented texture (FT) and un-oriented dispersion (UD, the finest grain type).

The ratio (J/C_{Me} or J/J_d) varies directly with varying overpotential when the process is under mass-transfer control, while the inhibition intensity parameter is more complex to quantify. The development of the crystal lattice depends on the competition between growth parallel to and perpendicular to the substrate surface. At increasing current densities and decreasing inhibition intensity, limited energy is available, 2D nucleation is not frequent, the growth layer thickness increases and formation of isolated crystals (FI type) or dendrites or whiskers may occur (Fischer, 1954; Andersen *et al*., 1985; Winand, 1994). At conditions of intermediate inhibition and/or current density, lateral growth is promoted, large crystals develop and surface roughness increases. BR-type deposits prevail, which may degrade to FI-type deposits over time. At a specific current density, lateral growth rate increases and dense, coherent deposits should prevail as inhibition intensity increases, i.e., at constant current density and increasing inhibition

intensity, morphology should change from BR to FT to UD. At high inhibition and high J/C_{Me}, 3D nucleation should be more frequent and more desirable types of deposits should be formed (Fischer, 1954; Andersen *et al*., 1985; Winand, 1994). Under these conditions, coherent deposits of many elongated crystals are formed perpendicular to the substrate surface. This type of deposit is described as the FT type. If the inhibition intensity and/or the current density is high, and a large number of small crystals are formed, the UD type of morphology prevails (Winand, 1991; Winand, 1994; Adcock *et al*., 2002).

Industrially, the most desired type of deposit is the UD type. This comprises coherent, compact, fine-grained deposits developed from frequent 3D nucleation. The Winand diagram (Winand, 1994) predicts that this type of deposit would prevail under conditions of high inhibition intensities over a fairly wide range of current densities. Therefore, a shift in the inhibition intensity and control thereof during electrocrystallisation could promote the process in such a way that the overall morphology shifts from FT type to UD type.

A specific type of inhibition relevant to nickel electrodeposition should be considered. Nickel is an inert metal with a high melting point and low exchange current density (Crundwell *et al*., 2011). A phenomenon called secondary inhibition is observed. This results from the absorbed $NiOH^+$ layer on the substrate surface. Under these conditions, inhibition occurs naturally, even in the absence of typically added inhibitory species. The pH of the electrolyte directly influences the degree of secondary inhibition (Budevski *et al*., 2000). At higher pH values, the $NiOH^+$ species are more easily formed and secondary inhibition should increase. If the electrolyte pH is more acidic, more H^+ ions are freely available and secondary inhibition decreases. Cations such as Na^+, which are not dischargeable at the cathode, generally have a negligible inhibitory effect on the electrodeposition of nickel. The SO_4^{2-} anions present in sulfate electrolytes as an intermediate species can either inhibit or activate the electrodeposition reaction (Budevski *et al*., 2000). The possible nickel species present that can cause inhibition are shown in Figure 2.14. At approximately pH 3, at which nickel electrowinning is typically conducted, $NiOH^+$ and $Ni(SO_4)_2^{2-}$ species are prevalent and therefore can be responsible for inhibition of this kind.

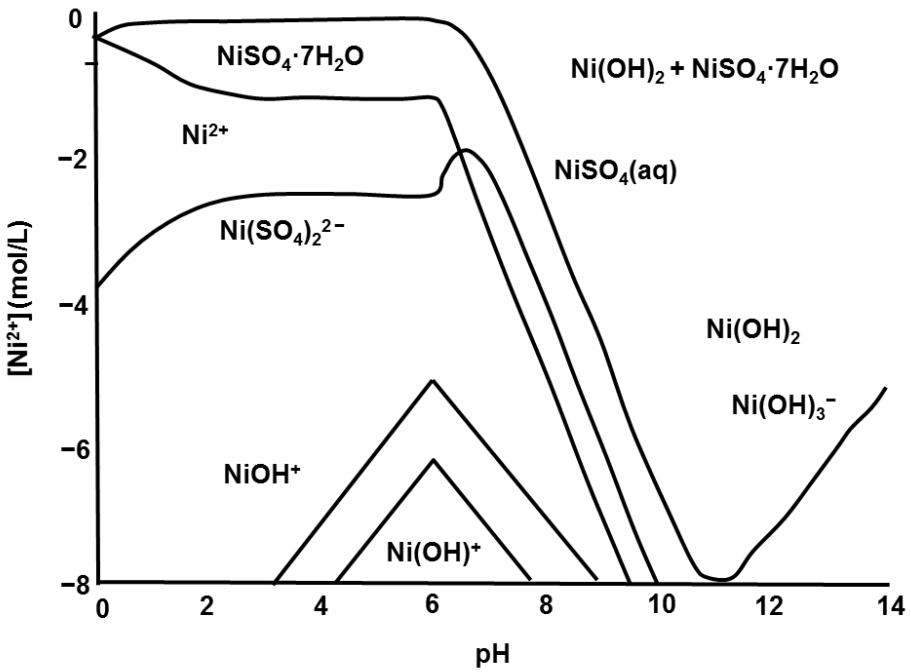

Figure 2.14. Concentration vs pH diagram indicating the possible nickel species present in the electrolyte (adapted from *Factsage* software).

2.4. Practical aspects of electrocrystallisation – measurement and control of nucleation and growth

2.4.1. Introduction

Monitoring and on-line control of the electrocrystallisation process during electrowinning is industrially crucial in order to optimise production processes in a cost-effective manner. Prediction of the morphological outcome of the electrodeposit in the early stages of electrocrystallisation is desired. No reliable technique for such prediction currently exists. If a concise, quick, easily usable technique could be implemented at the start of an electrowinning process, the parameters and conditions could, as necessary, be adjusted in order to shift the morphology from FT to UD type and therefore obtain a deposit of desired quality and characteristics.

The polarisation techniques generally used for the investigation of electrowinning processes include current- or potential-controlled methods. In many instances, a combination of techniques

is used and compared to obtain more accurate and reliable information. Some techniques elucidate more information regarding the electrocrystallisation process and kinetic parameters while other methods relate more to deposit characteristics and properties. Many of these techniques are laborious and it is generally difficult to compare results from previous studies owing to the use of many different techniques and many varying conditions. There are various techniques used to specifically investigate deposit morphology and the influence of impurities, additives and operating conditions on the morphology. It is, however, still difficult to quantitatively investigate differences in morphology and effects of various factors on such changes. Therefore, it is important to consider carefully which methods are reliable and capable of giving statistically meaningful results that are comparable between different experiments.

This section looks at the development and evolution of electrochemical polarisation techniques and how these have been used in the past to investigate and gain understanding of the electrocrystallisation process and morphology development. The limitations of potentiodynamic techniques are explored and the benefit of galvanodynamic techniques are investigated.

2.4.2. Overpotential, nucleation overpotential and plating overpotential

Overpotential is defined as the difference between the potential of metal deposition and the reversible potential (the potential at which deposition and dissolution of the same metal are in equilibrium). The total overpotential (E) measured during electrodeposition in an electrochemical cell is equal to the sum of the charge–transfer overpotential (E_t), the diffusion overpotential (E_d), the reaction overpotential (E_r), the crystallisation overpotential (E_c) and the resistance overpotential (E_Ω), given in Reaction [28] (Di Bari, 2010; Winand, 1991; Winand, 1994).

$$E = E_t + E_d + E_r + E_c + E_\Omega \qquad [28]$$

The crystallisation overpotential (E_c) (or the difference between the nucleation overpotential (E_n) and the plating overpotential (E_p)) is proportional to the energy available for electrocrystallisation but this overpotential cannot be directly measured or determined. An interesting perspective on the magnitude of various overpotentials to explain E_c specifically was given by Popov *et al*. (2002). In this particular experiment, overpotential was measured as a

function of time at constant current during electroplating of cadmium onto a platinum substrate. The results are illustrated in Figure 2.15.

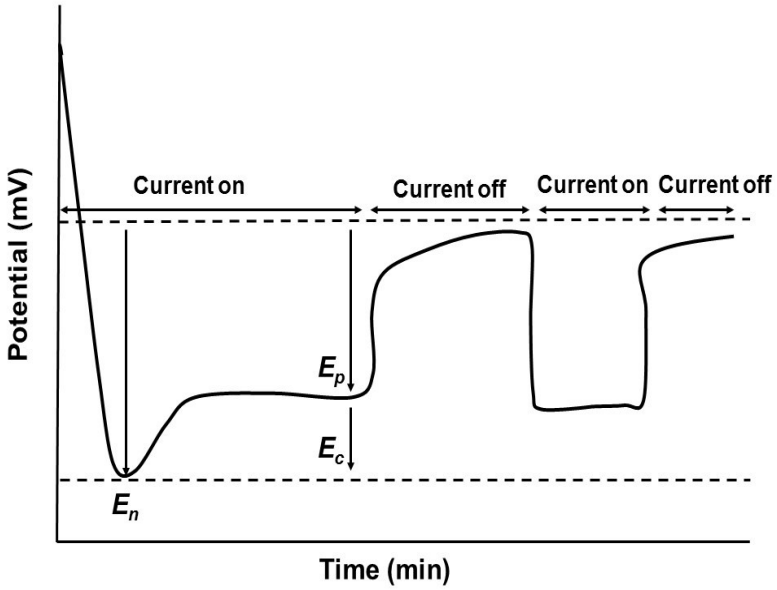

Figure 2.15. Electrode potential with the application of a cathodic current of 65 μA to a platinum electrode in a cadmium sulfate electrolyte (adapted from Popov *et al*., 2002).

This study showed that a larger initial overpotential, i.e., the nucleation overpotential (E_n), was required for plating to start and therefore for initial nucleation of cadmium onto platinum to take place. Once the electrodeposition reaction was initiated, the required overpotential decreased, the electrodeposition progressed, and growth occurred at the plating overpotential (E_p). The difference between these two overpotential values is an indication of the magnitude of the crystallisation overpotential (E_c) required for the electrodeposition reaction to occur. After some time, the current was switched off and the measured overpotential steadily returned to the reversible potential for this cadmium half-cell. Sometime later, the current was switched on again and growth of the deposit proceeded at a lower overpotential (approximately the same overpotential as the previously measured plating overpotential). This indicated that nucleation on the initial substrate was not required again and growth of cadmium onto the already deposited cadmium layer could proceed in the same manner as before the current interruption (Popov *et al*., 2002).

Such measurements of E_n, E_p or E_c are, however, extremely difficult to make accurately and repeatably due to many factors, such as the variation in substrate surface characteristics and preparation, differences in experimental setup, the increase in surface area and consequent variation in effective current density as growth of the electrodeposit proceeds and inherent error in sample and electrolyte preparation as well as the stability of conditions during the measurements. The development of more reliable techniques with quick and concise measurement parameters is therefore still key to understand, monitor and control nucleation and growth during the electrocrystallisation process.

2.4.3. Typical changes in polarisation behaviour during electrodeposition

Polarisation behaviour refers to the relationship between current and potential during electrodeposition processes. In order to monitor polarisation parameters, one needs to understand what the effects of parameter changes and addition agents could be on the measured overpotential as current is applied. Parameter changes, such as increased temperature or metal ion concentration, can cause depolarisation (less negative cathodic overpotential). If an organic additive, such as a surfactant, is added to the electrolyte, a polarizing effect might be observed (measured potential more negative) (Andersen *et al*., 1985).

A specific example for electroplated lead from fluorosilicic acid electrolyte is shown in Figure 2.16 (adapted from Andersen *et al*., 1985). This illustrates the effect of additives (a grain refiner and leveller) on the polarisation behaviour during the electrodeposition process, as well as the correlation of the polarisation parameters with the expected morphological properties of deposits obtained under these varying conditions. The observations made here are fundamental and typically expected for any electrocrystallisation process, including that of nickel deposition from sulfate electrolyte with and without additives.

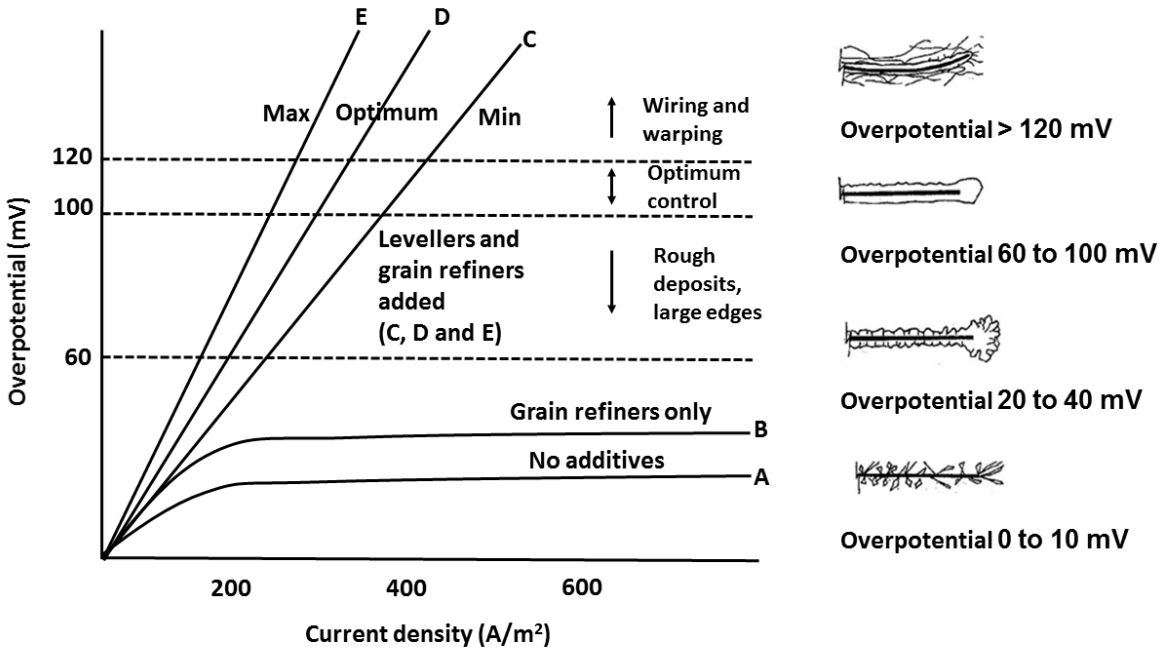

Figure 2.16. Observed changes in polarisation parameters related to changes in morphology for a specific experiment during lead electrodeposition from fluorosilicic acid electrolyte (adapted from Andersen *et al*., 1985).

Figure 2.16 shows the effect of changing parameters and conditions of the electrolyte on polarisation parameters. The curves labelled A and B were typically obtained when the metal ion concentration was low and the electrodeposition process was controlled by diffusion. The deposits produced under such conditions were of poor morphology, typically with increased roughness, pinholes, irregular growth and large edges. Curves C, D and E were obtained when the electrolyte contained excess metal ions and the electrodeposition was chemically controlled. Deposits from such electrolytes and conditions showed more controlled growth with closely packed grains and acceptable morphology.

Curve D shows the typical relationship between current density and overpotential as electrodeposition proceeds. Conditions under which depolarisation occurs produced a relationship for depolarisation, as shown in curve C. This could be, for example, due to an increase in electrolyte temperature. If an organic additive was, for example, added to the electrolyte, the curve shifted to position E, causing a polarizing effect. The importance of these observations is that changes in conditions and parameters cause shifts in polarisation parameters

and changes in morphology development. Therefore, there exists a relationship between polarisation parameters and morphology: if an optimum range of polarisation parameters can be determined for a particular electrodeposition system, the developing morphology might be predicted and controlled. If specific working ranges can be determined for which the relationship between the polarisation parameters is ideal, and the system is controlled in this way, the way in which morphology develops can be adjusted and ultimately controlled (Andersen *et al*., 1985).

A challenge that still remains is to determine the working range of polarisation parameters specific to nickel electrowinning from sulfate electrolyte. If a range of current and potential values can be determined for which desired developing morphology is obtained, and the conditions under which these desirable polarisation parameters are repeatably obtained, the production of good quality nickel electrodeposits can be predicted.

2.4.4. Conventional techniques used to measure polarisation parameters

An early technique to measure and investigate changes in polarisation parameters was cyclic voltammetry, in which potential is controlled and changes in current are measured (Kerby *et al*., 1977; Mackinnon *et al*., 1979a; Mackinnon *et al*., 1987). Cyclic voltammetry and subsequent techniques involve scanning of the potential or voltage in the negative potential direction (the forward sweep) up to a specific current density value and then reversing the potential scan direction (the backward sweep) in order to find the reversible potential at the current cross-over potential.

A typical example of a cyclic voltammetry study applicable to nickel electrodeposition from an electrolyte containing boric acid is shown in Figure 2.17.

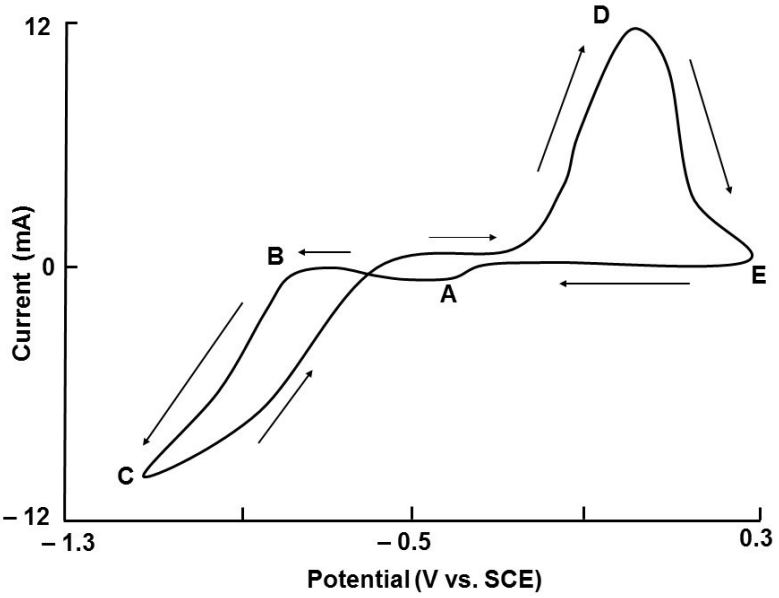

Figure 2.17. Typical cyclic voltammogram for a nickel electrodeposition system in the presence of boric acid (adapted from Ramachandran *et al*., 1993).

The peak indicated as ‘A’ shows the initiation of the hydrogen reduction reaction. This peak becomes smaller as the boric acid concentration increases. At ‘B’ the nickel electrodeposition reaction starts. The point marked ‘C’ indicates the point at which the nickel cations are depleted and the scan direction is reversed. Points ‘D’ and ‘E’ are points on the anodic sweep (Ramachandran *et al*., 1993).

An idea of the nucleation and plating overpotentials is obtained. It is, however, often difficult to identify the exact potential at which the onset of plating occurs because some metastable nucleation can generate small currents preceding stable nucleation. Potential measurements in electrochemical experiments suffer from the problem that the potential at the surface of the electrode cannot be directly measured and thus always includes some current-resistance (IR)-drop due to the solution resistance between the electrode and the point of measurement (Adcock *et al*., 2002; Adcock *et al*., 2004).

Compensation may be made afterwards for this error, but, in the case of controlled-potential experiments, the results are also a function of the rate at which the potential is scanned and this cannot sensibly be corrected for afterwards. Thus, if significant IR errors are predicted, as with

the high currents typical of electrowinning processes, the use of controlled-current rather than controlled-potential techniques are preferred (Kerby *et al*., 1977; Mackinnon *et al*., 1979a; Mackinnon *et al*.,1987; Adcock *et al*., 2002; Adcock *et al*., 2004).

A continuous electrochemical quality monitoring (CEQM) technique was later developed by Warren (1985). This has wider application but is still limited by various challenges. Obtaining repeatability of the inert substrate surface is problematic and the overall sensitivity of the measured plating potential as electrolyte composition changes is a challenge (Adcock *et al*., 2002). The later-developed and improved dual–channel CEQM technique made use of two moving wires that monitored the nucleation and plating potentials simultaneously (as a measure of cathode potential). Two types of additives are added in this technique – a levelling agent (additive that increases the plating overpotential) and a grain-refining agent (additive that reduces the nucleation overpotential). A comparison between traditional cyclic voltammetry and the dual-channel CEQM is shown in Figure 2.18.

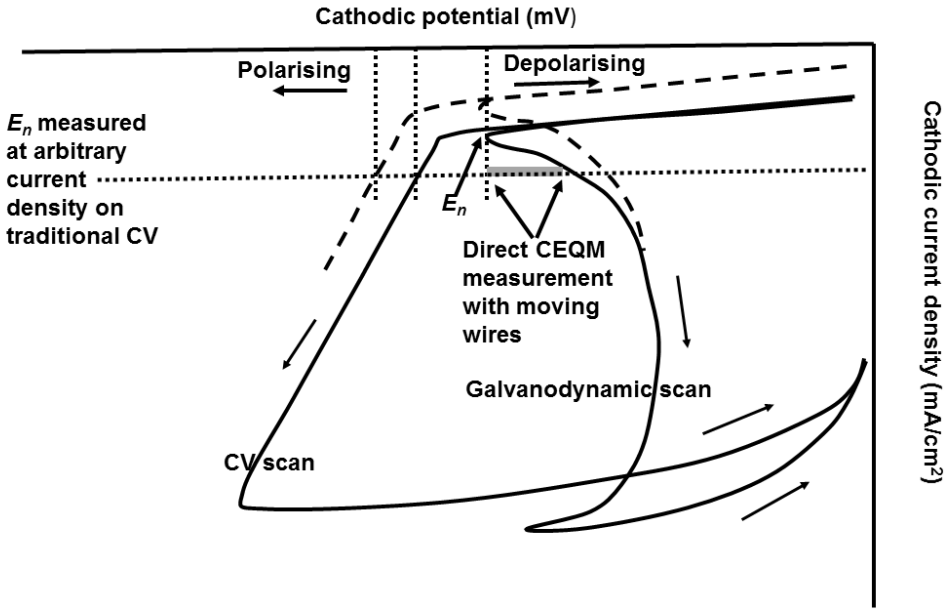

Figure 2.18. Graphical comparison of traditional cyclic voltammetry (CV) and the dual–channel CEQM galvanodynamic scan (adapted from Adcock *et al*., 2002).

This technique enables a more in-depth evaluation to investigate and understand the exact relationship between the morphology of the deposit and electrochemical polarisation measurements under controlled-current conditions. The measurement of nucleation overpotential

E_n alone is, however, not a completely accurate measurement to correlate with morphology, because the optimum E_n value may vary with additives and contaminants in the electrolyte solution. In situations where surfactants or additives are added, both the CEQM technique and cyclic voltammetry are difficult to apply because they do not necessarily give an accurate measure of the optimal concentration of additives (Mackinnon *et al*., 1979a; Warren, 1985; Adcock *et al*., 2002).

A technique developed by Adcock *et al*. (2002), specifically for zinc electrowinning, is based on these galvanodynamic polarisation principles. Measurements are made under controlled-current (galvanodynamic) conditions during plating on a foreign substrate. A very slow scan rate is used on the initial forward scan to accurately determine the point at which nucleation (E_n) initiates. Thereafter, a faster scan rate is used on the forward scan after the nucleation point up to the plating current density. A moderate scan rate is used on the backward scan towards zero, during which a measurement of the plating overpotential (E_p) is made. A typical scan in shown in Figure 2.19.

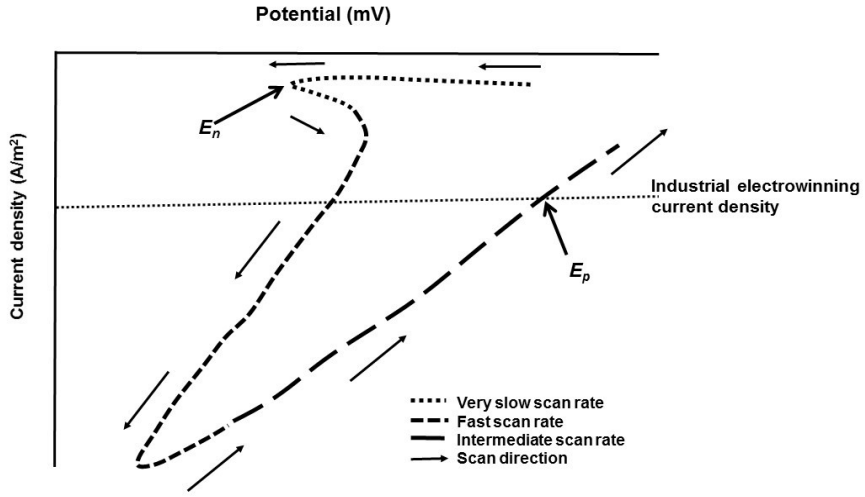

Figure 2.19. Schematic of the galvanodynamic method for zinc electrowinning indicating the different scan rates (adapted from Adcock *et al*., 2002).

One of the benefits of this method is that IR compensation can be done offline after a particular scan is completed because the scan rate is unaffected by the uncompensated potential. Although

the accuracy and reliability of galvanodynamic techniques appear more favourable compared with potential-controlled methods, the challenge still remains to correlate measured potentials logically to the morphological outcome of the produced electrodeposit. The idea is that if E_p is more cathodic (negative) than E_n, then the ΔE or crystallisation overpotential is positive so frequent 3D nucleation simultaneous to growth would be promoted and UD-type deposits would preferentially be produced (Adcock *et al*., 2002; Adcock *et al*., 2004).

The work on zinc electrowinning from sulfate electrolyte by Adcock *et al*. (2002 and 2004), identified the two most crucial factors (E_n and E_p) that are polarisation indicators of morphological shifts during the electrocrystallisation process. If a substrate performs ideally, the magnitude of ΔE can be used as a rough indication of grain size. As ΔE increases in magnitude, grain refinement of the metal deposit should occur. The magnitude of the measured E_p can be an indication of levelling. As E_p becomes more negative, the extent of levelling increases. The proposed correlation between the polarisation measurements and the metallographic structure of the deposit is shown in Figure 2.20.

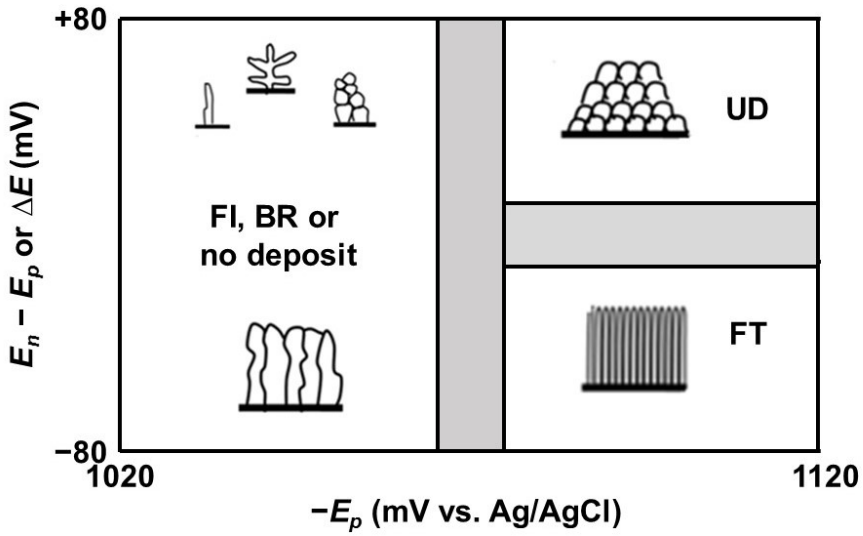

Figure 2.20. Possible relationships between ΔE and E_p indicating developing morphology (adapted from Adcock *et al*., 2004).

If the crystallisation potential (ΔE) is large (positive), then E_p is more negative than E_n and nucleation and growth occur simultaneously during electrocrystallisation. In this case, UD-type

deposits would preferentially form. The addition of a depolarising impurity or additive, however, will shift the E_p to more negative potential values and a shift will occur to the region where FI- or BR-type deposits are dominant. The current density may be too low under such conditions and a high enough rate of plating will then not be achieved. Low-quality, strained, irregular growth deposits will be produced under such conditions. In situations where E_p is smaller than E_n (negative ΔE values) the growth rate will be higher than the nucleation rate and therefore more FT-type deposits would be produced. These deposits are still good quality with low strain, but crystallites will be larger and more columnar compared with the UD-type (Adcock *et al*., 2002; Adcock *et al*., 2004).

This analysis is, however, simplified here for illustrative purposes. Hydrogen evolution may still occur at some values corresponding to the intermediate or in-between zones (grey areas in Figure 2.20) and, in some cases, optimal deposits would perhaps therefore not be produced. Zones are also likely to overlap and not be as clearly defined as depicted here (Adcock *et al*., 2002; Adcock *et al*., 2004).

Based on the work of Adcock, it seems theoretically possible to develop a galvanodynamic method for any electrowinning system which can be practically implemented to accurately determine nucleation and plating potentials. These potentials may then be used to predict the morphological changes obtained during the electrocrystallisation process.

Moats and Derrick (2012) used the same principles to develop a similar galvanodynamic method for copper electrowinning. The repeatability of the result measurements as well as deposit morphology were not reproducible and results were contradictory to the typical morphologies observed during copper electrowinning. Therefore, this study recommended that the Winand principles (Winand, 1991) are more applicable in the case of copper electrowinning. It is, however, noted that repeatability of the measurement and morphology are dependent on the precision of the electrochemical setup and that the slightest adjustment causes reproducibility errors – this is true for both the zinc methods developed by Adcock *et al*. (2002) as well as the nickel work presented here.

Chapter 3
Materials, methods and experimental techniques

This chapter describes the reagents, materials, instrumentation, experimental setup and techniques used in the experimental work conducted. It contains detailed descriptions of methods and procedures for all electrowinning investigations, the development of electrodeposition techniques, deposit characterisation and morphological studies, as well as investigations of the buffer characteristics and capacity of various electrolyte solutions.

3.1. Reagents and solution preparation

All electrolyte solutions were prepared by weighing the required amount of each analytical-grade reagent (AR), dissolving it in deionised water (supplied by Merck) and then making the solution up to a certain volume. The quality of the deionised water was monitored by means of inductively coupled plasma optical emission spectroscopy (ICP-OES) (indicated in Table 3.3) and the conductivity was measured as 5.6 ± 0.2 µS/m (characteristic of pure water, as documented by Thermo Fisher Scientific, 2014). Each solution was freshly prepared, magnetically stirred and heated to 65°C ± 1°C on a standard hotplate. The temperature and pH of the solution were measured with a calibrated Thermo Scientific, Orion 2 Star, bench-top pH meter/thermometer. Once the desired temperature was reached, the pH of the solution was adjusted to the desired value by the addition of either sodium hydroxide (0.1 M) or sulfuric acid (0.1 M). The pH was measured and recorded to two decimal places. The conductivity of the solution was measured at 65°C ± 1°C using a calibrated Toledo 2001 SG23 four-electrode conductivity meter. The meter has automatic temperature compensation and a full calibration with three standards of 84 µS/cm, 1413 µS/cm and 12.88 mS/cm was done before each measurement. Conductivity measurements were made and recorded to 0.1 µS/cm. Each solution was directly used for a particular experiment.

A small portion of each solution was kept aside for impurity analysis by ICP-OES (described in Section 3.1.1.), determination of the Ni^{2+} concentration by simple titration (detailed in Section 3.1.2.) and surface tension measurement. The ICP-OES results showed that no significant cation traces were detected in any of the prepared solutions.

Surface tension measurements were performed using a Rame–Hart imaging system. The electrolyte solution was injected with a syringe to form a droplet on the tip of the needle. The

drop was observed optically and the surface tension was calculated from the shape of the drop (pendant-drop shape method) (Arashiro and Demarquette, 1999; Berry *et al*., 2015). Deionised water was used as the reference sample. Surface tension measurements were recorded to 0.001 N/m.

Table 3.1 summarises the various chemical reagents used in the electrolyte and additive solutions.

Table 3.1. Chemical reagents used for electrolyte and additive solutions.

Reagent		Supplier	*Chemical grade
Nickel sulfate hexahydrate	$NiSO_4 \cdot 6H_2O$	Saarchem / Merck	AR
Sulfuric acid	H_2SO_4	Saarchem / Merck	AR
Sodium sulfate (anhydrous)	Na_2SO_4	Saarchem / Merck	AR
Boric acid	H_3BO_3	Saarchem / Merck	AR
Sodium hydroxide	NaOH	Saarchem / Merck	AR
Saccharin	$C_7H_5NO_3S$	Merck	CP
Sodium laurel sulfate (SLS)	$CH_3(CH_2)_{10}CH_2OSO_3Na$	Saarchem / Merck	AR
Pyridine	C_5H_5N	Emsure / Merck	CP
Aluminium sulfate octadecahydrate	$Al_2(SO_4)_3 \cdot 18H_2O$	Saarchem / Merck	AR
Cobalt sulfate hydrate	$CoSO_4 \cdot H_2O$	Saarchem	AR
Copper sulfate pentahydrate	$CuSO_4 \cdot 5H_2O$	Saarchem	AR
Sodium selenite	Na_2SeO_3	ACE Chemicals	AR
Sodium selenate	Na_2SeO_4	Merck	AR
Citric acid	$C_6H_8O_7$	Merck	AR
Nitric acid	HNO_3	Merck	AR

*The abbreviations AR refer to analytical-reagent grade and CP to chemically pure reagents.

Table 3.2 indicates the concentrations and characteristics of various electrolyte and additive solutions that were used in the experimental investigations. Each specified solution has a reference number for ease of reference throughout the following chapters. The solution

numbered “1” refers to the standard solution used for initial experiments and serves as a reference solution with a composition representative of commonly used industrial electrolyte conditions and concentrations (Kittelty, 2002; Crundwell *et al*., 2011).

Table 3.2. Compositions of various electrolytes.

Number	$[Ni^{2+}]$ (g/L)	$[Na_2SO_4]$ (g/L)	$[H_3BO_3]$ (g/L)	pH	Temperature (°C)	Additive(s)
1	***75***	***80***	***4***	***3.0***	***65***	***None***
2	**50**	80	4	3.0	65	None
3	**65**	80	4	3.0	65	None
4	**90**	80	4	3.0	65	None
5	75	**50**	4	3.0	65	None
6	75	**70**	4	3.0	65	None
7	75	**100**	4	3.0	65	None
8	75	80	**8**	3.0	65	None
9	75	80	**12**	3.0	65	None
10	75	80	**0**	**2.0**	65	None
11	75	80	**0**	**5.0**	65	None
12	75	80	4	**2.0**	65	None
13	75	80	4	**3.5**	65	None
14	75	80	4	**5.0**	65	None
15	75	80	4	3.0	**35**	None
16	75	80	4	3.0	**45**	None
17	75	80	4	3.0	**80**	None
18	75	80	**0**	3.0	65	4 g/L citric acid
19	75	80	**0**	3.0	65	8 g/L citric acid
20	75	80	**0**	3.0	65	12 g/L citric acid
21	75	80	4	3.0	65	4 mg/L SAC
22	75	80	4	3.0	65	10 mg/L SAC
23	75	80	4	3.0	65	20 mg/L SAC
24	75	80	4	3.0	65	5 mg/L SLS

Number	$[Ni^{2+}]$ (g/L)	$[Na_2SO_4]$ (g/L)	$[H_3BO_3]$ (g/L)	pH	Temperature (°C)	Additive(s)
25	75	80	4	3.0	65	20 mg/L SLS
26	75	80	4	3.0	65	40 mg/L SLS
27	75	80	4	3.0	65	20 mg/L PYR
28	75	80	4	3.0	65	60 mg/L PYR
29	75	80	4	3.0	65	100 mg/L PYR
30	75	80	4	3.0	65	5 mg/L Al
31	75	80	4	3.0	65	10 mg/L Al
32	75	80	4	3.0	65	5000 mg/L Al
33	75	80	4	3.0	65	100 mg/L Cu
34	75	80	4	3.0	65	250 mg/L Cu
35	75	80	4	3.0	65	500 mg/L Cu
36	75	80	4	3.0	65	250 mg/L Co
37	75	80	4	3.0	65	500 mg/L Co
38	75	80	4	3.0	65	1000 mg/L Co
39	75	80	4	3.0	65	10 mg/L Se(IV)
40	75	80	4	3.0	65	15 mg/L Se(IV)
41	75	80	4	3.0	65	25 mg/L Se(IV)
42	75	80	4	3.0	65	10 mg/L Se(VI)
43	75	80	4	3.0	65	15 mg/L Se(VI)
44	75	80	4	3.0	65	25 mg/L Se(VI)

3.1.1. Impurity analysis

ICP-OES measurements were performed on a Perkin Elmer Arcoss instrument after appropriate calibration and background correction. A typical ICP-OES analysis of the standard reference electrolyte, as well as tolerance limits of impurities, are shown in Table 3.3. The certified values for the deionised water obtained from Merck are also indicated.

Table 3.3. Determined concentration of typical impurities in the reference electrolyte.

Element	Deionised water (Merck) (mg/L)	Electrolyte solution concentration (mg/L)	Tolerance limit (mg/L) relative to 98 % pure Ni
Fe	<0.0121	<0.0028	5
Al		<0.0145	5
Ca		<0.0090	
Cr		<0.0003	30
Mg		<0.0004	500
Cu	<0.0132	<0.0024	100
Zn		<0.0010	100
Co	<0.0123	<0.0025	500
Pb	<0.0524	<0.0042	
Cd			500
Mn			250
Mo			40

3.1.2. Determination of Ni^{2+} concentration

The Ni^{2+} concentration of each electrolyte solution was determined to confirm the actual concentration of Ni^{2+} ions before and after each experiment, to ensure that an approximately constant supply of Ni^{2+} ions was available during the experiment and that the volume of electrolyte was therefore sufficient to maintain a constant Ni^{2+} concentration. A simple titration with disodium ethylene diamine tetra acetic acid (EDTA) was performed, as suggested by Kittelty (2002). Murexide indicator (Merck) was prepared by adding 0.1 g of ground murexide with 10 g of ground potassium nitrate (Saarchem) and mixing the powder well. A 1 M ammonium chloride (Merck) solution was prepared by dissolving 26.75 g of ammonium chloride power in 500 mL of deionised water. A 0.01 M solution of EDTA was prepared by dissolving 3.7224 g of EDTA in 1000 mL of deionised water.

For each titration, 0.05 mL ± 0.01 mL of electrolyte solution was accurately pipetted with a micropipette into a conical flask and 0.05 g of the murexide indicator was added. The prepared ammonium chloride solution (10 mL) was added and the murexide dissolved. The pH of the solution was then adjusted by adding 25 % ammonia drop-wise until pH 7 was reached. The solution was bright yellow. This solution was then titrated with 0.01 M EDTA until the endpoint (violet in colour) was reached. The volume of EDTA used was noted. The titration was done in triplicate for each electrolyte. The concentration of Ni^{2+} was then calculated using Equation [29].

$$\text{Nickel ion concentration } \left(\frac{g}{L}\right) = \frac{\text{titre (ml)}.\ [\text{EDTA}]\left(\frac{mol}{l}\right).\ 58.69\left(\frac{g}{mol}\right)}{0.05\ (mL)} \qquad [29]$$

3.2. Electrochemical experimental setup

The general experimental setup is shown in Figure 3.1. Electrochemical measurements were performed in a standard three-electrode cell setup with a Ag/AgCl reference electrode (saturated KCl) (Metrohm) which has a potential of 0.199 V vs. SHE. The sensing point of the Luggin tip of the reference electrode was placed at a fixed position approximately 3 mm away from the surface of the cathode. The cathode consisted of insulated titanium metal (commercial grade) with a square surface area of 2.25 cm^2. The auxiliary electrode was a coiled platinum wire. The auxiliary and working electrodes were separated by a polyethylene membrane (product code D21A05, obtained from Ecotao). Fresh electrolyte (300 mL) was used for each experiment. The electrolyte was heated to a specific temperature for each experiment (as indicated in Table 3.2) by an encased water jacket with water flowing from a water bath. The temperature of the electrolyte solution was measured, monitored and adjusted throughout the experiments using a standard thermometer with 1 °C accuracy. The temperature was kept within ± 1 °C of the desired temperature during each experiment. The system was connected to a potentiostat/galvanostat (Solartron Schlumberger 1286 interface) and computer fitted with the appropriated software (*Corrwave* and *Corrview*, obtained from Solartron Analytical).

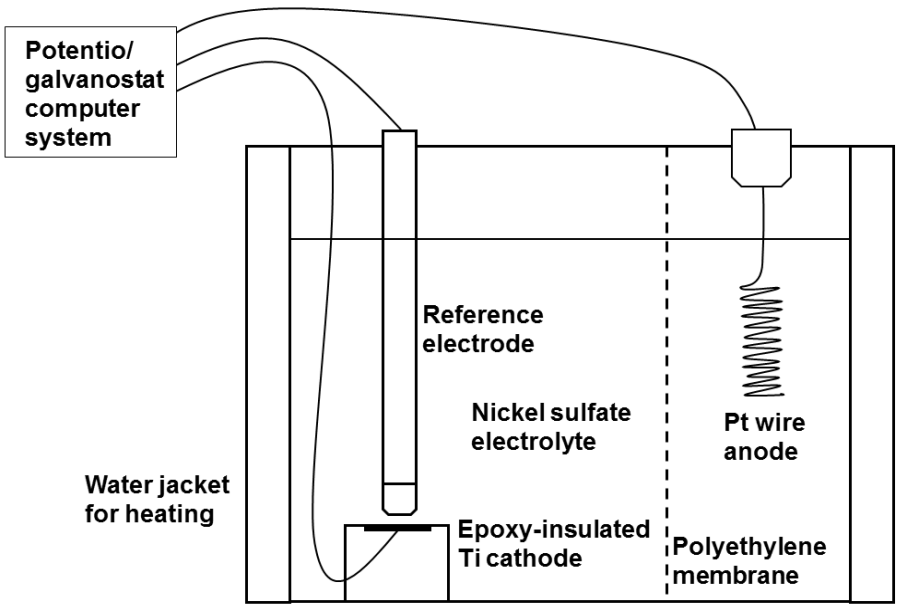

Figure 3.1. Schematic representation of the experimental setup for the electrochemical measurements during nickel electrowinning.

The experimental setup and methods were planned and designed carefully in order to produce repeatable laboratory results relevant to the operating conditions of the Anglo American Platinum Rustenburg Base Metals Refinery (RBMR) plant.

A few assumptions were made during the design of the experiments. Firstly, the deposition time of 2 h to obtain thicker deposits was assumed to be representative of longer deposition times typically used industrially. The focus was on the initial nucleation and growth processes of nickel onto titanium and the roughness of the titanium cathode was prepared to simulate the rough surface of titanium cathodes used at Anglo RBMR. The titanium blanks are sandblasted at Anglo RBMR to increase roughness (Voogt *et al*., 2017). The nucleation in the first few minutes was assumed to be representative of deposition of nickel onto nickel in thicker deposits. Secondly, the pH of the electrolyte was assumed to stay relatively constant over the period of 2 h of nickel electrodeposition.

3.2.1. Preparation of working electrode

Titanium cathodes were cut into 1.5 cm × 1.5 cm squares, connected to copper conducting wire by means of silver epoxy (Agar Scientific), then baked for 10 minutes at 100 ºC to ensure conductivity and then insulated by means of cold mounting with epoxy resin (Technoviz 4006 cold mounting resin). Each working electrode surface was then prepared by stepwise wet polishing with silicon carbide (SiC) paper from P800 to P1200 grit. Each electrode was ultrasonically cleaned for 120 s to remove abrasion debris from the electrode surface between each polishing step. The surface was then hot-air dried. Each working electrode was used directly after surface preparation.

3.3. Calculation of current efficiency

The masses of each prepared cathode directly before and directly after deposition were measured using a Sartorius analytical balance with 0.1 mg accuracy. The difference between these masses was used to determine the mass of the deposited material.

The theoretical mass of the electrodeposit was calculated using Equation [30]:

$$\text{Theoretical mass} = \frac{i \times t \times M}{n \times F} \qquad [30]$$

where: i = current in Ampere (A); t = plating time in seconds (s); M = atomic mass of nickel (g/mol); n = moles of electrons per mole of nickel; F = Faraday's constant of 96 485.33 C.

The current efficiency (CE) was calculated using Equation [31]:

$$\% \text{ Current efficiency (CE)} = \frac{\text{measured mass of the electrodeposit (g)}}{\text{theoretical mass of electrodeposit (g)}} \times 100 \quad [31]$$

3.4. Physical properties, quality and morphological evaluation of the nickel deposits

The obtained nickel deposits were examined and classified according to their colour and brightness, evident strain, pitting, and ease of removal from the cathode. Each of the obtained nickel deposits was removed from the cathode surface and ultrasonically cleaned. Thereafter, a cross-section was epoxy-mounted. The samples were sequentially polished using 400, 800, 1200 and 2400 grit paper, followed by 6 μm, 3 μm and then <1 μm diamond paste to remove any scratches. The deposits were then etched with 46 % nitric acid solution for 10 s. Thereafter, each deposit was washed with deionised water followed by ethanol. The sample was then air-dried before using optical microscopy (Olympus BX51M microscope) to observe the microstructures, evident strain and physical characteristics. Typical characteristics used for morphological classification is indicated in Table 3.4.

Table 3.4. Characteristics used for morphological classification of nickel electrodeposits.

Morphological type	Characteristics observed
UD	Fine grains, compact, no pinholes, grain size uniform throughout deposit, level, no peeling or strain cracks, no pitting
FT	Compact deposits, elongated grains, low strain and cracks, no peeling
BR/FI	Loosely packed grains, pinholes, pitting, irregular structure and grain size, not level, strained, cracked

3.5. Investigation of buffer characteristics of various electrolytes

Each of the electrolyte solutions was prepared in duplicate in the same manner as described in Section 3.1. Solutions of 0.1 M NaOH and 0.1 M H_2SO_4 were also freshly prepared. The first of each duplicate electrolyte solution was magnetically stirred and heated to 65 ºC. The pH of the solution was measured and recorded. The 0.1 M NaOH solution was then added in 0.5 mL aliquots and the pH of the solution was measured after each addition. The pH values

were recorded. The second of the duplicate electrolyte solutions was stirred and heated as the first. After recording the pH of the solution, the 0.1 M H_2SO_4 solution was added in 0.5 mL aliquots and the pH measured and recorded in the same way. The measured pH values were plotted against the volume of titrant added. The values were compared for all of the electrolyte solutions.

Another set of tests was then conducted. Each electrolyte solution was freshly prepared as previously described. The described three–electrode cell was set up and a galvanostatic experiment was conducted at a constant applied current density of 220 A/m^2 (the typical current density used at the Anglo RBMR plant (Voogt *et al*., 2017)) for 120 min. The pH was measured before current was applied and then monitored at 5-minute intervals over 120 min. This was carried out in triplicate for each electrolyte solution. The average pH values were plotted against time and the results for all the electrolytes were compared.

3.6. Industrial application

Industrial electrolytes and associated deposits were supplied by Anglo American Platinum's RBMR. The developed measurement technique was used to measure polarisation parameters on various industrial electrolytes, similar in composition to some of the synthetic electrolytes. Deposits were also produced from these specific electrolytes and compared with laboratory-produced deposits in terms of quality, strain and morphology. Samples received from RBMR are indicated in Table 3.5.

Polarisation parameters were measured and recorded in the same way as described for the synthetic electrolyte. Deposit samples were prepared in the same way as for the laboratory electrodeposits and the morphology and strain characteristics were determined by optical microscopy, as previously described.

Table 3.5. Compositions of industrial electrolytes received from Anglo American Platinum Rustenburg Base Metal Refiners.

Sample name	$[Ni^{2+}]$ (g/L)	$[Na_2SO_4]$ (g/L)	$[H_3BO_3]$ (g/L)	pH	Temperature (°C)	Additive(s)
Ref	***75***	***80***	***4***	***3.0***	***65***	***None***
A	75	80	4	3.0	65	5 mg/L Se(IV)
B	75	80	4	3.0	65	8 mg/L Se(IV)
C	75	80	4	3.0	65	10 mg/L Se(IV)
D	75	80	4	3.0	65	4 mg/L SAC
E	75	80	4	3.0	65	10 mg/L SAC
F	75	80	4	3.0	65	80 mg/L SAC
G	75	80	4	3.0	65	5 mg/L SLS
H	75	80	4	3.0	65	20 mg/L SLS
I	75	80	4	3.0	65	40 mg/L SLS
J	75	80	4	3.0	65	250 mg/L Cu
K	75	80	4	3.0	65	250 mg/L Co

Chapter 4
Development of repeatable galvanodynamic measurement technique

4.1. Initial experiments

The reference electrolyte was initially used to determine the scan rates at which repeatable values for both E_n and E_p could be measured. Preliminary experiments included cyclic voltammetry in order to establish typical potential and current density ranges for this electrolyte. Thereafter, the first galvanodynamic experiments were performed at various scan rates. The first aim was to determine the slow scan rate at which the initial nucleation point could be identified. The obtained scans are shown in Figure 4.1. All measured potential values are given vs Ag/AgCl (saturated KCl) reference electrode.

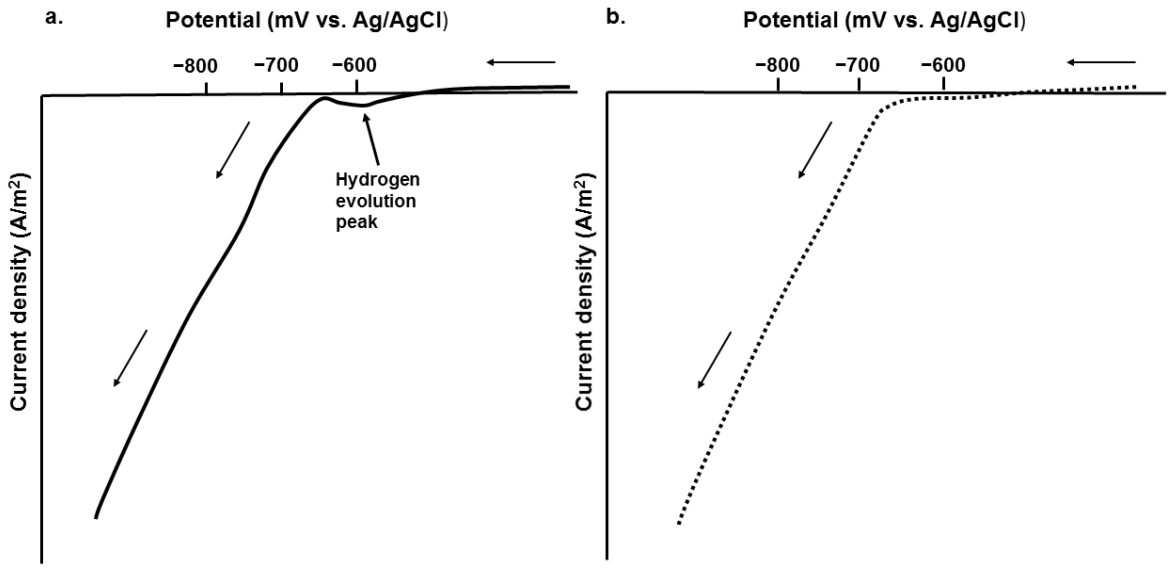

Figure 4.1. Initial scans to determine the optimal scan rate for establishing the nucleation point on the forward scan: a. a peak for hydrogen evolution is observed (scan rate 0.3000 mA/s), b. no hydrogen evolution peak is observed (scan rate 0.2000 mA/s).

Initial experiments showed a peak where hydrogen evolution initiated (Figure 4.1a). This was confirmed by observations of large bubbles as soon as a potential of −600 mV was achieved. After minor adjustments to the electrochemical setup (further separation of the electrodes and

insertion of the polyethylene membrane), the scan observed in Figure 4.1b was obtained. No hydrogen peak was observed, hydrogen bubbles were isolated from the cathode surface and the setup was stable. This scan was, however, not very repeatable and therefore the scan rate was slowed to achieve a clear nucleation point. The result is shown in Figure 4.2.

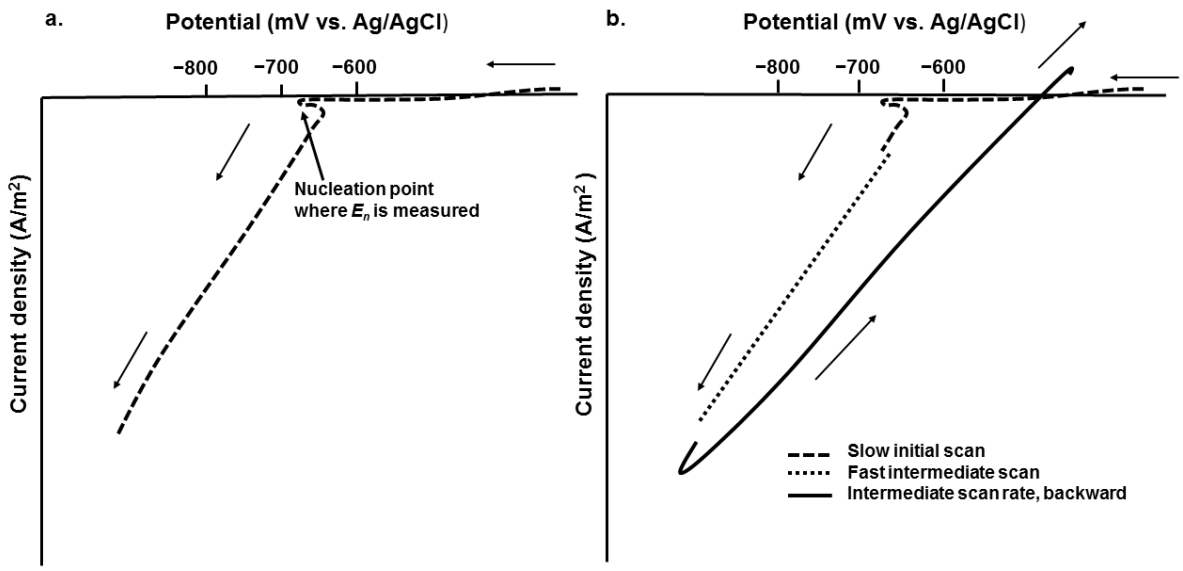

Figure 4.2. Results of the slow forward scan showing the exact nucleation point for the reference electrolyte: a. forward slow scan with nucleation point (0.1125 mA/s); b. shortened slow forward scan (0.1125 mA/s), followed by a fast intermediate scan (scan rate 1.000 mA/s) and then followed by the backward scan done at an intermediate rate of 0.5625 mA/s.

The slow forward scan rate was typically repeatable within 6 mV (detailed values presented in Appendix A). Once this was established for the reference electrolyte, the intermediate and backward scan rates needed to be optimised to measure the E_p value repeatably. The three scan-rate method described by Adcock *et al*. (2002) was used as a starting point: a fast scan rate was used after the E_n value was obtained followed by an intermediate scan rate on the backward scan, where E_p was measured at an arbitrary current density. As mentioned previously, a current density of 220 A/m^2 was chosen because this is typical of the working current density on the RBMR plant. This is shown in Figure 4.2b.

It was found that the scan rates needed to be balanced in such a way that the switch over between scan rates could be achieved fast enough for the curve to be continuous. In this work this was not achievable with three different scan rates, as shown by the gaps between the three

scan rates in Figure 4.2. The E_p value was also found to be less repeatable compared with the E_n value and therefore further work was done to limit the number of scans (to two instead of three) and thereby adapt the method to the capabilities of the potentiostat used. The results thereof and the finalised scan rates are discussed in detail in the following section.

4.2. Finalising the galvanodynamic technique

A preferred galvanodynamic scanning method was developed using the above measurements in order to measure E_n and E_p repeatably. The finalised method used for all polarisation measurements is summarised in this section. A newly prepared working electrode was introduced into the cell with prepared electrolyte for 1 min to stabilise at zero current in galvanostatic mode. Thereafter, two sequential galvanodynamic scans were applied. The first forward cathodic scan was done at a slow rate of 0.1125 mA/s in order to show the detailed turning point at which nucleation started. This scan rate was applied from −0 mA to −90 mA in the cathodic direction with a vertex current of −0.3 mA at which the nucleation turning point was identified. The second scan was done at a much faster rate of 0.5625 mA/s directly thereafter from −90 mA to 0 mA in the anodic direction. Each scan consisted of small increments in current with potential measurements made and recorded at the end of each increment. A total of 2000 points was recorded for each of the two scans.

The E_n was measured on the first, slow, cathodic scan at the most cathodic potential point. The E_p was measured on the fast, return, anodic scan at a current density of −220 A/m^2. This galvanodynamic scanning procedure was repeated five times for each electrolyte to obtain five repeat values of E_n and E_p to determine repeatability. The specific parameters of the galvanodynamic scanning procedure are summarised in Table 4.1.

Table 4.1. Experimental parameters used in the waveform for E_n and E_p measurement.

Experimental parameter	Value or description
Instrument mode	Galvanodynamic
Initial current	0 mA
Vertex current on the cathodic scan	−0.3 mA
Final current on the cathodic scan	−90 mA
Initial current on the anodic scan	−90 mA
Final current on the anodic scan	0 mA
Scan rate of cathodic scan	0.1125 mA/s
Scan rate of anodic scan	0.5625 mA/s

A typical galvanodynamic scan, after IR adjustment (Section 4.3), for the standard reference electrolyte is shown in Figure 4.3.

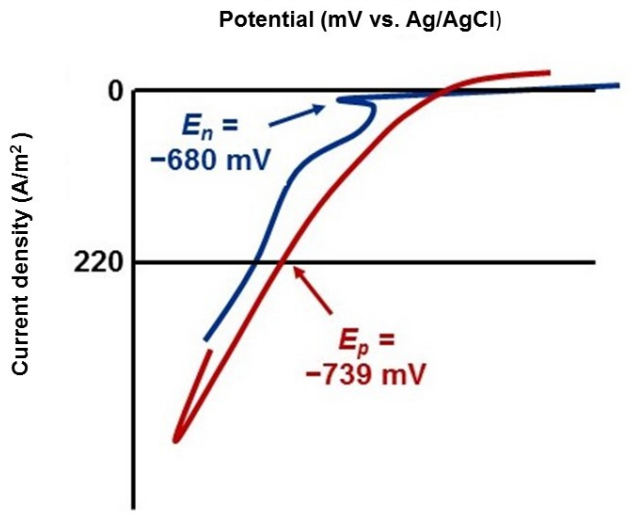

Figure 4.3. Typical galvanodynamic scans using the standard reference electrolyte (75 g/L Ni^{2+}; 80 g/L Na_2SO_4; 4 g/L H_3BO_3; 60 °C; pH 3). The slow cathodic scan (blue) shows the measured E_n and the fast, anodic scan (red) shows the measured E_p.

After each galvanodynamic scan was performed and the E_n and E_p measured, a newly prepared cathode was used and the programme was set to galvanostatic deposition mode, during which nickel was galvanostatically deposited for 2 h at a set current density of 220 A/m^2 under the same conditions. This was done in order to obtain a thick deposit for morphological, quality and characteristics evaluation. This was also repeated five times per electrolyte for repeatability purposes.

4.3. IR compensation

IR compensation was used to account for noise and numerical error in the measured data due to the distance between the substrate surface and reference electrode tip. IR compensation was done offline on completion of each two-step galvanodynamic scanning procedure. The electrolyte resistance (*Rs*) between the tip of the reference electrode and the cathode surface was determined before each experiment using frequency response analysis (FRA). The electrode was first polarised for 5 min at the base potential. A perturbation of 10 mVrms (millivolt root mean square) was then applied in a sine wave format through the frequency range of 100 kHz to 10 mHz. The *Rs* value was then determined from the Bode plot obtained at 100 kHz. Each value of *Rs* was then used to correct measured potential values in the

polarisation experiments by subtracting it from the calculated IR values to obtain the actual values.

The effect of the solution resistance, *Rs*, on the measured E_n values was found to be negligible and therefore compensation was only done for E_p values. The developed two-step galvanodynamic scanning method was repeated in triplicate for each specific electrolyte to determine the repeatability of the method. All results presented are IR-compensated.

The applied current flowing from the working electrode towards the auxiliary electrode, the resistance inherent to the electrolyte solution and the placement of the reference electrode to the working electrode were the main factors that determined the extent of the error in the potential measurement.

The experimental setup used for all experiments was such that the sensing point of the Luggin tip of the reference electrode was placed 3 mm away from the working electrode. The solution resistance (*Rs*) was measured by means of FRA to be approximately 0.7 Ω for typical electrolyte solutions used. The applied polarizing current at which the E_n and E_p values were measured was used to calculate the potential measurement error. This applied current at which E_n values were measured was approximately 0.7 mA for typical electrolytes used. This caused a measurement error of approximately 0.5 mV. The standard deviation in the measured E_n values was at least 3.0 mV, therefore the measurement error in these values due to *Rs* was found to be negligible and IR compensation of the E_n values was therefore discarded. The applied current at which the E_p values were measured was much larger (49.5 mA or a current density of 220 A/m^2). The measurement error in the E_p values was therefore found to be in the range of 37 mV and the correction was done for all measured E_p values.

A summary of the results of the IR compensation of the E_p values is given in Tables 4.2 and 4.3. One calculated value for each type of electrolyte solution is shown. The values are also expressed as a percentage of the total measured E_p value in order to compare the effect of IR compensation for the various electrolytes. All the results shown in the following sections are the uncorrected E_n values and the compensated E_p values.

Table 4.2. Calculated values for *Rs*, IR and percentage changes in the $-E_p$ values for electrolyte solutions without additives and impurities. The values were calculated from the *Rs* values obtained from FRA.

Number	$[Ni^{2+}]$ (g/L)	$[Na_2SO_4]$ (g/L)	$[H_3BO_3]$ (g/L)	pH	Temperature (°C)	*Rs* (Ω)	IR (mV)	$-E_p$ after IR compensation (mV)	IR as % of measured $-E_p$
1	***75***	***80***	***4***	***3***	***65***	***0.73***	***36***	***739***	***5***
2	**50**	80	4	3	65	0.61	30	768	4
3	**65**	80	4	3	65	0.68	34	748	5
4	**90**	80	4	3	65	0.77	38	768	5
5	75	**50**	4	3	65	0.66	33	618	5
6	75	**70**	4	3	65	0.71	35	673	5
7	75	**100**	4	3	65	0.72	36	699	5
8	75	80	**8**	3	65	0.66	33	740	4
9	75	80	**12**	3	65	0.73	36	779	5
10	75	80	**0**	**2**	65	0.71	35	624	6
11	75	80	**0**	**5**	65	0.70	35	619	6
12	75	80	4	**2**	65	0.71	35	759	5
13	75	80	4	**3.5**	65	0.72	36	727	5
14	75	80	4	**5**	65	0.72	36	818	4
15	75	80	4	3	**35**	0.73	36	829	4
16	75	80	4	3	**45**	0.72	36	674	5
17	75	80	4	3	**80**	0.71	35	817	4

Table 4.3. Calculated values for *Rs*, IR and percentage changes in the $-E_p$ values for electrolyte solutions with additives and impurities. The values were calculated from the *Rs* values obtained from FRA.

Number	$[Ni^{2+}]$ (g/L)	$[Na_2SO_4]$ (g/L)	$[H_3BO_3]$ (g/L)	pH	Temperature (°C)	Additive(s)	*Rs* (Ω)	IR (mV)	$-E_p$ after IR compensation	IR as % of measured $-E_p$
18	75	80	0	3	65	4 g/L Citric acid	0.69	34	675	5
19	75	80	0	3	65	8 g/L Citric acid	0.71	35	696	5
20	75	80	0	3	65	12 g/L Citric acid	0.71	35	679	5
21	75	80	4	3	65	4 mg/L SAC	0.69	34	788	4
22	75	80	4	3	65	10 mg/L SAC	0.72	36	775	5
23	75	80	4	3	65	20 mg/L SAC	0.68	34	765	4
24	75	80	4	3	65	5 mg/L SLS	0.71	35	788	4
25	75	80	4	3	65	20 mg/L SLS	0.73	36	760	5
26	75	80	4	3	65	40 mg/L SLS	0.73	36	741	5
27	75	80	4	3	65	20 mg/L PYR	0.70	35	779	4
28	75	80	4	3	65	60 mg/L PYR	0.74	37	764	5
29	75	80	4	3	65	100 mg/L PYR	0.71	35	755	5
30	75	80	4	3	65	5 mg/L Al	0.68	34	665	5
31	75	80	4	3	65	10 mg/L Al	0.72	36	659	5
32	75	80	4	3	65	5000 mg/L Al	0.80	40	716	6
33	75	80	4	3	65	100 mg/L Cu	0.74	37	696	5
34	75	80	4	3	65	250 mg/L Cu	0.74	37	683	6
35	75	80	4	3	65	500 mg/L Cu	0.76	38	644	5
36	75	80	4	3	65	250 mg/L Co	0.74	37	699	5
37	75	80	4	3	65	500 mg/L Co	0.77	38	671	6
38	75	80	4	3	65	1000 mg/L Co	0.78	39	650	6
39	75	80	4	3	65	10 mg/L Se(IV)	0.76	41	672	4
40	75	80	4	3	65	15 mg/L Se(IV)	0.81	39	684	4
41	75	80	4	3	65	25 mg/L Se(IV)	0.77	37	699	6
42	75	80	4	3	65	10 mg/L Se(VI)	0.76	38	712	4
43	75	80	4	3	65	15 mg/L Se(VI)	0.81	44	697	5
44	75	80	4	3	65	25 mg/L Se(VI)	0.72	41	724	6

4.4. Repeatability of polarisation measurements

One of the main objectives of this study was to develop a galvanodynamic measurement method that can be used to measure both E_n and E_p accurately and repeatably. The more repeatable the measurements, the more reliable the technique would be and the more likely the

technique can really be of value to elucidate information during the electrowinning process. The aim was to develop a technique with repeatable results for E_n and E_p within approximately 4 mV because this precision was previously shown for a similar technique developed for zinc electrowinning (Adcock *et al*., 2002). Each electrolyte and parameter set was repeated five times. The standard deviation for E_n and E_p were calculated from the five repeat measurements. The standard deviation for ΔE values were calculated as the sum of the standard deviations calculated for E_n and E_p. It was found that the results for all the electrolytes investigated varied within 4 – 10 mV for the measured E_n values and 3 – 8 mV for the obtained E_p values.

The repeatability of the developed technique is illustrated in Table 4.4. Detailed repeatability results for all electrolyte solutions prepared are shown in Appendix A. The results of five repeat measurements of E_n and E_p for electrolytes with different nickel concentrations are shown. The [Na_2SO_4] was at 80 g/L, the [boric acid] at 4 g/L, the temperature 65 ºC and the pH constant at 3. The results shown in italics are for the reference electrolyte.

Table 4.4. Results of the measured E_n and E_p values and the calculated ΔE values for electrolytes with varying nickel concentration, indicating repeatability of the developed technique.

[Ni^{2+}] (g/L)	$(-E_n)$ (mV)	Average $(-E_n)$ (mV)	Standard deviation (mV)	$(-E_p)$ (mV)	Average $(-E_p)$ (mV)	Standard deviation (mV)	ΔE (mV)	Average ΔE (mV)	Standard deviation (mV)
	688			*741*			*53*		
	676			*743*			*67*		
	677			*735*			*58*		
	680			*740*			*60*		
75	*678*	*680*	*5*	*738*	*739*	*3*	*60*	*60*	8
	813			768			−45		
	819			769			−50		
	815			767			−48		
	817			768			−49		
50	818	816	2	770	768	1	−48	−48	3
	694			777			83		
	685			763			78		
	689			767			78		
	692			762			70		
90	696	691	4	772	768	6	76	77	10

Chapter 5
Variation in polarisation parameters with changes in the electrolyte and effect thereof on developing morphology

5.1. Introduction

Once the galvanodynamic measurement method was developed and the results were repeatable for both E_n and E_p, it could now be further used to investigate the relationship between polarisation parameters and changes in the electrolyte. The idea was to characterise various electrolytes with differing compositions and conditions according to features such as surface tension and conductivity, changes in polarisation and current efficiency of thick deposits produced from each electrolyte. The results presented in this chapter explore the effect of changes in the electrolyte on the measured E_n and E_p values and compare the findings with theoretical expectations.

It was clear that changes in the electrolyte composition and conditions cause changes in polarisation parameters, which provided a way to measure the effect of changes in the electrolyte. If this could be related directly to changes and shifts in the growing morphology of the electrodeposit, during the early stages of nucleation and growth, it could be useful to correlate electrolyte changes, polarisation parameters and deposit morphology. Therefore, this chapter also explored changes in observed morphology and developing strain of nickel electrodeposits under various conditions and compositions of the sulfate electrolyte. The idea was to classify electrodeposits produced under various conditions according to the characteristics described by Fischer (1954) and later by Winand (1991).

5.2. Effect of nickel concentration

As nickel concentration increases, the growth rate decreases and more frequent nucleation of nickel ions takes place. Therefore, at higher nickel concentrations more fine-grained, closely packed, ductile, level, flat deposits are expected. Poor quality deposits with large, loosely packed crystallites, produced at high growth rates, are expected at low concentrations of nickel – typically below 60 g/L. At low nickel concentrations, 3D nucleation decreases, side reactions such as hydrogen evolution occur, the current efficiency is lower and early death of

growing nickel crystals is more feasible (Holm and O'Keefe, 2000; Kittelty, 2002; Di Bari, 2010).

As the concentration of nickel increased, the following was expected: the conductivity of the electrolyte should change due to an increase in number of ions in the electrolyte, the wettability should increase and the density of the electrolyte should increase due to higher nickel ion mobility (Abyaneh *et al*., 1994; Holm and O'Keefe, 2000). Higher current efficiencies should be achieved, better adhesion should be observed, the deposits should be low-strained and the crystal size should decrease (Abyaneh *et al*., 1994; Wu *et al*., 2003). At higher nickel concentrations, the substrate surface pH decreases. The possibility of $Ni(OH)_2$ precipitation decreases, ensuring better purity of the deposits, and hydrogen evolution is more limited (Di Bari, 2010).

Results for surface tension, conductivity and current efficiency for the same electrolytes with differing nickel concentration are shown in Table 5.1. The nickel concentration of the reference electrolyte was 75 g/L and the other concentrations tested were 50, 65 and 90 g/L. The five measurements for each type of electrolyte are shown in Appendix B1.

Table 5.1. Measured features for electrolytes with varying nickel concentration.

$[Ni^{2+}]$ (g/L)	$[Na_2SO_4]$ (g/L)	[Boric acid] (g/L)	pH	Temperature (°C)	Additive(s)	Current efficiency (%)	Conductivity (µS/cm)	Surface tension (N/m)
75	***80***	***4***	***3.0***	***65***	***None***	***98***	***141***	***0.036***
50	80	4	3.0	65	None	75	132	0.044
65	80	4	3.0	65	None	85	141	0.041
90	80	4	3.0	65	None	97	136	0.037

After galvanostatic deposition to obtain thick deposits, the highest current efficiencies were calculated for the higher nickel concentrations of 75 g/L (reference electrolyte) and 90 g/L. The current efficiency increased with increasing nickel concentration. The conductivity increased with increasing nickel concentration, as expected. The surface tension decreased with increasing concentration, indicating better wettability and therefore substrate surface interaction with nickel ions or increased ease of removal of hydrogen bubbles from the substrate surface.

Effect of changes in the nickel concentration on the measured polarisation parameters (E_n, E_p and ΔE) is shown in Figure 5.1. All of the measured result duplicates are detailed in Appendix A1.

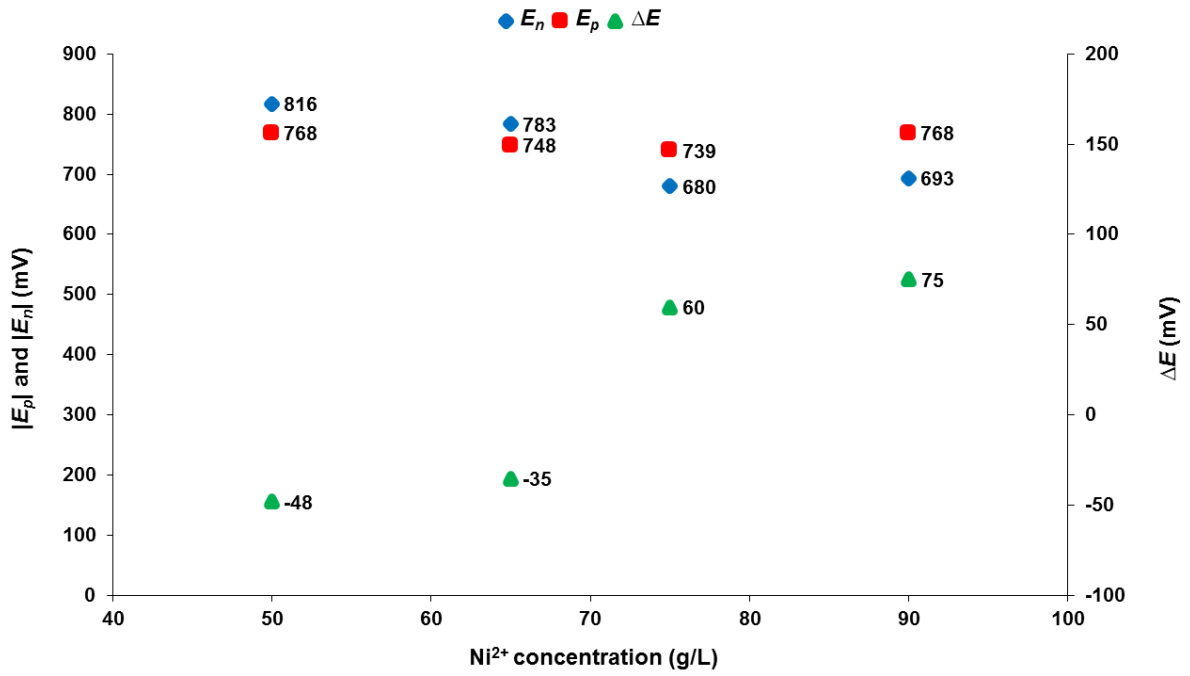

Figure 5.1. Variation of E_n, E_p and ΔE as a function of nickel concentration.

For the reference electrolyte (75 g/L Ni^{2+}), the E_p value was more cathodic compared with the E_n value, and therefore the ΔE value was positive. This was an ideal relationship between E_n and E_p and therefore a good quality deposit of desired morphology was expected – possibly of UD type (Adcock *et al*., 2002; Adcock *et al*., 2004). This relationship between E_n and E_p predicted that frequent nucleation was possible with relative growth of each newly developed nucleation crystallite. The same relationship (ΔE) was observed for a higher nickel concentration of 90 g/L. For lower nickel concentrations, the ΔE values were negative, which indicated more cathodic E_n values compared with the E_p values. This relationship predicted fast growth rates relative to nucleation, therefore producing larger crystal structures. Deposits of lower quality and less ideal characteristics were expected.

Deposits of UD-type morphology were obtained at both 75 g/L and 90 g/L nickel, as also predicted by the polarisation parameters. Highly strained, hydrogen pitted, cracked and peeled deposits were obtained at lower concentrations (65 g/L and 50 g/L) of nickel even though these deposits were of the FT type. The most desirable quality deposits were produced

at higher concentrations of nickel in the electrolyte, as expected. It is therefore recommended that a higher concentration of nickel (at least 75 g/L) is beneficial in producing nickel electrodeposits of high quality and preferred morphological characteristics. The differences in morphology are shown in Figure 5.2.

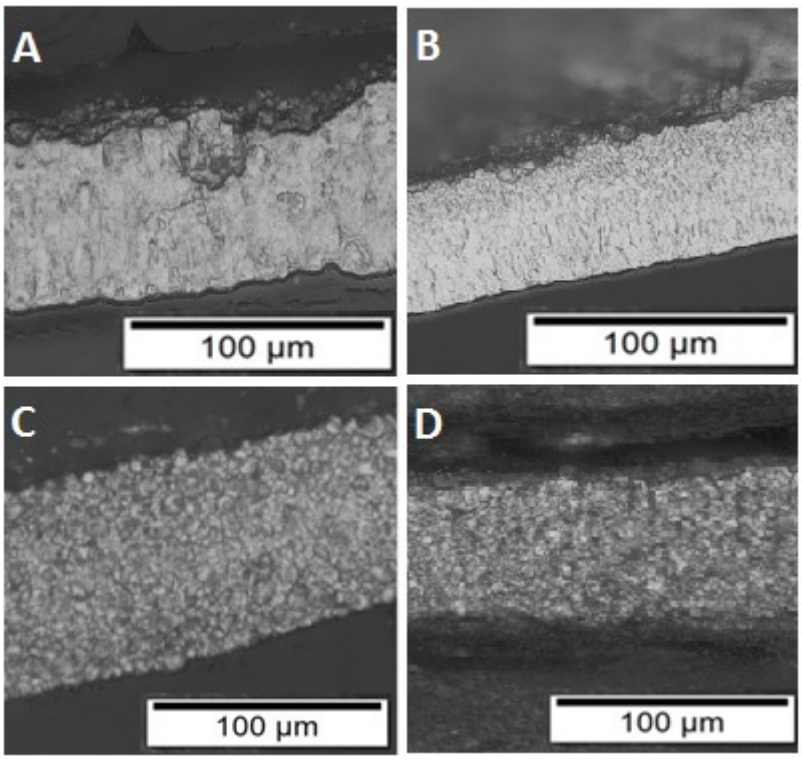

Figure 5.2. Micrographs of electrodeposits at various nickel concentrations indicating differences in morphology: A. 50 g/L Ni^{2+}, FT, strained and pitted; B. 65 g/L Ni^{2+}, FT, pitted; C. 75 g/L Ni^{2+} (standard electrolyte), UD; D. 90 g/L Ni^{2+}, UD.

The structure of the deposits at low nickel concentrations (A and B) was irregular with longer FT-type grains, indicative of large growth rates compared with nucleation processes. The top surfaces were uneven and hydrogen pitted. Grains were bound more loosely. The structure of the standard electrolyte (75 g/L Ni^{2+}) in Figure 5.2 C, showed smaller, tightly packed grains typical of the UD-type morphology. This was also seen at the higher concentration of 90 g/L Ni^{2+} (Figure 5.2 D). The bottom surface was, however, damaged upon removal of the deposit from the substrate surface for deposits produced at 90 g/L Ni^{2+}. This was symptomatic of compressive stresses during initial nickel deposition.

It therefore seemed that the most ideal morphology could be obtained for electrolyte with a Ni^{2+} concentration between 75 g/L and 90 g/L. The relationship of the measured polarisation

parameters also suggested a more favourable balance between nucleation and growth at Ni^{2+} concentrations of 75 and 90 g/L.

5.3. Effect of sodium sulfate concentration

The main purpose of adding sodium sulfate to the electrolyte is to improve conductivity of the solution and therefore improve the deposition process and reduce the power and energy requirements. As the concentration of Na_2SO_4 increases in the electrolyte solution, the conductivity of the solutions also increases up to a maximum. At higher concentrations, the conductivity is dominated by the H^+ concentration and therefore a further increase in Na_2SO_4 concentration does not have a definite effect (Ji and Cooper, 1996; Di Bari, 2010). At higher concentrations, the density and viscosity of the electrolyte also increase (Abyaneh *et al*., 1994). Sodium sulfate decreases the probability of nickel hydroxide precipitation by lowering the cathode surface pH (Ji and Cooper, 1996). At very high concentrations, the ionic strength of the electrolyte changes, a lower growth rate is expected and larger fan-shaped crystals should be produced because more frequent nucleation is possible (Abyaneh *et al*., 1994; Ji and Cooper, 1996).

Results for surface tension, conductivity and current efficiency are shown in Table 5.2. The sodium sulfate concentrations were 50 g/L, 70 g/L, 80 g/L (for the reference electrolyte) and 100 g/L. The detailed results for all electrolytes tested are shown in Appendix B2.

Table 5.2. Surface tension, conductivity and current efficiency of electrolytes with various Na_2SO_4 concentrations.

[Ni^{2+}] (g/L)	[Na_2SO_4] (g/L)	[Boric acid] (g/L)	pH	Temperature (°C)	Additive(s)	Current efficiency (%)	Conductivity (µS/cm)	Surface tension (N/m)
75	***80***	***4***	***3.0***	***65***	***None***	***98***	***141***	***0.036***
75	**50**	4	3.0	65	None	72	135	0.043
75	**70**	4	3.0	65	None	84	136	0.042
75	**100**	4	3.0	65	None	99	131	0.043

The highest current efficiencies were calculated for the 80 g/L and 100 g/L Na_2SO_4 electrolytes. The conductivity of the electrolytes increased with an increase in Na_2SO_4 concentration, with a slightly decreased conductivity at the highest concentration of 100 g/L.

The surface tension of the electrolytes decreased with increasing Na_2SO_4 concentration. It was therefore clear that higher concentrations of Na_2SO_4 were needed for acceptable current efficiency and better wettability, as expected.

Measured polarisation parameters with changes in sodium sulfate concentration are shown in Figure 5.3. The measurements for each electrolyte are shown in Appendix A2.

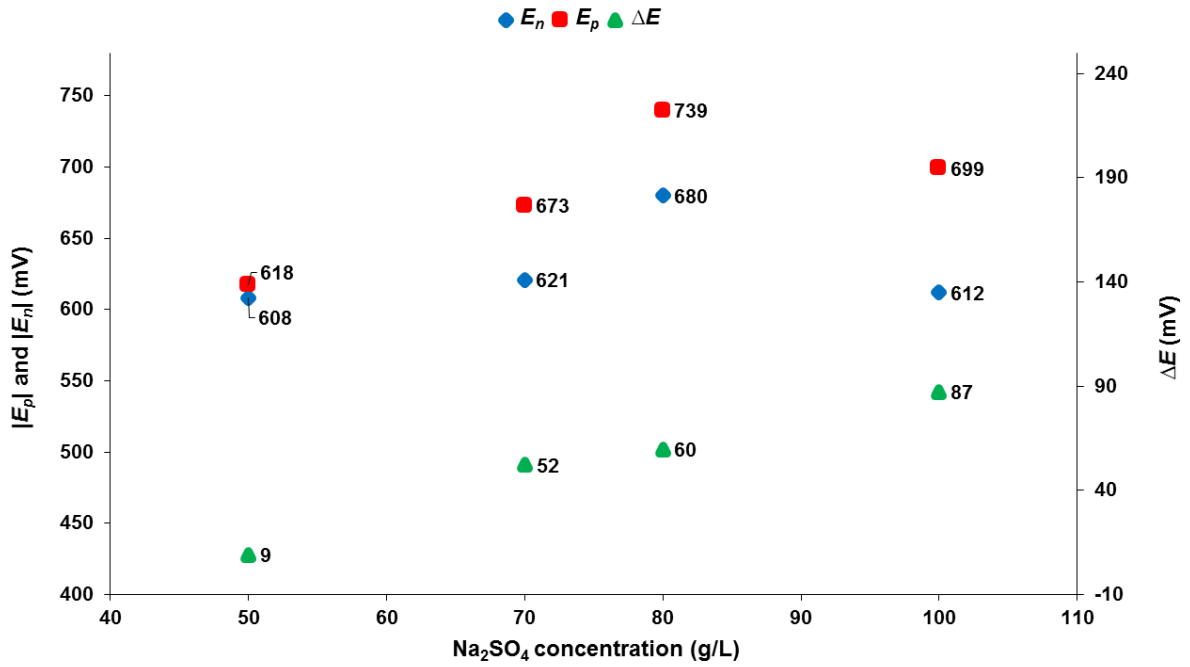

Figure 5.3. Variation of E_n, E_p and ΔE as a function of Na_2SO_4 concentration.

Polarisation parameters indicated that better quality deposits should be produced at higher concentrations. An initial increase (more cathodic) in the E_n values was observed for an increase in Na_2SO_4 concentrations from 50 g/L to 80 g/L. At 100 g/L, the E_n value became even less cathodic. The same trend was observed for the E_p values with increasing Na_2SO_4 concentration. The ΔE values were all positive and increased with increasing Na_2SO_4 concentration. The most cathodic E_n value was obtained at 80 g/L Na_2SO_4 in the electrolyte, which was indicative of high inhibition compared with the other electrolytes. The even more cathodic E_p value indicated a desirable relationship between E_n and E_p (positive ΔE) where frequent nucleation and an appropriate growth rate of each new crystallite were obtained.

Even though the ΔE value was highly positive for the 100 g/L electrolyte, the less cathodic E_n value was indicative of less inhibition and a decrease in frequent nucleation. The values obtained for the 70 g/L electrolyte were similar to those of the 100 g/L electrolyte. Good quality, overall fine-grained, UD- and FT-type deposits were predicted for the 70, 80 and 100

g/L electrolyte solutions from these measured polarisation parameters. The results indicated that a concentration of 80 g/L to 100 g/L Na_2SO_4 was ideal to produce nickel deposits of desirable characteristics and a concentration in this range is therefore recommended.

Figure 5.4. shows the different morphological types and quality characteristics of the produced thick deposits.

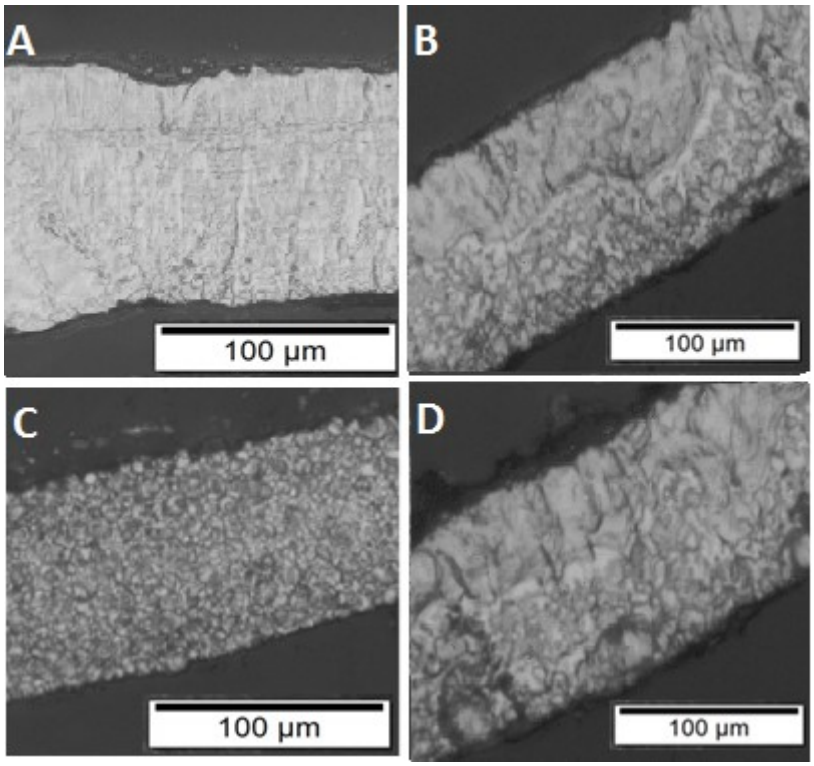

Figure 5.4. Micrographs of electrodeposits at various Na_2SO_4 concentrations indicating differences in morphology: A. 50 g/L Na_2SO_4, FT, irregular and pitted; B. 70 g/L Na_2SO_4, UD, C. 80 g/L Na_2SO_4 (standard electrolyte), UD; D. 100 g/L Na_2SO_4, UD, compressive stress.

Severe pitting and strain were observed in the deposits produced from electrolytes with 50 g/L Na_2SO_4 even though the morphological structure was FT type. Low strain and pitting were observed for both 70 g/L and 80 g/L electrolytes. The deposits produced from 100 g/L electrolytes also had very low pitting but some compressive strain was observed (strong adhesion to the substrate surface). It was therefore clear that the 80 g/L solution seemed to produce the deposits of most desirable quality.

The morphologies of all the deposits were compact. The grains were, however, quite different. The lower Na_2SO_4 concentrations (Figures 5.4 A and B) were more of the FT type

compared with the standard electrolyte in Figure 5.4 C. The general structure and morphology of the highest concentration (Figure 5.4 D) was very similar to the structure in Figure 5.4 B. This suggested that the concentration of 80 g/L Na_2SO_4 was optimum.

5.4. Effect of changes in temperature

Temperature plays a major role in the electrocrystallisation process and the morphological outcome of the electrodeposits. As temperature increases, the solubility and conductivity of the electrolyte increase, which promotes mobility of ions and therefore increases the nickel deposition reaction rate. At higher temperatures, the current efficiency increases and the power consumption decreases (Kuhn, 1971; Ji and Cooper, 1996; Lantelme and Seghiouer, 1998).

Deposits obtained at higher temperatures (typically above 60 °C) are flat, smooth, ductile and fine-grained due to increased nucleation during crystal growth. At lower temperatures, the internal strain increases significantly and deposits obtained under such conditions are brittle, pinholed and of poor morphological characteristics (Holm and O'Keefe, 2000; Kittelty, 2002; Lupi *et al*., 2006).

Results for surface tension, conductivity and current efficiency are shown in Table 5.3. The results for each electrolyte are shown in Appendix B3.

Table 5.3. Surface tension, conductivity and current efficiency for electrolytes with varying temperature.

$[Ni^{2+}]$ (g/L)	$[Na_2SO_4]$ (g/L)	[Boric acid] (g/L)	pH	Temperature (°C)	Additive(s)	Current efficiency (%)	Conductivity (µS/cm)	Surface tension (N/m)
75	***80***	***4***	***3.0***	***65***	***None***	***98***	***141***	***0.036***
75	80	4	3.0	**35**	None	67	78	0.048
75	80	4	3.0	**45**	None	87	90	0.042
75	80	4	3.0	**80**	None	91	177	0.048

The lowest current efficiency was obtained for the lowest temperature of 35 °C. Current efficiency and conductivity increased with increasing temperature. Very low and undesirable conductivities were measured at both 35 °C and 45 °C. The surface tension of the electrolytes was fairly constant for the temperatures tested. It therefore seemed that temperature did not

have a large effect on wettability but mainly influenced the conductivity and therefore the mobility of nickel ions in solution. The higher the temperature of the electrolyte, the higher the conductivity and therefore the better the mobility and transport of nickel ions in solution.

Measured polarisation parameters at varying temperature (35, 45, 65 and 80 °C) are shown in Figure 5.5. Measured values for each electrolyte are shown in Appendix A3.

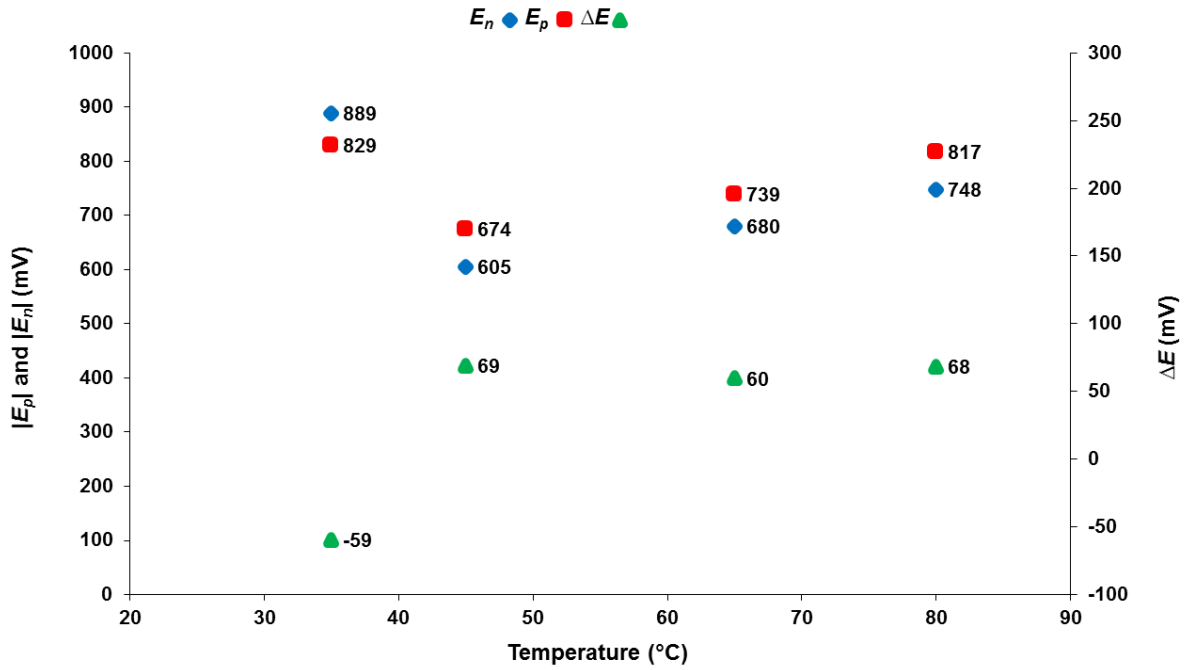

Figure 5.5. Variation of E_n, E_p and ΔE as a function of temperature (ºC).

As the temperature increased from 45 °C to 80 °C, the polarisation parameters changed in such a manner that the difference between E_n and E_p (ΔE) stayed approximately constant. The relationship between E_n and E_p therefore changed with increasing temperature in such a way that nucleation and growth and the relative rates of these processes were balanced. As temperature increased from 45 to 65 to 80 °C, more frequent inhibition and nucleation together with appropriate growth were obtained.

At an electrolyte temperature of 35 °C, the relationship between E_n and E_p was largely negative and the E_n and E_p values were both much more cathodic compared with the values for the standard electrolyte. This was indicative of fast growth processes with lower nucleation frequency. This unbalanced relationship between nucleation and growth was indicative of increasing internal strain during deposition of nickel ions.

The most desirable polarisation relationship was observed at the highest temperature of 80 °C and the best quality deposit was obtained at this temperature. An increase in temperature therefore caused an increase in inhibition, more frequent nucleation simultaneous to growth of the crystals and therefore a more desirable electrodeposit. This was most likely due to increased conductivity and therefore higher mobility of ions in solution. Higher temperatures were therefore recommended to produce deposits of good quality and preferred morphology. To limit energy usage and power consumption, a temperature of 65 ºC was acceptable.

The differences in strain and morphology are shown in Figure 5.6.

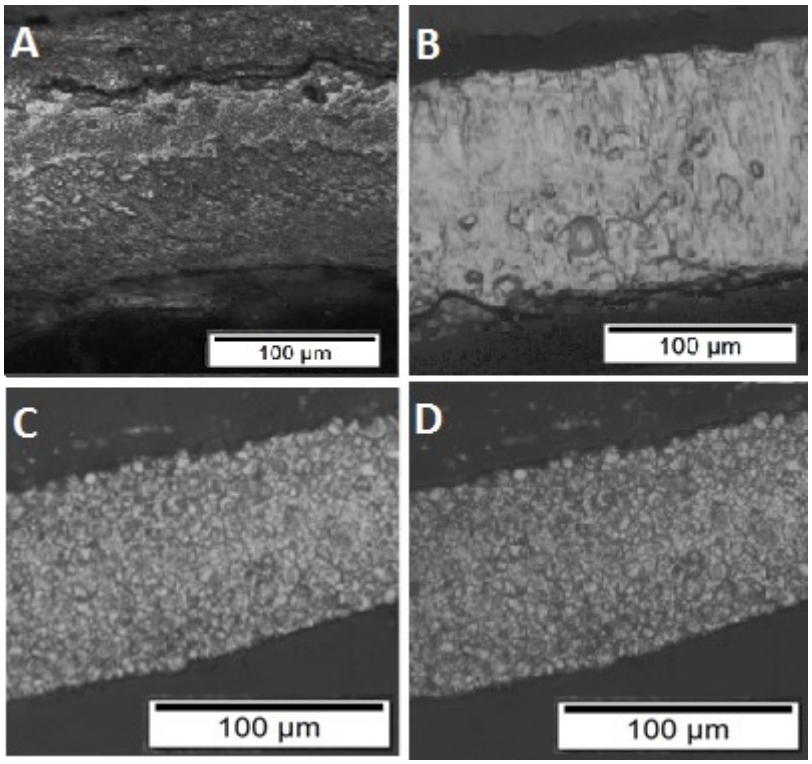

Figure 5.6. Micrographs of electrodeposits at various temperatures indicating differences in morphology: A. 35 °C, FT, strained, pitted brittle, a strain crack visible; B. 45 °C, FT, strained, pitted; C. 65 °C (standard electrolyte), UD; D. 80 °C, UD, strong adhesion to substrate surface.

Highly strained and pitted deposits were produced at 35 °C. A large strain crack is visible throughout most of the deposit (Figure 5.6 A) even though the morphology suggested some FT grains. The grains were large and irregular in structure, indicative of faster growth rates compared with nucleation.

Deposits of low strain and low pitting were produced at 45, 65 and 80 °C. This was expected due to increased mobility of ions and faster reaction rates at higher temperatures. At 45 °C, FT-type morphology was observed but hydrogen pitting and strain were also frequent. The deposits at 65 and 80 °C were of UD-type morphology and of good quality without strain. Some compressive strain was, however, observed upon removal of the deposit from the substrate surface at 80 °C. It therefore seemed that a temperature of 65 °C was adequate to promote nickel deposition and the rate at which nucleation and growth proceed and it was not necessary to use temperatures higher than 65 °C.

5.5. Effect of changes in pH

Hydrogen ion production is an inevitable secondary reaction (Reaction [4]) during nickel electrodeposition. As hydrogen ions combine to form H_2 gas, the pH at the cathode surface increases compared with the pH of the bulk electrolyte. If the pH increases above 5, the precipitation of $Ni(OH)_2$ becomes feasible. The electrodeposits are contaminated with these precipitates and the current efficiency decreases (Amblard *et al*., 1983; Armyanov and Sotirova-Chakarove, 1992; Ji and Cooper, 1996). At low electrolyte pH values, deposits are expected to be ductile, flat, smooth and overall of good quality. At high pH values of the electrolyte solution, curled, cracked, degraded, brittle deposits are normally observed (Ji and Cooper, 1996; Holm and O'Keefe, 2000; Kittelty, 2002). High pH values cause strong polarisation of the nucleation overpotential, which is indicative of very high inhibition. Nucleation is therefore expected to be less frequent, which should cause larger growth and therefore undesirable deposits. At lower pH, the inhibition is slightly decreased but still adequate and frequent 3D nucleation with appropriate growth is possible (Amblard, 1983; Armyanov and Sotirova-Chakarove, 1992; Ji and Cooper, 1996; Lantelme *et al*., 1998; Kittelty, 2002).

Conductivity, surface tension and current efficiency are shown in Table 5.4. The pH values tested were 2, 3, 3.5 and 5 with 4 g/L of boric acid added to the electrolyte, and pH 2 and 5 without any boric acid in the electrolyte. All replicate results are shown in Appendix B4. The pH of each freshly prepared electrolyte was measured and then adjusted to the desired value by either adding 0.1 M sulfuric acid (to adjust to more acidic values) or 0.1 M sodium hydroxide (to adjust to more alkaline values) in a dropwise fashion.

Table 5.4. Conductivity, surface tension and current efficiency for electrolytes at various pH values.

$[Ni^{2+}]$ (g/L)	$[Na_2SO_4]$ (g/L)	[Boric acid] (g/L)	pH	Temperature (°C)	Additive(s)	Current efficiency (%)	Conductivity (µS/cm)	Surface tension (N/m)
75	***80***	***4***	***3.0***	***65***	***None***	***98***	***141***	***0.036***
75	80	**0**	**2.0**	65	None	73	142	0.050
75	80	**0**	**5.0**	65	None	86	142	0.051
75	80	4	**2.0**	65	None	75	136	0.044
75	80	4	**3.5**	65	None	98	137	0.043
75	80	4	**5.0**	65	None	83	139	0.040

Current efficiency, conductivity and surface tension under conditions without boric acid (at pH 2 and pH 5) were not ideal and the obtained deposits were strained and pitted. The deposits produced at pH 3 and 3.5 had high current efficiencies of 97 % and 98 %. The conductivity of the electrolytes did not show a specific trend and ranged from 136 to 142 µS/m for all of the electrolytes. The surface tension of the electrolyte at pH 3 was the lowest and therefore indicative of good wettability. Deposits with low pitting and strain were produced at both pH 3 and 3.5. The strain was low at pH 2 but some pitting was observed in these deposits. Strain and pitting were observed for deposits produced from the solutions at pH 5. The physical characteristics of the electrodeposits suggested that the most desirable pH values are 3 and 3.5.

The responses of measured polarisation parameters to changes in pH of the electrolyte are shown in Figure 5.7. Replicate results are shown in Appendix A4. Points without boric acid buffer in the electrolyte are indicated. The potential ranges for E_n, E_p and ΔE were large and therefore the pH of the electrolyte clearly had an important, pronounced effect on the polarisation parameters. The ΔE values ranged from −69 mV to 60 mV and therefore deposits of various characteristics and properties were expected in relation to pH changes. The most positive ΔE values were obtained for electrolyte solutions at pH 3, 3.5 and pH 2 with 4 g/L of boric acid added. The most desirable deposits were therefore expected from these particular electrolytes.

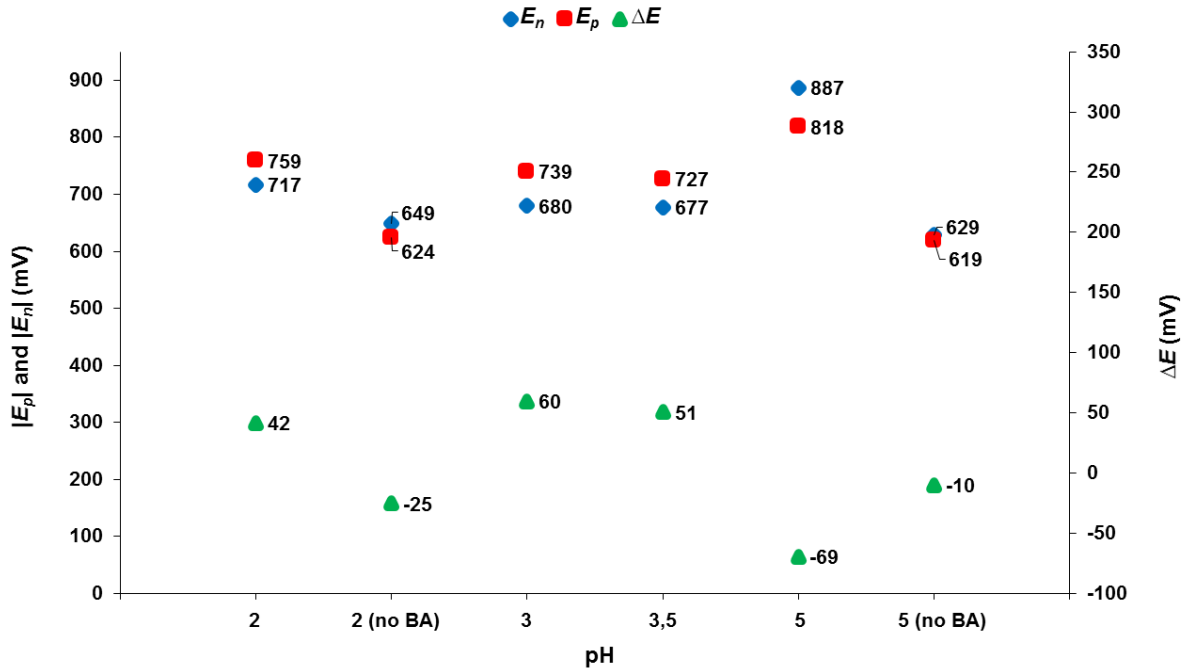

Figure 5.7. Variation of E_n, E_p and ΔE as a function of pH.

The E_n, E_p and ΔE values for electrolytes at pH 3 and pH 3.5 were similar. The E_n and E_p values were less cathodic (more positive) as the pH increased from 2 to 3.5. At pH 5, the E_n and E_p values shifted to the most cathodic potentials. Without boric acid present in the solution, the E_n values were less cathodic than for the standard electrolyte solution and the E_n values, irrespective of pH, were similar. The E_p values seemed to be more influenced by the absence of boric acid. The E_p values in this case were much less cathodic compared with that of the standard electrolyte.

Figure 5.8 shows the typical morphology and characteristics of thick deposits produced at various pH values. Nickel deposits obtained at pH 2 (Figure 5.8 E), 3 (Figure 5.8 D) and 3.5 (Figure 5.8 F) in the presence of boric acid buffer in the electrolyte were of desirable quality and preferred morphological characteristics. The deposits were smooth, flat, ductile, level and fine-grained. The morphology represented the typical UD type, which was indicative of frequent nucleation simultaneous to growth of the crystals. Very low pitting was also observed. The structure and fine-grained, even, regular morphology also suggested that $Ni(OH)_2$ precipitation was limited and therefore purity of the nickel deposit was improved.

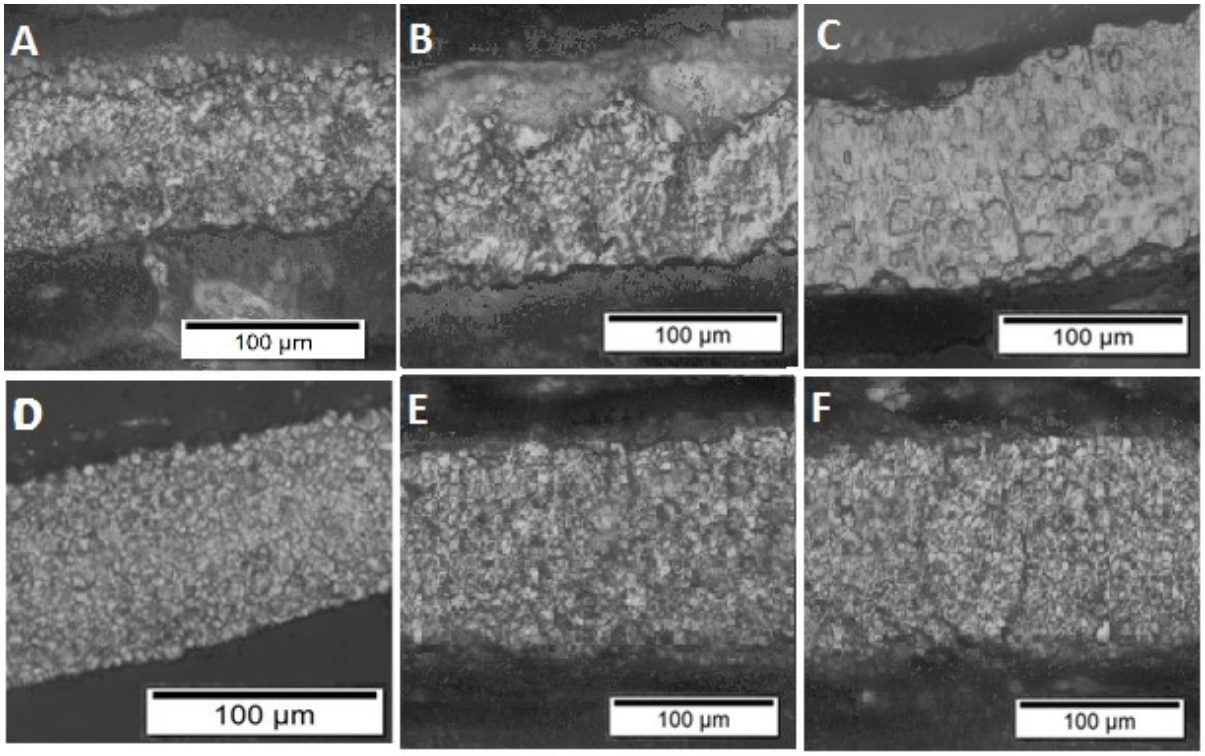

Figure 5.8. Micrographs of electrodeposits at various pH values indicating differences in morphology: A. pH 2 (no boric acid), FT, strained, brittle, irregular growth; B. pH 5 (no boric acid), FT, strained, brittle, irregular growth; C. pH 5, FT/BR, Large loose grains; D. pH 3 (standard electrolyte), UD; E. pH 2, FT/UD, mostly fine grains, compact, bright; F. pH 3.5, FT/UD, mostly fine-grained, bright, compact.

Deposits produced in the presence of boric acid at pH 5 (Figure 5.8 C) had FT/BR morphology with large loosely packed grains and irregular structure. This could possibly be due to the onset of $Ni(OH)_2$ precipitation within the deposit structure.

Deposits produced both at pH 2 (Figure 5.8 A) and pH 5 (Figure 5.8 B) without any boric acid were similar in morphological structure. Both were of FT type with irregular structures. It therefore seemed that boric acid played a crucial role, together with the pH of the electrolyte, in determining the morphology and strain characteristics.

Results showed that the presence of boric acid in the electrolyte was important and that pH alone was not sufficient to control deposition. These two parameters need to be considered carefully and in conjunction when controlling the electrocrystallisation of nickel. Electrolyte pH of 2 – 3.5, in the presence of 4 g/L of boric acid, was acceptable and must be maintained during nickel electrodeposition from sulfate electrolyte.

5.6. Effect of boric acid

Boric acid can act as a surface agent to manage the reduction of the nickel species in solution. It is a buffering component, which is proposed to act either as a catalyst for the reaction or as a carrier ligand for the Ni^{2+} species towards the substrate surface. This is proposed to be done via the formation of nickel–borate complexes (as the p*K*a value for boric acid itself is much higher than the working pH of the electrolyte solutions) (Yin *et al*., 1996; Gadad and Harris, 1998; Lupi *et al*., 2006). Without boric acid, $Ni(OH)_2$ precipitates are formed, which passivate the substrate surface and are incorporated into the nickel deposit. Boric acid is believed to act as a polariser that influences the overpotential for the nickel deposition reaction, as well as that of the hydrogen evolution process, in such a way that nickel is preferentially reduced onto the cathode surface (Yin *et al*., 1996; Lupi *et al*., 2006).

Surface tension, conductivity and current efficiency results are shown in Table 5.5. Boric acid was varied from 0 (at pH 2 and 5) to 4, 8 and 12 g/L (pH 3). Polarisation parameters compared with changes in boric acid concentration are shown in Figure 5.9. Replicate results are shown in Appendices A5 and B5.

Table 5.5. Surface tension, conductivity and current efficiency for electrolytes with varying boric acid concentration and pH.

$[Ni^{2+}]$ (g/L)	$[Na_2SO_4]$ (g/L)	[Boric acid] (g/L)	pH	Temperature (°C)	Additive(s)	Current efficiency (%)	Conductivity (µS/cm)	Surface tension (N/m)
75	***80***	***4***	***3.0***	***65***	***None***	***98***	***141***	***0.036***
75	80	**8**	3.0	65	None	94	126	0.061
75	80	**12**	3.0	65	None	95	137	0.061
75	80	**0**	**2.0**	65	None	73	142	0.050
75	80	**0**	**5.0**	65	None	86	142	0.051

Very low current efficiencies were obtained for solutions without any boric acid added, both at pH 2 and pH 5. Very high and desirable current efficiencies were obtained for all the solutions containing boric acid, with the highest current efficiency for the 4 g/L standard solution. The conductivity decreased with increasing boric acid concentration. This was not expected as an increase in ions in solution should increase conductivity. The highest conductivity was measured for the 4 g/L reference electrolyte. The surface tension of the

electrolytes without any boric acid was high and therefore wettability of these solutions was predicted to be quite poor. The surface tension of the 4 g/L solution was the lowest and therefore the most desired. The surface tensions of the 8 g/L and 12 g/L solutions were also acceptable.

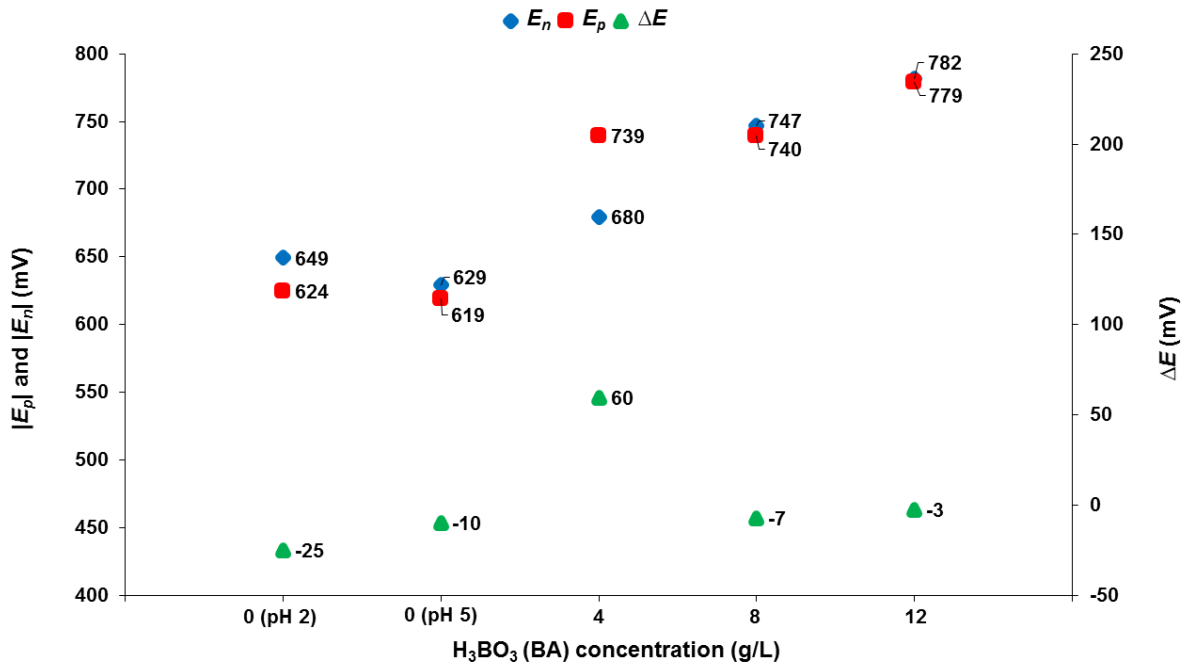

Figure 5.9. Variation of E_n, E_p and ΔE as a function of boric acid concentration.

Analysis of the polarisation parameters for the variation in boric acid concentration showed that 4 g/L of boric acid (standard solution) gave the most desirable relationship between E_n and E_p and would therefore be predicted to produce the most preferred UD-type deposit. The solutions with higher boric acid concentrations (8 g/L and 12 g/L) were also expected to produce deposits of good quality and UD-type morphological characteristics even though the ΔE values were slightly negative. This observation could not at this stage be explained and once again suggests that the mechanism of boric acid needs further investigation and understanding.

Figure 5.10 shows the morphological differences in thick deposits produced at various boric acid concentrations.

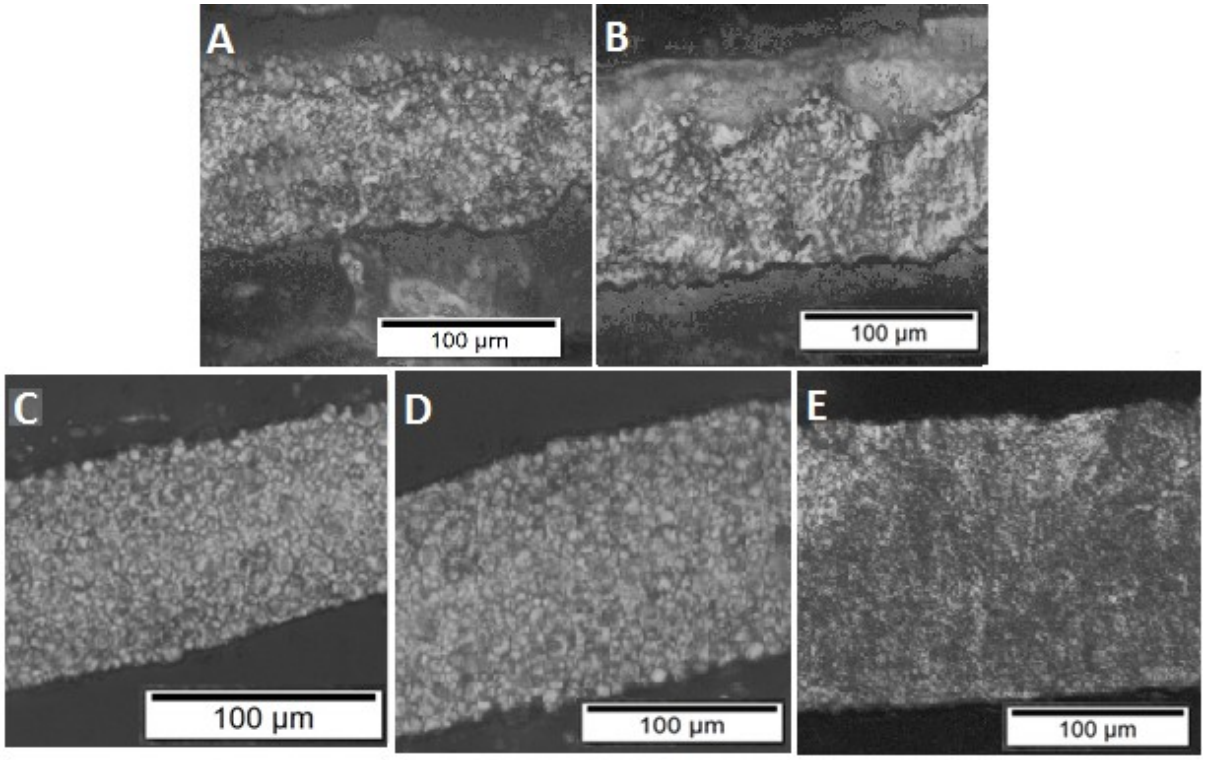

Figure 5.10. Micrographs of electrodeposits at various boric acid concentrations indicating differences in morphology: A. 0 g/L boric acid (pH 2), FT, strained, brittle, irregular growth; B. 0 g/L boric acid (pH 5), FT, strained, brittle, irregular growth; C. 4 g/L boric acid (standard electrolyte), UD; D. 8 g/L boric acid, FT/UD, mostly fine-grained, compact; E. 12 g/L, FT/UD, finest grains, bright, compact.

Acceptable UD-type deposits were indeed produced when boric acid was present in the electrolyte (Figure 5.10 C, D and E). These deposits were all fine-grained, round, nodular, level and compact and no signs of strain or hydrogen pitting were observed. Deposits obtained in the absence of boric acid (at both pH 2, Figure 5.10 A, and pH 5, Figure 5.10 B) were highly strained, pitted and of very poor quality. Compressed strain in the middle of these deposits towards the edges was observed in all these deposits.

The addition of boric acid to the electrolyte is clearly recommended according to the results reported. Both the morphological and quality outcome of the produced deposits, as well as the measured polarisation parameters, indicated that boric acid served a definite purpose in producing preferred quality nickel electrodeposits. In the presence of boric acid, and at an appropriate working pH of the electrolyte, hydrogen evolution, and therefore pitting, was limited or eliminated. Appropriate inhibition and therefore a suitable nucleation and growth relationship was promoted by the presence of boric acid. It was also observed that the pH of

the electrolyte could be more easily controlled and maintained in the presence of boric acid. The mechanism of the action of boric acid is still unclear and the fact that the p*K*a values (approximately 9) for boric acid reactions were above the working pH (approximately 3) for nickel electrodeposition cannot be explained by the findings thus far. Therefore, two other investigations were done in order to investigate this further: firstly, boric acid was replaced by citric acid, which has a p*K*a value closer to the working pH (Section 5.6.1.); secondly, buffer studies (Section 5.10) were done on all the electrolytes investigated.

5.6.1. Replacing boric acid with citric acid

Alternative buffers with p*K*a values in the same range as the working pH for nickel electrodeposits from sulfate electrolyte have been proposed (Chao-qun *et al*., 2007). One such possible buffer is citric acid or, more specifically, citrate ions. It is also proposed that citric acid itself, as well as nickel–citrate complexes, might be responsible for buffering of the electrolyte solution. The complexes adsorb to the cathode surface, thereby influencing inhibition and wettability and ultimately contributing to the nickel electrocrystallisation reaction. The adsorption is also believed to inhibit the hydrogen evolution reaction and thereby promote nickel deposition. A particular study by Chao-qun *et al*. (2007) found that the addition of citric acid caused an increase in buffering capacity at high current efficiencies. The nickel deposits were of high quality and desirable morphological characteristics under optimum conditions of pH, temperature and nickel concentrations. The deposits were generally fine-grained and compact.

Surface tension, conductivity and current efficiency results for these experiments are shown in Table 5.6 (Appendix B6).

Table 5.6. Surface tension, conductivity and current efficiency for electrolytes with varying citric acid concentration.

$[Ni^{2+}]$ (g/L)	$[Na_2SO_4]$ (g/L)	[Boric acid] (g/L)	pH	Temperature (°C)	Additive(s) (g/L)	Current efficiency	Conductivity (µS/cm)	Surface tension (N/m)
75	***80***	***4***	***3.0***	***65***	***None***	***98***	***141***	***0.036***
75	80	**0**	3.0	65	4 g/L citric acid	93	140	0.040
75	80	**0**	3.0	65	8 g/L citric acid	90	141	0.040
75	80	**0**	3.0	65	12 g/L citric acid	92	140	0.039

Current efficiencies for all concentrations of citric acid added were slightly lower compared with the standard conditions but still ranged from 90 – 92%. The conductivity measurements of the electrolytes were similar to that of the standard solution and were fairly constant for all the citric acid concentrations tested. The surface tension of the electrolytes in the presence of citric acid was fairly constant and similar to the standard electrolyte. The lowest surface tension was obtained for the highest citric acid concentration.

Measured polarisation parameters for electrolytes of varying citric acid concentration are shown in Figure 5.11 and compared with those of the reference electrolyte (0 g/L citric acid and 4 g/L boric acid). Results for all electrolytes are shown in Appendix A6.

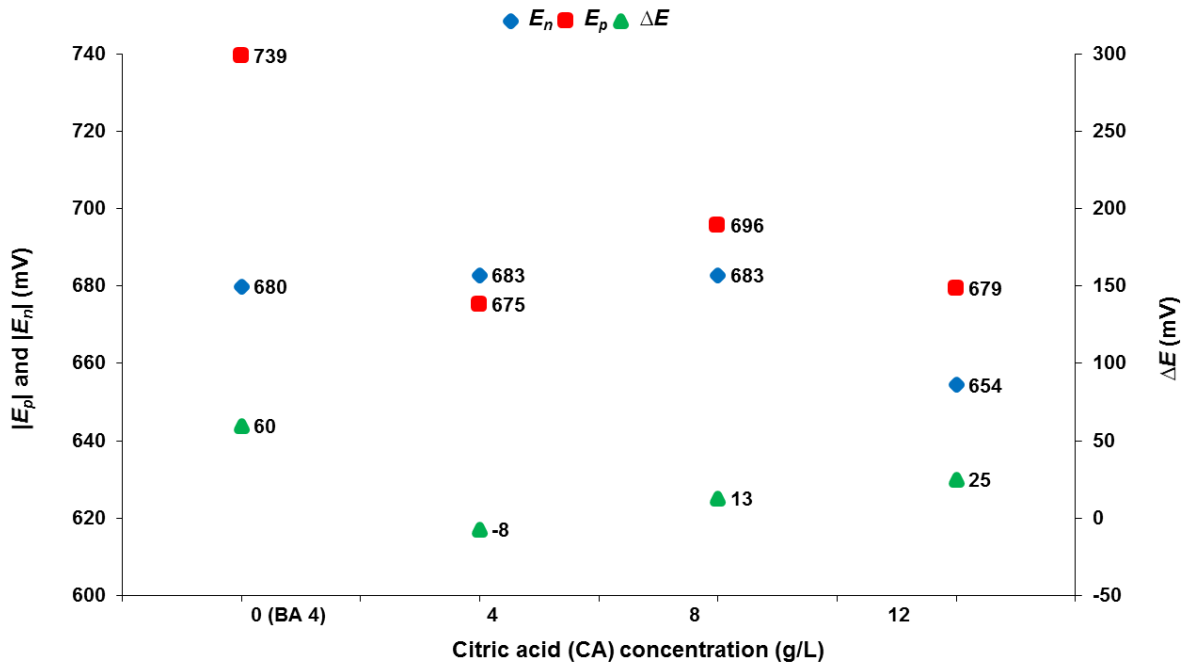

Figure 5.11. Variation of E_n, E_p and ΔE as a function citric acid concentration (g/L).

The polarisation values for citric acid used as buffer were repeatable within about 8 mV. E_p values were more affected by the presence of citric acid in the electrolyte compared with the E_n values. The measured E_n values were constant up to an added citric acid concentration of 8 g/L but decreased significantly at an even higher value of 12 g/L. The E_p values did not follow a specific trend but decreased overall with the addition of citric acid to the electrolyte. The ΔE values were positive (more favourable) at both 8 and 12 g/L of added citric acid. The ΔE values were less positive compared with the standard electrolyte solution, but were still positive and therefore it was likely that produced deposits would be of good quality.

Figure 5.12 shows differences in morphology for deposits at various concentrations of citric acid.

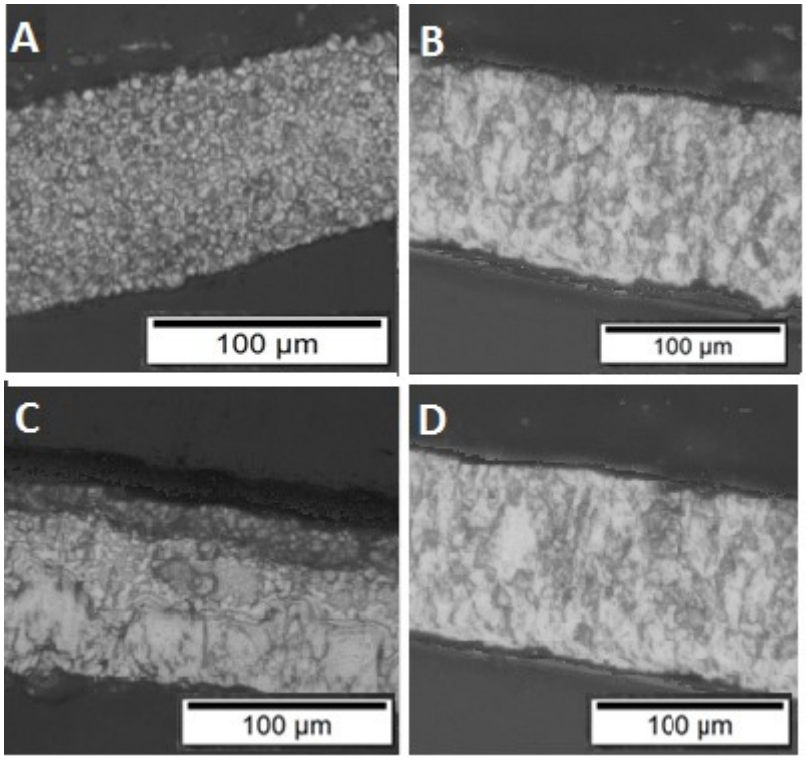

Figure 5.12. Micrographs of electrodeposits at various citric acid concentrations indicating differences in morphology: A. 0 g/L citric acid (standard electrolyte), UD; B. 4 g/L citric acid, UD/FT; C. 8 g/L citric acid, UD/FT; D. 12 g/L citric acid, UD/FT.

The deposits obtained in the presence of citric acid were all UD/FT type with some indications of strain and hydrogen pitting. Grains were generally fine and compact. The deposits were slightly less bright but still level and of acceptable quality. The morphology of the deposit obtained at the highest citric acid concentration was most comparable with that of the deposits obtained from the standard electrolyte solution.

The results showed that boric acid had a more definite and preferred effect in the electrolyte compared with citric acid, even though the p*K*a of citric acid is much closer to the working pH of the electrolyte. It is therefore recommended that boric acid is more beneficial in the electrolyte for nickel electrodeposition. Buffering characteristics are further explored and compared in Section 5.10.

5.7. Effect of additives

5.7.1. Effect of sodium lauryl sulfate

SLS is an anionic surfactant that increases the wettability of the electrolyte by adhering to the substrate surface thereby preventing hydrogen bubbles from interfering at the cathode surface during nickel electrodeposition. Therefore, SLS in the electrolyte should reduce hydrogen pitting and also improve the quality of the deposit. Deposits are generally smooth, bright, fine-grained and low-strained. SLS increases inhibition as it adheres to the substrate, which usually causes a shift to more negative overpotentials without changes in current efficiency (Kittelty and Nicol, 2003; Mohanty *et al*., 2009; Jing *et al*., 2010).

Results for surface tension, current efficiency and conductivity are shown in Table 5.7. Detailed results are shown in Appendix B7.

Table 5.7. Surface tension, conductivity and current efficiency at various SLS concentrations.

$[Ni^{2+}]$ (g/L)	$[Na_2SO_4]$ (g/L)	[Boric acid] (g/L)	pH	Temperature (°C)	Additive(s)	Current efficiency (%)	Conductivity (µS/cm)	Surface tension (N/m)
75	***80***	***4***	***3.0***	***65***	***None***	***98***	***142***	***0.036***
75	80	4	3.0	65	5 mg/L SLS	84	146	0.030
75	80	4	3.0	65	20 mg/L SLS	86	136	0.031
75	80	4	3.0	65	40 mg/L SLS	82	125	0.030

Addition of SLS to the electrolyte caused a decrease in current efficiency. The electrolyte conductivity decreased with increasing SLS concentration and surface tension decreased at all concentrations. This showed that SLS did increase the wettability of the electrolyte, as expected. Therefore, nickel electrodeposition should be more efficient and hydrogen pitting and strain should be limited in the presence of SLS.

Measured polarisation parameters at various SLS concentrations (0, 5, 20 and 40 mg/L) are shown in Figure 5.13. Replicate results are shown in Appendix A7.

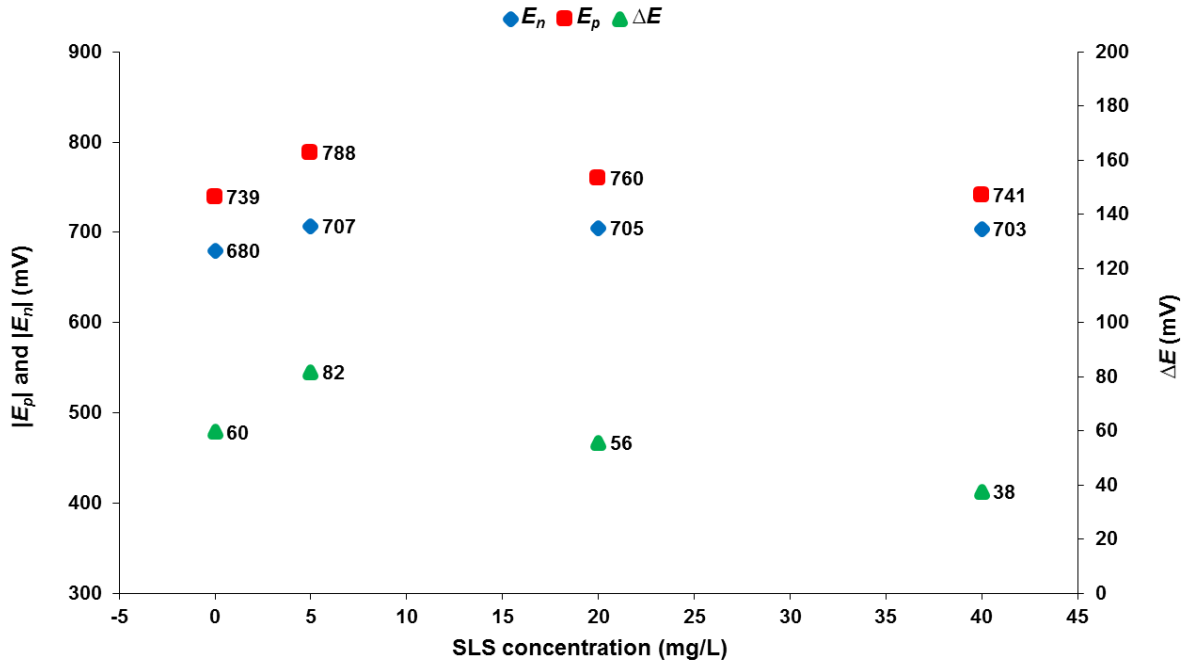

Figure 5.13. Variation of E_n, E_p and ΔE as a function SLS concentration.

Measured polarisation parameters at varying SLS concentrations in the electrolyte were repeatable within 7 mV. A polarisation effect on both E_n and E_p was observed in the presence SLS. The calculated ΔE values were all positive, indicating a desired relationship between nucleation and growth. The ΔE, E_n and E_p values for the 20 mg/L SLS electrolyte compared well with the values for the reference electrolyte. The ΔE decreased with increasing SLS concentration. It was therefore proposed that a concentration around 20 mg/L was beneficial to promoting a good relationship between nucleation and growth, as well as optimising inhibition and wettability without causing too strong adherence to the substrate.

According to the polarisation parameters, good quality deposits of desirable characteristics were expected from all solutions containing SLS. The measured E_n values were highly cathodic, indicating sufficient inhibition and frequent nucleation. The E_p values were even more cathodic, which showed that FT- and UD-type deposits should prevail. Microstructures of deposits are shown in Figure 5.14.

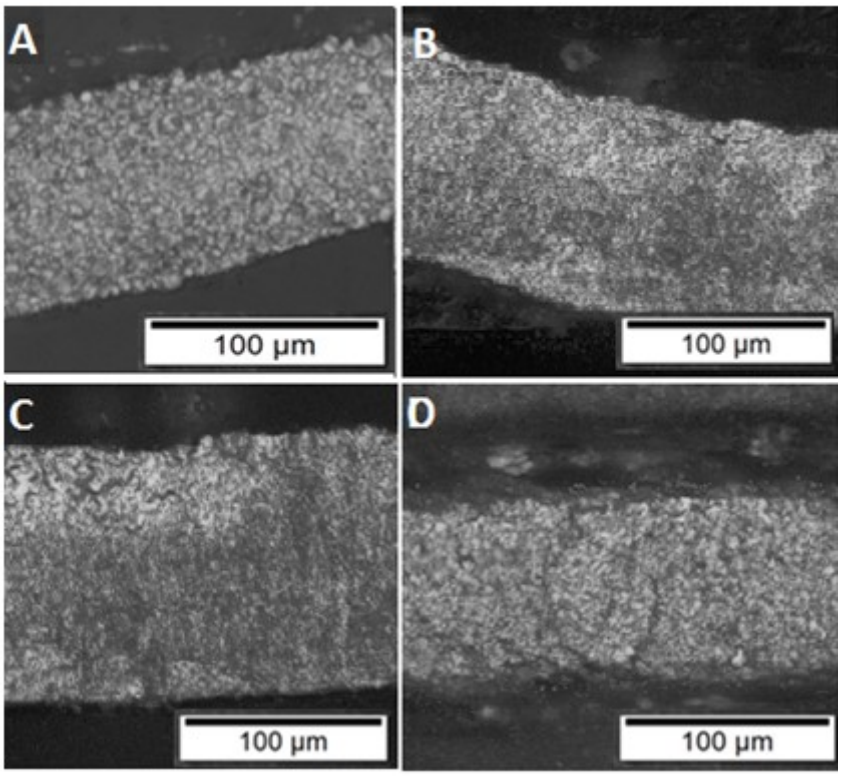

Figure 5.14. Micrographs of electrodeposits at various SLS concentrations indicating differences in morphology: A. 0 mg/L SLS (standard electrolyte), UD; B. 5 mg/L SLS, UD; C. 20 mg/L SLS, UD; D. 40 mg/L SLS, UD.

All of the nickel deposits were bright, fine-grained, smooth and level. The grains were round and fine and similar to or finer than grains obtained for the standard electrolyte. No hydrogen pitting was observed in the presence of SLS and the deposits were all of acceptable quality.

Most of the thick deposits, however, especially at the higher SLS concentrations, were difficult to remove from the cathode surface after deposition. This was indicative of increased interaction of the nickel with the substrate (better wettability) in the presence of SLS. It seemed that the higher the concentration of SLS in the electrolyte, the higher the wettability and inhibition and therefore this induced compressive internal strain at high concentrations. The concentration of SLS was therefore important and should be optimised in order to still remove the deposit with ease after deposition is complete.

5.7.2. Effect of saccharin

SAC is an aromatic organic compound added to the electrolyte to produce level, bright and fine-grained deposits and improve ductility. Grains are generally finer with an increase in SAC concentration due to direct inhibition, which in turn promotes nucleation and changes cathodic overpotentials, especially E_n (Xuetao *et al*., 2008; Rashidi and Amadeh, 2009). SAC has also been proposed to act as a carrier molecule to promote transport and interaction through the double layer. It does, however, seem that the beneficial effects of SAC reaches a plateau at very high concentrations, possibly due to saturation of adsorption sites on the cathode surface (Ciszewski *et al*., 2004; Xuetao *et al*., 2008; Rashidi and Amadeh, 2009).

Current efficiency, surface tension and conductivity are shown in Table 5.8. Results for all electrolytes are detailed in Appendix B8.

Table 5.8. Surface tension, current efficiency and conductivity with varying SAC concentration.

$[Ni^{2+}]$ (g/L)	$[Na_2SO_4]$ (g/L)	[Boric acid] (g/L)	pH	Temperature (°C)	Additive(s)	Current efficiency (%)	Conductivity (µS/cm)	Surface tension (N/m)
75	***80***	***4***	***3.0***	***65***	***None***	***98***	***141***	***0.036***
75	80	4	3.0	65	4 mg/L SAC	86	126	0.034
75	80	4	3.0	65	10 mg/L SAC	83	123	0.037
75	80	4	3.0	65	20 mg/L SAC	70	130	0.034

Current efficiency decreased with increasing SAC concentration. The conductivity decreased at all concentrations of SAC. The surface tension of all the solutions was low and in approximately the same range as that of the standard electrolyte. Deposits produced at 4, 10 and 20 mg/L of added SAC were low in strain and without pitting. The deposits were extremely bright compared with the standard electrolyte deposits and very fine-grained. These deposits, however, were all extremely difficult to remove from the substrate surface after galvanostatic plating. It is proposed that SAC caused an alteration in the substrate surface chemistry due to interaction or an increase in compressive internal strain in the nickel electrodeposit. The exact mechanism still needs further understanding and exploration.

The effect of SAC concentration on measured polarisation parameters is shown in Figure 5.15. Concentration was varied from 0 to 20 mg/L. Detailed results are shown in Appendix A8.

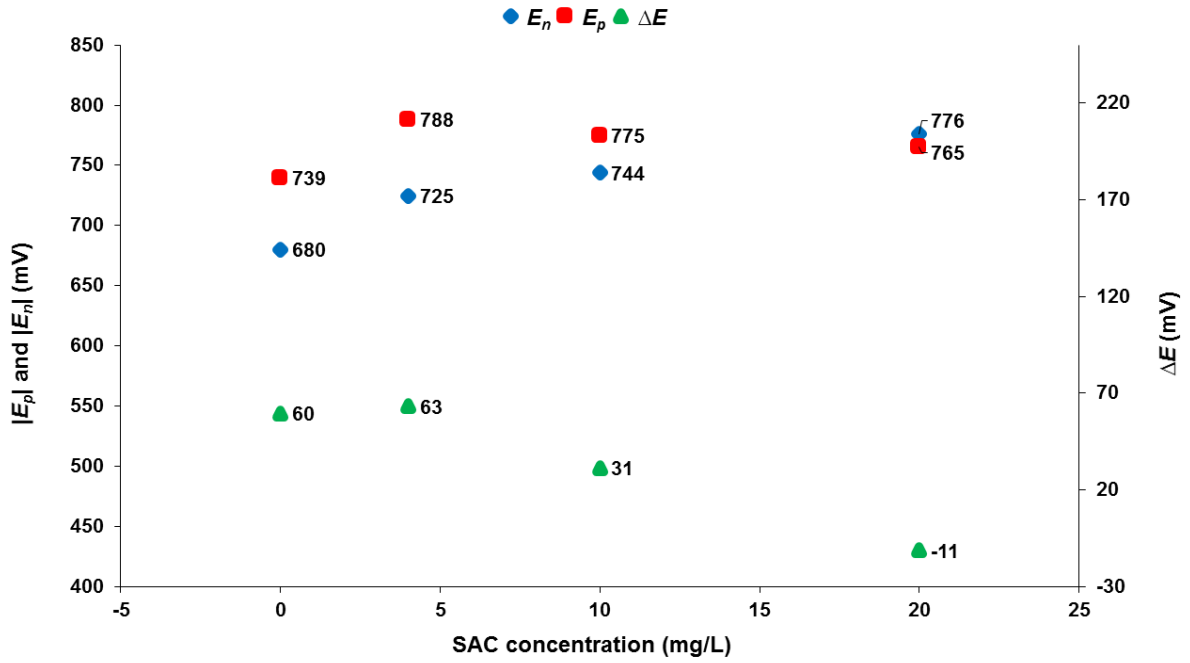

Figure 5.15. Variation of E_n, E_p and ΔE as a function of SAC concentration (mg/L).

Polarisation parameters measured at various SAC concentrations were repeatable within 7 mV. The addition of SAC to the electrolyte solution had a polarizing effect with both E_n and E_p values becoming more cathodic. The ΔE values were highly positive for the electrolyte containing 4 and 10 mg/L of SAC. At 20 mg/L of SAC, the ΔE value was negative. It was not clear at this stage why this was observed and should be further investigated.

As the concentration of SAC increased, the E_n value also increased, which was indicative of an increase in inhibition and also an increase in 3D nucleation. The changes in E_p as SAC was added to the electrolyte also indicated that grain refinement was promoted.

Typical morphologies obtained for various SAC concentrations are shown in Figure 5.16.

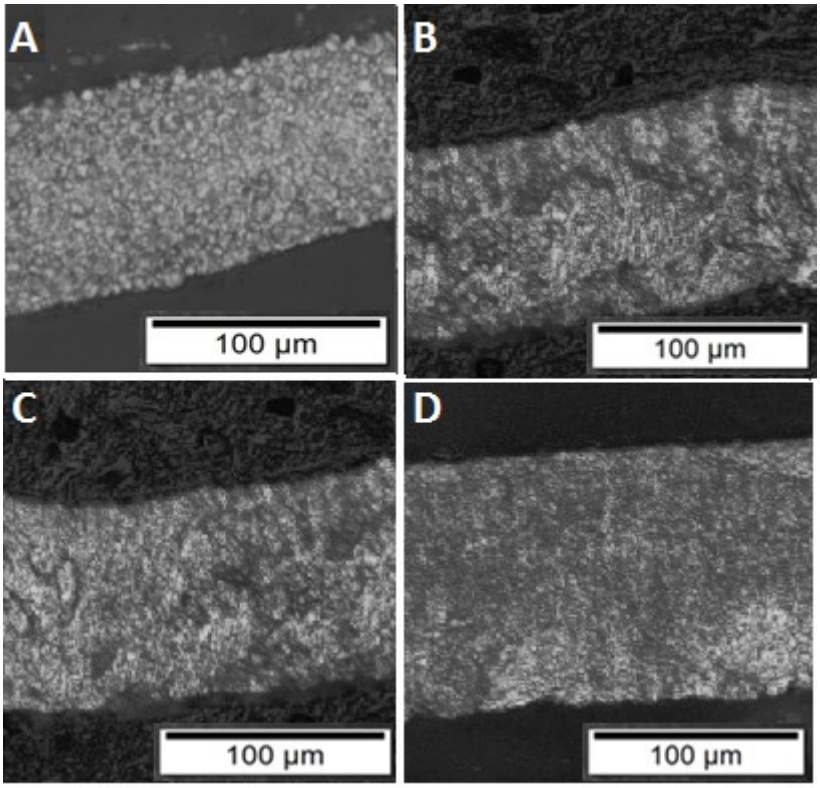

Figure 5.16. Micrographs of electrodeposits at various SAC concentrations indicating differences in morphology: A. 0 mg/L SAC (standard electrolyte), UD; B. 4 mg/L SAC, UD; C. 10 mg/L SAC, UD; D. 20 mg/L SAC, UD.

Good quality, bright, fine-grained and low-strained deposits were obtained in the presence of SAC at all concentrations tested. The morphology and general grain size were very similar to that of the standard electrolyte. Some compressive strain was observed upon removal of the deposits from the substrate surface. This was similarly observed in the presence of SLS. Some irregular grains were observed for deposits from the 5 mg/L and 10 mg/L electrolytes but, overall, the deposit structure, quality and morphology were acceptable and similar to the standard electrolyte. No definite improvements in the quality and morphology of deposits were observed in the presence of both SLS and SAC.

At the highest concentration of 20 mg/L SAC, the deposit morphology was acceptable and very fine-grained, even though the ΔE was slightly negative. It was proposed that, due to the high concentration of SAC as grain refiner, frequent nucleation was still possible even though the ΔE value was slightly negative (indicative of less frequent nucleation). Therefore, the addition of SAC to the electrolyte may be useful in situations where frequent nucleation is

prevented by some other factor, to assist in promoting nucleation and therefore creating better balance between nucleation and growth.

5.7.3. Effect of pyridine

PYR is added to electrolytes to increase levelling and inhibit corrosion. It is an organic molecule containing electron-releasing methyl groups that can donate electrons when absorbed onto the substrate surface. As it absorbs onto the substrate surface, inhibition increases. PYR is a cathodic polariser. Deposits produced in the presence of PYR are bright, level and fine-grained. The current efficiency is normally unaffected by the addition of PYR to the electrolyte solution (Mohanty *et al*., 2001; Mohanty *et al*., 2005).

Concentration was varied from 0 to 100 mg/L. Results for the current efficiency, surface tension and conductivity are presented in Table 5.9. Replicate results are shown in Appendix A9.

Table 5.9. Surface tension, conductivity and current efficiency at various PYR concentrations.

$[Ni^{2+}]$ (g/L)	$[Na_2SO_4]$ (g/L)	[Boric acid] (g/L)	pH	Temperature (°C)	Additive(s)	Current efficiency (%)	Conductivity (µS/cm)	Surface tension (N/m)
75	***80***	***4***	***3.0***	***65***	***None***	***98***	***142***	***0.036***
75	80	4	3.0	65	20 mg/L PYR	90	136	0.031
75	80	4	3.0	65	60 mg/L PYR	94	135	0.031
75	80	4	3.0	65	100 mg/L PYR	92	132	0.029

Current efficiency decreased slightly with the addition of PYR, but all current efficiencies ranged from 90 – 94%. Conductivity and surface tension decreased with increasing PYR concentration. The lowest surface tension of 0.029 N/m was measured at 100 mg/L of PYR, indicating good wettability and therefore increased interaction with the substrate surface during the deposition of nickel. All deposits were low-strained, bright, level, fine-grained and of desired quality but all were difficult to remove from the substrate. The general effects of PYR addition, therefore, were similar to effects observed in the presence of SLS and SAC.

Measured polarisation parameters in response to changes in the PYR concentration are shown in Figure 5.17. Replicate results for all electrolytes are given in Appendix A9.

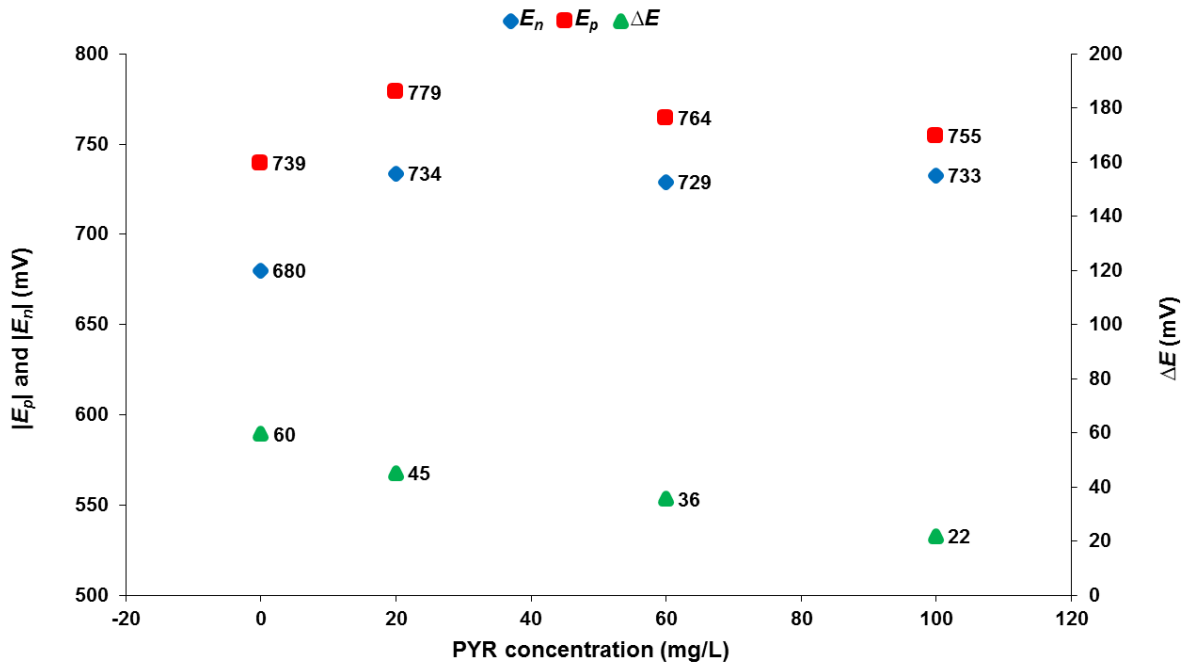

Figure 5.17. Variation of E_n, E_p and ΔE as a function PYR concentration.

Results for the measured polarisation parameters at varying PYR concentrations in the electrolyte were repeatable to within approximately 6 mV. A polarisation effect on both E_n and E_p was observed in all cases. Calculated ΔE values were all positive and therefore good quality deposits were expected at all concentrations of PYR. The effect of PYR on the E_n value was approximately constant – E_n was fairly constant but higher than the E_n for the standard electrolyte. In the presence of PYR, E_p changed (decreased) with increasing PYR concentration. Therefore, ΔE values also decreased with increasing PYR concentration.

It seems that PYR behaved as a polariser, as expected, which influenced growth processes more than nucleation processes. The benefits of PYR addition were obtained even at a low concentration, such as 5 mg/L, and therefore a higher concentration was not more beneficial and not needed to achieve the same effect.

Typical morphologies obtained for electrodeposits in the presence of PYR are shown in Figure 5.18.

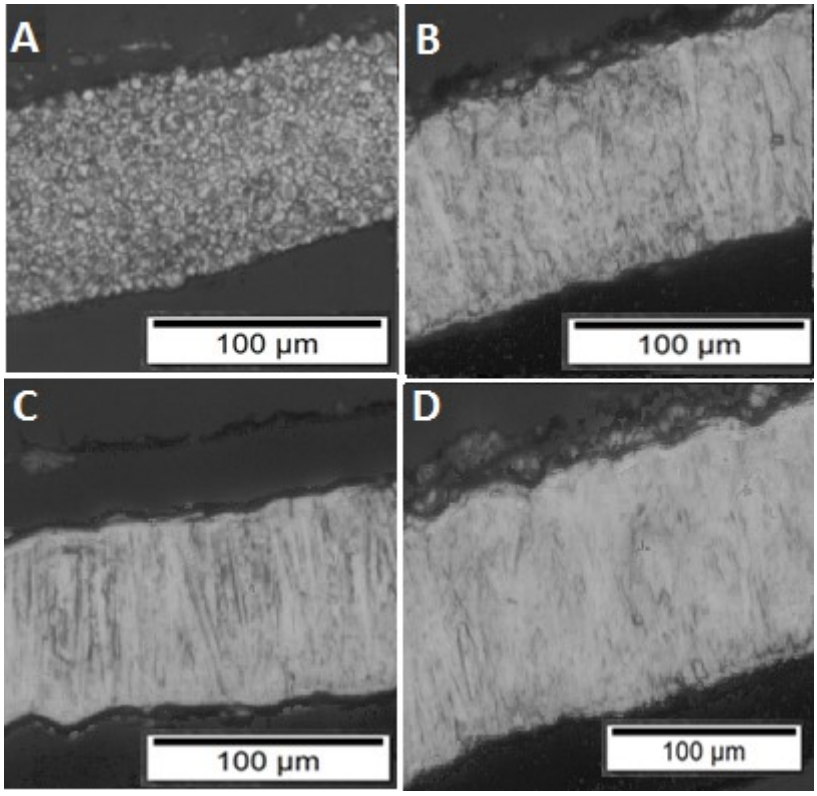

Figure 5.18. Micrographs of electrodeposits at various PYR concentrations indicating differences in morphology: A. 0 mg/L PYR (standard electrolyte), UD; B. 20 mg/L PYR, FT; C. 60 mg/L PYR, FT; D. 100 mg/L PYR, FT.

The effect of the presence of PYR in the electrolyte was clearly observed. The deposit grains were much more elongated, larger and of the FT type when compared with the structure of the deposits from the standard electrolyte. No strain or hydrogen pitting were observed.

All deposits were compact, fairly level and of acceptable quality, but the morphology was very different compared with the fine-grained structures for the standard electrolyte and the SLS- and SAC-containing electrolytes. The deposit morphology and structure were very similar for all concentrations of PYR and therefore a concentration of 5 mg/L was sufficient to achieve this FT-type morphology. No extra benefits in the morphological characteristics were observed with an increase in PYR concentration.

5.8. Effect of impurities

5.8.1. Effect of cobalt

Cobalt may co-deposit with nickel, thereby reducing purity and decreasing current efficiency (Gogia and Das, 1991). Concentrations of 500 mg/L or lower do not have a definite effect on the morphological outcome of the nickel deposits. At higher concentrations nickel deposits are severely degraded, cracked, peeled and more spongy. Increased internal strain is observed, especially if cobalt atoms are incorporated into the growing crystal lattice. Shifts in polarisation are observed with cobalt present in the electrolyte, depending on the cobalt concentration. At low concentrations of cobalt, nickel electrodeposition is less noble. At higher concentrations of cobalt, nickel electrodeposition is shifted to more negative values (Gogia and Das, 1991; Kittelty, 2002).

Solution measurements are shown in Table 5.10. The concentrations tested were 250, 500 and 1000 mg/L. Replicate results are shown in Appendix B10.

Table 5.10. Current efficiency, conductivity and surface tension of electrolyte with various cobalt concentrations.

$[Ni^{2+}]$ (g/L)	$[Na_2SO_4]$ (g/L)	[Boric acid] (g/L)	pH	Temperature (°C)	Additive(s)	Current efficiency (%)	Conductivity (µS/cm)	Surface tension (N/m)
75	***80***	***4***	***3.0***	***65***	***None***	***98***	***141***	***0.036***
75	80	4	3.0	65	250 mg/L Co	88	140	0.040
75	80	4	3.0	65	500 mg/L Co	82	140	0.036
75	80	4	3.0	65	1000 mg/L Co	85	139	0.041

Current efficiencies in the presence of cobalt impurities (at all concentrations) were low compared with that of the standard electrolyte. The conductivity decreased and the surface tension increased (poor wettability) with increasing cobalt concentration. The deposits were highly strained, cracked and hydrogen pits were prevalent. This was observed at all concentrations of cobalt.

The response of measured polarisation parameters to changes in the cobalt concentration are shown in Figure 5.19. Replicate results are shown in Appendix A10.

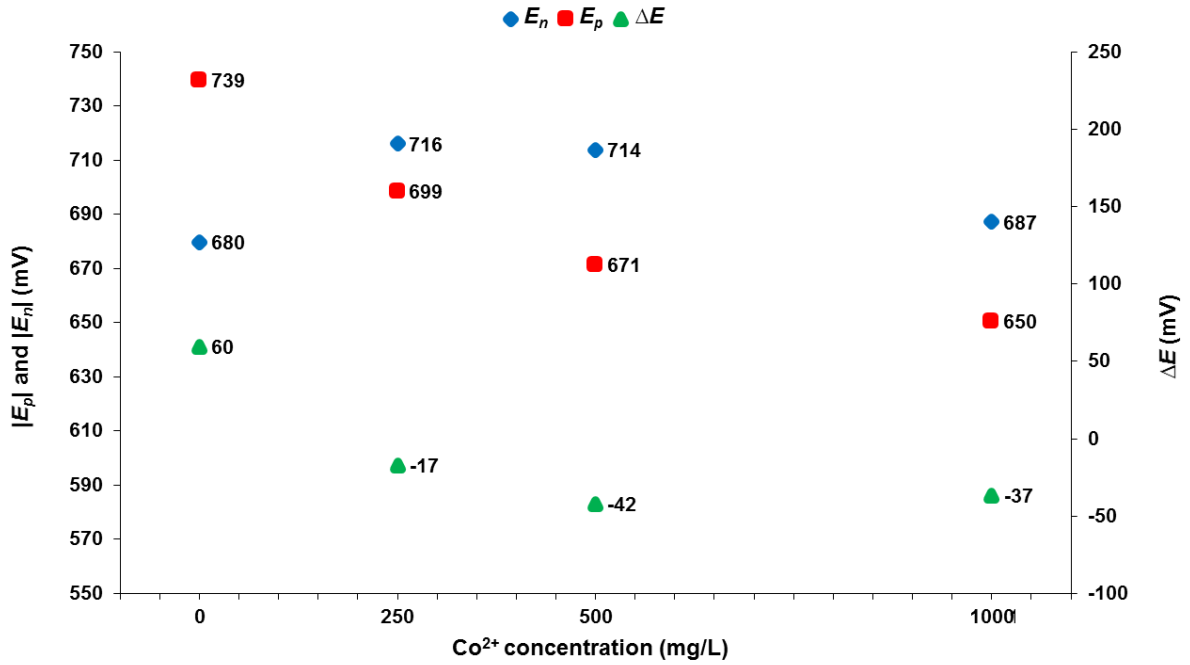

Figure 5.19. Variation of E_n, E_p and ΔE as a function of cobalt concentration.

The E_n, E_p and ΔE values obtained for varying cobalt concentration were repeatable within 10 mV. Depolarisation was observed in the E_p values as the cobalt concentration increased, indicating fast, irregular growth of deposited crystallites. The E_n values also showed a polarizing effect upon initial addition of cobalt to the solution, indicating increased inhibition.

The ΔE values for all the investigated cobalt concentrations were highly negative and therefore deposits of poor quality and undesirable characteristics were expected with cobalt in the electrolyte. The changes in polarisation parameters also suggested that cobalt may be incorporated into the growing crystal lattice, especially at higher cobalt concentrations. The deposits were very brittle and spongy with very irregular grain size; the decrease in current efficiency also suggested that this morphology would result.

Morphology of deposits obtained in the presence of cobalt is shown in Figure 5.20.

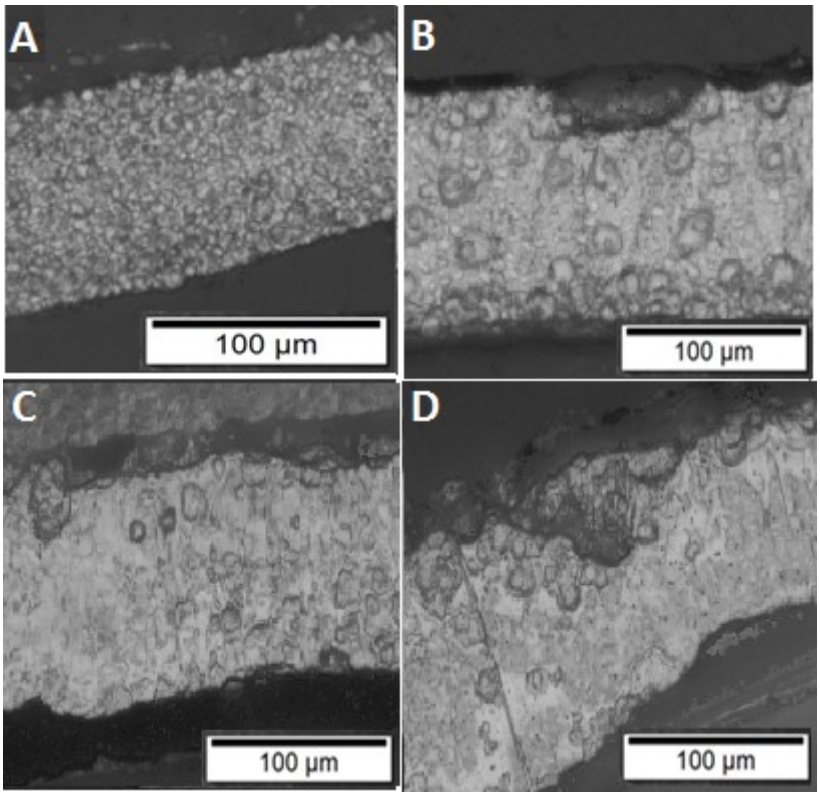

Figure 5.20. Micrographs of electrodeposits at various cobalt concentrations indicating differences in morphology: A. 0 mg/L Co (standard electrolyte), UD; B. 250 mg/L Co, FT/BR; C. 500 mg/L Co, FT/BR; D. 1000 mg/L Co, FT/BR.

Deposits obtained in the presence of cobalt were highly strained with hydrogen pitting and irregular structure. The grains were very irregular in size, which could be indicative of cobalt incorporation into the nickel deposit itself. The general structure of the grains of all deposits seemed to be FT/BR type and all deposits were of unacceptable quality. The deposits were also dull in colour in some areas, which might have been due to cobalt incorporation into the structure. The morphology of the deposits at 500 mg/L and 1000 mg/L cobalt were similar in structure but, even at lower concentration, the presence of cobalt seemed to be detrimental. This suggested that cobalt, even at concentrations below the tolerance limit of 500 mg/L (Table 2.1.) (Gogia and Das, 1991), had severe effects on the polarisation parameters, the deposition process of nickel and the ultimate structure of the nickel deposit.

5.8.2. Effect of copper

Copper is expected to co-deposit with nickel and therefore the current efficiency obtained and purity were expected to decrease. The tolerance limit of copper in the electrolyte is approximately 200 mg/L and the effect of copper increases with increasing concentration (Gogia and Das, 1991). Nickel deposits are generally discoloured, nodular and strained in the presence of copper. Growth is irregular at copper concentrations higher than the tolerance limit. Copper also influences the polarisation behaviour depending on the concentration of the copper impurity (Dennis and Fuggle, 1968; Gogia and Das, 1991; Kittelty, 2002).

Current efficiency, surface tension and conductivity of the electrolyte are shown in Table 5.11. Replicate measurements are shown in Appendix B11. The copper impurity concentration was varied from 100 to 250 to 500 mg/L.

Table 5.11. Current efficiency, conductivity and surface tension for results at varying copper concentrations.

$[Ni^{2+}]$ (g/L)	$[Na_2SO_4]$ (g/L)	[Boric acid] (g/L)	pH	Temperature (°C)	Additive(s)	Current efficiency (%)	Conductivity (µS/cm)	Surface tension (N/m)
75	***80***	***4***	***3.0***	***65***	***None***	***98***	***142***	***0.036***
75	80	4	3.0	65	100 mg/L Cu	89	144	0.041
75	80	4	3.0	65	250 mg/L Cu	89	141	0.041
75	80	4	3.0	65	500 mg/L Cu	79	140	0.041

The current efficiencies were low for all electrolytes containing copper. The lowest current efficiency of 78 % was obtained at the highest copper concentration. Conductivity of all the solutions was approximately the same as that of the standard solution. The surface tension seemed unaffected by the added copper ions in the electrolyte. The obtained deposits for the higher concentrations of copper (250 and 500 mg/L) in the electrolyte solutions were highly strained and pitted. At a concentration of 100 mg/L copper, the deposits were strained and pitted more than those obtained from the standard electrolyte solution, but not as severely as those from electrolytes containing higher concentrations of copper.

Measured polarisation parameters in response to changes in the copper concentration are shown in Figure 5.21. Replicate results are shown in Appendix A11.

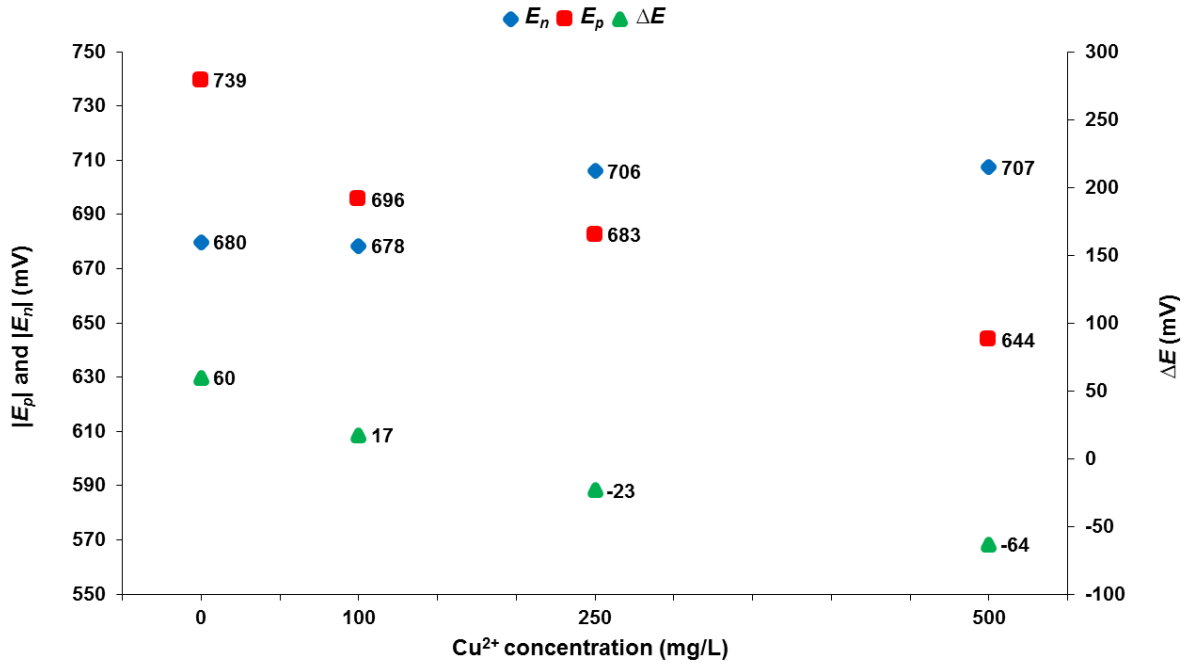

Figure 5.21. Variation of E_n, E_p and ΔE as a function of copper impurity concentration.

The repeatability of the measured polarisation results was 8 mV. The E_n values showed a polarizing effect at concentrations of 250 mg/L and higher. The E_p values decreased with increasing copper concentration. The ΔE values at the higher concentrations of 250 and 500 mg/L were negative, indicating an unfavourable relationship between nucleation and growth. Polarisation parameters therefore indicated desirable deposits at the low copper concentration of 100 mg/L. Higher concentrations were expected to cause large irregular crystallites, produced under conditions of low inhibition and less frequent nucleation. Deposits were also expected to contain copper in the structure, causing strain and cracking.

Figure 5.22 shows the differences in morphology of the nickel deposits with various concentrations of copper present in the electrolyte.

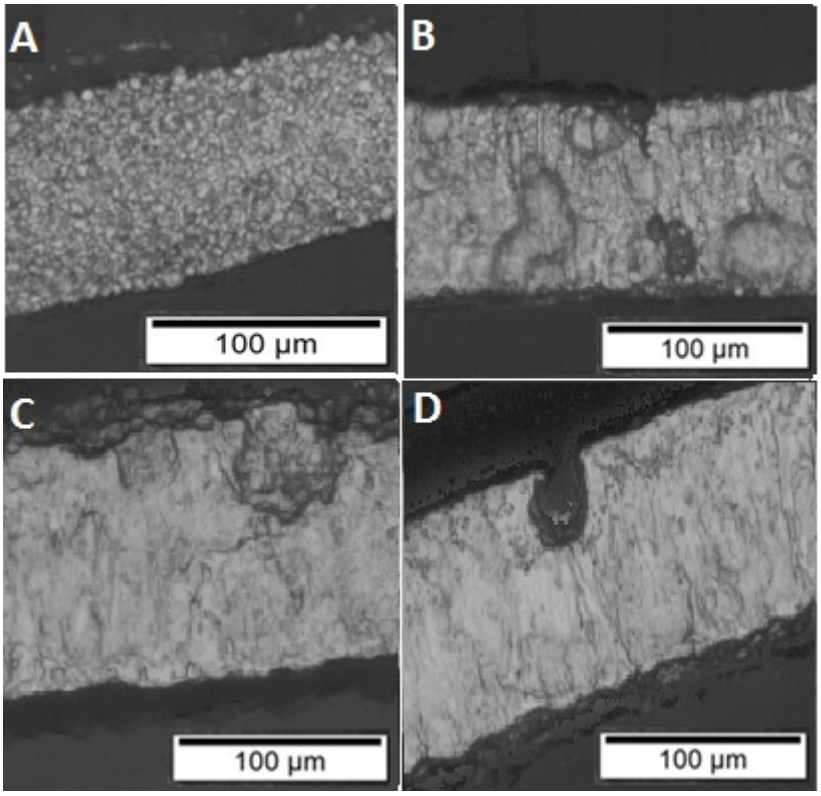

Figure 5.22. Micrographs of electrodeposits at various copper concentrations indicating differences in morphology: A. 0 mg/L Cu (standard electrolyte), UD; B. 100 mg/L Cu, FT/BR; C. 250 mg/L Cu, FT/BR; D. 500 mg/L Cu, FT/BR.

The morphology of all deposits in the presence of copper was much deteriorated compared with that of the standard electrolyte. The structures were all strained and showed large cracks, holes and hydrogen pits. The morphology was typical of FT/BR type with large, elongated grains growing in an irregular direction and of non-uniform size. The morphology of the deposits at 250 mg/L and 500 mg/L seemed very similar while the grains at 100 mg/L were finer. The deposits from the 100 mg/L electrolyte, however, were very strained, even though the tolerance limit for copper impurities is reportedly around 200 mg/L (Table 2.1.) (Gogia and Das, 1991). The morphology and general structure of the deposits obtained in the presence of copper strongly suggested that copper may be incorporated into the crystal structure. Copper impurities should therefore be avoided at all costs.

5.8.3. Effect of aluminium

The tolerance limit of aluminium in any nickel electrowinning process or application is much lower compared with that of other metallic impurities and a concentration of as low as 5 mg/L of aluminium can have a strong effect on polarisation parameters and morphology. Even if such low concentrations are present, nickel deposits are cracked, curled, peeled, cracked, brittle and severely pitted (Gogia and Das, 1988; Zhou and O'Keefe, 1997; Holm and O'Keefe, 2000). The effect increases with increasing aluminium concentration up to approximately 2000 mg/L (Küzeci and Kammel, 1994; Holm and O'Keefe, 2000). The polarisation parameters are shifted to more negative values in the presence of aluminium impurities and the effect increases with increasing concentration and current efficiency (Gogia and Das, 1988; Küzeci and Kammel, 1994; Holm and O'Keefe, 2000; Kittelty, 2002).

At low concentrations of 20 and 40 mg/L aluminium impurity, Kittelty (2002) found that deposits were severely cracked, delaminated and strained. Intermediate impurity concentrations of 270 and 540 mg/L aluminium in the electrolyte caused delamination and discolouration of the nickel deposits and internal cracks were evident throughout the nickel deposits. Increased concentrations of 1350 and 2700 mg/L in the electrolyte improved the morphology and strain characteristics and the nickel deposits produced were smooth, level and regular in growth structure. Deposits that were highly strained and cracked (produced from electrolytes with low concentrations of aluminium impurities) were found to contain aluminium (most probably as $Al(OH)_3$) in the crystal lattice. This was indicative of aluminium co-deposition at low concentrations of aluminium impurity in the electrolyte. Nickel deposits produced at concentrations of 1350 and 2700 mg/L of aluminium impurity in the electrolyte were found not to contain aluminium in the nickel crystal lattice (Kittelty, 2002). The conclusions from this study showed that at low concentrations of aluminium impurity (20, 40, 270 and 540 mg/L), $Al(OH)_3$ is most likely to form at the working pH of the electrolyte and co-deposit or precipitate during electrodeposition of nickel itself. At higher concentrations of aluminium (1350 and 2700 mg/L), the aluminium is most likely to form other species, such as $AlOH^{2+}$, $Al(OH)_2^{+}$ and $Al(OH)_2^{4+}$, which are more likely to be involved in buffering or transport in the electrolyte instead of co-depositing with nickel, thereby promoting better morphology of the nickel deposit (Kittelty, 2002).

Low internal strain without aluminium contamination in the nickel electrodeposit was also found at 2500 mg/L aluminium impurity in the electrolyte by Nsiengani (2017). The deposits were smooth, level and compact.

In this study, it was therefore decided to evaluate the effect of two extremely low aluminium impurity concentrations (5 and 10 mg/L) and one high concentration (5000 mg/L) that was even higher than the concentrations evaluated by Kittelty (2002). The morphology and polarisation parameters were expected to be indicative of poor characteristics, poor quality and high internal strain for the low concentrations, while the 5000 mg/L of aluminium impurity was expected to improve the overall polarisation characteristics, strain and morphology of the nickel electrodeposits.

Results for conductivity, surface tension and current efficiency are presented in Table 5.12. The aluminium concentrations tested were 5, 10 and 5000 mg/L. Detailed results are included in Appendix B12.

Table 5.12. Results for current efficiency, conductivity and surface tension at varying aluminium concentrations.

$[Ni^{2+}]$ (g/L)	$[Na_2SO_4]$ (g/L)	[Boric acid] (g/L)	pH	Temperature (°C)	Additive(s)	Current efficiency (%)	Conductivity (µS/cm)	Surface tension (N/m)
75	***80***	***4***	***3.0***	***65***	***None***	***98***	***141***	***0.036***
75	80	4	3.0	65	5 mg/L Al	87	141	0.039
75	80	4	3.0	65	10 mg/L Al	90	140	0.040
75	80	4	3.0	65	5000 mg/L Al	91	142	0.041

Current efficiency in the presence of low aluminium impurity concentrations (5 and 10 mg/L) decreased. Conductivity stayed almost constant compared with the conductivity measured for the standard electrolytes. The surface tension of the electrolytes increased with increasing aluminium concentration. The deposits obtained at 5 and 10 mg/L of aluminium added to the electrolytes were strained, peeled, cracked and hydrogen pitting was observed over the deposit surfaces. These observations were consistent with aluminium (probably as $Al(OH)_3$) being incorporated into the growing crystal lattice and therefore decreasing the deposit purity.

At 5000 mg/L of added aluminium, the current efficiency was 91 %, the conductivity of the electrolyte was the same as the standard electrolyte and the surface tension slightly higher than the standard electrolyte. The obtained deposits were not strained and much less pitted than the other electrolytes with added aluminium. It therefore seemed that there was a critical concentration of aluminium at which it might become a beneficial impurity and at which good quality deposits were produced.

The response of measured polarisation parameters to changes in the aluminium concentration are shown in Figure 5.23. Detailed results are shown in Appendix A12.

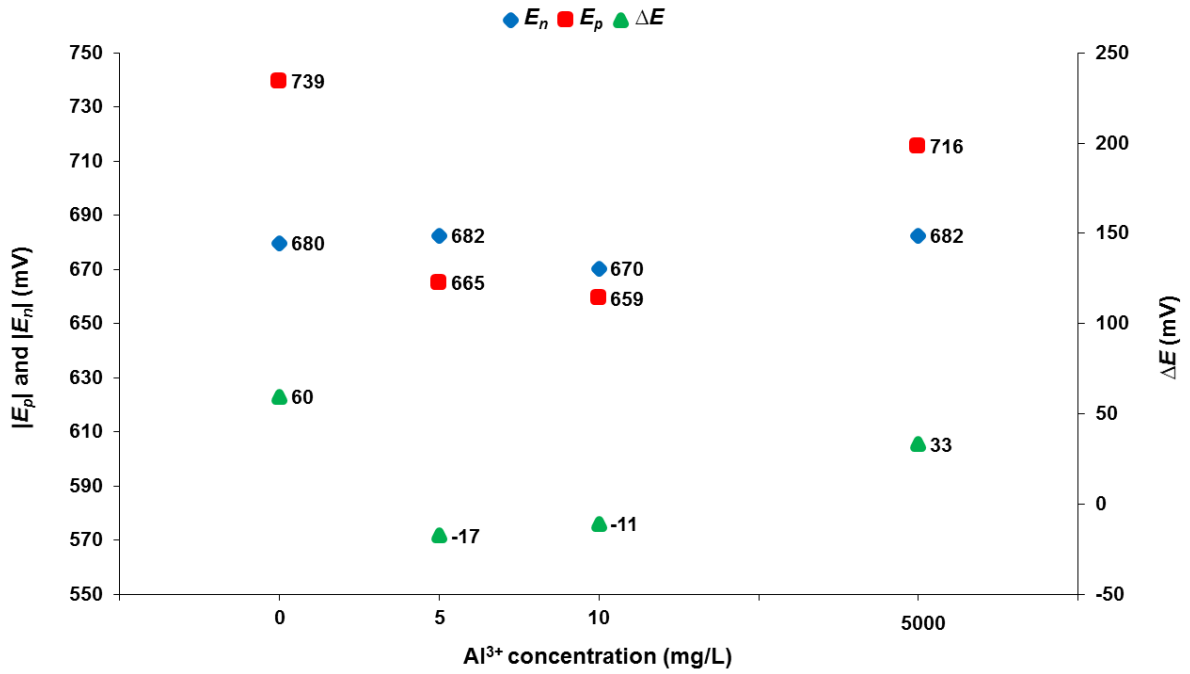

Figure 5.23. Results of the variation of E_n, E_p and ΔE as a function of aluminium concentration.

Polarisation results were repeatable within approximately 7 mV. An increase in aluminium influenced the E_p values more than the E_n values. The E_n value was fairly constant for 0, 5 and 10 mg/L of added aluminium. The E_n value slightly increased cathodically at the much higher concentration of aluminium added of 5000 mg/L. The E_p value initially decreased cathodically at 5 and 10 mg/L but increased significantly at 5000 mg/L. The ΔE values were negative for the 5 mg/L and 10 mg/L electrolytes. At 5000 mg/L, the ΔE value was positive and the relationship between E_n and E_p therefore favourable. A good relationship between nucleation and growth was therefore expected at 5000 mg/L. This was confirmed by the improved quality and morphology of the deposits obtained at 5000 mg/L aluminium, and the

purity of the deposits was therefore also likely to be higher compared with the deposits at 5 and 10 mg/L aluminium.

The different morphological structures obtained at various concentrations of aluminium are shown in Figure 5.24.

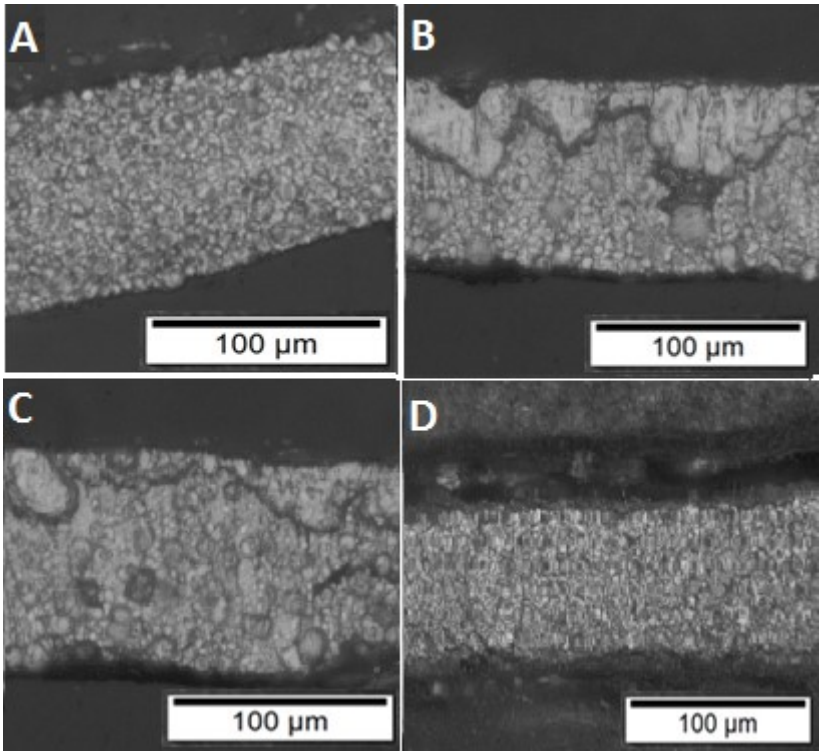

Figure 5.24. Micrographs of electrodeposits at various aluminium concentrations indicating differences in morphology: A. 0 mg/L Al (standard electrolyte), UD; B. 5 mg/L A, BR; C. 10 mg/L Al, BR; D. 5000 mg/L Al, UD.

The morphologies of the deposits at both 5 mg/L and 10 mg/L of aluminium impurity were very similar. The grains were very irregular and some areas showed faster growth and low nucleation, while other areas seemed to be relatively fine-grained. The deposits were cracked, pitted and highly strained with holes inside the deposits at some points. This could have been due to incorporation of aluminium compounds into the nickel deposit causing increased strain in the crystal structure. The morphology was mainly of BR type with some fine-grained areas. The presence of low concentrations of aluminium impurity was therefore detrimental to the morphology and strain of the deposit. This confirmed the morphology described by Kittelty (2002) for deposits formed from electrolytes containing 20, 40, 270 and 540 mg/L of aluminium.

The deposits obtained in the presence of 5000 mg/L of aluminium had low strain, no cracks, low pitting and were fine-grained, level and smooth. The morphology seemed to be of UD type and was very similar to the morphology and grain size of deposits from the standard electrolyte. In some areas, grain refinement was even observed (Figure 5.24 D) compared with the standard electrolyte deposit (Figure 5.24 A). Such a high concentration of aluminium appeared beneficial to the overall structure, strain characteristics and morphology of nickel electrodeposits. The possible buffering characteristics of these electrolytes were further investigated in order to explain these findings. The results are presented in Section 5.10.

5.9. Effect of amphoterics

5.9.1. Effect of selenium

Selenium is known to co-deposit during electrowinning at all concentrations and in both selenite (Se(IV)) and selenate (Se(VI)) forms (Crundwell *et al*., 2011). The presence of selenium also causes cracking, internal strain and severe delamination during electrowinning (Voogt *et al*., 2017). It is therefore expected that selenium impurities will have severe effects on the morphology and strain characteristics due to their incorporation into the crystal lattice during electrodeposition. Table 5.13 shows results for various selenium impurities on the current efficiency, surface tension and conductivity of the electrolyte. Concentrations were varied from 10 – 25 mg/L. Results of the five repeat measurements are shown in Appendixes A13 and A14.

Table 5.13. Results for current efficiency, conductivity and surface tension at varying Se(IV) and Se(VI) concentrations.

$[Ni^{2+}]$ (g/L)	$[Na_2SO_4]$ (g/L)	[Boric acid] (g/L)	pH	Temperature (°C)	Additive(s)	Current efficiency (%)	Conductivity (µS/cm)	Surface tension (N/m)
75	***80***	***4***	***3.0***	***65***	***None***	***98***	***142***	***0.036***
75	80	4	3.0	65	10 mg/L Se(IV)	84	136	0.035
75	80	4	3.0	65	15 mg/L Se(IV)	88	140	0.038
75	80	4	3.0	65	25 mg/L Se(IV)	79	138	0.035
75	80	4	3.0	65	10 mg/L Se(VI)	87	133	0.041
75	80	4	3.0	65	15 mg/L Se(VI)	88	138	0.039
75	80	4	3.0	65	25 mg/L Se(VI)	78	140	0.033

The current efficiency decreased at all concentrations of selenium impurities (for both selenite and selenate). The lowest current efficiencies were obtained at the highest concentrations of selenium. The conductivity of the electrolyte seemed to be only slightly affected at all selenium concentrations. The surface tension also seemed less affected with only a slight decrease in surface tension as the concentration of the selenite and selenate impurity increased. The wettability therefore seemed to be less influenced by the presence of selenium compared with other impurities.

The effects of selenium on the polarisation parameters are shown in Figures 5.25 and 5.26.

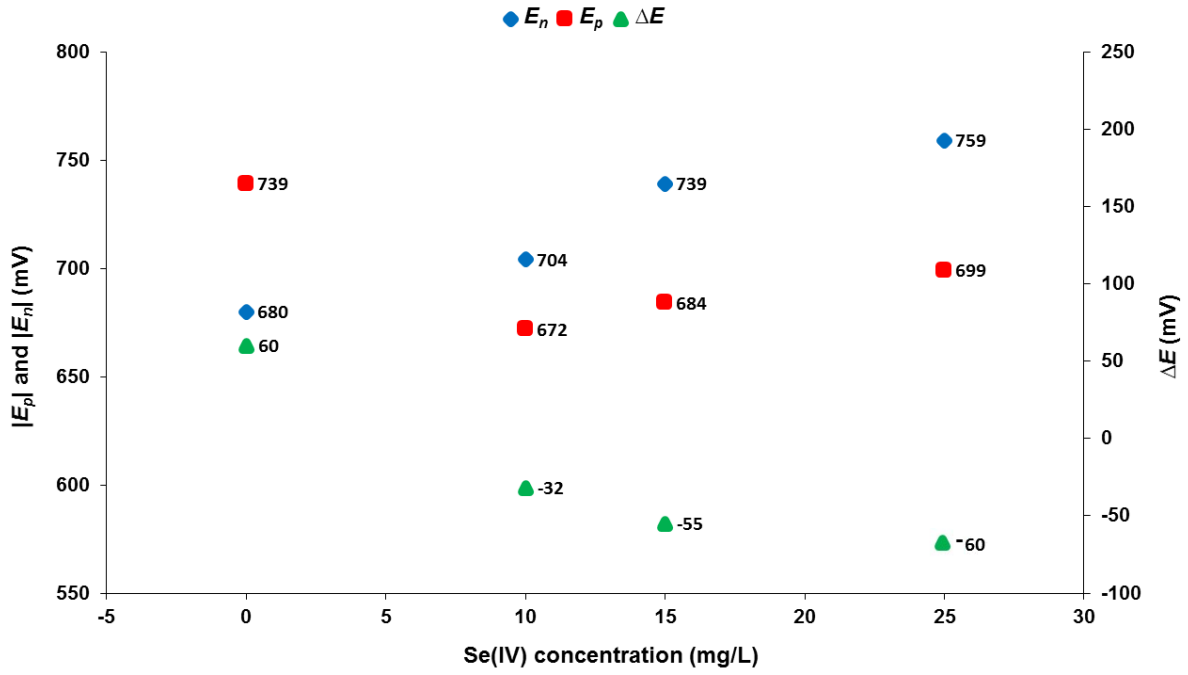

Figure 5.25. Variation of E_n, E_p and ΔE as a function of Se(IV) concentration.

The polarisation parameters were severely changed by the presence of selenite. The E_n increased with increasing concentration of selenite and the E_p initially decreased with increasing selenite. At higher concentration, the E_p only slightly increased. Therefore, the ΔE was negative for all concentrations and ΔE decreased with increasing concentration of selenite. The presence of selenite in the solution therefore suggested low inhibition, ineffective nucleation and high rates of growth. Therefore, irregular structures with high internal strain were expected.

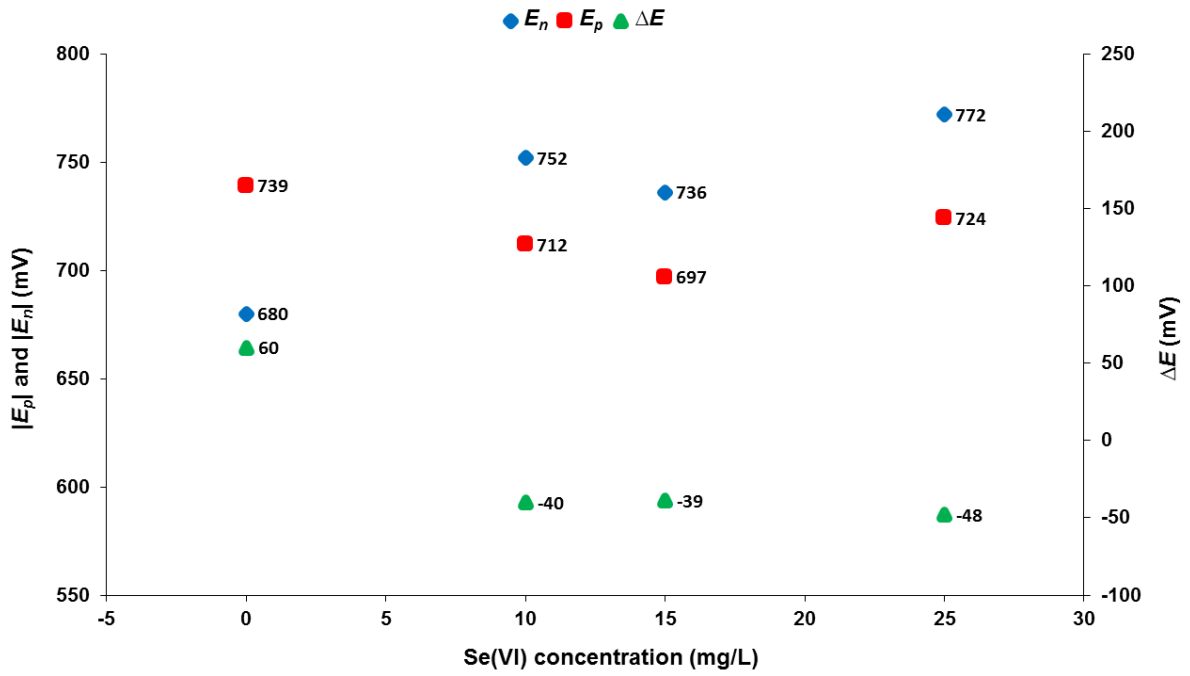

Figure 5.26. Variation of E_n, E_p and ΔE as a function of Se(VI) concentration.

Polarisation parameters were also greatly changed in the presence of selenate. The E_p decreased with increasing concentration of selenate, with a slight increase at the highest concentration. The E_n increased with the addition of selenate to the electrolyte. The relationship between E_n and E_p changed such that ΔE was negative for all concentrations and the ΔE was fairly similar at the three concentrations of selenate. It therefore seemed that, irrespective of selenate concentration, the presence of selenate promoted strain development in the deposit structure with an undesirable relationship of nucleation, inhibition and growth processes. Poor morphology and high strain were therefore expected.

The effects of the presence of selenite and selenate on the polarisation parameters were similar. All of the ΔE values calculated at all of the concentrations in both cases were highly negative and the current efficiencies low. The effects on the morphology of the deposits at all concentrations of selenite and selenate are therefore expected to be similar.

The morphologies for deposits obtained from electrolytes with various selenite and selenate concentrations are shown in Figures 5.27 and 5.28, respectively.

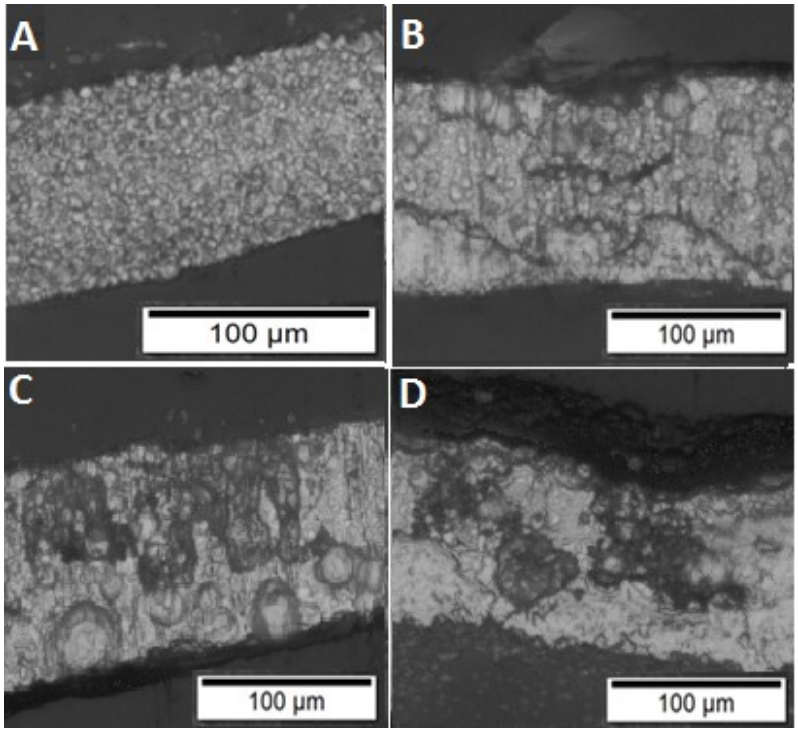

Figure 5.27. Micrographs of electrodeposits at various selenite concentrations indicating differences in morphology: A. 0 mg/L Se(IV) (standard electrolyte), UD; B. 10 mg/L Se(IV), BR; C. 15 mg/L Se(IV), BR; D. 25 mg/L Se(IV), BR.

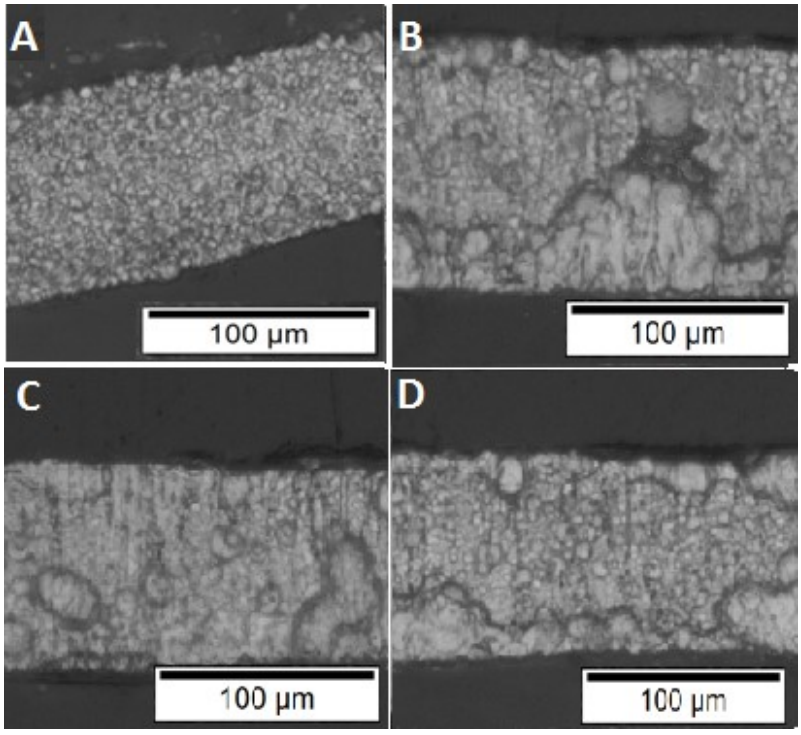

Figure 5.28. Micrographs of electrodeposits at various selenate concentrations indicating differences in morphology: A. 0 mg/L Se(VI) (standard electrolyte), UD; B. 10 mg/L Se(VI), BR; C. 15 mg/L Se(VI), BR; D. 25 mg/L Se(VI), BR.

The morphologies of the deposits from electrolytes with both selenite and selenate were irregular. Large grains with irregular growth and high internal strain, pitting, holes and cracks were produced. Delamination along the side edges of the deposits was also observed during the electrodeposition process of almost all of the deposits, irrespective of the oxidation state of the impurity. The effect of the selenium impurities was the most severe of all of the impurities and the strain was certainly the highest.

No significant differences were observed in the morphology and quality of the deposits at increasing concentration of the impurities and the morphology at all concentrations was similar and of the BR type. Some finer grains were also observed in between large irregular growth grains for all of the concentrations.

An interesting observation was that the ΔE value calculated could be related to not only the general morphology and structure of the deposits, but also to the internal stress and developing strain during electrodeposition. For deposits produced from electrolytes with all of the impurities (except 5000 mg/L aluminium), the ΔE value was low. This observation and the relation of ΔE to E_p and strain is further explored in Chapter 6.

5.10. Investigation of buffering capabilities of various electrolytes

In order to better understand findings regarding the differences in polarisation parameters in the presence of boric acid and aluminium, the buffering characteristics of various electrolytes were investigated. The idea was to test which electrolytes buffered the system better and which composition of the electrolyte was more effective to keep the pH more constant throughout the nickel electrodeposition process.

Various electrolytes of differing composition were prepared without any pH adjustment prior to these tests. Therefore, most of the starting pH values were approximately 2. The standard electrolyte (with boric acid concentration of 4 g/L) was first tested, as well as the two electrolytes with increased boric acid concentrations to 8 g/L and 12 g/L. As a baseline, the standard electrolyte was also prepared exactly as before, but no boric acid (0 g/L) was added. Comparing the buffering characteristics of these electrolytes was used to investigate the buffering capabilities specific to the presence of boric acid in the electrolyte. The effect of the nickel in the electrolyte was also investigated as it has been proposed that boric acid might complex with nickel, forming nickel–borate complexes that might be responsible for buffering (instead of boric acid itself). The standard electrolyte was prepared in the same way

but with different nickel concentrations – 0 g/L and 50 g/L, all at the standard boric acid concentration of 4 g/L. Another electrolyte was prepared with 4 g/L of citric acid, to compare the buffering capabilities of citric acid and boric acid because the p*K*a of citric acid is similar to the working pH of the electrolyte. The last electrolytes prepared were to investigate the buffering characteristics of aluminium impurity in the electrolyte in the presence of boric acid. Two electrolytes were prepared with low (10 mg/L) and high (5000 mg/L) aluminium with the standard electrolyte boric acid concentration of 4 g/L.

A summary of the compositions of electrolytes prepared for the buffer investigation is given in Table 5.14.

Table 5.14. Compositions of electrolytes prepared for testing of buffering characteristics.

$[Ni^{2+}]$ (g/L)	$[Na_2SO_4]$ (g/L)	[Boric acid] (g/L)	pH	Temperature (°C)	Additive(s)
75	***80***	***4***	***3.0***	***65***	***None***
75	80	**8**	3.0	65	None
75	80	**12**	3.0	65	None
75	80	**0**	3.0	65	None
0	80	4	3.0	65	None
50	80	4	3.0	65	None
75	80	**0**	3.0	65	**4 g/L Citric acid**
75	80	4	3.0	65	**10 mg/L Al^{3+}**
75	80	4	3.0	65	**5000 mg/L Al^{3+}**

Buffering characteristics of the electrolytes were tested in two ways (Chapter 3, Section 3.5). The first was a titration with either NaOH or H_2SO_4 that monitored of the pH of the electrolyte after each addition. The results were compared to evaluate which composition was able to keep the pH more constant. The second method was a typical three- electrode cell setup with each electrolyte and a constant current density of 220 A/m^2 applied. The pH of the solution was monitored over time to investigate which composition was able to buffer the electrolyte more effectively. The results are presented in Figures 5.29 to 5.32.

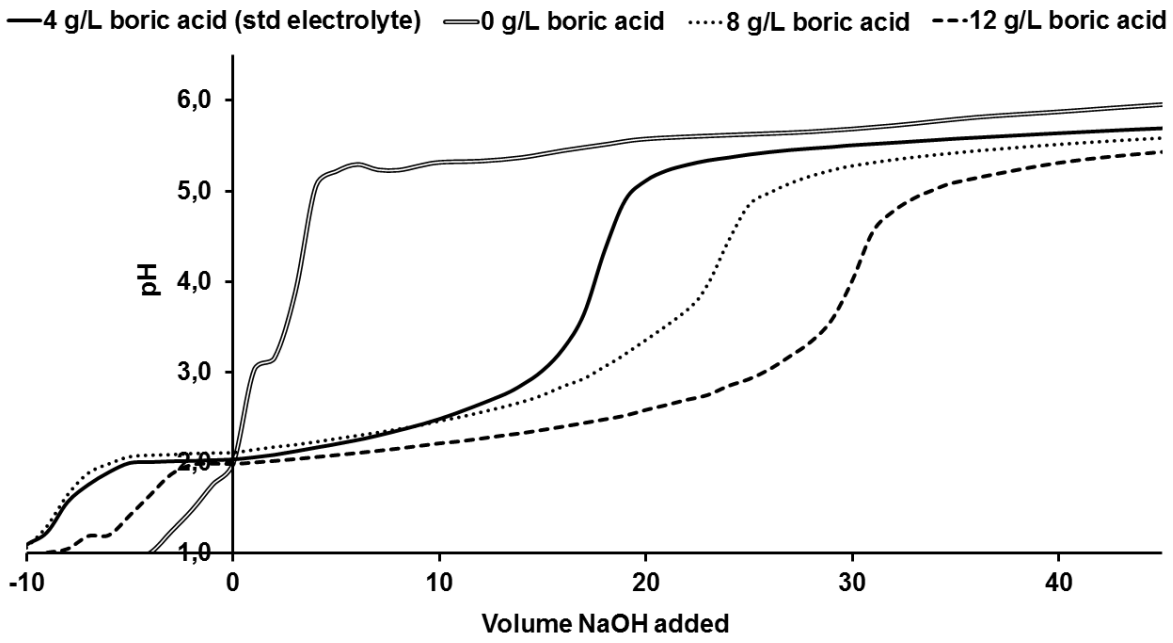

Figure 5.29. Changes in electrolyte pH with increasing NaOH or H_2SO_4 volume of electrolytes with various boric acid concentrations.

Results presented in Figure 5.29 showed that the pH of the electrolyte increased sharply upon the first additions of NaOH for the electrolyte without any boric acid. After more NaOH was added, a plateau was reached after which the pH did not further increase significantly with more added NaOH. This showed that the electrolyte without boric acid did not buffer the pH of the solution. The pH of the electrolytes containing boric acid stayed more constant with the first additions of NaOH and only started increasing after the addition of approximately 10 mL of NaOH. The pH of the electrolyte with the highest concentration of boric acid (12 g/L) stayed constant for longer as more NaOH added and only started sharply increasing at a volume of about 15 mL of NaOH. Therefore, the buffering action and capacity of the electrolyte increased as the boric acid concentration increased.

Optimum buffering capacity of these electrolytes was found between pH 2 and 3 as this was the range at which the pH was most constant upon NaOH addition. Therefore, even though the p*K*a of boric acid is 9.2 (Ji and Cooper, 1996), the solutions containing boric acid had buffering capabilities at the lower pH values of 2 to 3 at which nickel electrodeposition takes place.

Figure 5.30 shows results of experiments to determine the effect of nickel concentration on the buffering capabilities of the electrolyte.

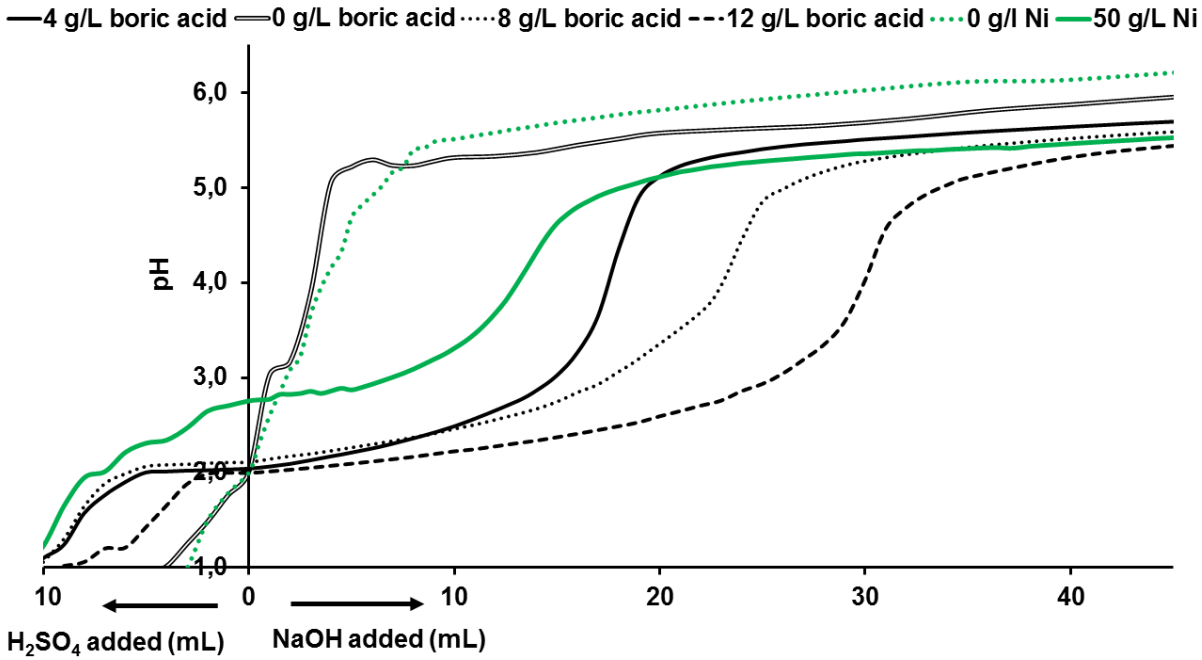

Figure 5.30. Changes in electrolyte pH with increasing NaOH or H_2SO_4 volume of electrolytes with various boric acid and nickel concentrations.

The electrolyte without any nickel in solution showed results similar to that of the electrolyte without any boric acid. The pH increased sharply upon the addition of the first few aliquots of NaOH. The electrolyte without nickel therefore showed low buffering capacity. The solution containing only 50 g/L nickel showed a slightly better buffer capacity but much lower compared with the normal standard electrolyte that contained 80 g/L nickel. This was a clear indication that not only boric acid is needed to achieve good buffer capacity, but that nickel in the electrolyte is also essential. This suggests that a certain nickel–borate complex or various nickel–borate complexes are responsible for the buffer capacity of the nickel sulfate electrolytes. It is, however, also an indication that buffering of the electrolyte takes place during nickel electrodeposition and that boric acid is at least partially responsible. Boric acid might also therefore play an important role in nickel ion transport to the substrate surface as these results suggest that nickel–borate complexes are formed.

Figure 5.31 shows results obtained for the electrolyte containing 4 g/L citric acid instead of 4 g/L boric acid of the standard electrolyte.

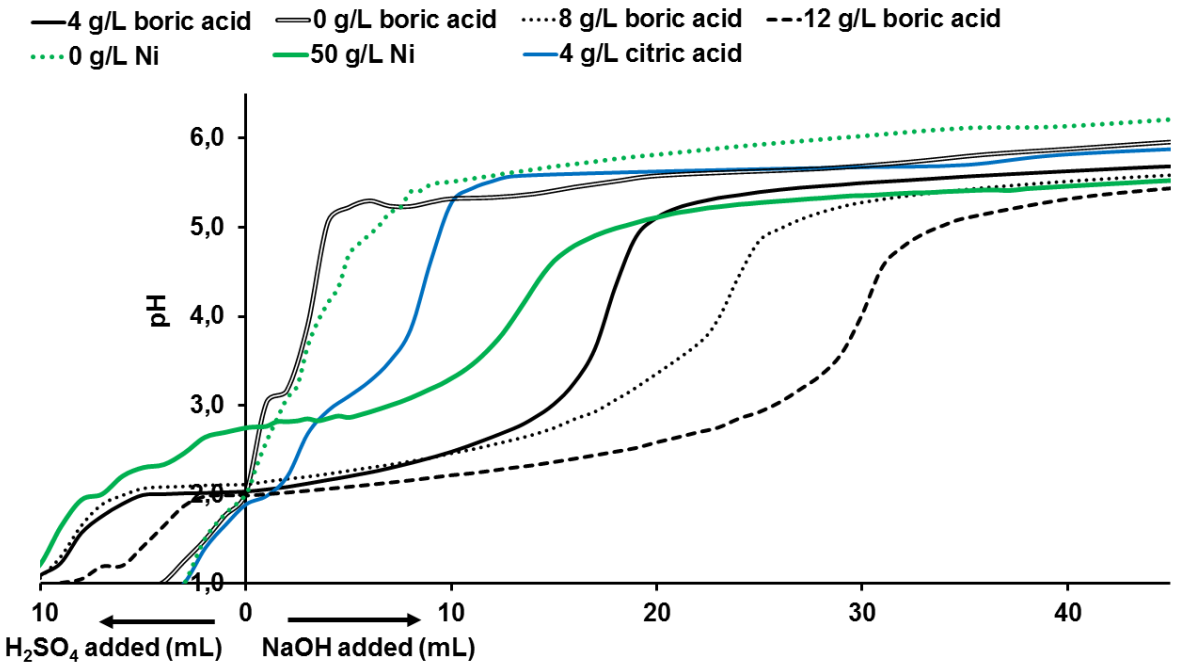

Figure 5.31. Changes in electrolyte pH with increasing NaOH or H_2SO_4 volume of electrolytes with various boric acid, nickel and citric acid concentrations.

The electrolyte containing 4 g/L citric acid instead of boric acid showed slightly better buffer capacity than the solution without boric acid but much less buffer capacity compared with the solutions containing boric acid. This suggested that citric acid was not as effective as a buffer as boric acid and was therefore less recommended.

This observation was not as expected. Citric acid is a tri-protonated acid with p*K*a values of 2.9, 4.3 and 5.2. Therefore, it was expected that citric acid itself, as acid or citrate, should be able to buffer the solution better than boric acid. The fact that the electrolyte is less buffered with the addition of citric acid therefore also suggests that buffering might have been due to citric acid not forming nickel–citrate complexes as effectively under the specific conditions compared with nickel–borate complexes.

Results including the aluminium-containing electrolytes are shown in Figure 5.32.

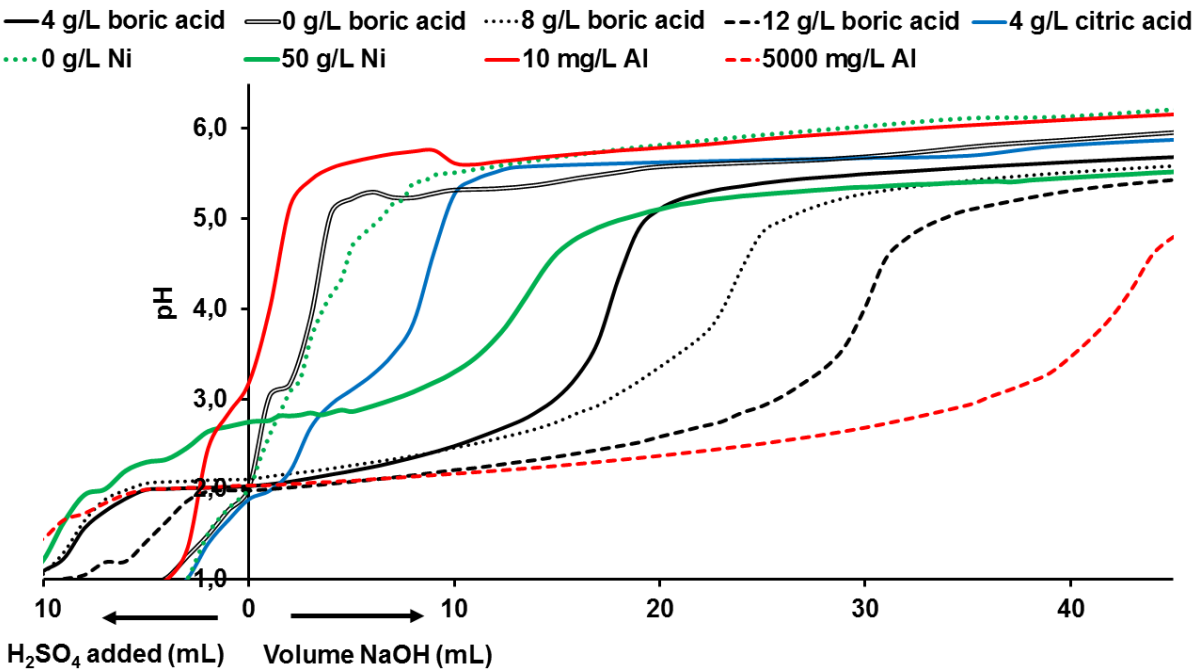

Figure 5.32. Changes in electrolyte pH with increasing NaOH or H_2SO_4 volume of electrolytes with various boric acid, nickel and citric acid concentrations.

Very interesting observations were made for the addition of aluminium impurities to the standard electrolyte. At a low impurity concentration of 10 mg/L, the lowest buffer capacity was observed of all of the electrolytes compared. This was expected as low concentrations of aluminium in the nickel electrolyte are known to be detrimental to the electrodeposition process as well as the morphological outcome. At a very high concentration of aluminium (5000 mg/L), the best buffer capacity of all of the electrolytes was observed. The measured pH of the electrolyte stayed much more constant for up to approximately 40 mL of NaOH added before increasing sharply. Therefore, aluminium at high concentrations improved the buffer capacity and therefore the electrocrystallisation process of nickel from typical sulfate electrolytes. It is proposed that high concentrations of aluminium might be responsible for interaction with nickel and/or borate ions in solution to form complexes that aid in buffer capacity as well as nickel transport towards the substrate surface.

In order to confirm these buffer capacity observations, another test was done. The pH of each electrolyte was monitored during a typical galvanostatical plating process over a period of 2 h at a current density of 220 A/m^2. The results are shown in Figures 5.33 to 5.36. It was expected that the pH of the solution (bulk pH) should decrease with time as more hydrogen ions were produced as electrodeposition of nickel proceeded.

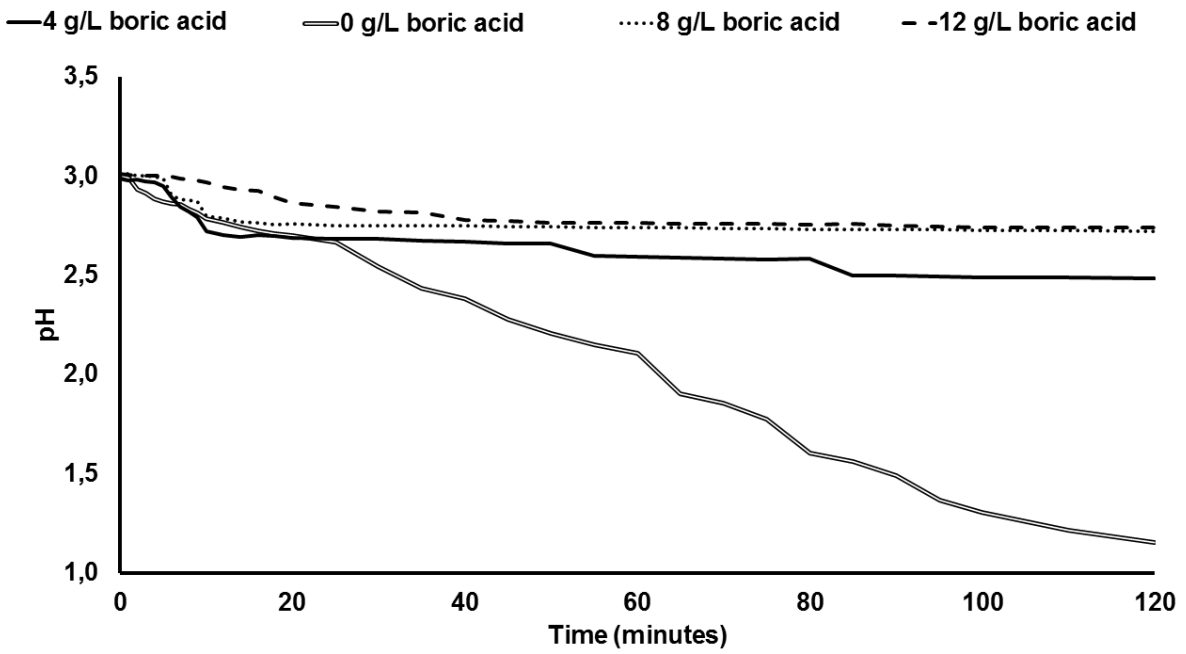

Figure 5.33. Changes in electrolyte pH with increasing time of electrolytes containing various concentrations of boric acid.

The pH of the electrolyte was maintained for longer with increasing boric acid concentration. The buffering of the electrolytes with 8 and 12 g/L boric acid was similar and better compared with the 4 g/L standard electrolyte and the electrolyte without boric acid. The electrolytes with 4, 8 and 12 g/L showed stable pH and good buffering capacity between pH 2.5 and 3. Therefore, an increase in boric acid from 4 g/L to 8 and 12 g/L was not necessarily more beneficial if the plating time was only 120 min. The pH of the electrolyte with 4 g/L boric acid, however, did decrease more toward the end of the 120 min cycle and higher concentrations might have been necessary if longer plating times were used. The pH of electrolytes with 8 and 12 g/L boric acid was still stable after 120 min of plating time. The results from this second pH monitoring technique therefore also suggested that boric acid did play a crucial role in maintaining the pH of the electrolyte and that boric acid was responsible for buffering of the electrolyte. Therefore, the mechanism of boric acid appeared to involve, at least partially, buffering, thereby reducing the effect of the hydrogen evolution reaction.

The influence of nickel concentration compared with boric acid concentration is displayed in Figure 5.34.

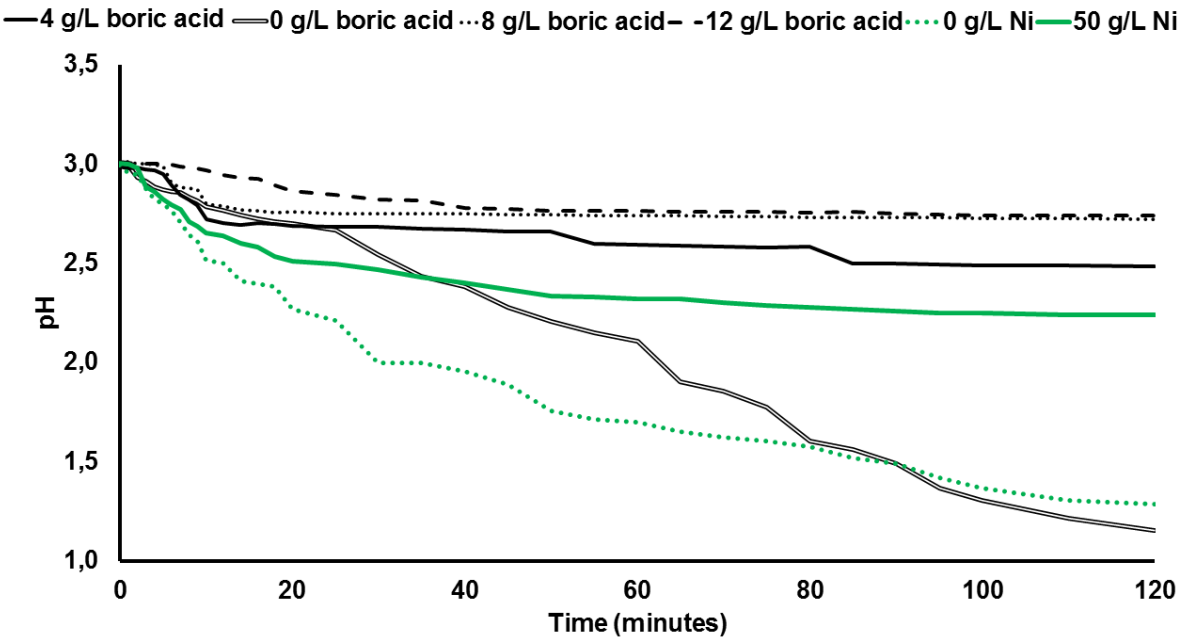

Figure 5.34. Changes in electrolyte pH with increasing time of electrolytes containing various concentrations of nickel and boric acid.

The results showed that the buffering capacity of the electrolytes increased with increasing nickel concentration – from 0 g/L to 50 g/L to 75 g/L (standard electrolyte containing 4 g/L of boric acid). Therefore, the nickel and boric acid combination (and therefore nickel–borate complexes) was essential to obtained effective buffering of the electrolyte in the pH range of 2 – 3.

The electrolyte with 4 g/L boric acid and 0 g/L nickel and the electrolyte with 75 g/L nickel and 0 g/L boric acid both had a low buffering capacity over time. This showed that both nickel and boric acid are important in buffering. The relationship between the concentration of nickel and boric acid is also important and needs to be in equilibrium to achieve desired buffering of the electrolyte.

Results for citric acid- (Figure 5.35) and aluminium-containing electrolytes (Figure 5.36) are included below.

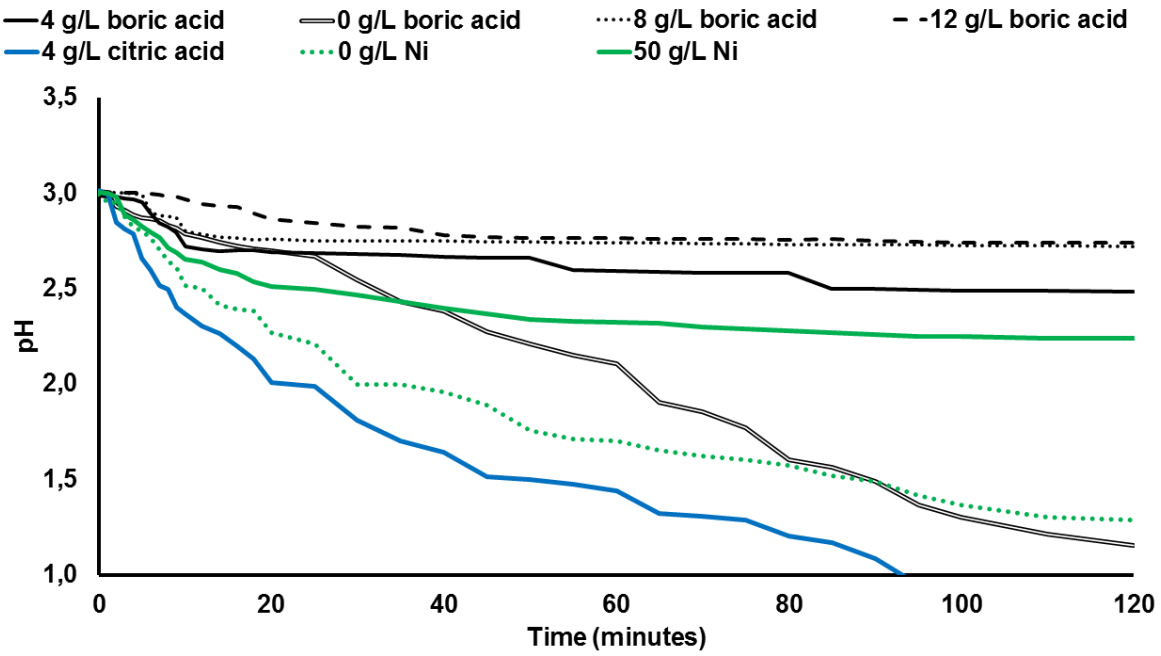

Figure 5.35. Changes in electrolyte pH with increasing time of electrolytes containing various concentrations of nickel, boric acid and citric acid.

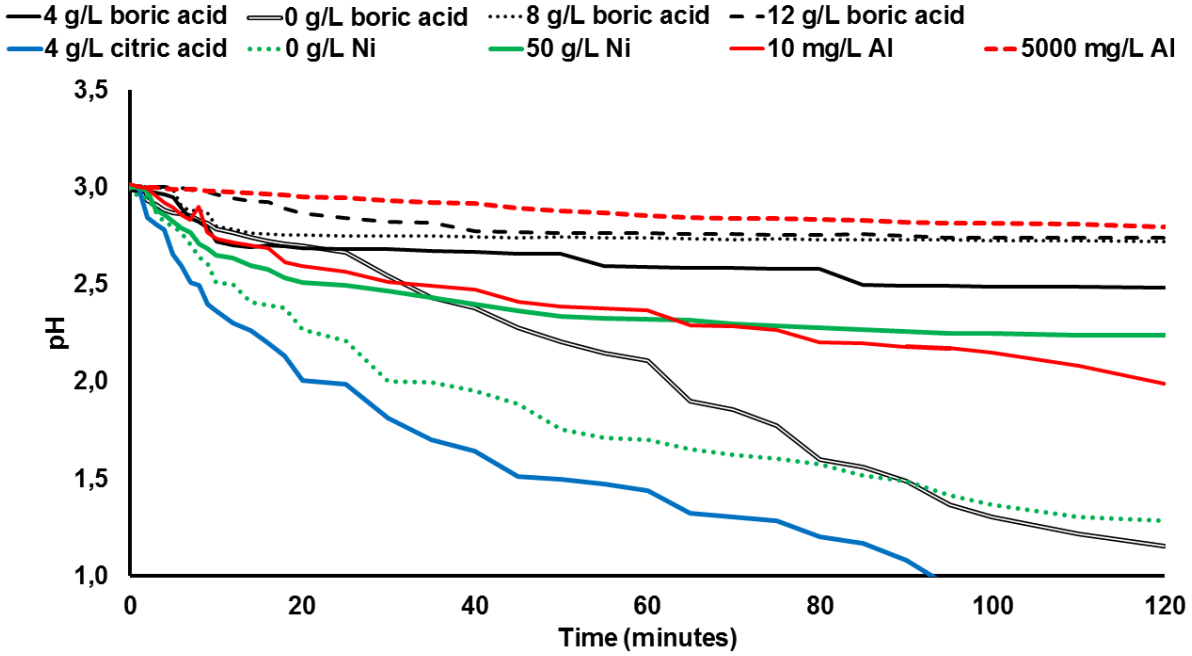

Figure 5.36. Changes in electrolyte pH with increasing time of electrolytes containing various concentrations of nickel, boric acid, citric acid and aluminium.

The lowest buffer capacity was observed for the electrolyte containing citric acid instead of boric acid. The pH of the electrolyte dropped significantly in the first few minutes of applied current and the overall maintenance of the pH of the solution was the lowest of all electrolytes. This confirmed that citric acid was not an effective replacement for boric acid and that even though the p*K*a of citric acid and its derivatives were within the working pH of the electrolyte, it did not buffer the electrolyte effectively.

The electrolyte with 10 mg/L aluminium showed a buffering capacity similar to the electrolyte with 50 g/L nickel. This suggested that aluminium had an effect on buffering of the system and that 10 mg/L aluminium lowered the maintenance of pH, even in the presence of 4 g/L boric acid. Therefore, aluminium appeared to interfere with the relationship between nickel and boric acid, by possibly binding to nickel, boric ions or nickel–borate complexes. The electrolyte with aluminium of 5000 mg/L had the highest buffering capacity of all electrolytes and only dropped very slightly over the plating time of 120 min. At such a high concentration, the aluminium ion itself may bind or complex to nickel, borate or nickel–borate complexes in a different way compared with solutions containing 10 mg/L aluminium, such that a beneficial effect is achieved.

Typical stability data for a system such as this are shown in Figure 5.37.

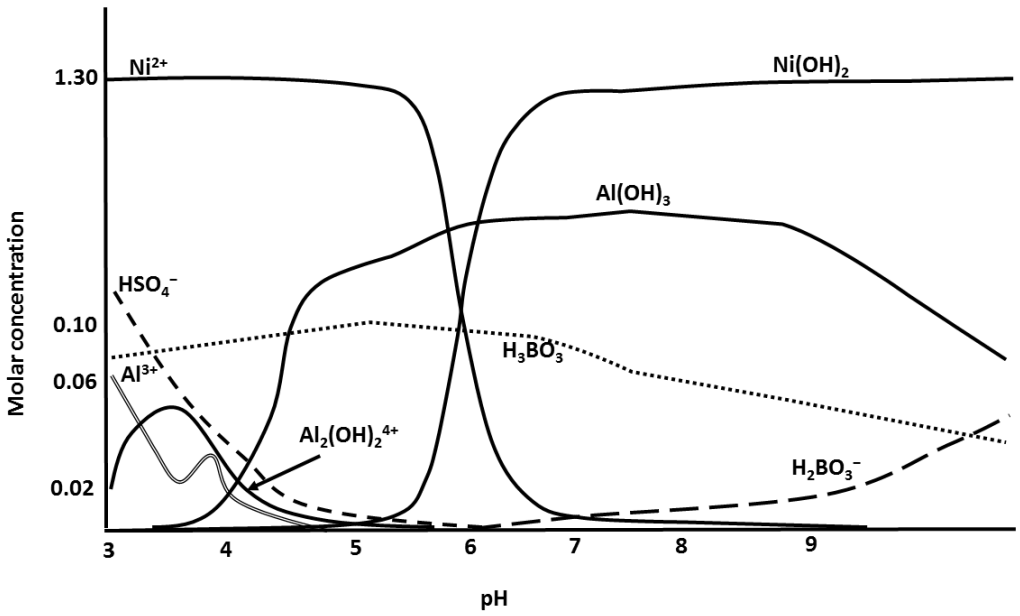

Figure 5.37. Stability data for nickel, aluminium and boric acid at 60 °C (obtained with *Factsage* software).

The most predominant aluminium species at the typical working pH and the reaction thereof is shown in Reaction [32].

$$2Al^{3+} + 2H_2O \rightarrow Al_2(OH)_2^{4+} + 2H^+ \quad [32]$$

At approximately pH 4, aluminium can precipitate as $Al(OH)_3$ and this is probably was what was observed in the deposits at low concentrations of aluminium, such as 5 and 10 mg/L in this study. This was also observed at concentrations of 20, 40, 270 and 540 mg/L of aluminium by Kittelty (2002). At much higher concentrations of aluminium (1350 and 2700 mg/L investigated by Kittelty (2002) and 5000 mg/L in this study), growth of fine-grained, regular morphology and ductile nickel deposits without contamination could be promoted due to a delay in the formation of nickel and aluminium hydroxide species.

Chapter 6
Correlation of changes in polarisation parameters with changes in developing morphology

6.1. Introduction

The results and findings presented thus far clearly show that changes in operating conditions and composition of the nickel sulfate electrolyte can directly be related to changes in polarisation parameters. A method for measuring E_n and E_p was presented and the relationship between E_n and E_p is shown to change with changes in the relationship between nucleation and growth processes during nickel electrodeposition. Therefore, these polarisation parameters can be measured and used as an indication of changes in the electrolyte.

It is also shown that changes in the composition and conditions of the electrolyte can be directly related to changes in the developing morphology as the nickel deposit grows. The differences in morphology due to changes in concentrations in the electrolyte, temperature and pH, the addition of buffering agent and the presence or absence of impurities or additives are shown to directly influence the structure, morphology, strain and hydrogen pitting of the nickel electrodeposits. This chapter explores whether there is any correlation between the measured E_n and E_p and the morphology of nickel deposits produced from various electrolytes.

6.2. First region of similar morphology and strain – highly cathodic E_p and positive ΔE values

By using the measured E_n and E_p and the calculated ΔE values, a diagram relating these parameters can be drawn. Taking E_p, as the measure of growth itself, as the independent variable plotted on the x-axis, then grain refinement (or a measure of inhibition) expressed by ΔE is plotted as the dependent variable on the y-axis. A diagram specific to nickel electrodeposition from sulfate electrolyte can then be drawn. The diagram for the standard electrolyte of 75 g/L Ni^{2+}, 80 g/L Na_2SO_4, temperature of 60 °C, pH 3 and 4 g/L boric acid added is shown in Figure 6.1. This point is also used as a reference point for all the other deposits from various electrolytes. This point refers to the average polarisation parameters of five repeat measurements (Appendix A).

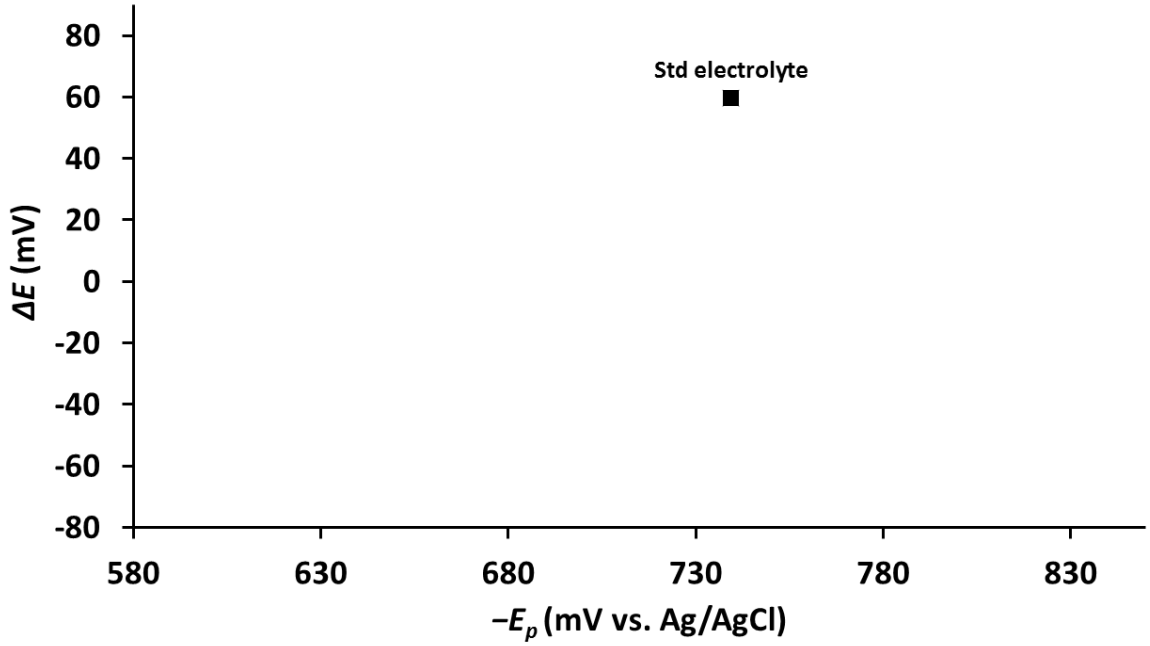

Figure 6.1. Polarisation diagram for parameters measured for the standard electrolyte.

Figure 6.2 shows this reference point in relation to other points obtained for electrolytes with varying conditions.

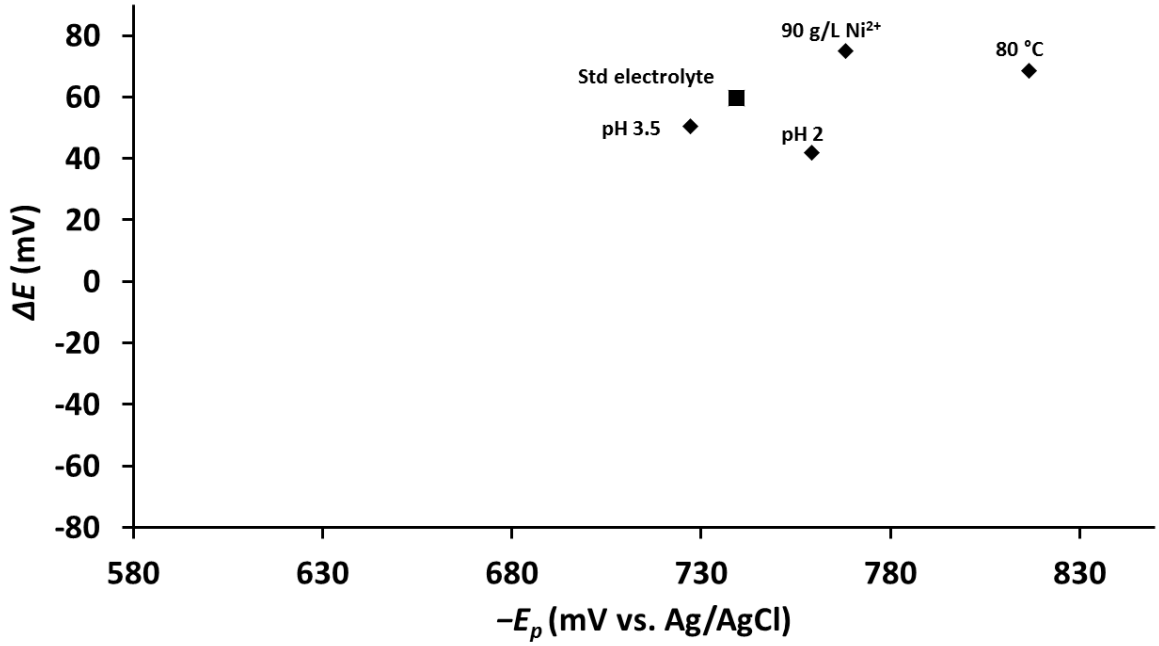

Figure 6.2. Polarisation diagram measured for changes in conditions of the electrolyte to 90 g/L Ni^{2+}, 80 °C, pH 2 and pH 3.5.

Other polarisation measurements for the increase in boric acid are shown in Figure 6.3.

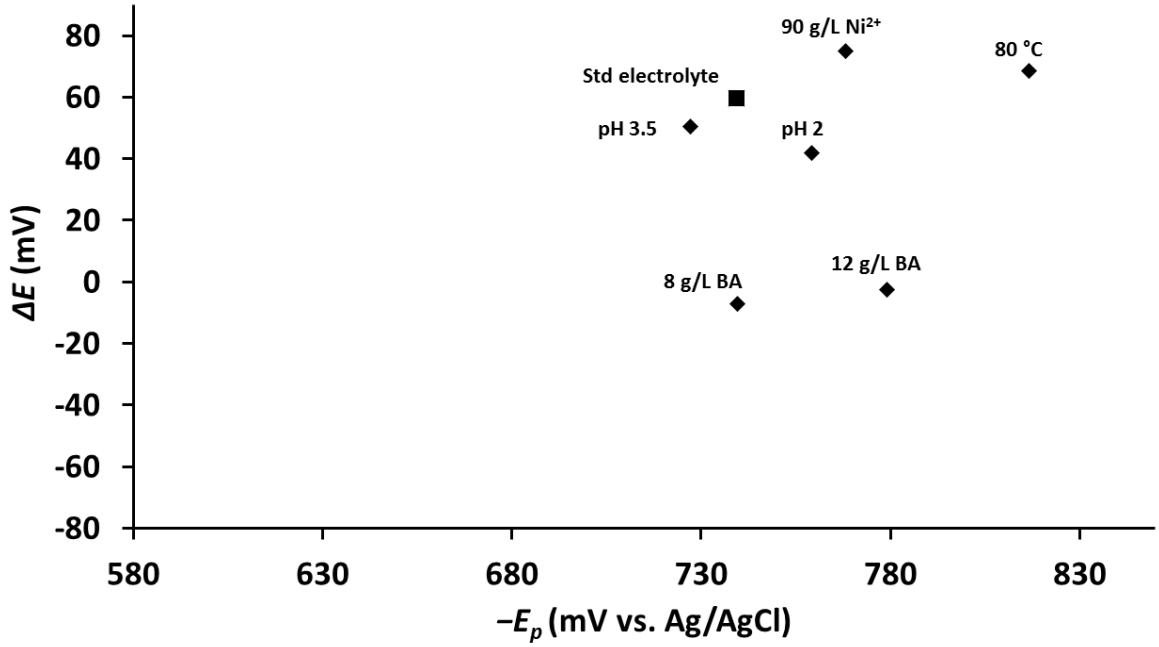

Figure 6.3. Polarisation diagram including points for increases in boric acid (BA) to 8 g/L and 12 g/L.

The points in closest proximity to that of the standard electrolyte are those at pH 2 and pH 3.5. The E_p values for these points are fairly cathodic and their ΔE values are highly positive. Therefore, the E_p relates to high growth rates while the ΔE indicates frequent nucleation during these growth processes. This observation is also made for the higher nickel concentration of 90 g/L Ni^{2+} and the increased temperature to 80 °C. For all of these points, the polarisation diagram indicates that the inhibition, nucleation and growth processes are in balance.

The points obtained for the increased boric acid concentrations of 8 g/L and 12 g/L also show cathodic E_p values similar to the other points discussed, but both of these points have slightly negative ΔE values. This therefore indicates that the growth of the deposits is adequate but that inhibition or nucleation is less ideal. It is not clear why this is observed because good quality, desired morphology deposits were obtained at increased boric acid concentrations (Chapter 5, Section 5.6). Therefore, this observation is attributed to the buffering or transport effect of the boric acid mechanism that is still not fully understood.

Figures 6.4, 6.5 and 6.6 show the stepwise inclusion of polarisation points obtained for electrolytes with the additives SLS, SAC and PYR in relation to the standard electrolyte.

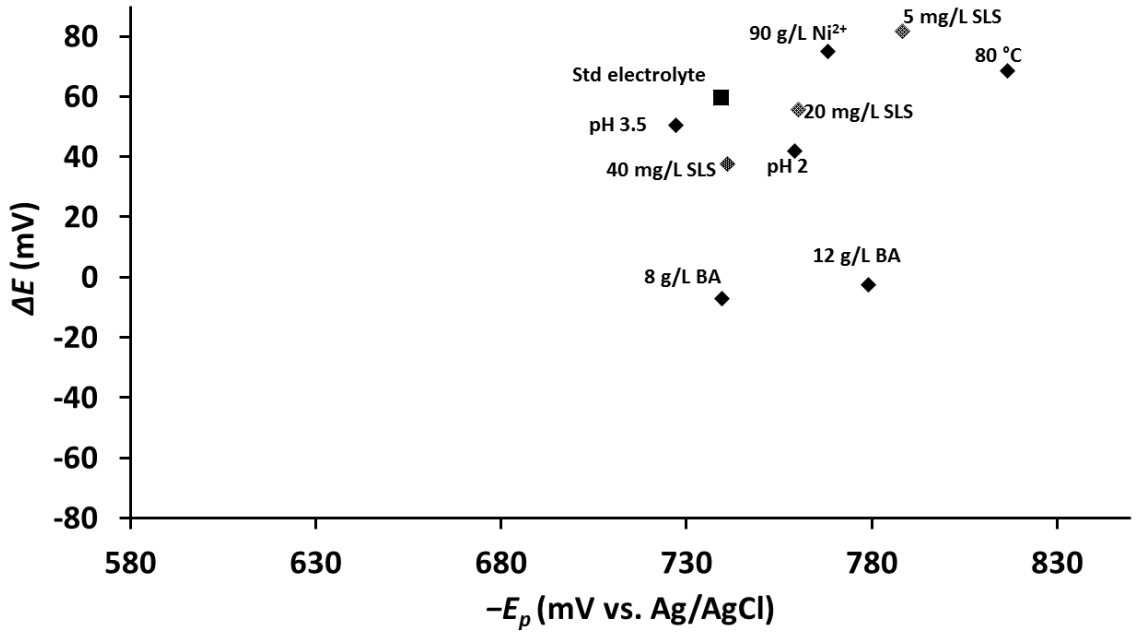

Figure 6.4. Polarisation diagram including polarisation parameters for electrolytes with varying concentrations of SLS additive.

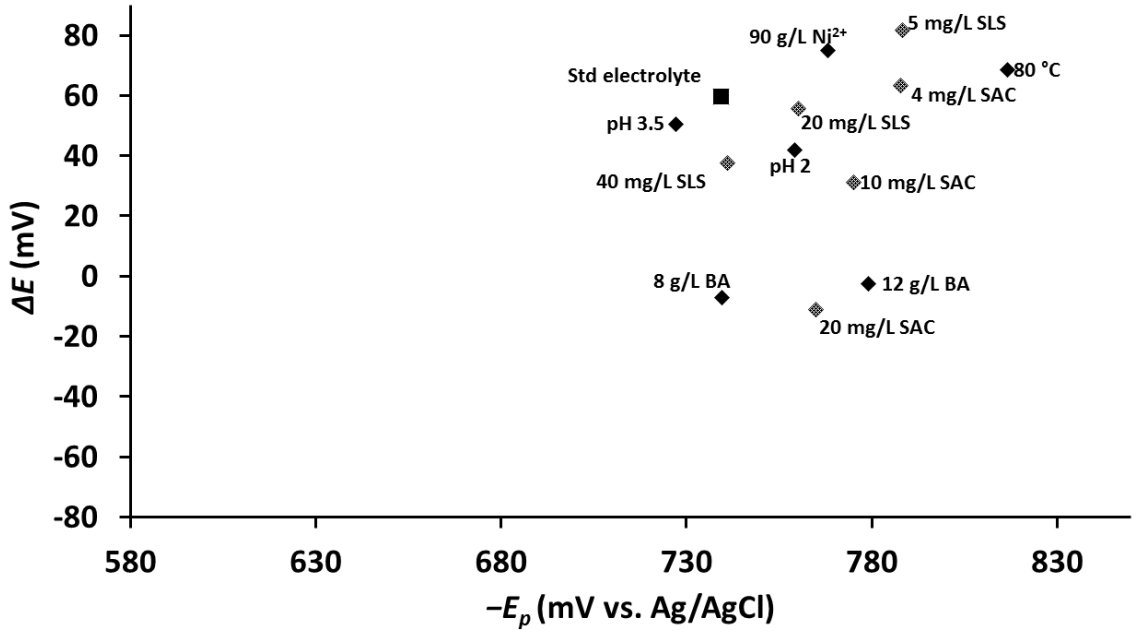

Figure 6.5. Polarisation diagram including polarisation parameters for electrolytes with varying concentrations of SAC additive.

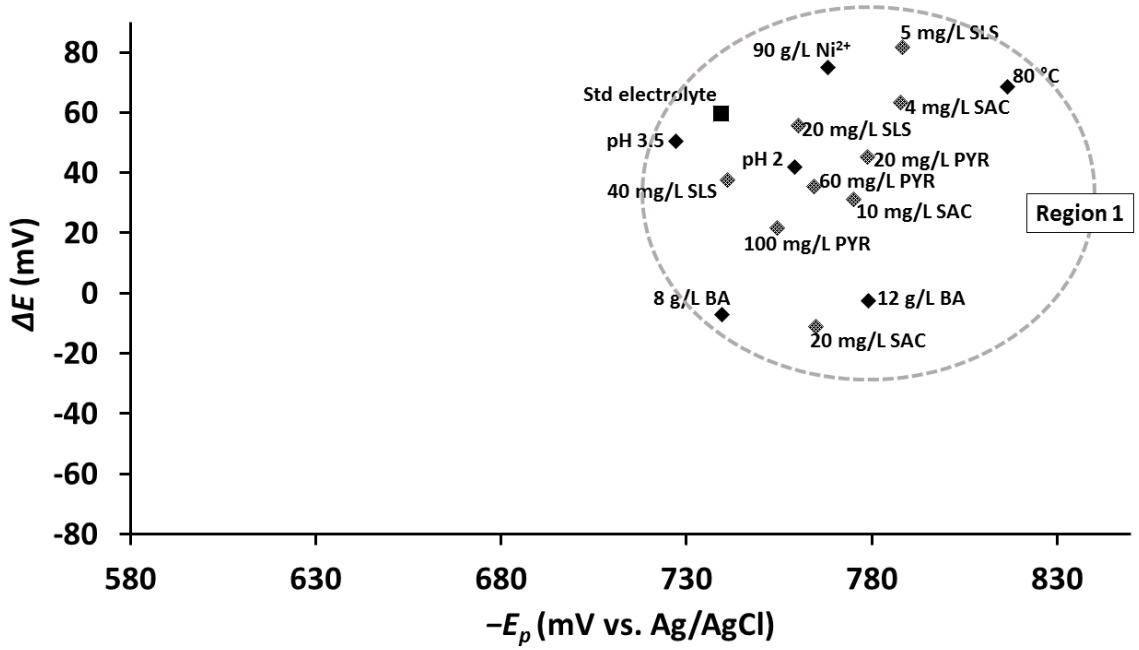

Figure 6.6. Polarisation diagram including polarisation parameters for electrolytes with varying concentrations of PYR additive. Region 1 of similar morphologies is also indicated by a dotted line.

Polarisation parameters for the following electrolytes are shown in Region 1 (Figure 6.6): standard electrolyte, higher Ni^{2+} concentration of 90 g/L, increased temperature to 80 °C, higher boric acid concentrations of 8 and 12 g/L, pH changes to 2 and 3.5 and all concentrations of SLS, SAC and PYR. Morphologies are compared in Figure 6.7.

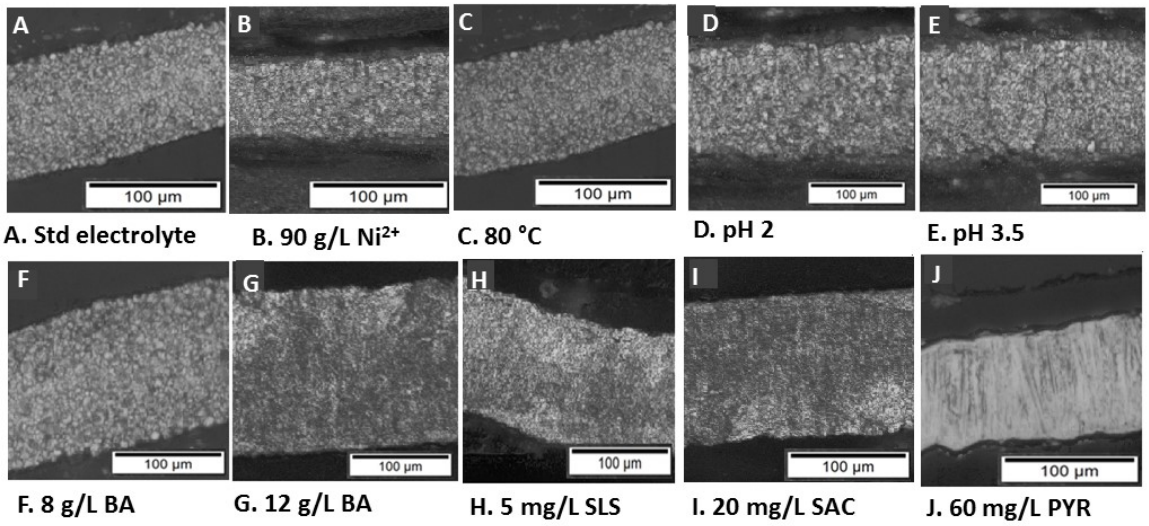

Figure 6.7. Microstructures obtained for deposits from electrolytes from Region 1. BA refers to boric acid.

Deposits obtained from all electrolytes in Region 1 were very similar in morphology. All of the deposits were either UD, FT or UD/FT type. All were fine-grained, low in strain and hydrogen pitting, level and regular in structure. High current efficiencies were calculated for these deposits and the wettability and conductivity of the electrolytes were acceptable (Chapter 5, Sections 5.2, 5.4, 5.5 and 5.7). All of these deposits had polarisation parameters with E_p more cathodic than approximately −700 mV. This indicated that the rate of growth, as well as the manner in which growth proceeds, are ideal in this range.

The ΔE values for these points were mostly positive and even very large, such as the values for the 80 °C, 90 g/L Ni^{2+} and 5 mg/L SLS electrolytes. Most of the electrolytes included in this region had ΔE values between 20 and 60 mV. Three points had slightly negative ΔE values: 8 g/L and 12 g/L boric acid and the 20 mg/L SAC electrolytes. The ΔE value, and therefore E_n, plays a very crucial role in the balance between nucleation and growth processes. This balance is more complicated than to expect a desired relationship between nucleation and growth at all positive ΔE values. It can, however, be said that at a combination of E_p more cathodic than 700 mV and ΔE between 20 and 60 mV, a good relationship can be expected and a desired, good quality deposit of UD/FT-type morphology and low strain is produced.

The three points with negative ΔE values also included the electrolyte with the highest concentration of SAC (20 mg/L). The presence of SAC, especially at higher concentrations, might therefore also be involved in transport of nickel ions or buffering of the electrolyte in some way. This could be related to the fact that SAC has a lone pair of electrons to donate to nickel ions, thereby causing a stabilisation effect and more frequent nucleation of the formed nickel ions (Ciszewski *et al*., 2004; Rashidi and Amadeh, 2009).

It is interesting that the morphology of the deposits obtained from electrolytes at all PYR concentrations was far more FT than the other deposits within this region. It is known that PYR molecules aid in nickel deposition by directly adhering to the substrate surface, thereby influencing inhibition (Mohanty *et al*., 2001; Mohanty *et al*., 2005). This alters the mechanism of nickel deposition onto the substrate itself. The PYR electrolyte points were still included in Region 1 because all deposits were still very low-strained and almost no hydrogen pitting was observed. Deposits were compact and regular and still of desired morphology, even though the morphological type was more FT compared with the overall morphology in this region of UD or UD/FT.

It is also observed that the ΔE values decreased with increasing concentrations of SAC, SLS and PYR. The E_p values also followed this trend. This indicated that, at higher concentrations of additives, the growth frequency and rate decreased slightly to compensate for changes in nucleation frequency and inhibition intensity in order to maintain the balance between nucleation and growth. The effect of additives on the substrate surface (inhibition) or transport of nickel ions towards the substrate or the nickel reduction rate (because the additives can donate electrons) is therefore proposed to increase at increasing concentration of the specific additive.

6.3. Second region – highly cathodic E_p and negative ΔE values

Polarisation parameters for the next four electrolytes are shown in Figure 6.8. These points are grouped together as Region 2.

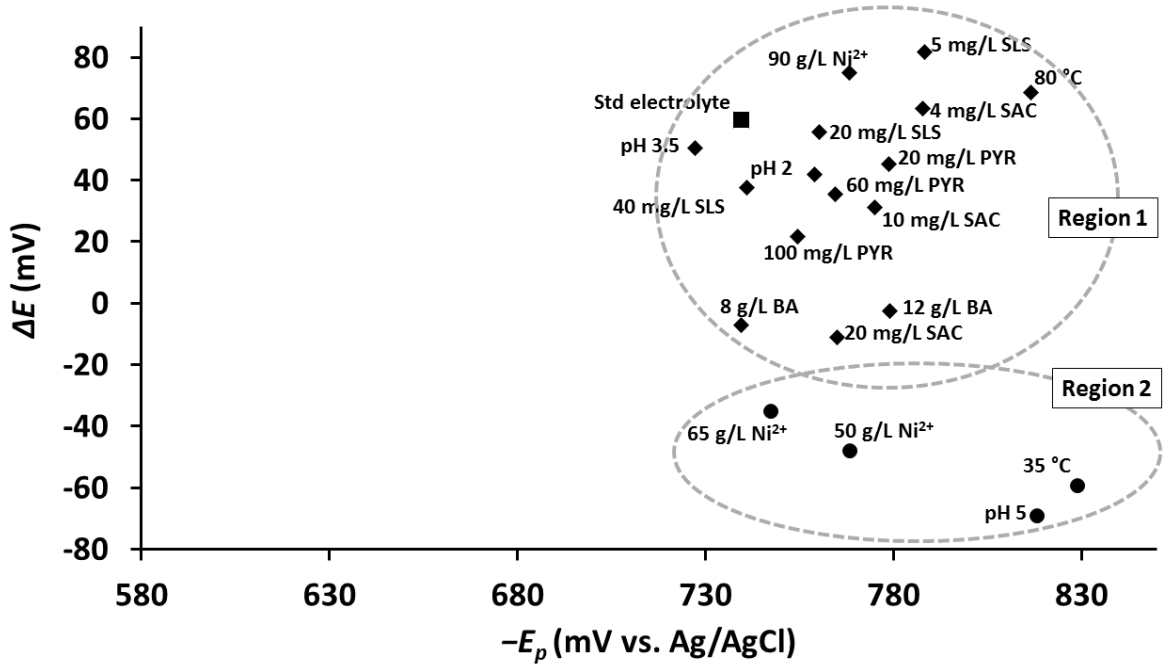

Figure 6.8. Polarisation diagram including polarisation parameters for the following electrolytes: lower Ni^{2+} concentrations of 50 g/L and 65 g/L, pH 5 and lower temperature of 35 °C. Region 2 of similar morphologies is also indicated by a dotted line.

The points in Region 2 are for the electrolytes containing low Ni^{2+}, and of low temperature and high pH. The fact that the E_p in this region is highly cathodic (more negative than 730 mV) indicates fast and frequent growth. These points all have highly negative ΔE values, which is indicative of less frequent or slower nucleation and inadequate inhibition. The polarisation parameters therefore indicate or predict the formation of large irregular grains

with high internal strain. This is observed (Figure 6.9): the morphologies of these deposits were generally of BR type and pitting and strain cracks were commonly observed.

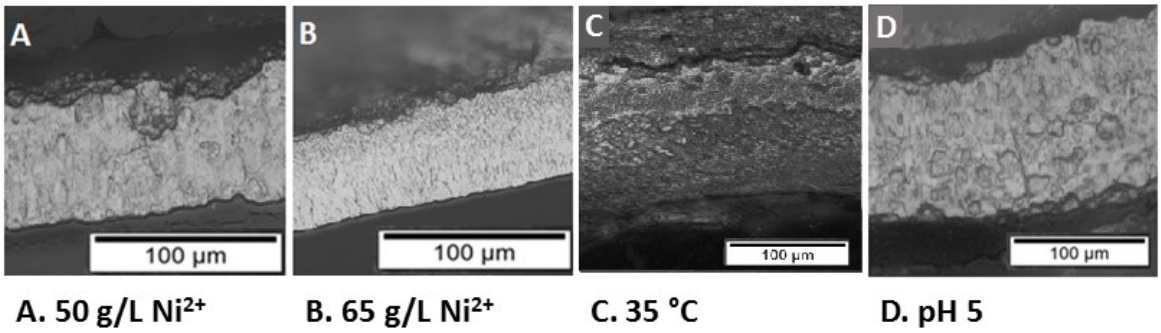

Figure 6.9. Microstructures obtained for deposits from electrolytes included in Region 2.

This was expected at a pH of 5, considering that this is the pH at which $Ni(OH)_2$ is likely to form and can co-deposit or cause internal strain (Amblard *et al*., 1983; Armyanov and Sotirova-Chakarove, 1992; Ji and Cooper, 1996; Lantelme and Seghiouer, 1998; Kittelty, 2002).

At low temperatures, the transport of nickel ions and the rate of reaction are expected to be lower and therefore loosely packed, brittle deposits with high strain are expected (Kuhn, 1971; Ji and Cooper, 1996; Lantelme and Seghiouer, 1998; Holm and O'Keefe, 2000; Kittelty, 2002; Lupi *et al*., 2006).

At low Ni^{2+} concentrations, the viscosity, density and conductivity of the electrolyte are affected. Formation and transport of nickel ions are limited, causing poor morphology, irregular growth and high internal strain (Ji and Cooper, 1996; Holm and O'Keefe, 2000; Kittelty, 2002; Wu *et al*., 2003).

Even though the effects of high pH, low temperature and low Ni^{2+} concentration are very different, as are the mechanisms by which the nickel electrodeposition is influenced by these changes in the electrolyte, their effect on the morphology is similar. It is clear that the effect on the measured polarisation parameters is also similar and therefore data points in this region measured for any electrolyte indicated similar poor morphology and highly strained deposits.

6.4. Third region – less cathodic E_p and negative ΔE values

The effect of the presence of impurities of cobalt and copper are shown in Figure 6.10.

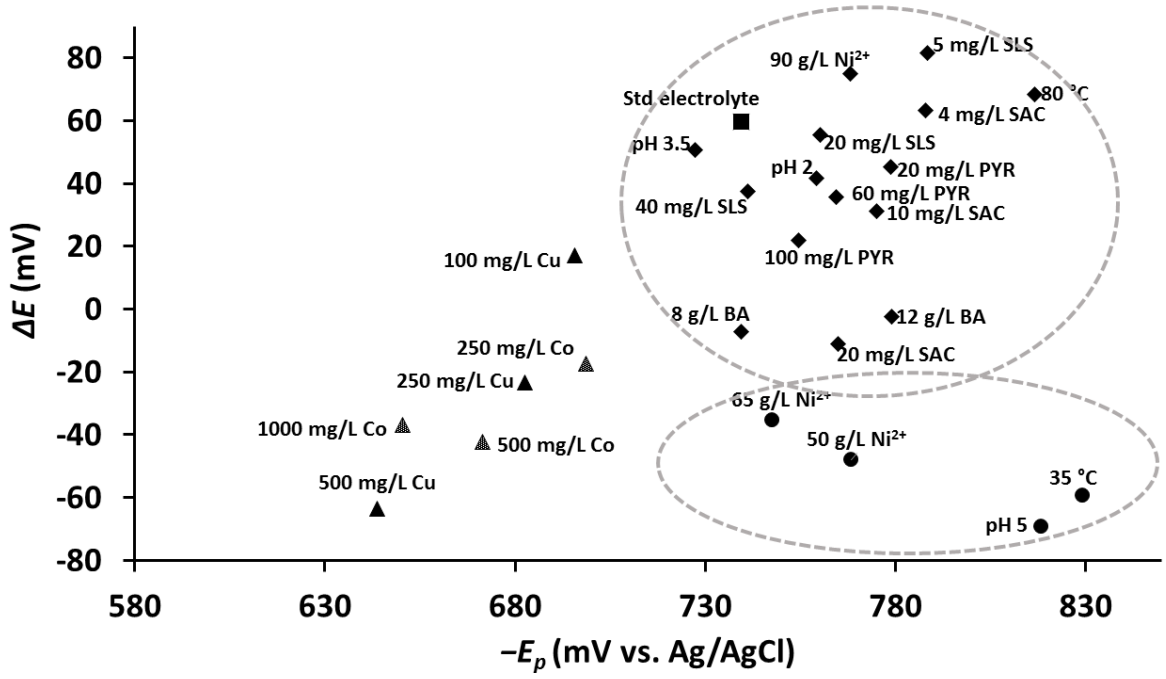

Figure 6.10. Polarisation diagram including points for electrolytes containing cobalt and copper impurities.

The points for the electrolytes with cobalt and copper impurities have less cathodic E_p values (between 630 mV and 730 mV). This is indicative of lower growth rates that produce poor quality, irregular BR-type deposits. The ΔE values are also largely negative, indicating ineffective inhibition and nucleation. The ΔE and E_p values decreased with increasing concentration of the impurity, especially for copper. This is indicative of the increasing effect of the impurity as the concentration increased.

Cobalt and copper are known to co-deposit with nickel and therefore highly strained deposits are expected (Gogia and Das, 1991; Kittelty, 2002). The relationship between nucleation and growth suggested by the measured polarisation parameters for electrolyte with these impurities concurs with this and suggests that highly strained, cracked deposits with irregular large growth crystals and large pinholes would preferentially form. The results also suggest that the effects of cobalt and copper are fairly similar and therefore similar morphologies are expected.

The polarisation points for aluminium impurities are included in Figure 6.11.

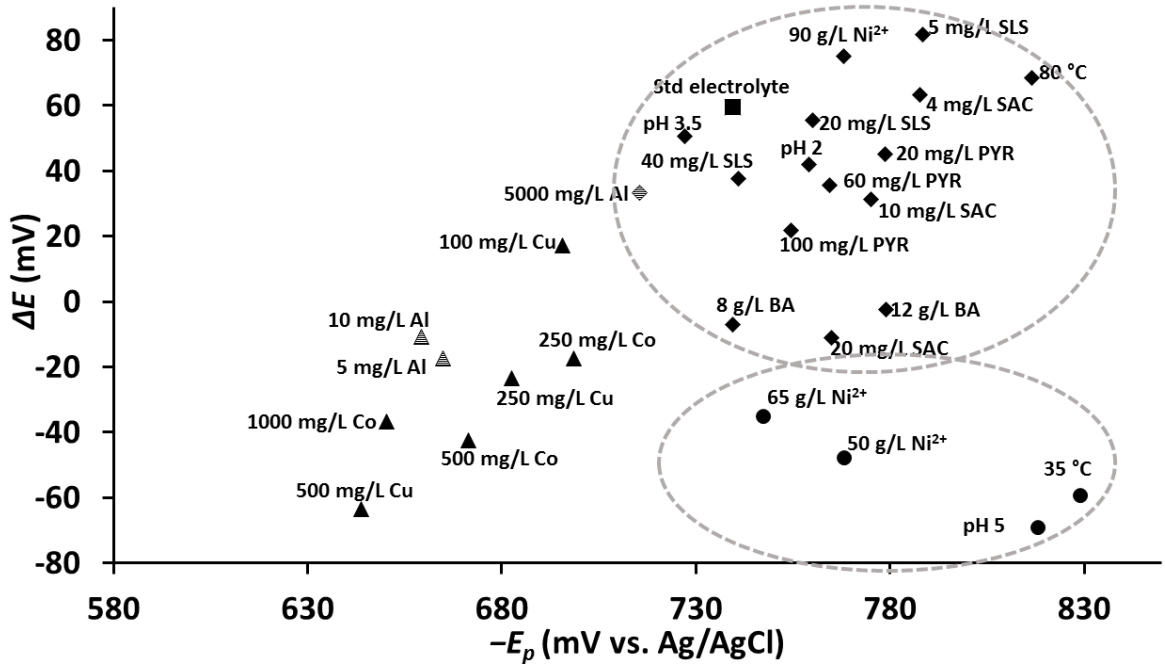

Figure 6.11. Polarisation diagram including polarisation parameters for aluminium impurities of 5 mg/L, 10 mg/L and 5000 mg/L.

The electrolytes with low concentrations of aluminium (5 and 10 mg/L) showed polarisation points in the same region as the cobalt and copper impurities. The E_p values were less cathodic compared with those of Regions 1 and 2 and the ΔE values were negative. The electrolyte containing 5000 mg/L aluminium, however, had very different polarisation parameters, which can be included in Region 1. The ΔE value was positive and the E_p value much more cathodic compared with the other aluminium electrolytes. This compares well to expectations, because the morphology obtained for deposits in the presence of high concentrations of aluminium (more than 2700 mg/L) (Kittelty, 2003) was similar to UD type and compared well with the morphology obtained from the standard electrolyte. Therefore, the polarisation parameters also predicted that a 5000 mg/L aluminium impurity in the electrolyte is beneficial to the morphology and internal strain.

The effect of selenium in the electrolyte is included in Figure 6.12. The polarisation points for selenite and selenate impurities are similar to those obtained for the other impurities. The ΔE values were negative and the E_p values less cathodic. Therefore, the polarisation parameters predict highly strained, brittle deposits. The morphologies of deposits from these electrolytes confirmed this prediction. This confirmed the results of high strain and delamination in the presence of selenium, as described by Voogt *et al*. (2017).

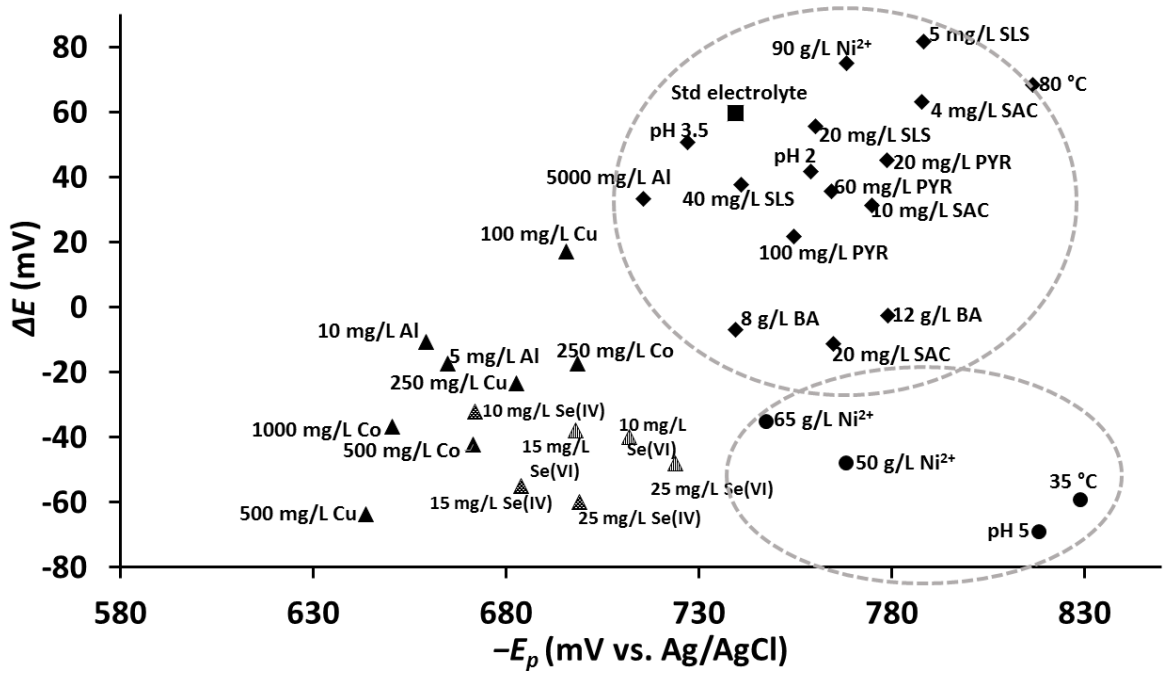

Figure 6.12. Polarisation diagram also containing polarisation parameters for selenium impurities: Se(IV) and Se(VI) at concentrations of 10, 15 and 25 mg/L.

Figure 6.13 contains polarisation data for the electrolytes without boric acid added. Similarly, these polarisation parameter points fall in the region with low E_p and negative ΔE values.

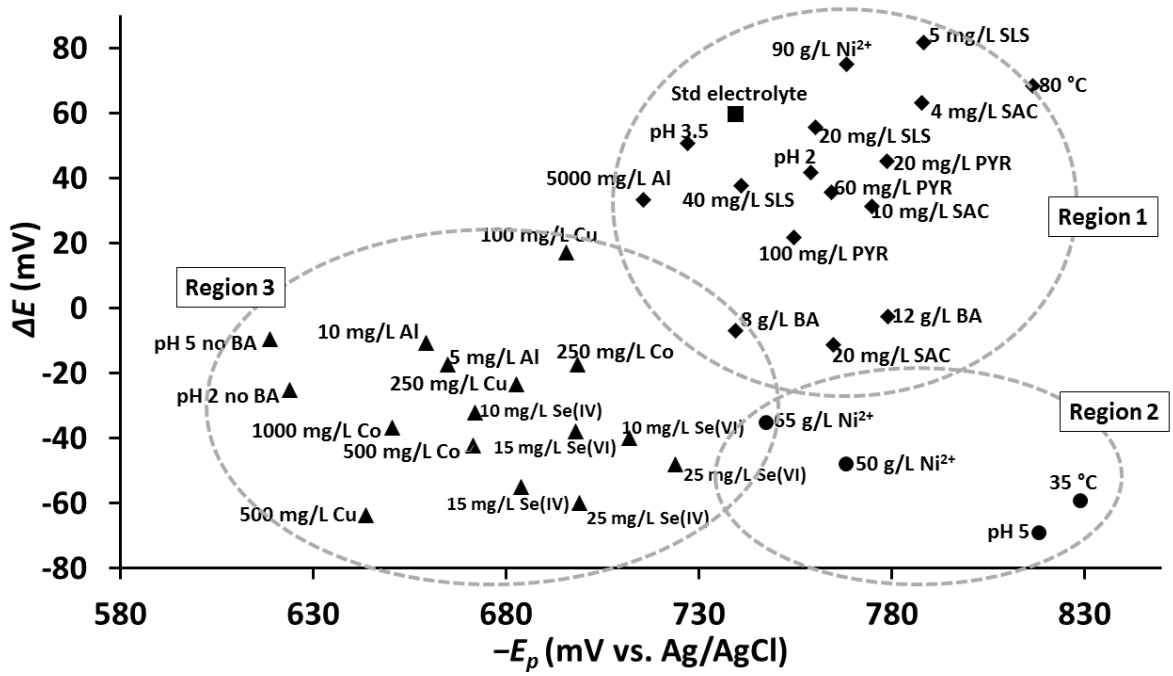

Figure 6.13. Polarisation diagram containing points for electrolytes containing no boric acid (BA) at different pH values of 2 and 5.

Polarisation parameters for the electrolytes without any boric acid had the lowest E_p values of all electrolytes. This is indicative that irregular growth at low rates was obtained, irrespective of the pH. Boric acid has a more important function compared with electrolyte pH itself, because the effect of changes in the boric acid concentration shift the polarisation parameters much more, compared with that of changes in pH. The ΔE values for both electrolytes were negative, indicating less ideal nucleation and inhibition. These polarisation parameters therefore also suggested that boric acid plays a crucial role in either transport or buffering during deposition of the nickel from its complex on the cathode surface.

It was also interesting to find that the polarisation points on the diagram for high aluminium concentration (5000 mg/L) and the standard electrolyte (4 g/L of boric acid), as well as the increased boric acid electrolytes (8 and 12 g/L), were in the same region, while the electrolytes without boric acid fell in another region. It therefore appears that Region 1 may also be indicative of electrolytes with desired buffering or transport capabilities. Considering that the electrolytes with additives fell in the same region may even suggest that high concentrations of aluminium and ideal concentrations of boric acid influence inhibition and the species adhere to the substrate surface, thereby promoting nickel deposition in the same mechanistic way as surface agents such as SLS. Further investigations of this method might even shed some light on more accurate mechanisms.

The morphologies of the deposits from Region 3 were either FT-, BR- or FT/BR-type grains with large pinholes, strain, cracks, hydrogen pitting and irregular surfaces. Dark areas were also visible within the structures of deposits, which might be indicative of contamination of the deposits – especially in the case of copper, cobalt, aluminium and selenium impurities.

A comparison is shown of the morphologies of points in Region 3 in Figure 6.14.

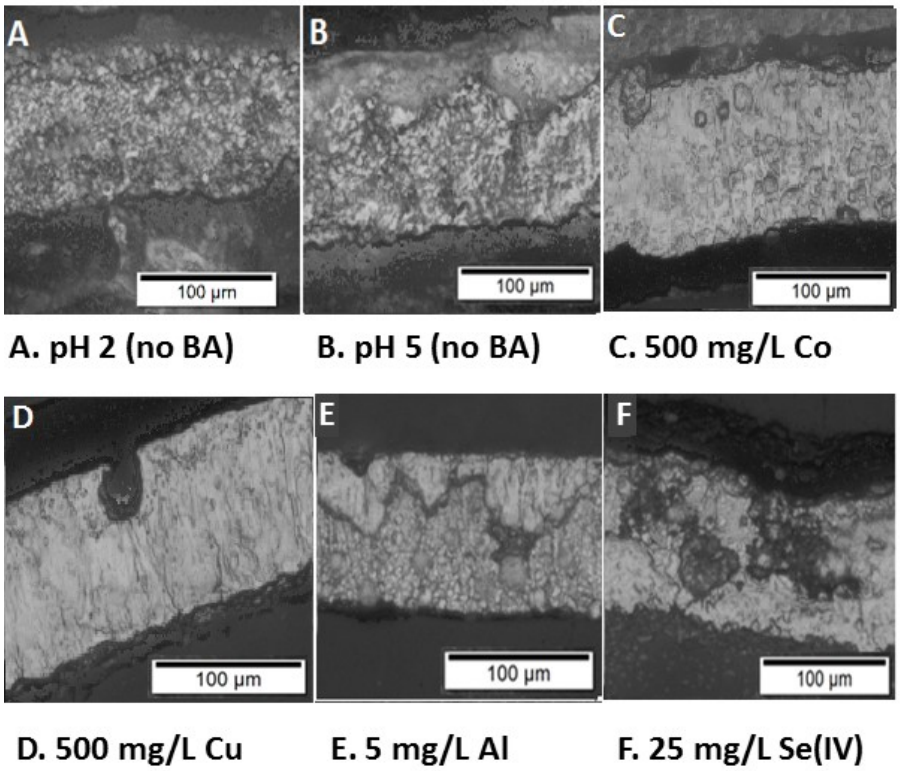

Figure 6.14. Micrographs showing morphology and strain characteristics of various deposits produced from electrolytes from Region 3. BA refers to boric acid.

6.5. Fourth region – less cathodic E_p and positive ΔE values

Electrolytes with citric acid added (without boric acid) had polarisation parameters with lower E_p values and low but positive ΔE values. The 4 g/L and 8 g/L citric acid electrolytes had similar polarisation values compared with the impurity parameters in Region 3. The ΔE value for the 12 g/L electrolyte was the most positive. The addition of citric acid to the electrolyte caused a decrease in E_p at all concentrations, such that growth was more affected than nucleation.

The morphology of the samples obtained under these conditions was mostly FT-type grains with some irregular growth areas and even some fine grains. Some strain and pitting were observed, but not for all the deposits. The morphology and strain characteristics seemed to be more acceptable than deposits from Region 3, and less desirable than deposits from Region 1.

Polarisation parameters for electrolytes containing citric acid instead of boric acid are shown in Figure 6.15.

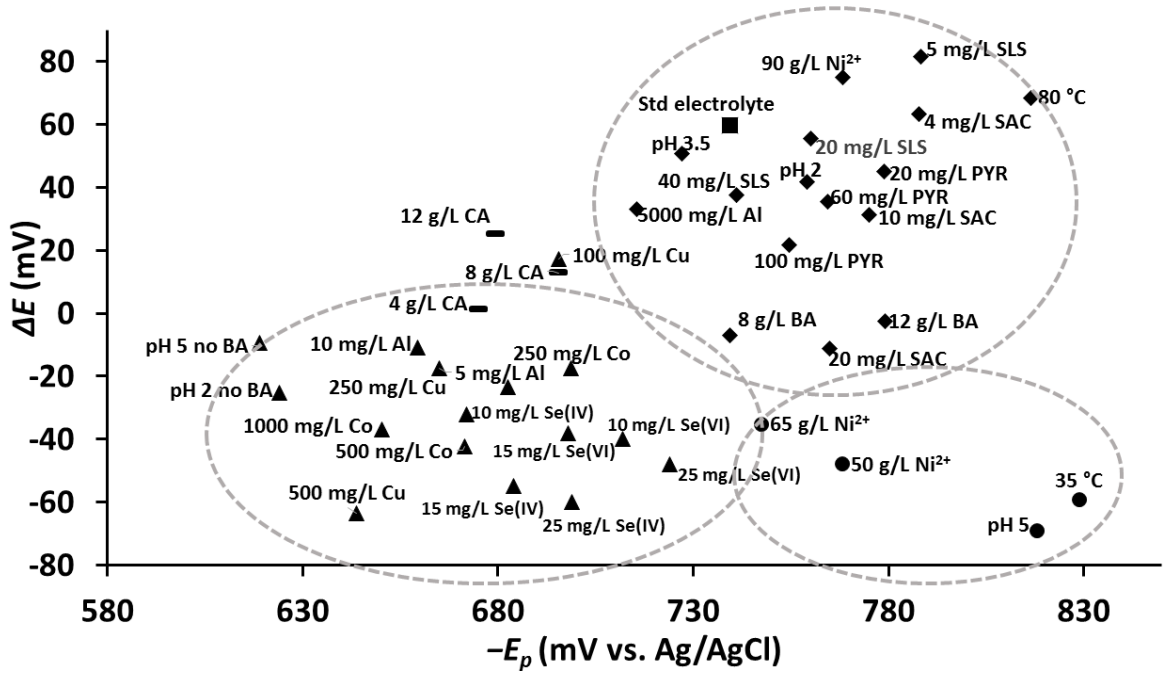

Figure 6.15. Polarisation diagram containing parameters for electrolytes containing 4, 8 and 12 g/L citric acid (CA) instead of boric acid (BA).

Other points in this range include the intermediate temperature of 45 °C and the electrolytes with Na_2SO_4 concentrations of 70 g/L and 100 g/L. All of these points are shown in Figure 6.16.

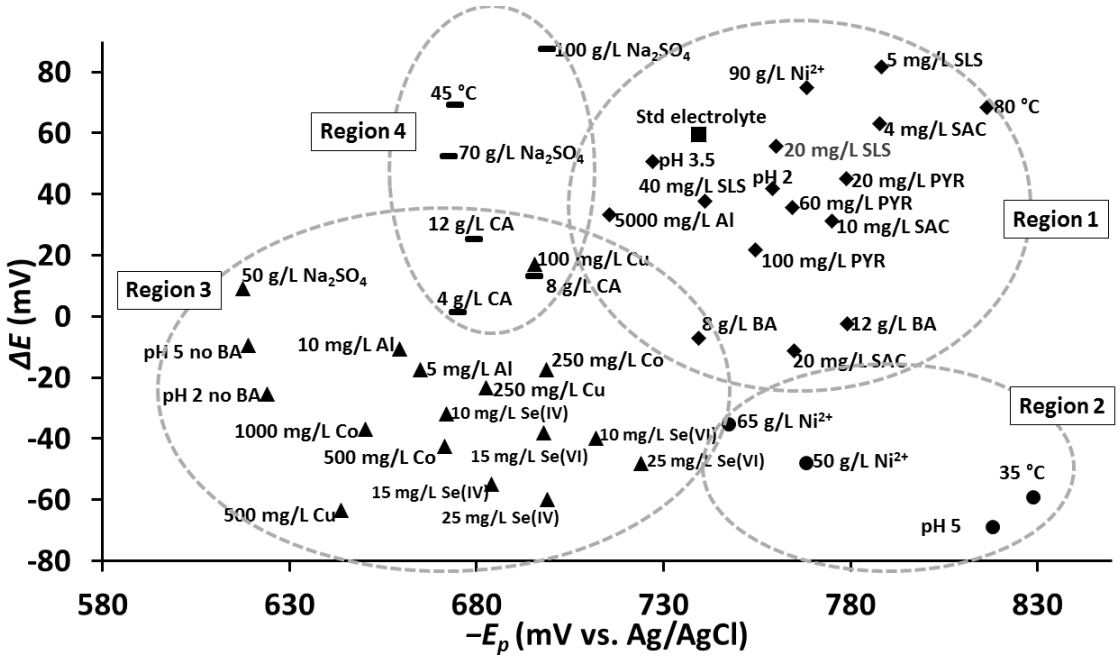

Figure 6.16. Polarisation diagram showing polarisation points for 4, 8 and 12 g/L citric acid (CA) as well as 70 and 100 g/L Na_2SO_4 and the intermediate temperature of 45 °C.

The main purpose of Na_2SO_4 in the electrolyte is to increase the conductivity but it is known that the effect is only observed up to a certain maximum concentration. Thereafter, an increase in concentration has no beneficial effect on the conductivity (Di Bari, 1994; Ji and Cooper, 1996). This effect was also observed in the polarisation parameters. The lowest concentration of 50 g/L Na_2SO_4 falls in Region 3 and highly undesirable quality and morphology deposits were produced. An increase to 70 g/L Na_2SO_4 shifted E_p to more cathodic values and ΔE became positive. An even further increase to 80 g/L (standard electrolyte) shifted the polarisation parameters into Region 1, giving an ideal relationship between nucleation, inhibition and growth. Deposit morphology was UD type and ideal in quality and strain characteristics. A further increase to 100 g/L Na_2SO_4 shifted the polarisation parameters into Region 4 with a less cathodic E_p but a highly positive ΔE value. Morphology of deposits from this electrolyte was also more FT type and showed some internal strain when compared with the deposits from the standard electrolyte. The polarisation parameters therefore also showed that 80 g/L Na_2SO_4 is a high enough concentration to improve quality and morphology by increasing conductivity and transport in the electrolyte but that increases above 80 g/L have no further benefit.

Deposits produced at 45 °C had relatively fine-grained morphology and showed slight pitting and strain. Polarisation parameters showed a similar relationship to that of the 70 and 100 g/L Na_2SO_4 electrolytes. It was therefore concluded that Region 4 is a region of intermediate morphology – in between the characteristics of Region 3 and Region 1. The morphology is UD/FT type and some strain and pitting were observed. The inhibition or nucleation frequency is not ideal in this region in order to balance with growth processes, but it can be sufficient in instances where UD-type morphology is not specifically required for a certain application. The morphological differences for points in Region 4 are shown in Figure 6.17.

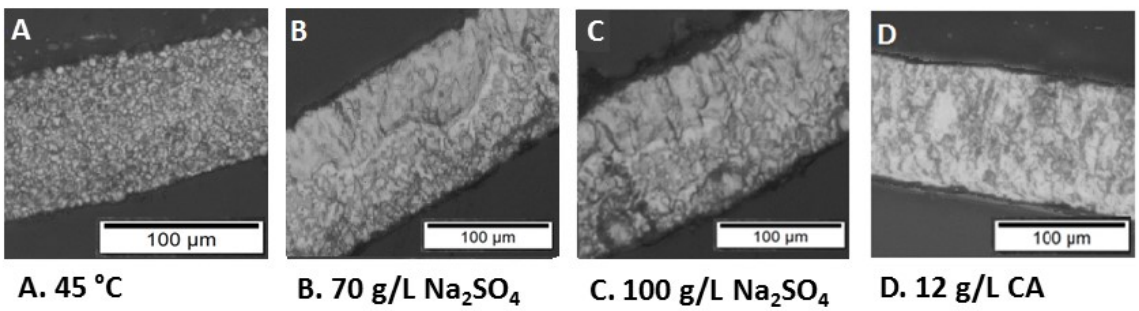

Figure 6.17. Morphological characteristics of deposits from polarisation points for Region 4.

It should be mentioned that the regions specified here are not mathematically calculated and therefore the regions may coincide and have some intermediate areas of overlapping morphology. This concept was simply chosen to give ranges of polarisation parameters that provide a general measure of whether a deposit from an electrolyte will have acceptable morphology and low internal strain.

Chapter 7
Correlation of results with industrial electrolyte

7.1. Introduction

The applicability of the polarisation method to industrial electrolytes and conditions needed to be evaluated. The aim was to test the polarisation method on various industrial electrolytes with conditions, parameters and compositions typically observed in the Anglo RBMR plant. Reproducibility of the measured polarisation parameters was evaluated and the polarisation values were compared with those obtained for synthetic electrolytes of similar composition. This comparative evaluation was important to establish the validity of the measurement method to the industrial environment and the feasibility of implementing the method on-line or at-line.

7.1.1. Introduction to RBMR tankhouse for nickel electrowinning

Leaching, precipitation and electrowinning processes are used at RBMR to ultimately produce nickel and copper metal from copper nickel matte (NCM) (Biley, 2016; Bryson and Biley, 2016).

Leaching processes are shown in Figure 7.1.

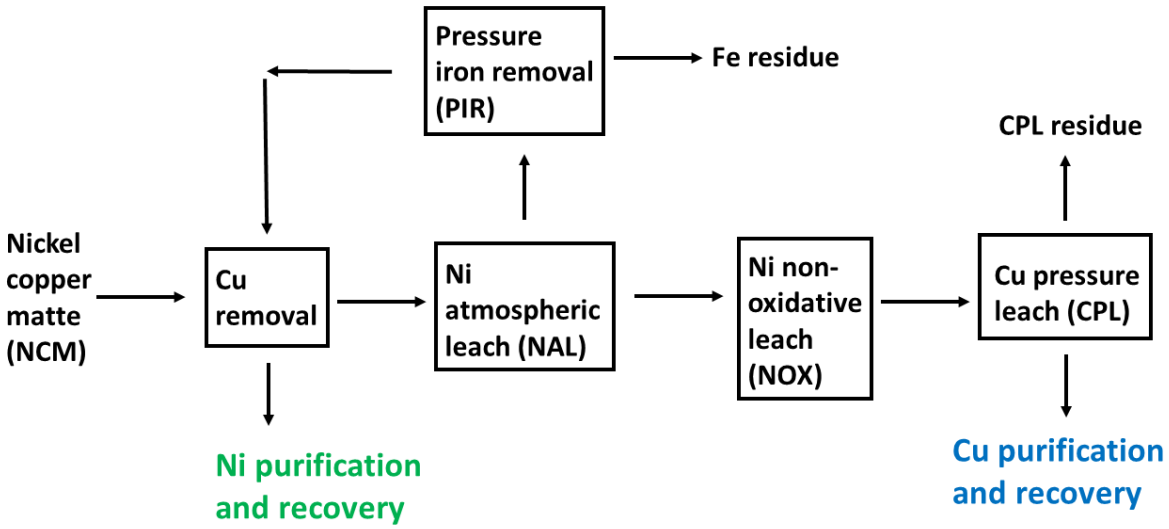

Figure 7.1. Schematic of the leaching processes at RBMR (after Bryson *et al.*, 2008a; Biley, 2016).

NCM contains most of the base metals (as sulfides) obtained from the converter matte after platinum-group metals (PGM) have been removed. The leaching circuit consists of the copper removal, the nickel atmospheric leach (NAL) and the nickel non-oxidative leach (NOX) processes that primarily separate nickel and copper by metathesis, which is found to be more beneficial than hydrolysis (Bryson *et al.*, 2008a; Summerton *et al.*, 2012; Bryson and Biley, 2016). The pressure iron removal (PIR) is a process during which iron is precipitated from the nickel leach solution, thereby removing iron and increasing purity of the nickel solution before electrowinning. It is an oxidative process at elevated temperature of 145 °C. The filtrate is fed back to the copper removal stage. Here, the pH allows for iron and copper to precipitate as sulfates, which are fed back to the nickel leaching circuit. The copper removal process therefore serves as a second step for iron removal, thereby minimizing breakthrough of impurities (Bryson *et al.*, 2008a; Biley, 2016; Bryson and Biley, 2016).

The nickel and copper circuits are shown in Figure 7.2.

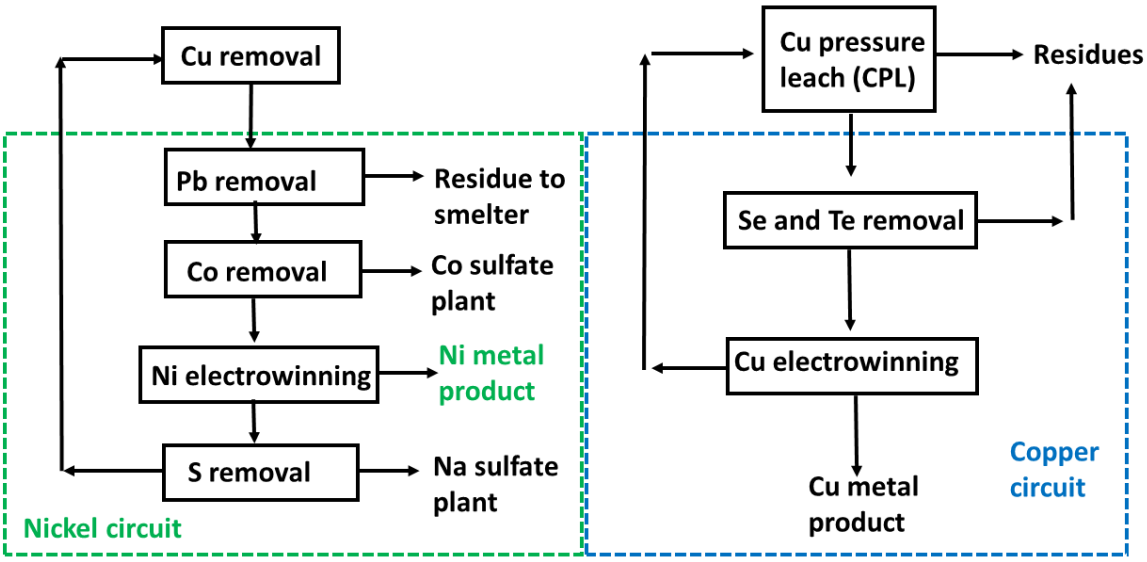

Figure 7.2. Schematic overview of nickel and copper production processes at RBMR (after Hofirek and Kerfoot, 1992, Biley, 2016).

During the first stages in the nickel circuit, lead and cobalt are removed from the solution. The residual solution is fed to nickel electrowinning cells where nickel metal is produced. After electrowinning, the nickel from spent electrolyte is recycled and sulfur is removed by crystallisation with sodium hydroxide. This produces nickel hydroxide, which is later

dissolved and fed back into the leaching circuit, and sodium sulfate, which is further processed elsewhere (Hofirek and Nofal, 1995; Bryson and Biley, 2016).

The first step in the copper circuit entails removal of selenium and tellurium. Thereafter, the solution is fed to copper electrowinning cells where copper metal is produced. The copper spent electrolyte is fed back to both of the pressurised leach stages: this, firstly, supplies an acidic medium for leach processes and, secondly, contains base metals to be further recycled and processed (Hofirek and Nofal, 1995; Biley, 2016).

7.1.2. Nickel electrowinning process at RBMR

RBMR has recently been expanded, with the construction of a new tankhouse exclusively for nickel electrowinning in order to increase the nickel production capacity to 32 400 tpa (Voogt *et al*., 2017) and to limit the exposure of tankhouse employees to nickel aerosols produced during electrowinning. Hoods were installed to cover the cells during electrowinning, anode skirts with slits were introduced (Figure 7.3) and automation of the harvesting process of nickel cathodes after electrowinning was implemented. Titanium blanks are used for deposition of nickel and the nickel can be plated for up to 10 days before harvesting (Bryson *et al*., 2008b; Voogt *et al*., 2017).

The cells with hanging cathode and anode with anode skirt are shown in Figure 7.3.

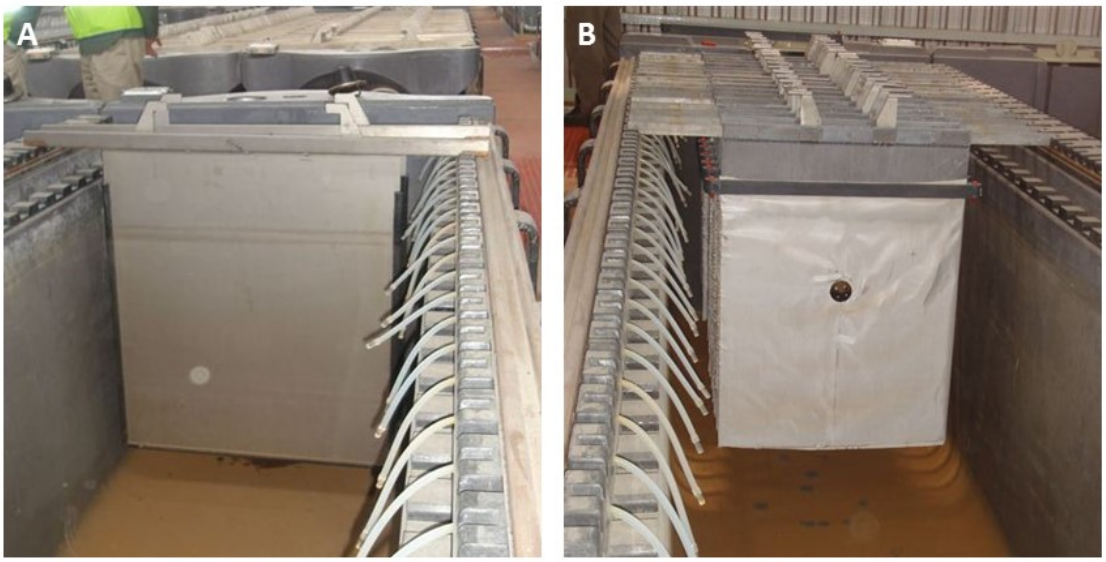

Figure 7.3. Industrial nickel electrowinning cell at RBMR showing A: titanium cathode blank and B: the anode with anode skirt (Photographs courtesy of Anglo American Platinum RBMR).

The RBMR electrowinning cells and setup are unique because each cathode–anode pair is separated from the next, with feed electrolyte supplied to each pair individually (shown by the white rubber pipes on the side of the cells in Figure 7.3). Cathode bags are used (not shown here), which allow control and monitoring of the pH surrounding each individual cathode. This is especially useful to test the effect of impurities on an industrial scale because each catholyte can be dosed individually with a certain impurity of additive without affecting the catholyte of other cathodes in the electrowinning cell (Voogt *et al*., 2017).

The electrolytes supplied for the current test work were therefore dosed during industrial electrowinning operations at RBMR and sampled from individual catholytes for further laboratory testing. This was extremely useful, because the impurities and additives were representative of industrial conditions and could still be obtained without contamination of large electrowinning cells or influencing targeted nickel production. The samples that were produced at RBMR in this way contained SLS, SAC, Cu and Co; a reference electrolyte from each of these catholytes was also taken before dosing. The reference electrolytes contained 80 g/L Ni^{2+}, 100 g/L Na_2SO_4 and 8 g/L H_3BO_3. These were also tested by ICP-OES for other possible impurities. No significant concentrations of Fe, Co, Cu or Se were measured in the reference electrolytes (Appendix C, Table C5).

Results presented here are average values of five repeat measurements. The complete data with all replicate measurements for each RBMR electrolyte are shown in Appendix C.

7.2. Comparison of results for electrolytes containing sodium lauryl sulfate

Three industrial electrolytes with 5, 20 and 40 mg/L of SLS were received. The polarisation parameters were measured. Results comparing polarisation data for the RBMR SLS electrolytes and the synthetic SLS electrolytes (containing 5, 20 and 40 mg/L) are shown in Figure 7.4. The reference points for the laboratory standard electrolyte and RBMR reference electrolyte are also indicated.

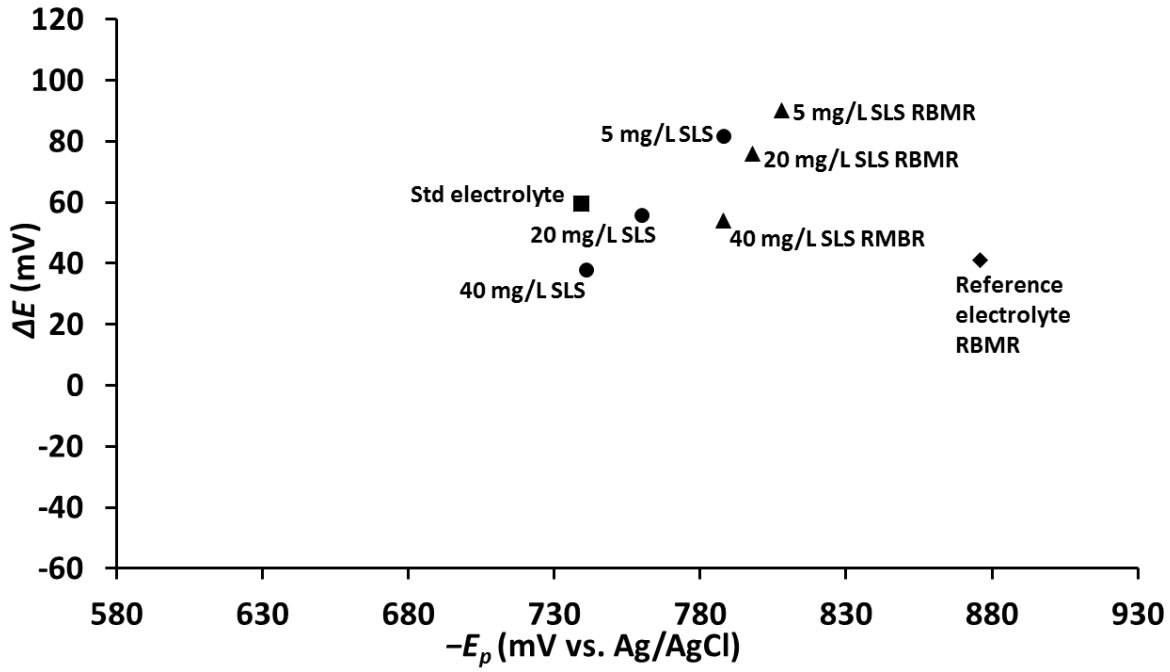

Figure 7.4. Results comparing polarisation parameters of synthetic and industrial electrolytes containing various concentrations of SLS.

Polarisation data for the industrial electrolytes were similar to those of the laboratory solutions. All of the points measured had highly cathodic E_p and positive ΔE values. The polarisation parameters for the RBMR electrolytes were also situated in the upper right region (Region 1, Figures 6.6 and 6.7). Therefore, a good balance between nucleation and growth was expected and typical UD-type morphology and low strain were also expected for the deposits from industrial electrolytes. The same trend in polarisation data with increasing concentrations of SLS was observed for the industrial samples compared with the synthetic electrolytes. The mechanism and action of working of SLS in both synthetic and RBMR electrolytes of similar composition were comparable.

Morphological characteristics for deposits produced from the electrolytes with various SLS additive concentrations are shown in Figure 7.5.

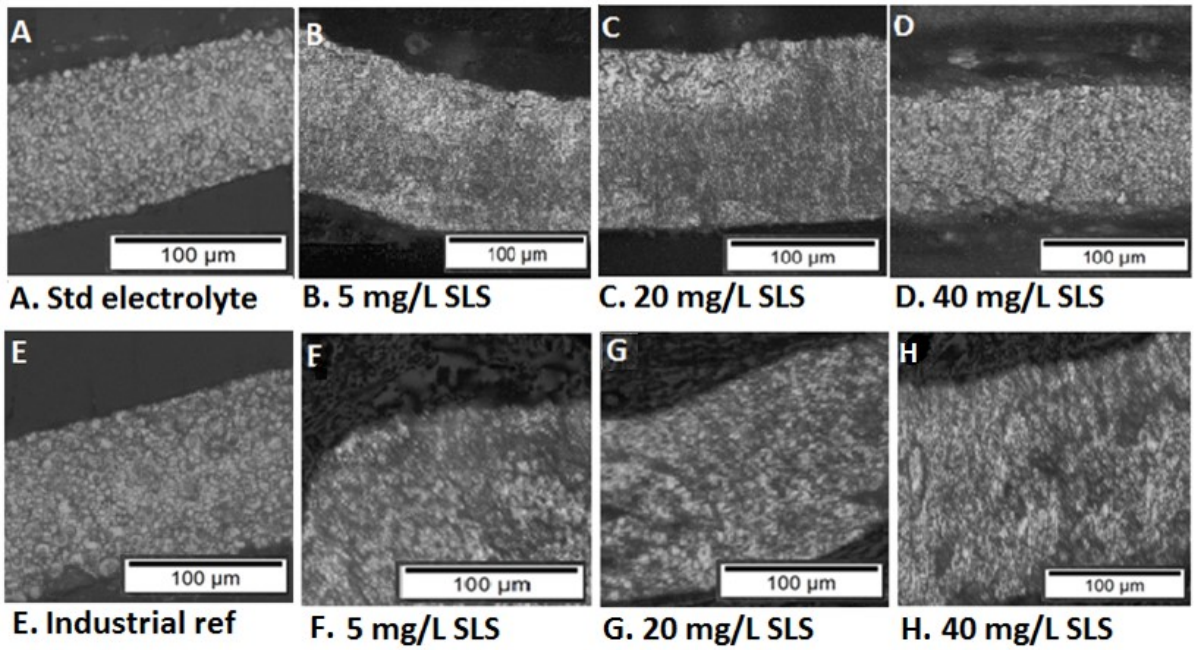

Figure 7.5. Micrographs showing morphology of deposits with varying concentrations of SLS: A – D represent deposits from synthetic electrolytes while E – H are for deposits from RBMR electrolytes.

Deposit morphology and characteristics were similar for deposits without any additive – the standard electrolyte compared with the RBMR reference electrolyte (presented in Fig 7.5 A and E). The deposits were of UD type, fine-grained, level, bright and compact and showed no signs of internal strain. The measured polarisation points and the fact the that morphology and strain characteristics were similar for these reference electrolytes confirmed that these two polarisation points could be grouped together into a region of similar morphology and therefore also suggested that points measured surrounding these polarisation points could be included in this region.

Morphology and general structural characteristics of the deposits in the presence of SLS compared well. All deposits were fine-grained and of UD type. The deposits shown in Figure 7.5 E – H, produced from the RBMR electrolytes, were extremely difficult to remove from the substrate surface without breaking the deposit itself. This was indicative of compressive stresses, which were also observed for the laboratory samples. It was therefore extremely difficult to photograph these deposits and the quality of the micrographs was not ideal. It was, however, still clear that the fine-grained, low-strained, UD-type morphology was prevalent in these deposits as well.

7.3. Comparison of results for electrolytes containing saccharin

Three industrial RBMR electrolytes with 4, 10 and 80 mg/L of SAC were received. The polarisation parameters were measured. Results comparing polarisation data for the industrial SAC electrolytes and the synthetic SAC electrolytes (containing 4, 10 and 20 mg/L) are shown in Figure 7.6. The reference point for the laboratory standard electrolyte is also indicated.

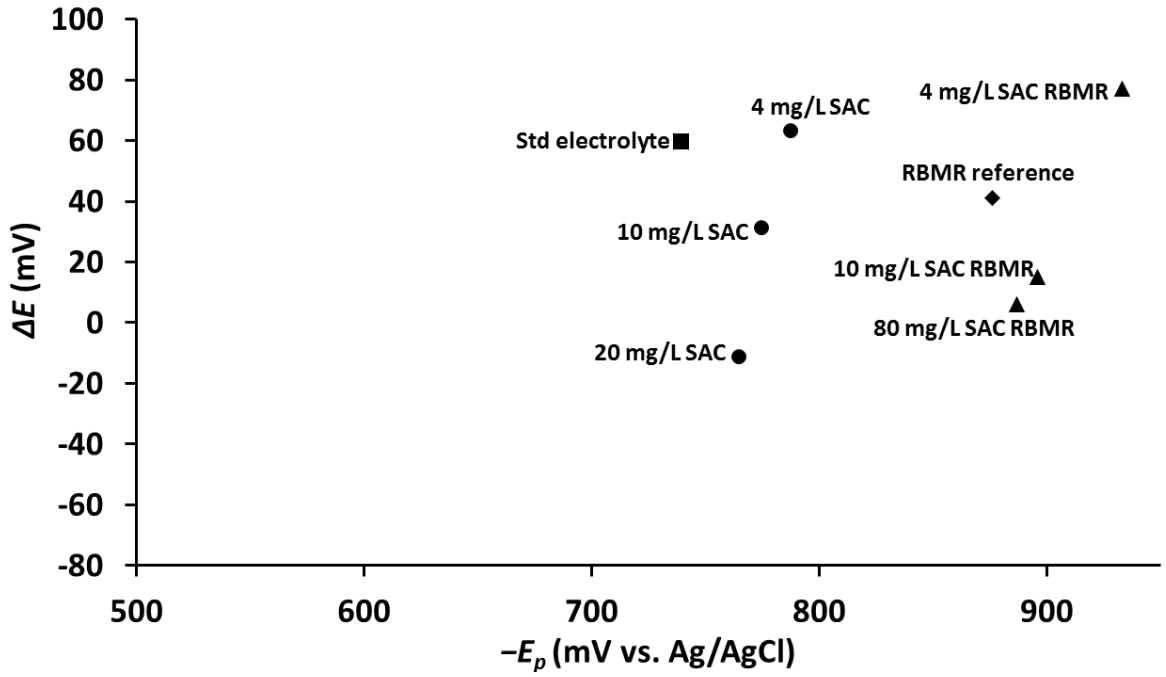

Figure 7.6. Results comparing polarisation parameters of synthetic and industrial electrolytes containing various concentrations of SAC.

Polarisation parameters for the industrial electrolytes containing SAC were similar to the data measured for the synthetic electrolytes containing SAC. The E_p values were large and the ΔE values were all positive. Therefore, the balance between inhibition, nucleation of new nickel ions and growth of deposited clusters seemed to be ideal. The same trend was observed for increasing SAC concentration in the electrolyte: $-E_p$ and ΔE decreased with increasing concentration. The increase in concentration therefore influenced not only nucleation, but also growth, in such a way that the relationship stayed balanced even at a high concentration of SAC of 80 mg/L.

It was observed that the E_p values obtained for the RBMR electrolytes (electrolytes containing SAC as well as the industrial reference electrolyte) were even more cathodic compared with the synthetic electrolytes. This is not fully understood at this stage but the

compositional differences in the synthetic standard electrolyte compared with the industrial reference electrolyte might be the cause thereof. The polarisation point for the RBMR reference electrolyte was also measured on the higher, more cathodic E_p side, compared with the synthetic standard electrolyte.

Micrographs of the thick deposits obtained from all electrolytes (synthetic and industrial) containing various concentrations of SAC are shown in Figure 7.7.

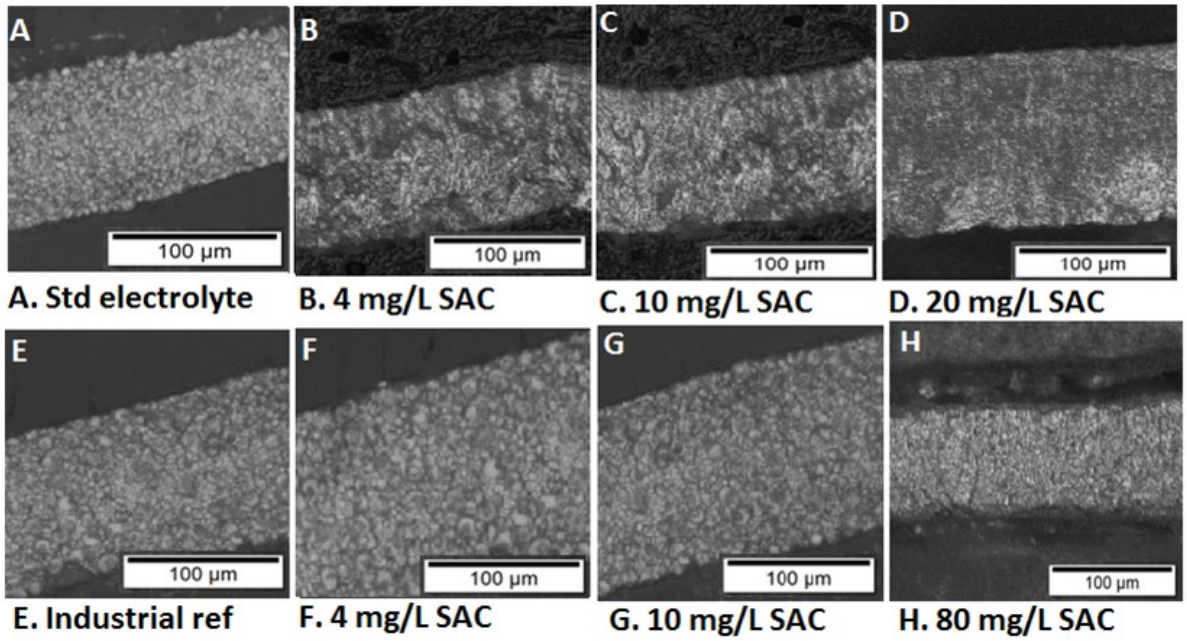

Figure 7.7. Micrographs showing morphology of deposits with varying concentrations of SAC: A – D represent deposits from synthetic electrolytes while E – H are for deposits from industrial electrolytes.

The deposits with added SAC were also all similar in structure and the characteristics and morphology comparable for the industrial and laboratory electrolytes. The morphologies of all the deposits were comparable with the typical morphology described for Region 1 (Figures 6.6 and 6.7). The finest grains were observed for the deposits from the RBMR electrolyte containing 80 mg/L of SAC and 20 mg/L of SAC (synthetic electrolyte). It was therefore found that grain refinement improves with an increase in SAC concentration for both electrolytes.

7.4. Comparison of results for electrolytes containing cobalt

One industrial RBMR electrolyte with a cobalt impurity of 250 mg/L was received and tested in the same way to measure the polarisation parameters. The results were compared with the polarisation data for the synthetic electrolytes containing 250, 500 and 1000 mg/L of cobalt impurity. This is presented in Figure 7.8.

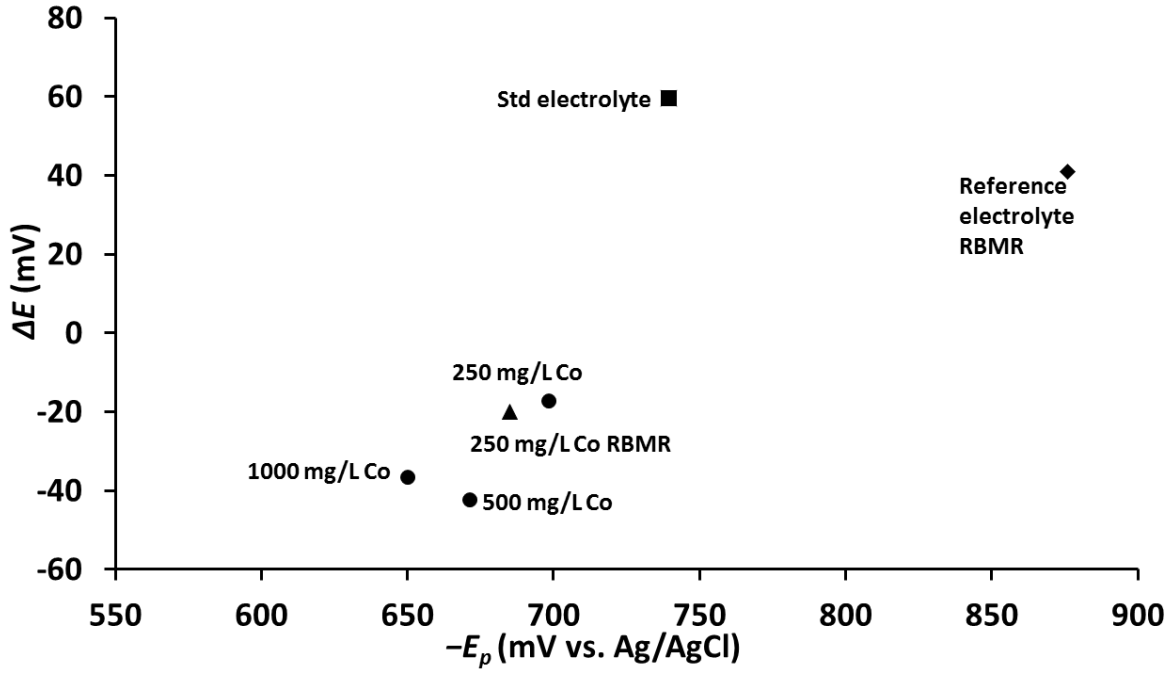

Figure 7.8. Results comparing polarisation parameters of synthetic and industrial electrolytes containing various concentrations of cobalt.

Polarisation parameters measured for the industrial electrolyte compared well with the data for the synthetic electrolyte with the same cobalt impurity concentration. The measured polarisation point for the industrial electrolyte containing cobalt was in the same region as the synthetic cobalt-containing electrolytes. This suggested that the morphology and strain characteristics would also be similar for the industrial deposit compared with the synthetic deposits. Polarisation points found in this region of low (negative) ΔE values and less cathodic E_p values were expected to indicate low growth rates, undesirable inhibition and nucleation and therefore poor morphology and high strain.

Morphology and strain characteristics for deposits produced from electrolytes containing various concentrations of cobalt are shown in Figure 7.9.

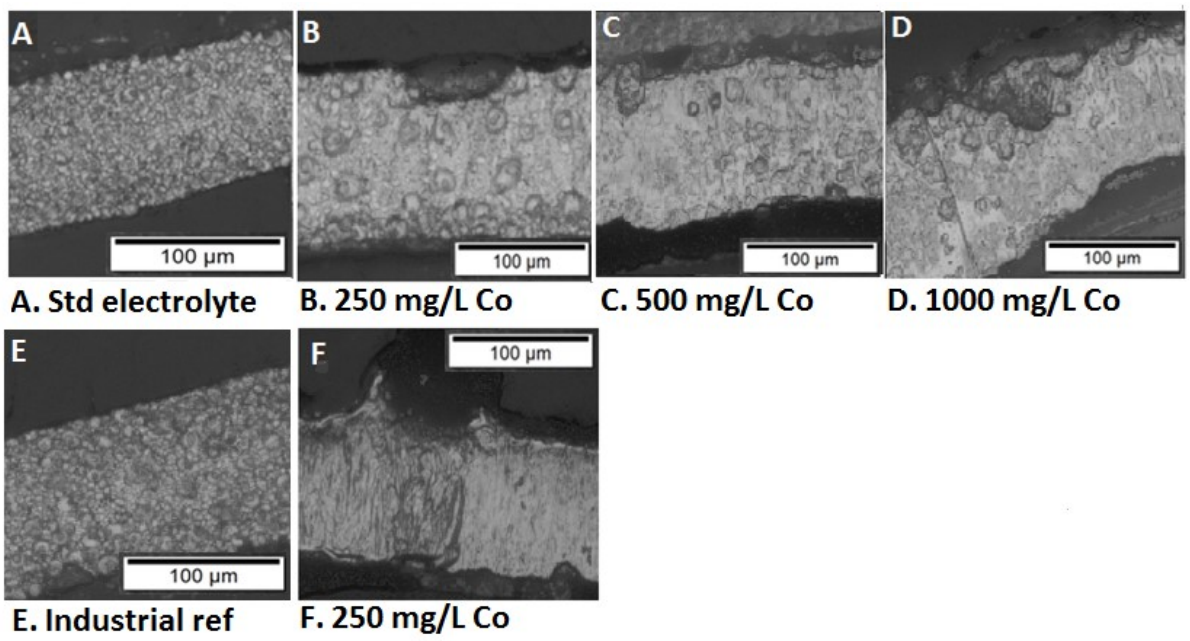

Figure 7.9. Micrographs showing morphology of deposits with varying concentrations of cobalt impurity: A – D represent deposits from synthetic electrolytes while E – F are for deposits from industrial electrolytes.

The morphologies of all deposits (synthetic and industrial) were similar. Large pinholes and irregular structures were observed throughout the deposits. The morphology of the industrial cobalt-containing electrolyte was more FT type compared with the synthetic electrolytes containing cobalt (more BR type), but the internal strain characteristics were similar and some darker areas on all deposits were observed, which were indicative of possible cobalt co-deposition and therefore incorporation of cobalt into the nickel structure during electrodeposition.

7.5 Comparison of results for electrolytes containing copper

One industrial RBMR electrolyte with a copper impurity of 250 mg/L was received and tested in the same way to measure the polarisation parameters. The results were compared with the polarisation data for the synthetic electrolytes containing 100, 250 and 500 mg/L of copper impurity. This is presented in Figure 7.10. The morphologies of the thick deposits obtained in the presence of copper impurities are compared in Figure 7.11.

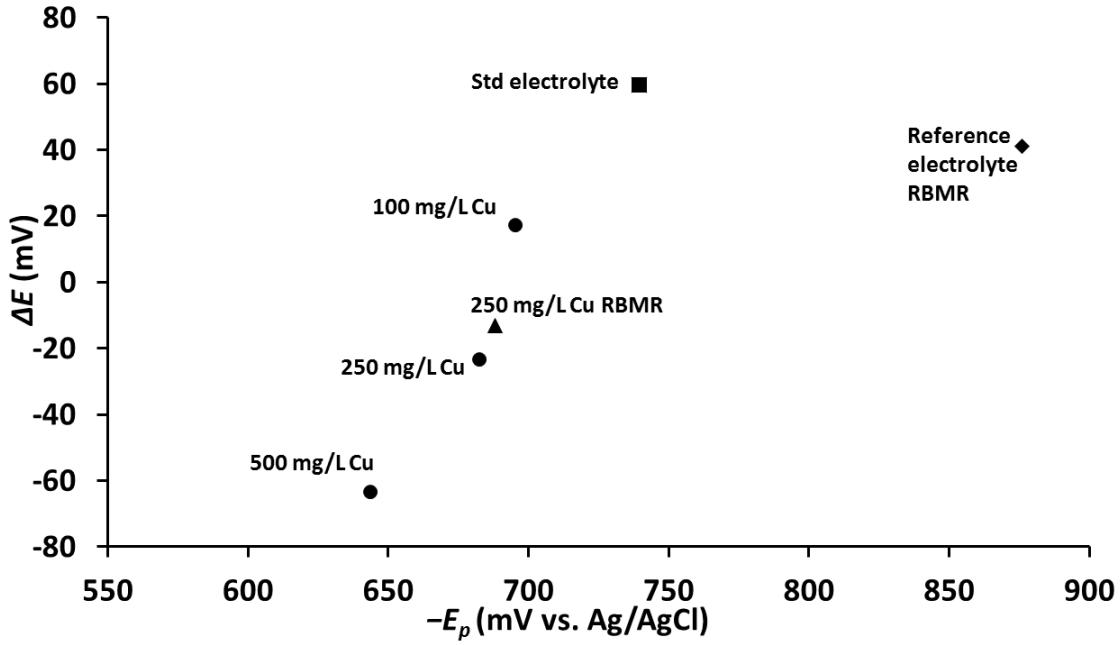

Figure 7.10. Results comparing polarisation parameters of synthetic and industrial electrolytes containing various concentrations of copper.

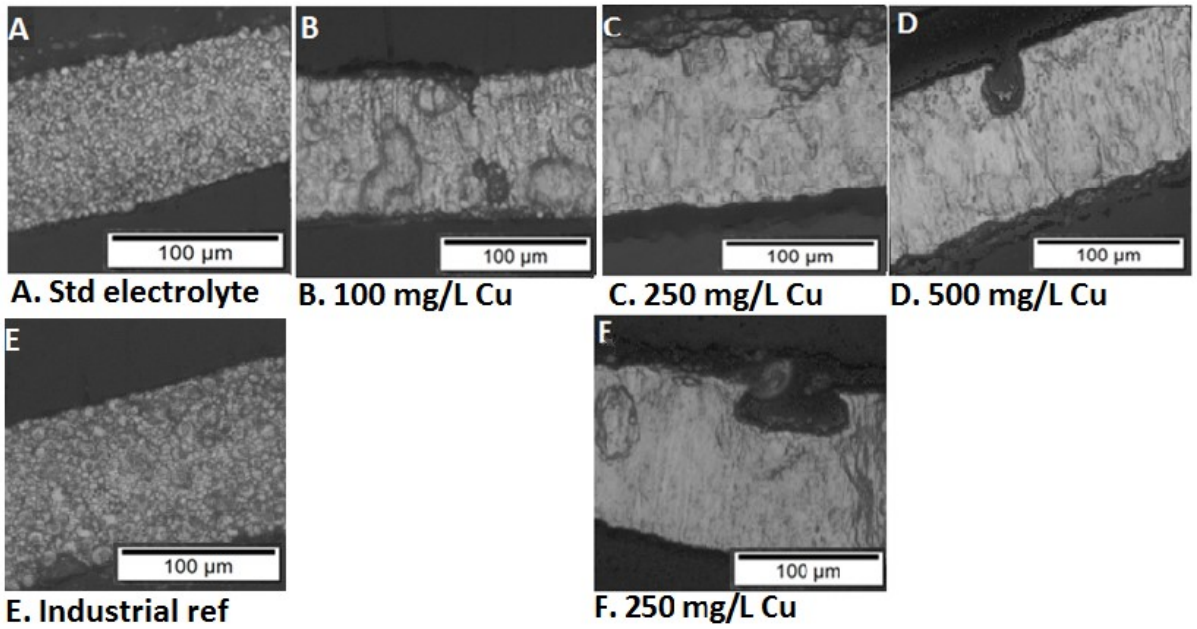

Figure 7.11. Micrographs showing morphology of deposits with varying concentrations of copper impurity: A – D represent deposits from synthetic electrolytes while E – F are for deposits from industrial electrolytes.

The polarisation measurements for the industrial electrolyte containing copper (250 mg/L) were similar to that of the 250 mg/L copper-containing synthetic electrolyte. The measured ΔE and E_p values were negative, which indicated undesirable inhibition, nucleation and growth processes, similar to that measured for the synthetic electrolytes. The morphologies of these deposits were therefore also expected to be similar and of poor characteristics.

The morphology and internal strain characteristics for all of the electrolytes containing copper impurities were similar. All deposits (synthetic and industrial) were of the FT/BR-type with irregular structures, large pinholes and signs of internal strain. The morphology of the synthetic and industrial electrolytes containing 250 mg/L of copper were particularly comparable and showed similar type of morphology but also similar large surface pinholes.

7.6. Comparison of results for electrolytes containing selenite

Three RBMR electrolytes with selenite impurities of 5, 8 and 10 mg/L were received and tested in the same way to measure the polarisation parameters. The results were compared with the polarisation data for the synthetic electrolytes containing 10, 15 and 25 mg/L of selenite impurity. This is presented in Figure 7.12.

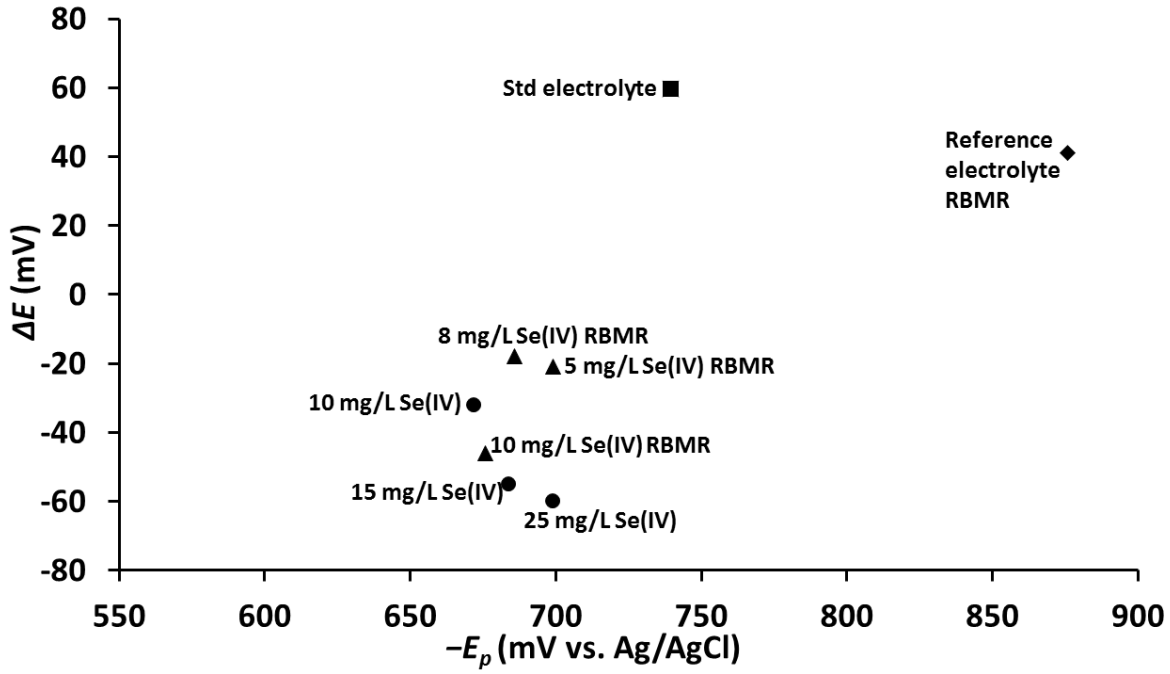

Figure 7.12. Results comparing polarisation parameters of synthetic and industrial electrolytes containing various concentrations of selenite.

The polarisation parameters measured for all concentrations were again similar for the synthetic and industrial electrolytes containing selenite. All polarisation parameters were measured in Region 3 (Section 6.3, Figure 6.13) where ΔE was negative and E_p less cathodic. The morphology suggested by polarisation parameters in this region was BR/FT type with highly strained structures.

The morphologies obtained for thick deposits from these electrolytes are shown in Figure 7.13. The morphological structures of the deposits obtained from industrial electrolytes containing selenite were very similar to those obtained from the synthetic electrolytes. All deposits were BR type, with highly strained internal structures, large pits, cracks and delaminated areas. The severity of the strain did not seem to be affected by selenite concentration as all deposits were cracked and brittle.

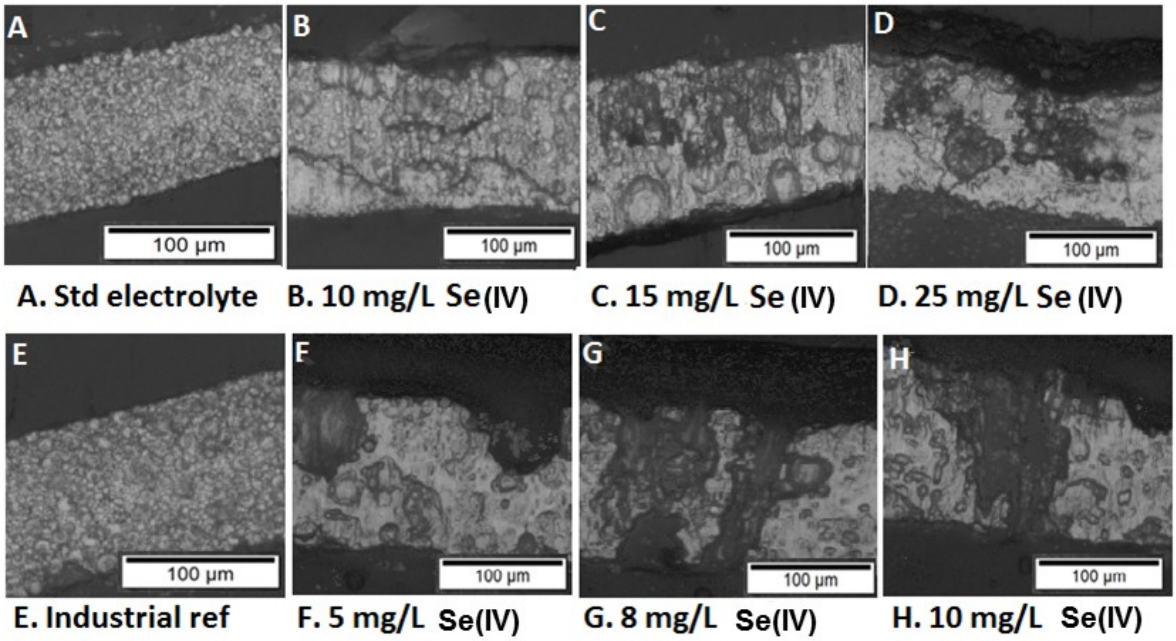

Figure 7.13. Micrographs showing morphology of deposits with varying concentrations of selenite impurity: A – D represent deposits from synthetic electrolytes while E – H are for deposits from industrial RBMR electrolytes.

7.7. Industrial applicability

The results for the industrial and synthetic electrolytes were very similar. Measured polarisation parameters for all electrolytes, with or without additives and impurities, were comparable and fell in the same regions of suggested morphology. Therefore, the ΔE and E_p values were similar in each case. The morphology and strain characteristics for each type of

electrolyte were also comparable for industrial and synthetic electrolytes. This indicates that the morphologies suggested by measured polarisation parameters and the relationship between ΔE, E_n and E_p were applicable to laboratory conditions as well as industrial, large-scale operations. However, only a few electrolytes were tested in this way, so further study should be conducted with more typical conditions, parameters, impurities and additives specifically applicable to the RBMR plant.

The idea is that this measuring method could be adapted to a plant environment and implemented such that the production effects of sudden changes in electrolyte or breakthrough of impurities can be predicted. The effects that these changes are predicted have on the morphology of thick deposits could then be suggested in the early stages of the deposition cycle and, if necessary, adaptive changes could be made before the morphology of the deposit became completely affected. This technique could therefore possibly serve as a predictive tool to monitor the effect of electrolyte changes on the morphology and give early warning that corrective action should be taken.

Another possibility is to apply this method to the use of additives. Should a certain additive be considered to achieve a particular purity, quality or morphology of nickel deposits, this method could be used to check, at a laboratory scale, what the possible outcome would be. It could also serve as a method to determine the optimum concentration needed of such an additive to obtain a certain characteristic.

Even though the technique is proved repeatable and was found to be a fast way to suggest what the outcome of changes in the electrolyte on the morphology and strain would be, it is important to determine whether it can be implemented on-line or at-line with the same repeatability and precision. If the technique is found to be repeatable in a plant environment, it should be considered for automated on-line or at-line application in a plant process. The possibility of a setup could be investigated where continuous sampling of the electrolyte from industrial cells takes place with continuous polarisation measurements made automatically. These polarisation measurements should be sensitive enough to change with any particular change in electrolyte conditions, parameters or composition. If changes occur, an automated alert could be created and adaptive changes made timeously.

Chapter 8
Conclusions and future work

8.1. Galvanodynamic measuring technique

In earlier work a galvanodynamic technique was developed for measurement of polarisation parameters for zinc electrowinning by Adcock *et al*. (2002 and 2004), and the usefulness of these to predict morphological outcome specific to zinc electrowinning was established (Adcock *et al*., 2004). In this work, a galvanodynamic measuring technique was developed that is specific to nickel electrowinning from sulfate electrolyte. This technique gave repeatable measurements for both E_n and E_p within 6 mV. It was found that two scans at different scan rates could be used for this application and that this method was able to determine the nucleation and growth of deposits more accurately and reliably than typical cyclic voltammetry techniques. It was also found that the IR compensation for this technique could be done fairly easily and off-line after completion of the experimental scans. The IR compensation also only needed to be done for E_p as the current values for measured E_n values were small and therefore IR changes were negligible.

The electrochemical cell setup was found to be critical to enable this method to be repeatable and precise – as is the case with all electrochemical work. The slightest changes or movement in the cell setup or distance between electrodes had a large influence on the measurements. Therefore, the success of this method related mainly to the consistency and repeatability of the cell setup and the way in which measurements were made.

The measurements made with this technique for E_n and E_p could be used as indicators of inhibition, nucleation and growth processes during the deposition of nickel onto a substrate surface. The E_n and E_p values (and therefore also ΔE) were found to be representative values of the process of nickel depositing onto the cathode and were found to change with changes in the electrolyte and ultimately affect the morphology. These polarisation values were found to change with changes in deposition mechanism or action as impurities interfered or co-deposited or additives acted as transport molecules or altered inhibition. Changes in these values were also found with changes in buffering of the electrolyte, which could be used to shed some light on how buffering occurs and which compositional changes altered the buffering mechanism.

8.2. Inhibition, nucleation and growth

It was clear that the balance in the relationship of inhibition, nucleation and growth processes was essential to obtain a nickel deposit of desired morphology, low strain and good quality. It was also found that the polarisation parameters measured were indicative of this relationship and that E_n and E_p (and therefore ΔE) could be used as indicators of changes in the balance of this relationship.

At positive ΔE values and highly cathodic E_p values (higher than approximately 700 mV), the relationship between nucleation and growth was found to be ideal. Frequent nucleation could take place with simultaneous growth of nucleated nickel ions, thereby forming fine-grained, smooth, level, regular in structure, bright and low-strained deposits. Electrolytes with measured values in this range included the standard electrolyte, high nickel concentrations, high temperature, pH around 3, SLS, SAC and PYR additives and high boric acid concentrations. At high nickel concentrations, more ions were available to deposit, which made transport and deposition more effective. Increased temperature increased the rate of nickel deposition, making the deposition process more effective. Electrolytes with a pH of 2.5, 3 and 3.5 showed similar results. At these pH values, the effect of hydrogen evolution was limited and buffering of the electrolyte was optimum. Boric acid added to the electrolyte also promoted good buffering of the system. The addition of SLS, SAC and PYR additives to the electrolyte directly increased inhibition, promoted frequent nucleation and caused grain refinement. The morphology of deposits obtained from these electrolytes were similar and of UD or FT/UD type – showing a desired balance between inhibition, nucleation and growth.

At negative ΔE values and highly cathodic E_p values, nickel ions nucleated less frequently and the few nucleated clusters had high growth rates, thereby forming large irregular growths with large grains and pinholes in the structure. Electrolytes found to have these deposit characteristics were those with low nickel concentrations, low temperature and a high pH of 5. Low nickel concentration was typically expected to produce deposits with less nucleation, as fewer ions were available and therefore only growth of these few deposited clusters took place. Low temperature had the same effect. Less frequent and slower nucleation processes with simultaneous growth prevailed and deposits were brittle and cracked. At an electrolyte pH of 5, buffering of the electrolyte was not sufficient and large hydrogen pits were observed due to H_2 gas generation at the surface.

At negative ΔE and less cathodic E_p values, the balance between nucleation and growth was irregular and non-ideal. Polarisation points obtained with this relationship were mostly from impurity-containing electrolytes. Nucleation and growth processes were unbalanced, which caused brittle, strained deposits with holes and cracks. Co-deposition of impurities into the nickel crystal structure was most likely to have caused additional strain in the lattice. Dark and light areas were observed in most of the micrographs, which was typical of impurities co-deposited with nickel. This was found for cobalt, copper, aluminium (at low values of 5 and 10 mg/L) and selenium impurities.

Other polarisation points that were observed in this region were for the electrolytes without any boric acid (both at pH 2 and 5). The structure of theses deposits was similar to that obtained from the electrolytes with impurities in strain and pitting characteristics and showed that boric acid was essential to obtained a desired relationship between nucleation and growth. These two polarisation points, especially, showed the importance of boric acid and that boric acid itself or boric acid complexation was involved in either buffering of the electrolyte or another form of transport of nickel ions or other action to improve the balance between inhibition, nucleation and growth.

For polarisation points where ΔE values were positive and E_p values were less cathodic (lower than approximately 700 mV), an intermediate region was obtained for which nucleation and growth processes seemed to be balanced but some strain and pitting were still observed. The morphology observed for deposits from electrolytes in this region was acceptable in quality but grains were larger and more elongated when compared with the morphology of typical UD-type deposits. The typical structure resulted from less frequent nucleation compared with the standard electrolyte, but with slower growth rates compared with points with more cathodic E_p values. Polarisation points with these characteristics were obtained from electrolytes with slightly lower and higher Na_2SO_4 concentrations (compared with the standard electrolyte), the electrolytes containing citric acid instead of boric acid and the electrolyte with a temperature of 45 °C. Deposits from electrolytes with these characteristics were of intermediate-type morphology and strain – not as ideal and UD type as the deposits in the region with the standard electrolyte but not as strained and cracked as electrolytes in the region of impurities.

8.3. Buffering characteristics of sulfate electrolytes

The polarisation results clearly showed that buffering of the electrolyte was extremely important, not only to stabilise the pH and limit the effect of hydrogen evolution, but also to ensure low strain in the nickel deposits and improve the overall morphology. It was found that boric acid was effective as a buffering agent at 4, 8 and 12 g/L even though the p*K*a of boric acid is much higher than the working pH of the sulfate electrolyte. It was therefore proposed that nickel–borate complexes are most likely to form and perform buffering action and most probably also improve transport of the nickel ions toward the substrate surface. Citric acid, with a p*K*a in the range of the working pH, was found to be less effective as a buffer and deposits produced from electrolytes at 4, 8 and 12 g/L, were acceptable in morphological and strain characteristics, but were not as fine-grained or compact as deposits obtained in the presence of boric acid.

It was also observed that the pH of the electrolyte, together with the boric acid concentration, played a crucial role in buffering of the system and therefore ultimately influencing the morphology and characteristics of the nickel deposits. At pH 5, in the presence of boric acid, deposits were highly strained and pitted. This was most likely to be due to nickel hydroxide species forming and co-depositing with nickel, causing strain and irregular crystal structures. The boric acid action was only effective if the starting pH of the electrolyte was between 2 and 3.5.

Another important conclusion regarding buffering was that high concentrations of aluminium impurity had a beneficial effect on the buffering of the electrolyte as well as the morphological outcome of the nickel deposits. At low concentrations of aluminium (5 and 10 mg/L), co-deposition of aluminium species into the crystal structure was most probable and highly strained deposits were formed. At high concentrations (5000 mg/L), however, the electrolyte pH was most stable – even more stable compared with electrolytes with only boric acid. It is proposed that aluminium also complexes with nickel to form stable complexes that improve buffering and nickel ion transport to the cathode.

8.4. Industrial application

Deposits produced from industrial electrolytes from RBMR containing the additives SAC and SLS and impurities copper, cobalt and selenite were compared with those from synthetic electrolytes. The galvanodynamic method was repeatable for measurement of E_n and E_p for

each industrial electrolyte to approximately 5 mV and the values for E_n and E_p were comparable to those obtained for synthetic electrolytes of similar composition.

Polarisation results (E_p vs. ΔE) compared well for RBMR and synthetic electrolytes of comparable composition and points could be plotted in the same polarisation regions. This was observed in the presence of additives as well as impurities. The addition of SAC and SLS to the industrial electrolytes shifted the polarisation parameters to highly positive ΔE and highly cathodic E_p values that indicated the required inhibition, frequent nucleation and balanced growth. Cobalt, copper and selenite impurities shifted the polarisation parameters to negative ΔE and less cathodic E_p values, where co-deposition of the impurity and large loose grains due to high growth rates and less frequent nucleation were observed.

The morphologies of deposits from both synthetic and industrial electrolytes were similar in all cases. The addition of SAC and SLS to the electrolytes caused grain refinement and level, bright, compact deposits of UD type were produced. This also indicated a good balance between inhibition, nucleation and growth. In the presence of cobalt, copper and selenite, highly strained deposits with cracks and pinholes were formed from both types of electrolytes, which confirmed high growth rates and most probably co-deposition of impurities into the nickel crystal structure.

These results are in agreement with morphological observations made industrially and confirmed that strained deposits are produced in the presence of cobalt, copper and selenite. The additives, SAC and SLS, were expected to improve the grain size as this is the case industrially. Grain refinement was observed for synthetic and industrial RBMR electrolytes containing SAC and SLS.

Use of the galvanodynamic method to measure polarisation parameters was therefore applicable to both synthetic and industrial electrolytes and was found to be useful to indicate the relationship between inhibition, nucleation and growth in the early stages of nickel electrodeposition. These polarisation parameters were an indication of the conditions, composition and concentrations in the electrolyte on the nucleation and growth processes. The measured polarisation parameters were found to be indicative of how the nickel electrodeposition mechanism changes with changes in the electrolyte and can therefore be used as a measure of what the possible morphological outcome would be. This was found for typical sulfate electrolytes (reference electrolytes) without any additives or impurities as well as for electrolytes containing SAC, SLS, cobalt, copper and selenite.

These results show that the technique is feasible for further investigation to implement at-line or on-line to investigate, monitor and possibly control the electrodeposition process. It could also be a useful technique to investigate what the outcome would be in cases where a new additive is considered to obtain a particular nickel morphology for a specific application.

8.5. Future work

The effects of combinations of conditions, parameters and concentration changes in the electrolyte have not yet been tested and the applicability of the developed method to such cases is not known. All of the current results are based on sulfate electrolyte and the applicability of the technique to chloride-containing electrolyte can be explored. Other changes to the electrolyte have not yet been investigated, such as the effect of current density. The work done in this study was based simply on the current density used at the RBMR plant (220 A/m^2), but the technique can certainly be adapted in future to assess different current densities, combinations of electrolyte changes and specific impurities and additives for specific plant applications. A lower current density of 200 A/m^2 might be worth investigating with the aim of reducing energy consumption and decreasing operational costs.

The classification of strain and morphology of the nickel deposits was done qualitatively for this study. It is worthwhile to investigate more quantitative techniques for measuring strain and grain characteristics. Strain can be more accurately measured by strain gauge experiments and measurement of roughness of deposits can be included to classify the deposits more quantitatively. Grain sizes can also be measured and included in the comparison and classification of morphology.

The mapping of the E_n, E_p and ΔE results should also be evaluated by means of statistical software to evaluate and define the regions of overlapping morphology more critically. This might be an interesting perspective to further evaluate regions and even distinguish morphology more critically according to the measured polarisation parameters.

The buffering mechanism of the sulfate electrolyte is still not fully understood and this study only touched on the possibility of buffering of nickel–borate complexes as well as the possibility of aluminium at high concentrations being responsible for buffering or transport. This should be further explored in order to better understand, define and fine-tune the buffering and transport actions in typical sulfate electrolyte for nickel electrodeposition processes.

This method could be of interest in the plant environment to monitor the incoming electrolyte and detect any changes in the composition or conditions that would cause a shift in polarisation parameters. For instance, if the incoming nickel sulfate electrolyte are continually monitored, and Pb or Co removal in the nickel circuit prior to nickel electrowinning is not effective, the polarisation parameters will change. Therefore, by monitoring the polarisation parameters, such changes could be identified almost instantly and dealt with appropriately and timeously before a large number of nickel electrodeposits are produced with contamination or undesirable morphology.

Reference list

Aaboudi, O., Amblard, J., Chopart, J.-P. and Olivier, A. (2001). A temperature and electrochemical impedance spectroscopy analysis of nickel electrocrystallization from a Watts solution. *Journal of Physical Chemistry B*, 105, 7205–7210.

Abyaneh, M.Y. (1982). Calculation of overlap for nucleation and three-dimensional growth of centres. Electrochimica Acta, 27, 1, 1329-1334.

Abyaneh, M.Y., and Hashemi-Pour, M. (1994). The effect of the concentration of boric acid on the kinetics of electrocrystallization of nickel. *Trans. Inst. Met.Finish.* 72, 1, 23–26.

Adcock, P.A., Adeloju, S.B. and Newman, O.M.G. (2002). Measurement of polarization parameters impacting on electrodeposit morphology I: Theory and development of technique. *Journal of Applied Electrochemistry,* 32, 1101–1107.

Adcock, P.A., Quillinan, A., Clark, B., Newman, O.M.G. and Adeloju, S.B. (2004). Measurement of polarization parameters impacting on electrodeposit morphology. II:conventional zinc electrowinning solutions. *Journal of Applied Electrochemistry*, 34, 771–780.

Agatzini-Leonardou, S., Tsakiridis, P.E., Oustadakis, P., Karidakis, T. and Katsiapi, A. (2009). Hydrometallurgical process for the separation and recovery of nickel from sulphate heap leach liquor of nickeliferrous laterite ores. *Minerals Engineering*, 22, 1181–1192.

Alfantazi, A.M. and Shakshouki, A. (2002). The effects of chloride ions on the electrowinning of nickel from sulfate electrolytes. *Journal of the Electrochemical Society*, 149, 10, 506–510.

Amblard, J., Froment, M., Maurin, G., Mercier, D. and Trevisan-Pikacz, E. (1982). The electrocrystallization of nickel on vitreous carbon. A kinetic and structural study of nucleation and coalescence. *Journal of Electroanalytical Chemistry*, 134, 345–352.

Amblard, J., Froment, M., Maurin, G., Spurellis, N. and Trevisan-Souteyrand, E. (1983). Nickel electrocrystallization - from nucleation to textures. *Electrochimica acta* 28, no. 7, 909–915.

Andersen, T.N. Kerby, R.C. and O'Keefe, T.J. (1985). Control techniques for industrial electrodeposition from aqueous solutions. *Journal of Metals*, 36–43.

Arashiro, E.Y. and Demarquette, N.R. (1999). Use of the pendant drop method to measure interfactial tension. *Materials Research*, 2, 1, 23–32.

Armyanov, S., and Sotirova-Chakarove, G. (1992). Hydrogen desorption and internal stress in nickel coatings obtained by periodic electrodeposition. *Journal of electrochemical society* 139, no. 12, 3454–3457.

Berry, J.D., Neeson, M.J., Dagastine, R.R., Chan, D.Y.C. and Tabor, R.F. (2015). Measurement of surface and interfacial tension using pendant drop tensiometry. *Journal of Colloid and Interface Science*, 454, 226–237.

Biley, C.A. (2016). The pressure iron removal section at Rustenburg Base Metal Refiners. IMPC 2016, XXVIII International Mineral Processing Congress Proceedings, September 11-15, Québec City Convention Center.

Bockris, J., Reddy, A. and Gamboa-Aldeco, M. (2000). The electrogrowth of metals on electrodes. *Modern electrochemsitry*, 2A, 1293–1347.

Bryson, L.J., Hofirek, Z., Collins, M.J., Berezowsky, R.M.G.S. and Stiksma, J. (2008a). New matte leaching developments at Anglo Platinum's Base Metal Refinery. In C.A. Ypung, P.R. Tay;or, C.G. Anderson & Y. Choi (Eds.), Hydrometallurgy 2008, Proceedings of the sixth international Symposium, pp. 570-579, Phoenix, Arizona.

Bryson, L.J., Graham, N.J., Bogosi, E.P. and Erasmus, D.L. (2008b). Nickel electrowinning tank house developments at Anglo Platinum's Base Metal Refinery. ALTA Ni/Co 2008, Melbourne, Australia.

Bryson, L.J. and Biley, C.A. (2016). The evolution of iron control at Rustenburg Base Metal Refiners. IMPC 2016, XXVIII International Mineral Processing Congress Proceedings, September 11-15, Québec City Convention Center.

Budevski, E., Staikov, G. and Lorenz, W.J. (2000). Electrocrystallization nucleation and growth phenomena. *Electrochimica Acta*, 45, 2559–2574.

Chao-qun, L., Xin-hai, L., Zhi-xin, W. and Hua-jun, G. (2007). Nickel electrodeposition from novel citrate bath. *Transactions of Nonferrous Metals Society of China*, 17, 1300–1306.

Ciszewski, A., Posluszny, S., Milczarek, G. and Baraniak, M. (2004). Effects of saccharin and quaternary ammonium chlorides on the electrodeposition of nickel from a Watts-type electrolyte. *Surface and Coatings Technology*, 183, 127–133.

Crundwell, F., Moats, M., Ramachandran, V., Robinson, T. and Davenport, W. (2011). *Extractive Metallurgy of Nickel, Cobalt and Platinum-Group Metals*. Elsevier. 327–346.

Dennis, J.K. and Fuggle, J.J. (1968). The effect of metallic contamination on the structure and ductility of electrodeposited nickel. *Transactions on the Institute of Metal Finishing*, 46, 185–193.

Di Bari, G.A. (2010). Electrodeposition of nickel. *Modern Electroplating, 5th edition*. Schlesinger, M. and Paunovic, M. (eds.) Wiley, Hoboken, New Jersey. 79–114.

Ebrahimi, F. and Ahmed, Z. (2003). The effect on the microstructure and tensile properties of electrodeposited nanocrystalline nickel. *Materials Characterization*, 49, 373–379.

Fischer, H. (1954). *Elektrolytische abscheidung und electrokristallisation van metallen.* Vol. 729. Springer Verlag.

Fornari, P. and Abbruzzese, C. (1999). Copper and nickel selective recovery by electrowinning from electronic and galvanic industrial solutions. *Hydrometallurgy*, 52, 209–222.

Franklin, T.C. (1987). Some mechanisms of action of additives in electrodeposition processes. *Surface and coatings technology*, 30, 415–428.

Gadad, S. and Harris, T.M. (1998). Oxygen incorporation during the electrodeposition of Ni, Fe, and Ni-Fe alloys. *Journal of the Electrochemical Society*, 145, 11, 3699–3703.

Gogia, S.K. and Das, S.C. (1988). The effects of Mg^{2+}, Mn^{2+}, Zn^{2+}, and Al^{3+} on the nickel deposit during electrowinning from sulfate bath. *Metallurgical Tansactions B*, 19B, 823–831.

Gogia, S.K. and Das, S.C. (1991). The effect of Co^{2+}, Cu^{2+}, Fe^{2+} and Fe^{3+} during electrowinning of nickel. *Journal of Applied Electrochemistry*, 21, 64–72.

Hofirek, Z. and Kerfoot, D.G.E. (1992). The chemistry of the nickel-copper matte leach and its application to process control and optimisation. *Hydrometallurgy*, 29, 357–381.

Hofirek, Z. and Nofal, P.J. (1995). Pressure leach capacity expansion using oxygen-enriched air at RBMR (Pty) Ltd. *Hydrometallurgy*, 39, 91–116.

Holm, M. and O'Keefe, T.J. (2000). Electrolyte parameter effects in the electrowinning of nickel from sulfate electrolytes. *Minerals Engineering*, 13, 2, 195–200. *Journal of the Electrochemical Society*, 145, 11, 3699–3703.

Ji, J. (1994). Fundamental aspects of nickel electrowinning from chloride electrolytes. PhD Thesis, Faculty of graduate studies, Department of metals and materials engineering, University of British Columbia, Vancouver, B.C., Canada.

Ji, J. and Cooper, W.C. (1996). Nickel speciation in aqueous chloride solutions. *Electrochimica Acta*, 41, 9, 1549–1560.

Jing, L., Qi-hua, Y. and Zhao, Z. (2010). Effects of additives on nickel electrowinning from sulfate system. *Transactions of nonferrous metals society of China* 20, 97–101.

Kerby, R., Jackson, H., O'Keefe, T. and Wang, Y-M. (1977). Evaluation of organic additives for use in zinc electrowinning. *Metallurgical Transactions B*, 8, 661–668.

Kittelty, D. (2002). The electrocrystallization of nickel and its relationship to the physical properties of the metal. PhD thesis, Murdoch University, Australia.

Kittelty, D. and Nicol, M.J. (2003). The effects of solution impurities on the properties of nickel cathodes. *Hydrometallurgy 2003*, The Minderals, Metals and Materials Society, Warrendale, Pennsylvania, 2, 1205–1218.

Kolb, D.M. (2001). Electrochemical surface science. *Angewandte Chemie International Edition*, 40, 1162–1181.

Kuhn, A.E. (1971). Electrodeposition of nickel. *Industrial electrochemical processes*, 348–352.

Küzeci, E. and Kammel, R. (1994). Effects of metallic and D2EHPA impurities on nickel electrowinning form aqueous sulphate baths. *Journal of Applied Electrochemistry*, 24, 730–736.

Lantelme, F. and Seghiouer, A. (1998). Model of nickel electrodeposition from acidic medium. *Journal of Applied Electrochemistry,* 28, 9, 907–913.

Lupi, C., Pasquali, M. and Dell'Era, A. (2006). Studies concerning nickel electrowinning from acidic and alkaline electrolytes. *Minerals Engineering*, 19, 1246–1250.

Mackinnon, D.J., Brannen, J.M. and Kerby, R.C. (1979a). The effect of cadmium on zinc deposit structures obtained from high purity industrial acid sulphte electrolyte. *Journal of Applied Electrochemistry*, 9, 71–79.

Mackinnon, D.J., Brannen, J.M. and Kerby, R.C. (1979b) The effect of lead on zinc deposit structures obtained from high purity synthetic and industrial acid sulphate electrolytes. *Journal of Applied Electrochemistry*, 9, 55–70.

Mackinnon, D.J., Brannen, J.M. and Fenn, P.L. (1987). Characterization of impurity effects in zinc electrowinning from industrial acid sulphate electrolyte. *Journal of Applied Electrochemistry*, 17, 1129–1143.

Malevich, D., Baron, J.Y., Szymanski, G. and Lipkowski, J. (2008). Optimization of the parameters for nickel electrowinning using interference microscopy and digital image analysis. *Journal of Solid State Electrochemistry*, 12, 453–459.

Moats, M.S. and Derrick, A. (2012). Investigation of nucleation and plating overpotentials during copper electrowinning using the galvanostatic staircase method. Electrometallurgy. Hoboken (NJ): John Wiley & Sons, Inc.

Mohanty, U.S., Tripathy, B.C., Singh, P. and Das, S.C. (2001). Effect of pyridine and its derivatives on the electrodeposition of nickel from aqueous sulfate solutions Part II: Polarization behaviour. *Journal of Applied Electrochemistry*, 31, 969–972.

Mohanty, U.S., Tripathy, B.C., Singh, P., Das, S.C. and Misra, V.N. (2005). Effect of pyridine and picolines on the electrocrystallization of nickel from sulphate solutions. *Surface and Coatings Technology*, 197, 247–252.

Mohanty, U.S., Tripathy, B.C., Das, S.C., Singh, P. and Misra, V.N. (2009). Effect of sodium lauryl sulphate (SLS) on nickel electrowinning from acidic sulphate solutions. *Hydrometallurgy*, 100, 60–64.

Moskalyk, R.R. and Alfantazi, A.M. (2002a). Nickel sulphide smelting and electrorefining practice: a review. *Mineral Processing and Extractive Metallurgy Review*, 23, 141–180.

Moskalyk, R.R. and Alfantazi, A.M. (2002b). Nickel laterite processing and electrowinning practice. *Minerals Engineering*, 15, 593–605.

Muñoz, A.G., Salinas, J.B. and Bessone, J.B. (2003). First stages of Ni deposition onto vitreous carbon from sulfate solutions. *Thin Solid Films*, 429, 119–128.

Muresan, L., Maurin, G., Oniciu, L. and Gaga, D. (1996). Influence of metallic impurities on zinc electrowinning from sulphate electrolyte. *Hydrometallurgy*, 43, 345–354.

Nicol, M.J. and Kittelty, D. (2001). The electrocrystallisation of nickel and its relationship to the physical properties of the metal. Electrometallurgy 2001, Canadian Institute of Mining, Metallurgy and Petroleum, Toronto, Canada.

Njau, K.N. and. Janssen, L.J.J. (1995). Electrochemical reduction of nickel ions from dilute solutions. *Journal of applied electrochemsitry* 25, 982–986.

Nsiengani, E.N. (2017). Effect of impurities in a nickel sulfate electrolyte on internal stress development, morphology and adhesion to titanium of electrodeposited nickel. Master of applied sciences, Dissertation, University of Pretoria, Department of Materials Science and Metallurgical Engineering, Pretoria, South Africa.

Oniciu, L. and Muresan, L. (1991). Some fundamental aspects of levelling and brightening in metal electrodeposition. *Journal of Applied Electrochemistry*, 21, 565−574.

Park, K.H., Reddy, B.R., Jung, S.H. and Mohapatra, D. (2006). Transfer of cobalt and nickel from sulphate solutions to spent electrolyte through solvent extraction and stripping. *Separation and Purification Technology*, 51, 265–271.

Paunovic, M. and Schlesinger, M. (2006). *Fundamentals of electrodeposition.* Vol. 2nd edition. Wiley.

Plieth, W. (2011). Electrocrystallization – factors influencing struture. *Journal of Solid State Electrochemistry,* 15, 1417–1423.

Popov, I., Djokic, S.S. and Grgur, B.N. (2002). *Fundamental aspects of electrometallurgy.* Springer US; Kluwer academic publishers.

Ramachandran, P. and Nanadakumar, V. (1993). Role of boric acid in nickel electrowinning – a cyclic voltammetry study. *Electrochimica Acta*, 289–296.

Rashidi, A.M. and Amadeh, A. (2009). The effect of saccharin addition and bath temperature on the grain size of nanocrystalline nickel coatings. *Surface and Coatings Technology*, 204, 353–358.

Rashkov, S.T., Petrova, M. and Bozhkov, C.H.R. (1990). The effect of nickel on the mechanism of the initial stages of zinc electrowinning from sulphate electrolytes. Part I. Investigations on a spectrally pure aluminium cathode. *Journal of Applied Electrochemistry*, 20, 11–16.

Rasmussen, A.A., Møller, P. and Somers, M.A.J. (2006). Microstructure and thermal stability of nickel layers electrodeposited from an additive-free sulphamate-based electrolyte. *Surface and Coatings Technology*, 200, 6037–6046.

Summerton, G.C, Craig, D.C, Dinham, P., McCulloch, N. & Dowling, S. (2012). The chemistry and mineralogy of a nickel copper matte leach. In M.J. Collins, D. Filippou, J.R. Harlamovs & E. Peek, (Eds.), 51st Conference of Metallurgists, COM2012, Held in Conjunction with Pressure Hydrometallurgy 2012 (pp.433-456), Niagara Falls.

Tripathy, B.C., Singh, P., Muir, D.M. and Das, S.C. (2001). Effect of organic extractants on the electrocrystallization of nickel from aqueous sulphate solutions. *Journal of Applied Electrochemsitry*, 31, 301–305.

Van den Brande, P., Dumont, A. and Winand, R. (1994). Nucleation and growth of nickel by electrodeposition under galvanostatic conditions. *Journal of Applied Electrochemistry*, 24, 201–205.

Voogt, K., Brits, J.H.W.M. and Bryson, L. (2017). Stress in full deposit electrowon nickel. Conference proceedings, CIM/COM 2017, conference of metallurgists, Vancouver, August 2017.

Warren, I.H. (1985). The application of polarization measurements in the control of zinc tankhouse operation. Proceedings of Zinc'85; Osaka, Japan. *Mining and Metallurgical Institute of Japan,* 251–264.

Whittington, B.I. and Muir, D. (2000). Pressure acid leaching of nickel laterites: a review. *Mineral Processing and Extractive Metallurgy Review*, 21, 527–600.

Wiart, R., Cachet, C., Bozhkov, C.H.R. and Rashkov, S.T. (1990). On the nature of the 'induction period' during the electrowinning of zinc from nickel containing sulphate electrolytes. *Journal of Applied Electrochemistry*, 20, 381–389.

Wiart, R. (1990). Elementary steps of electrodeposition analysed by means of impedance spectroscopy. *Electrochimica Acta*, 35, 10, 1587–1593.

Winand, R. (1991). Electrocrystallization: fundamental considerations and application to high current density continuous steel sheet plating. *Reviews of Applied Electrochemistry*, 27, 377–385.

Winand, R. (1994). Electrodeposition of metals and alloys – new results and perspectives. *Electrochimica Acta*, 39, 8/9, 1091–1105.

Wu, R., Oliazadeh, M. and Alfantazi, A.M. (2003). Electrical conductivity and density of $NiSO_4/H_2SO_4$ solutions in the range of modern nickel electrorefining and electrowinning electrolytes. *Journal of Applied Electrochemistry*, 33, 1043–1047.

Xuetao, Y., Yu, W., Dongbai, S. and Hongying, Y. (2008). Influence of pulse parameters on the microstructure and microhardness of nickel electrodeposits. *Surface and Coatings Technology*, 202, 1895–1903.

Yin, K.M. and Lin, B.T. (1996). Effects of boric acid on the electrodeposition of iron, nickel and iron-nickel. *Surface and Coatings Technology*, 78, 205–210.

Zhou, Z. and O'Keefe, T.J. (1997). Modification of anomalous deposition of Zn-Ni alloy by using tin additions. *Surface and Coatings Technology*, 96, 191–197.

Appendix A: Polarisation measurements

Table A1: Results for measured E_n and E_p values, the calculated ΔE values and standard deviation for four nickel concentrations evaluated.

$[Ni^{2+}]$ (g/L)	$-E_n$ (V)	$-E_p$ (V)	ΔE (V)	Average $-E_n$ (mV)	Average $-E_p$ (mV)	Average ΔE (mV)
	0.813	0.768	−0.045			
	0.819	0.769	−0.050			
	0.815	0.767	−0.048			
	0.817	0.768	−0.049			
50	0.818	0.770	−0.048	816 ± 2	768 ± 1	−48 ± 3
	0.787	0.744	−0.043			
	0.778	0.746	−0.032			
	0.780	0.750	−0.030			
	0.782	0.747	−0.035			
65	0.788	0.751	−0.037	783 ± 4	748 ± 3	−35 ± 7
	0.688	0.741	0.053			
	0.676	0.743	0.067			
	0.677	0.735	0.058			
	0.680	0.740	0.060			
75	0.678	0.738	0.060	680 ± 5	739 ± 3	60 ± 8
	0.694	0.777	0.083			
	0.695	0.763	0.068			
	0.689	0.767	0.078			
	0.692	0.762	0.070			
90	0.696	0.772	0.076	693 ± 3	768 ± 6	75 ± 9

Table A2: Results for measured E_n and E_p values, the calculated ΔE values and standard deviation for four Na_2SO_4 concentrations evaluated.

$[Na_2SO_4]$ (g/L)	$-E_n$ (V)	$-E_p$ (V)	ΔE (V)	Average $-E_n$ (mV)	Average $-E_p$ (mV)	Average ΔE (mV)
	0.604	0.612	0.008			
	0.609	0.620	0.011			
	0.608	0.618	0.010			
	0.610	0.621	0.011			
50	0.611	0.617	0.006	608 ± 3	618 ± 4	9 ± 7
	0.621	0.669	0.048			
	0.617	0.676	0.059			
	0.623	0.672	0.049			
	0.618	0.673	0.055			
70	0.624	0.674	0.050	621 ± 3	673 ± 3	52 ± 6
	0.688	0.741	0.053			
	0.676	0.743	0.067			
	0.677	0.735	0.058			
	0.680	0.740	0.060			
80	0.678	0.738	0.060	680 ± 5	739 ± 3	60 ± 8
	0.629	0.697	0.068			
	0.623	0.701	0.078			
	0.620	0.691	0.071			
	0.595	0.708	0.113			
100	0.592	0.698	0.106	612 ± 17	699 ± 6	87 ± 23

Table A3: Results for measured E_n and E_p values, the calculated ΔE values and standard deviation for four temperatures evaluated.

Temperature (ºC)	$-E_n$ (V)	$-E_p$ (V)	ΔE (V)	Average $-E_n$ (mV)	Average $-E_p$ (mV)	Average ΔE (mV)
	0.885	0.818	−0.067			
	0.893	0.836	−0.057			
	0.890	0.830	−0.060			
	0.887	0.828	−0.059			
35	0.888	0.834	−0.054	889 ± 3	829 ± 7	−59 ± 10
	0.603	0.672	0.069			
	0.608	0.677	0.069			
	0.605	0.676	0.071			
	0.604	0.676	0.072			
45	0.607	0.671	0.064	605 ± 2	674 ± 3	69 ± 5
	0.688	0.741	0.053			
	0.676	0.743	0.067			
	0.677	0.735	0.058			
	0.680	0.740	0.060			
60	0.678	0.738	0.060	680 ± 5	739 ± 3	60 ± 8
	0.751	0.820	0.069			
	0.744	0.815	0.071			
	0.748	0.817	0.069			
	0.750	0.812	0.062			
80	0.747	0.819	0.072	748 ± 3	817 ± 3	68 ± 6

Table A4: Results for measured E_n and E_p values, the calculated ΔE values and standard deviation for pH values evaluated.

pH	$-E_n$ (V)	$-E_p$ (V)	ΔE (V)	Average $-E_n$ (mV)	Average $-E_p$ (mV)	Average ΔE (mV)
	0.649	0.628	−0.020			
	0.652	0.624	−0.027			
	0.648	0.629	−0.019			
	0.649	0.623	−0.026			
2 (no boric acid buffer)	0.649	0.627	−0.022	649 ± 2	624 ± 2	−25 ± 4
	0.713	0.756	0.043			
	0.718	0.762	0.044			
	0.721	0.761	0.040			
	0.716	0.758	0.042			
2	0.719	0.759	0.040	717 ± 3	759 ± 2	42 ± 5
	0.688	0.741	0.053			
	0.676	0.743	0.067			
	0.677	0.735	0.058			
	0.680	0.740	0.060			
3	0.678	0.738	0.060	680 ± 5	739 ± 3	60 ± 8
	0.675	0.719	0.044			
	0.678	0.737	0.059			
	0.682	0.731	0.049			
	0.677	0.728	0.051			
3.5	0.671	0.721	0.050	677 ± 4	727 ± 7	51 ± 11
	0.625	0.616	−0.009			
	0.630	0.620	−0.011			
	0.631	0.621	−0.010			
	0.628	0.618	−0.010			
5 (no boric acid buffer)	0.627	0.620	−0.007	629 ± 2	619 ± 3	−10 ± 5
	0.892	0.824	−0.068			
	0.887	0.818	−0.069			
	0.891	0.819	−0.072			
	0.888	0.810	−0.078			
5	0.879	0.820	−0.059	887 ± 5	818 ± 5	−69 ± 10

Table A5: Results for measured E_n and E_p values, the calculated ΔE values and standard deviation for boric acid concentrations evaluated.

[Boric acid] (g/L)	$-E_n$ (V)	$-E_p$ (V)	ΔE (V)	Average $-E_n$ (mV)	Average $-E_p$ (mV)	Average ΔE (mV)
	0.688	0.741	0.053			
	0.676	0.743	0.067			
	0.677	0.735	0.058			
	0.680	0.740	0.060			
4	0.678	0.738	0.060	680 ± 5	739 ± 3	60 ± 8
	0.748	0.736	−0.012			
	0.746	0.743	−0.003			
	0.745	0.740	−0.005			
	0.745	0.738	−0.007			
8	0.749	0.741	−0.008	747 ± 2	740 ± 3	−7 ± 5
	0.781	0.785	0.004			
	0.782	0.782	0.001			
	0.780	0.780	0.000			
	0.784	0.772	−0.012			
12	0.781	0.776	−0.005	782 ± 2	779 ± 5	−3 ± 7
	0.625	0.616	−0.009			
	0.630	0.620	−0.011			
	0.628	0.618	−0.010			
	0.631	0.624	−0.007			
0 (pH 5)	0.631	0.619	−0.012	629 ± 2	619 ± 3	−10 ± 5
	0.649	0.628	−0.020			
	0.652	0.624	−0.027			
	0.651	0.622	−0.029			
	0.647	0.624	−0.023			
0 (pH 2)	0.648	0.623	−0.025	649 ± 2	624 ± 2	−25 ± 4

Table A6: Results for measured E_n and E_p values, the calculated ΔE values and standard deviation for citric acid concentrations evaluated.

[Citric acid] (g/L)	$-E_n$ (V)	$-E_p$ (V)	ΔE (V)	Average $-E_n$ (mV)	Average $-E_p$ (mV)	Average ΔE (mV)
	0.688	0.741	0.053			
	0.676	0.743	0.067			
	0.677	0.735	0.058			
	0.680	0.740	0.060			
0	0.678	0.738	0.060	680 ± 5	739 ±3	60 ± 8
	0.688	0.672	−0.016			
	0.687	0.675	−0.012			
	0.682	0.670	−0.012			
	0.676	0.678	0.002			
4	0.681	0.681	0.000	683 ± 5	675 ± 4	−8 ± 9
	0.682	0.694	0.012			
	0.684	0.697	0.013			
	0.680	0.695	0.015			
	0.689	0.698	0.009			
8	0.679	0.694	0.015	683 ± 4	696 ± 2	13 ± 6
	0.658	0.682	0.024			
	0.650	0.679	0.029			
	0.654	0.674	0.020			
	0.652	0.677	0.025			
12	0.658	0.685	0.027	654 ± 4	679 ± 4	25 ± 8

Table A7: Results for measured E_n and E_p values, the calculated ΔE values and standard deviation for sodium lauryl sulfate concentrations evaluated.

[SLS] (mg/L)	$-E_n$ (V)	$-E_p$ (V)	ΔE (V)	Average $-E_n$ (mV)	Average $-E_p$ (mV)	Average ΔE (mV)
	0.688	0.741	0.053			
	0.676	0.743	0.067			
	0.677	0.735	0.058			
	0.680	0.740	0.060			
0	0.678	0.738	0.060	680 ± 5	739 ± 3	60 ± 8
	0.713	0.794	0.081			
	0.712	0.782	0.070			
	0.699	0.786	0.087			
	0.711	0.788	0.077			
5	0.699	0.792	0.093	707 ± 7	788 ± 5	82 ± 12
	0.708	0.763	0.055			
	0.704	0.758	0.054			
	0.707	0.759	0.052			
	0.702	0.761	0.059			
20	0.702	0.760	0.058	705 ± 3	760 ± 2	56 ± 5
	0.707	0.739	0.032			
	0.699	0.745	0.046			
	0.702	0.741	0.039			
	0.703	0.738	0.035			
40	0.706	0.742	0.036	703 ± 3	741 ± 3	38 ± 6

Table A8: Results for measured E_n and E_p values, the calculated ΔE values and standard deviation for saccharin concentrations evaluated.

[SAC] (mg/L)	$-E_n$ (V)	$-E_p$ (V)	ΔE (V)	Average $-E_n$ (mV)	Average $-E_p$ (mV)	Average ΔE (mV)
	0.688	0.741	0.053			
	0.676	0.743	0.067			
	0.677	0.735	0.058			
	0.680	0.740	0.060			
0	0.678	0.738	0.060	680 ± 5	739 ± 3	60 ± 8
	0.723	0.786	0.063			
	0.729	0.784	0.055			
	0.721	0.793	0.072			
	0.728	0.787	0.059			
4	0.722	0.789	0.067	725 ± 4	788 ± 3	63 ± 7
	0.740	0.776	0.036			
	0.741	0.772	0.031			
	0.748	0.771	0.023			
	0.741	0.779	0.038			
10	0.749	0.777	0.028	744 ± 4	775 ± 3	31 ± 7
	0.777	0.769	−0.008			
	0.776	0.767	−0.009			
	0.776	0.761	−0.015			
	0.778	0.768	−0.010			
20	0.774	0.760	−0.014	776 ± 1	765 ± 1	−11 ± 2

Table A9: Results for measured E_n and E_p values, the calculated ΔE values and standard deviation for pyridine concentrations evaluated.

[PYR] (mg/L)	$-E_n$ (V)	$-E_p$ (V)	ΔE (V)	Average $-E_n$ (mV)	Average $-E_p$ (mV)	Average ΔE (mV)
	0.688	0.741	0.053			
	0.676	0.743	0.067			
	0.677	0.735	0.058			
	0.680	0.740	0.060			
0	0.678	0.738	0.060	680 ± 5	739 ± 3	60 ± 8
	0.731	0.782	0.051			
	0.733	0.776	0.043			
	0.738	0.779	0.041			
	0.730	0.777	0.047			
20	0.736	0.780	0.044	734 ± 3	779 ± 2	45 ± 5
	0.730	0.762	0.032			
	0.728	0.768	0.040			
	0.731	0.763	0.032			
	0.727	0.765	0.038			
60	0.728	0.764	0.036	729 ± 2	764 ± 2	36 ± 4
	0.734	0.754	0.020			
	0.733	0.758	0.025			
	0.730	0.759	0.029			
	0.732	0.753	0.021			
100	0.735	0.749	0.014	733 ± 2	755 ± 4	22 ± 6

Table A10: Results for measured E_n and E_p values, the calculated ΔE values and standard deviation for Co^{2+} concentrations evaluated.

$[Co^{2+}]$ (mg/L)	$-E_n$ (V)	$-E_p$ (V)	ΔE (V)	Average $-E_n$ (mV)	Average $-E_p$ (mV)	Average ΔE (mV)
	0.688	0.741	0.053			
	0.676	0.743	0.067			
	0.677	0.735	0.058			
	0.680	0.740	0.060			
0	0.678	0.738	0.060	680 ± 5	739 ± 3	60 ± 8
	0.720	0.699	−0.021			
	0.714	0.701	−0.013			
	0.709	0.710	0.001			
	0.719	0.694	−0.025			
250	0.718	0.989	−0.029	716 ± 5	699 ± 8	−17 ± 13
	0.711	0.675	−0.036			
	0.713	0.677	−0.036			
	0.709	0.664	−0.045			
	0.719	0.669	−0.050			
500	0.717	0.672	−0.045	714 ± 4	671 ± 5	−42 ± 9
	0.689	0.648	−0.041			
	0.690	0.652	−0.038			
	0.692	0.653	−0.039			
	0.684	0.642	−0.042			
1000	0.681	0.657	−0.024	687 ± 5	650 ± 6	−37 ± 11

Table A11: Results for measured E_n and E_p values, the calculated ΔE values and standard deviation for Cu^{2+} concentrations evaluated.

$[Cu^{2+}]$ (mg/L)	$-E_n$ (V)	$-E_p$ (V)	ΔE (V)	Average $-E_n$ (mV)	Average $-E_p$ (mV)	Average ΔE (mV)
	0.688	0.741	0.053			
	0.676	0.743	0.067			
	0.677	0.735	0.058			
	0.680	0.740	0.060			
0	0.678	0.738	0.060	680 ± 5	739 ± 3	60 ± 8
	0.682	0.690	0.008			
	0.677	0.692	0.015			
	0.681	0.698	0.017			
	0.676	0.697	0.021			
100	0.676	0.701	0.025	678 ± 3	696 ± 5	17 ± 8
	0.700	0.682	−0.018			
	0.709	0.687	−0.022			
	0.705	0.685	−0.020			
	0.710	0.680	−0.030			
250	0.706	0.679	−0.027	706 ± 4	683 ± 3	−23 ± 7
	0.710	0.642	−0.068			
	0.711	0.648	−0.063			
	0.698	0.647	−0.051			
	0.708	0.641	−0.067			
500	0.710	0.641	−0.069	707 ± 5	644 ± 3	−64 ± 8

Table A12: Results for measured E_n and E_p values, the calculated ΔE values and standard deviation for Al^{3+} concentrations evaluated.

$[Al^{3+}]$ (mg/L)	$-E_n$ (V)	$-E_p$ (V)	ΔE (V)	Average $-E_n$ (mV)	Average $-E_p$ (mV)	Average ΔE (mV)
	0.688	0.741	0.053			
	0.676	0.743	0.067			
	0.677	0.735	0.058			
	0.680	0.740	0.060			
0	0.678	0.738	0.060	680 ± 5	739 ± 3	60 ± 8
	0.681	0.668	−0.013			
	0.683	0.665	−0.018			
	0.684	0.660	−0.024			
	0.686	0.662	−0.024			
5	0.678	0.670	−0.008	682 ± 3	665 ± 4	−17 ± 7
	0.668	0.657	−0.011			
	0.669	0.658	−0.011			
	0.672	0.660	−0.012			
	0.676	0.656	−0.020			
10	0.666	0.666	0.000	670 ± 4	659 ± 4	−11 ± 8
	0.682	0.720	0.038			
	0.688	0.716	0.028			
	0.679	0.714	0.035			
	0.682	0.710	0.028			
5000	0.681	0.178	0.037	682 ± 3	716 ± 4	33 ± 7

Table A13: Results for measured E_n and E_p values, the calculated ΔE values and standard deviation for Se(IV) concentrations evaluated.

[Se(IV)] (mg/L)	$-E_n$ (V)	$-E_p$ (V)	ΔE (V)	Average $-E_n$ (mV)	Average $-E_p$ (mV)	Average ΔE (mV)
	0.688	0.741	0.053			
	0.676	0.743	0.067			
	0.677	0.735	0.058			
	0.680	0.740	0.060			
0	0.678	0.738	0.060	680 ± 5	739 ± 3	60 ± 8
	0.706	0.674	−0.032			
	0.710	0.677	−0.033			
	0.698	0.669	−0.029			
	0.702	0.672	−0.030			
10	0.703	0.668	−0.035	704 ± 4	672 ± 4	−32 ± 2
	0.741	0.683	−0.058			
	0.740	0.683	−0.057			
	0.739	0.686	−0.053			
	0.739	0.684	−0.055			
15	0.736	0.682	−0.054	739 ± 2	684 ± 2	−55 ± 2
	0.761	0.699	−0.062			
	0.754	0.702	−0.052			
	0.758	0.701	−0.057			
	0.754	0.696	−0.058			
25	0.757	0.697	−0.060	759 ± 3	699 ± 3	−60 ± 4

Table A14: Results for measured E_n and E_p values, the calculated ΔE values and standard deviation for Se(VI) concentrations evaluated.

[Se(VI)] (mg/L)	$-E_n$ (V)	$-E_p$ (V)	ΔE (V)	Average $-E_n$ (mV)	Average $-E_p$ (mV)	Average ΔE (mV)
	0.688	0.741	0.053			
	0.676	0.743	0.067			
	0.677	0.735	0.058			
	0.680	0.740	0.060			
0	0.678	0.738	0.060	680 ± 5	739 ± 3	60 ± 8
	0.741	0.712	−0.029			
	0.764	0.711	−0.053			
	0.752	0.707	−0.045			
	0.753	0.714	−0.039			
10	0.752	0.716	−0.036	752 ± 8	712 ± 3	−40 ± 9
	0.740	0.698	−0.042			
	0.741	0.699	−0.042			
	0.733	0.691	−0.042			
	0.736	0.700	−0.036			
15	0.731	0.699	−0.032	736 ± 4	697 ± 4	−39 ± 5
	0.769	0.721	−0.048			
	0.768	0.722	−0.046			
	0.777	0.728	−0.049			
	0.772	0.724	−0.048			
25	0.773	0.725	−0.048	772 ± 4	724 ± 3	−48 ± 1

Appendix B: Current efficiency, electrolyte conductivity and surface tension measurements

Table B1: Changes in parameters as a function of variation in nickel concentration

$[Ni^{2+}]$ (g/L)	Cathode mass before deposition (g)	Cathode mass after deposition (g)	Current efficiency (%)	Average current efficiency (%)	Conductivity (μS/cm)	Average conductivity (μS/cm)	Surface tension (N/m)	Average surface tension (N/m)
	15.6348	15.7338	99		140		0.036	
	15.6245	15.7221	98		142		0.036	
	14.9866	15.0841	98		143		0.037	
	15.2646	15.3599	96		142		0.036	
75	14.8976	14.9967	100	98 ± 2	140	142 ± 2	0.037	0.036 ± 1
	14.5267	14.6011	75		127		0.044	
	15.6238	15.7003	77		132		0.044	
	15.6659	15.7434	78		130		0.044	
	15.4424	15.5123	70		133		0.044	
50	15.9444	16.0200	76	75 ± 3	136	132 ± 3	0.045	0.044 ± 1
	14.8253	14.9096	85		142		0.041	
	14.5956	14.6775	82		141		0.042	
	14.6648	14.7549	90		141		0.041	
	14.5784	14.6648	87		141		0.042	
65	15.3074	15.3882	81	85 ± 4	140	141 ± 1	0.041	0.041 ± 1
	14.4704	14.5718	102		135		0.036	
	14.6598	14.7585	99		136		0.037	
	14.5635	14.6597	97		135		0.037	
	15.6489	15.7428	94		136		0.037	
90	15.6223	15.7166	95	97 ± 4	136	136 ± 1	0.038	0.037 ± 2

Table B2: Changes in parameters as a function of variation in sodium sulfate concentration

$[Na_2SO_4]$ (g/L)	Cathode mass before deposition (g)	Cathode mass after deposition (g)	Current efficiency (%)	Average current efficiency (%)	Conductivity (µS/cm)	Average conductivity (µS/cm)	Surface tension (N/m)	Average surface tension (N/m)
	15.6348	15.7338	99		140.2		0.036	
	15.6245	15.7221	98		141.0		0.036	
	14.9866	15.0841	98		141.1		0.037	
	15.2646	15.3599	96		141.6		0.036	
80	14.8976	14.9967	100	98 ± 2	139.6	141 ± 1	0.037	0.036 ± 1
	14.9465	15.0177	72		135.8		0.042	
	14.5688	14.6459	77		134.9		0.043	
	14.9466	15.0162	70		135.1		0.043	
	15.3265	15.3963	70		135.2		0.043	
50	15.6238	15.6948	71	72 ± 3	134.2	135 ± 1	0.043	0.043 ± 1
	15.2689	15.3546	86		136.5		0.042	
	15.2649	15.3449	80		135.9		0.042	
	15.6659	15.7556	90		136.3		0.041	
	14.9788	15.0649	86		136.0		0.042	
70	14.8552	14.9322	77	84 ± 5	135.9	136 ± 1	0.042	0.042 ± 1
	13.6586	13.7547	97		130.8		0.042	
	14.5565	14.6535	97		130.9		0.043	
	14.6458	14.7458	100		132.0		0.043	
	14.6499	14.7494	100		130.7		0.043	
100	14.6777	14.7783	101	99 ± 2	131.2	131 ± 1	0.044	0.043 ± 1

Table B3: Changes in parameters as a function of variation in temperature

Temperature (°C)	Cathode mass before deposition (g)	Cathode mass after deposition (g)	Current efficiency (%)	Average current efficiency (%)	Conductivity (µS/cm)	Average conductivity (µS/cm)	Surface tension (N/m)	Average surface tension (N/m)
	15.6348	15.7338	99		140.2		0.036	
	15.6245	15.7221	98		141.0		0.036	
	14.9866	15.0841	98		141.1		0.037	
	15.2646	15.3599	96		141.6		0.036	
60	14.8976	14.9967	100	98 ± 2	139.6	141 ± 1	0.037	0.036 ± 1
	14.9558	15.0378	82		90.4		0.042	
	14.9005	14.9885	88		90.5		0.042	
	14.9135	14.9985	85		90.5		0.042	
	15.9225	16.0116	89		90.2		0.042	
45	14.6487	14.7375	89	87 ± 3	90.6	91 ± 1	0.042	0.042 ± 1
	16.1316	16.2005	69		77.6		0.048	
	15.4698	15.5366	67		77.9		0.048	
	15.4487	15.5119	63		77.9		0.048	
	14.4495	14.5188	70		78.3		0.048	
35	15.8532	15.9183	65	67 ± 3	78.1	78 ± 1	0.048	0.048 ± 1
	14.9234	15.0163	93		177.4		0.048	
	14.8766	14.9656	89		177.2		0.047	
	14.9488	15.0352	87		176.8		0.048	
	15.0122	15.1059	94		177.4		0.048	
80	13.4430	13.5357	93	91 ± 3	176.9	177 ± 1	0.047	0.048 ± 1

Table B4: Changes in parameters due to variation in pH

pH	Cathode mass before deposition (g)	Cathode mass after deposition (g)	Current efficiency (%)	Average current efficiency (%)	Conductivity (µS/cm)	Average conductivity (µS/cm)	Surface tension (N/m)	Average surface tension (N/m)
	15.6348	15.7338	99		140.2		0.036	
	15.6245	15.7221	98		141.0		0.036	
	14.9866	15.0841	98		141.1		0.037	
	15.2646	15.3599	96		141.6		0.036	
3	14.8976	14.9967	100	98 ± 2	139.6	141 ± 1	0.037	0.036 ± 1
	15.6268	15.7188	92		137.8		0.043	
	15.2235	15.3162	93		136.9		0.043	
	16.1359	16.2344	99		137.2		0.043	
	14.8995	15.0025	103		136.9		0.043	
3.5	15.0344	15.1354	101	98 ± 5	136.2	137 ± 1	0.044	0.043 ± 1
	17.0712	17.1522	81		140.1		0.040	
	15.6465	15.7325	86		138.8		0.040	
	15.8976	15.9778	81		139.9		0.040	
	14.8895	14.9698	81		141.2		0.039	
5	15.271	15.3544	84	83 ± 3	136.1	139 ± 2	0.040	0.040 ± 1
	17.2966	17.3845	88		134.0		0.044	
	15.2665	15.3352	69		135.9		0.045	
	15.4865	15.5584	72		136.1		0.043	
	15.6944	15.7684	74		135.9		0.044	
2	13.0754	13.1455	70	75 ± 8	138.6	136 ± 2	0.044	0.044 ± 1
	14,4077	14,4962	89		142,4		0.050	
	14,5976	14,6885	91		141,6		0.050	
	15,0234	15,1099	87		142,0		0.050	
5	15,1862	15,2649	79		141,3		0.051	
(no boric acid)	11,8587	11,9425	84	86 ± 5	140,7	142 ± 1	0.051	0.051 ± 1
	16,5766	16,6454	69		143,0		0.050	
	15,4962	15,5677	72		142,0		0.051	
	14,5946	14,6635	69		141,8		0.051	
2	14,4458	14,5135	68		141,7		0.051	
(no boric acid)	15,5504	15,6348	85	73 ± 7	140,8	142 ± 1	0.051	0.050 ± 1

Table B5: Changes in parameters as a function variation in boric acid concentration

[Boric acid] (g/L)	Cathode mass before deposition (g)	Cathode mass after deposition (g)	Current efficiency (%)	Average current efficiency (%)	Conductivity (μS/cm)	Average conductivity (μS/cm)	Surface tension (N/m)	Average surface tension (N/m)
	15.6348	15.7338	99		140.2		0.036	
	15.6245	15.7221	98		141.0		0.036	
	14.9866	15.0841	98		141.1		0.037	
	15.2646	15.3599	96		141.6		0.036	
4	14.8976	14.9967	100	98 ± 2	139.6	141 ± 1	0.037	0.036 ± 1
	15.4968	15.5905	94		124.6		0.061	
	15.3344	15.4284	94		125.5		0.061	
	15.2944	15.3949	101		125.6		0.061	
	14.5977	14.6916	94		124.9		0.061	
8	15.0796	15.1659	87	94 ± 2	126.8	126 ± 1	0.061	0.061 ± 1
	14.6984	14.7952	97		131.8		0.061	
	14.5598	14.6495	90		131.9		0.061	
	15.0315	15.1255	94		132.1		0.061	
	15.6428	15.7402	98		131.6		0.061	
12	13.734	13.8277	94	95 ± 3	132.4	132 ±	0.061	0.061 ± 1
	14.4077	14.4962	89		142.4		0.050	
	14.5976	14.6885	91		141.6		0.050	
	15.0234	15.1099	87		142.0		0.050	
	15.1862	15.2649	79		141.3		0.051	
0 (pH 5)	11.8587	11.9425	84	86 ± 5	140.7	142 ± 1	0.051	0.051 ± 1
	16.5766	16.6454	69		143.0		0.050	
	15.4962	15.5677	72		142.0		0.051	
	14.5946	14.6635	69		141.8		0.051	
	14.4458	14.5135	68		141.7		0.051	
0 (pH 2)	15.5504	15.6348	85	73 ± 7	140.8	142 ± 1	0.051	0.050 ± 1

Table B6: Changes in parameters as a function of variation in citric acid concentration

[Citric acid] (g/L)	Cathode mass before deposition (g)	Cathode mass after deposition (g)	Current efficiency (%)	Average current efficiency (%)	Conductivity (μS/cm)	Average conductivity (μS/cm)	Surface tension (N/m)	Average surface tension (N/m)
	15.6348	15.7338	99		140.2		0.036	
	15.6245	15.7221	98		141.0		0.036	
	14.9866	15.0841	98		141.1		0.037	
	15.2646	15.3599	96		141.6		0.036	
0	14.8976	14.9967	100	98 ± 2	139.6	141 ± 1	0.037	0.036 ± 1
	14.5689	14.6621	94		139.9		0.040	
	14.5582	14.6541	96		139.8		0.040	
	15.6233	15.7194	97		141.1		0.040	
	16.5526	16.6421	90		140.9		0.040	
4	15.4623	15.5498	88	93 ± 4	141.2	141 ± 1	0.040	0.040 ± 1
	15.1519	15.2448	93		141.8		0.040	
	14.8797	14.9685	89		142.1		0.040	
	15.6266	15.7189	93		142.3		0.040	
	15.9464	16.0304	84		140.8		0.040	
8	14.1567	14.2448	88	90 ± 4	140.1	141 ± 1	0.040	0.040 ± 1
	14.1889	14.2754	87		138.8		0.039	
	15.6238	15.7094	86		138.9		0.039	
	16.6238	16.7154	92		140.9		0.038	
	17.1994	17.2908	92		140.8		0.039	
12	15.4884	15.5889	101	92 ± 6	141.1	140 ± 1	0.039	0.039 ± 1

Table B7: Changes in parameters as a function of variation in sodium lauryl sulfate concentration

[SLS] (mg/L)	Cathode mass before deposition (g)	Cathode mass after deposition (g)	Current efficiency (%)	Average current efficiency (%)	Conductivity (µS/cm)	Average conductivity (µS/cm)	Surface tension (N/m)	Average surface tension (N/m)
	15.6348	15.7338	99		140.2		0.036	
	15.6245	15.7221	98		141.0		0.036	
	14.9866	15.0841	98		141.1		0.037	
	15.2646	15.3599	96		141.6		0.036	
0	14.8976	14.9967	100	98 ± 2	139.6	141 ± 1	0.037	0.036 ± 1
	15.2133	15.2846	82		146.0		0.031	
	15.2663	15.3308	85		145.6		0.031	
	15.2398	15.3018	82		145.4		0.031	
	14.8495	14.9196	80		144.9		0.030	
5	15.0648	15.1240	89	84 ± 4	144.9	146 ± 1	0.031	0.030 ± 1
	14.9485	15.0088	81		135.7		0.031	
	14.8794	14.9371	88		135.8		0.031	
	14.4458	14.5019	86		135.4		0.030	
	14.6484	14.7075	89		136.0		0.031	
20	14.5520	14.6164	85	86 ± 3	136.1	136 ± 1	0.031	0.031 ± 1
	14.2265	14.2866	80		125.8		0.031	
	14.5662	14.6259	80		125.2		0.030	
	14.5846	14.6401	86		124.9		0.031	
	14.1414	14.2008	80		125.3		0.029	
40	15.6843	15.7402	86	82 ± 3	124.8	125 ± 1	0.029	0.030 ± 1

Table B8: Changes in parameters as a function of variation in saccharin concentration.

[SAC] (mg/L)	Cathode mass before deposition (g)	Cathode mass after deposition (g)	Current efficiency (%)	Average current efficiency (%)	Conductivity (µS/cm)	Average conductivity (µS/cm)	Surface tension (N/m)	Average surface tension (N/m)
	15.6348	15.7338	99		140.2		0.036	
	15.6245	15.7221	98		141.0		0.036	
	14.9866	15.0841	98		141.1		0.037	
	15.2646	15.3599	96		141.6		0.036	
0	14.8976	14.9967	100	98 ± 2	139.6	141 ± 1	0.037	0.036 ± 1
	14.5998	14.6795	80		129.7		0.034	
	14.5568	14.6382	82		125.8		0.033	
	14.6984	14.7777	80		125.6		0.034	
	15.6412	15.7355	95		124.8		0.034	
4	15.0224	15.1147	93	86 ± 7	121.6	126 ± 3	0.034	0.034 ± 1
	14.5362	14.6171	81		123.4		0.035	
	14.5623	14.6466	85		123.0		0.037	
	14.8895	14.9758	87		124.1		0.037	
	14.9566	15.0325	76		123.0		0.037	
10	14.3445	14.4285	84	83 ± 4	122.6	123 ± 1	0.038	0.037 ± 1
	15.6438	15.7171	74		130.5		0.034	
	15.6648	15.7309	66		130.2		0.034	
	15.4689	15.5399	71		130.1		0.034	
	15.5284	15.6008	73		130.2		0.034	
20	14.2155	14.2818	67	70 ± 3	129.8	130 ± 1	0.034	0.034 ± 1

Table B9: Changes in parameters as a function of variation in pyridine concentration

[PYR] (mg/L)	Cathode mass before deposition (g)	Cathode mass after deposition (g)	Current efficiency (%)	Average current efficiency (%)	Conductivity (μS/cm)	Average conductivity (μS/cm)	Surface tension (N/m)	Average surface tension (N/m)
	15.6348	15.7338	99		140.2		0.036	
	15.6245	15.7221	98		141.0		0.036	
	14.9866	15.0841	98		141.1		0.037	
	15.2646	15.3599	96		141.6		0.036	
0	14.8976	14.9967	100	98 ± 2	139.6	141 ± 1	0.037	0.036 ± 1
	15.5162	15.6059	90		134.6		0.031	
	15.6498	15.7421	93		135.2		0.032	
	14.9956	15.0891	94		135.8		0.031	
	15.6238	15.7096	86		136.7		0.032	
20	14.8667	14.9556	89	90 ± 3	135.6	136 ± 1	0.031	0.031 ± 1
	14.9236	15.0162	93		133.9		0.031	
	14.1919	14.2819	90		135.2		0.032	
	14.5679	14.6623	95		134.9		0.031	
	14.5587	14.6509	93		134.7		0.030	
60	15.6223	15.7212	99	94 ± 3	134.0	135 ± 1	0.031	0.031 ± 1
	15.2329	15.3255	93		132.8		0.029	
	14.6235	14.7199	97		131.9		0.029	
	15.9267	16.0152	89		131.2		0.028	
	14.8876	14.9785	91		131.8		0.029	
100	14.1918	14.2799	88	92 ± 3	130.9	132 ± 1	0.028	0.029 ± 1

Table B10: Changes in parameters as a function of variation in cobalt concentration

$[Co^{2+}]$ (mg/L)	Cathode mass before deposition (g)	Cathode mass after deposition (g)	Current efficiency (%)	Average current efficiency (%)	Conductivity (µS/cm)	Average conductivity (µS/cm)	Surface tension (N/m)	Average surface tension (N/m)
	15.6348	15.7338	99		140.2		0.036	
	15.6245	15.7221	98		141.0		0.036	
	14.9866	15.0841	98		141.1		0.037	
	15.2646	15.3599	96		141.6		0.036	
0	14.8976	14.9967	100	98 ± 2	139.6	141 ± 1	0.037	0.036 ± 1
	14.9546	15.0421	88		140.2		0.040	
	14.9156	15.0091	94		140.6		0.040	
	15.2668	15.3488	82		140.1		0.040	
	16.4995	16.5882	89		140.1		0.040	
250	14.6287	14.7168	88	88 ± 4	140.2	140 ± 1	0.039	0.040 ± 1
	14.1148	14.1958	81		140.5		0.036	
	14.1168	14.1985	82		138.8		0.036	
	15.6419	15.7205	79		139.2		0.036	
	15.6423	15.7294	87		139.4		0.036	
500	15.1864	15.2645	78	82 ± 4	140.1	140 ± 1	0.036	0.036 ± 1
	14.8898	14.9702	81		138.8		0.041	
	14.9478	15.0261	79		138.8		0.041	
	15.6234	15.7088	86		139.2		0.040	
	15.2236	15.3145	91		137.4		0.040	
1000	15.4996	15.5886	89	85 ±5	138.2	139 ± 1	0.041	0.041 ± 1

Table B11: Changes in parameters as a function of variation in copper concentration

$[Cu^{2+}]$ (mg/L)	Cathode mass before deposition (g)	Cathode mass after deposition (g)	Current efficiency (%)	Average current efficiency (%)	Conductivity (μS/cm)	Average conductivity (μS/cm)	Surface tension (N/m)	Average surface tension (N/m)
	15.6348	15.7338	99		140.2		0.036	
	15.6245	15.7221	98		141.0		0.036	
	14.9866	15.0841	98		141.1		0.037	
	15.2646	15.3599	96		141.6		0.036	
0	14.8976	14.9967	100	98 ± 2	139.6	141 ± 1	0.037	0.036 ± 1
	14.1659	14.2554	90		143.5		0.040	
	16.6658	16.7549	89		143.3		0.041	
	15.6684	15.7548	87		144.8		0.041	
	14.9462	15.0332	87		144.1		0.040	
100	14.1662	14.2549	89	89 ± 1	140.9	144 ± 1	0.042	0.041 ± 1
	15.6428	15.7289	86		140.8		41.82	
	15.9915	16.0845	93		140.9		40.98	
	14.6428	14.7288	86		140.8		41.22	
	15.2649	15.3512	87		140.7		41.61	
250	15.5546	15.6448	91	89 ± 3	140.6	141 ± 1	40.12	0.041 ± 1
	14.6646	14.7445	80		140.2		40.95	
	14.9185	15.0015	83		140.1		40.98	
	15.6445	15.7184	74		139.3		41.13	
	15.9488	16.0252	77		139.4		41.16	
500	16.2643	16.3465	83	79 ± 4	138.2	140 ± 1	41.16	0.041 ± 1

Table B12: Changes in parameters as a function of variation in aluminium concentration

$[Al^{3+}]$ (mg/L)	Cathode mass before deposition (g)	Cathode mass after deposition (g)	Current efficiency (%)	Average current efficiency (%)	Conductivity (μS/cm)	Average conductivity (μS/cm)	Surface tension (N/m)	Average surface tension (N/m)
	15.6348	15.7338	99		140.2		0.036	
	15.6245	15.7221	98		141.0		0.036	
	14.9866	15.0841	98		141.1		0.037	
	15.2646	15.3599	96		141.6		0.036	
0	14.8976	14.9967	100	98 ± 2	139.6	141 ± 1	0.037	0.036 ± 1
	15.6689	15.7564	88		141.3		0.038	
	15.6994	15.7865	87		141.6		0.038	
	14.6885	14.7799	92		140.9		0.039	
	14.9465	15.0294	83		141.2		0.039	
5	15.6294	15.7125	83	87 ± 4	141.2	141 ± 1	0.039	0.039 ± 1
	16.3599	16.4486	89		140.1		0.040	
	16.1572	16.2458	89		139.9		0.040	
	14.6659	14.7484	83		139.8		0.040	
	15.2622	15.3558	94		140.1		0.040	
10	15.2346	15.3296	95	90 ± 5	139.8	140 ± 1	0.040	0.040 ± 1
	14.9458	15.0423	97		142.3		0.041	
	15.2648	15.3562	92		142.8		0.041	
	15.4884	15.5764	88		142.0		0.040	
	15.1369	15.2264	90		142.1		0.041	
5000	14.8946	14.9844	90	91 ± 3	142.2	142 ± 1	0.041	0.041 ± 1

Table B13: Changes in parameters as a function of variation in Se(IV) concentration

[Se(IV)] (mg/L)	Cathode mass before deposition (g)	Cathode mass after deposition (g)	Current efficiency (%)	Average current efficiency (%)	Conductivity (µS/cm)	Average conductivity (µS/cm)	Surface tension (N/m)	Average surface tension (N/m)
	15.6348	15.7338	99		140.2		0.036	
	15.6245	15.7221	98		141.0		0.036	
	14.9866	15.0841	98		141.1		0.037	
	15.2646	15.3599	96		141.6		0.036	
0	14.8976	14.9967	100	98 ± 2	139.6	141 ± 1	0.037	0.036 ± 1
	15,2689	15,3525	84		132,8		0.036	
	14,8469	14,9325	86		136,0		0.035	
	15,1036	15,1882	85		136,2		0.036	
	15,2203	15,3049	85		134,4		0.036	
10	14,9986	15,0822	84	84 ± 1	139,6	136 ± 3	0.035	0.035 ± 1
	14,9765	15,0621	86		139,2		0.038	
	15,1362	15,2238	88		141,2		0.038	
	15,0689	15,1565	88		141,1		0.039	
	15,3221	15,4097	88		140,2		0.037	
15	14,9867	15,0684	82	88 ± 3	139,6	140 ± 1	0.037	0.038 ± 1
	14,9867	15,0654	79		138,2		0.035	
	14,9968	15,0755	79		139,1		0.035	
	15,3268	15,4075	81		139,1		0.035	
	15,0678	15,1435	76		137,7		0.036	
25	15,0689	15,1426	74	79 ± 3	136,9	138 ± 2	0.036	0.035 ± 1

Table B14: Changes in parameters as a function of variation in Se(VI) concentration

[Se(VI)] (mg/L)	Cathode mass before deposition (g)	Cathode mass after deposition (g)	Current efficiency (%)	Average current efficiency (%)	Conductivity (µS/cm)	Average conductivity (µS/cm)	Surface tension (N/m)	Average surface tension (N/m)
	15.6348	15.7338	99		140.2		0.036	
	15.6245	15.7221	98		141.0		0.036	
	14.9866	15.0841	98		141.1		0.037	
	15.2646	15.3599	96		141.6		0.036	
0	14.8976	14.9967	100	98 ± 2	139.6	141 ± 1	0.037	0.036 ± 1
	15,2668	15,3534	87		133,2		0.041	
	15,3264	15,4130	87		132,9		0.040	
	15,8894	15,9721	83		133,1		0.041	
	14,9976	15,0862	89		133,5		0.041	
10	15,2033	15,2889	86	87 ± 2	133,1	133 ± 1	0.041	0.041 ± 1
	15,0421	15,1297	88		138,2		0.040	
	14,9946	15,0822	88		139,1		0.040	
	14,9765	15,0631	87		138,5		0.039	
	15,2218	15,3114	90		137,8		0.039	
15	15,4684	15,5590	91	88 ± 2	137,1	138 ± 1	0.039	0.039 ± 1
	15,011	15,0867	76		140,1		0.033	
	14,9465	15,0222	76		140,2		0.033	
	14,5664	14,6441	78		141,1		0.034	
	14,9485	15,0302	82		140,4		0.034	
25	14,9965	15,0792	83	78 ± 3	139,6	140 ± 1	0.033	0.033 ± 1

Appendix C: Polarisation measurements for industrial application

Table C1: Results for measured E_n and E_p values, the calculated ΔE values and standard deviation for three sodium lauryl sulfate concentrations evaluated.

[SLS] (mg/L)	$-E_n$ (V)	$-E_p$ (V)	ΔE (V)	Average $-E_n$ (mV)	Average $-E_p$ (mV)	Average ΔE (mV)
	0.720	0.810	0.090			
	0.719	0.810	0.091			
	0.715	0.807	0.092			
	0.715	0.806	0.091			
5	0.721	0.808	0.087	718 ± 3	808 ± 2	90 ± 2
	0.721	0.799	0.078			
	0.724	0.799	0.075			
	0.722	0.795	0.073			
	0.720	0.798	0.078			
20	0.721	0.800	0.079	722 ± 4	798 ± 3	77 ± 3
	0.733	0.788	0.055			
	0.735	0.788	0.053			
	0.735	0.790	0.055			
	0.731	0.786	0.055			
40	0.736	0.788	0.052	734 ± 2	788 ± 1	54 ± 1

Table C2: Results for measured E_n and E_p values, the calculated ΔE values and standard deviation for three saccharin concentrations evaluated.

[SAC] (mg/L)	$-E_n$ (V)	$-E_p$ (V)	ΔE (V)	Average $-E_n$ (mV)	Average $-E_p$ (mV)	Average ΔE (mV)
	0.884	0.897	0.013			
	0.881	0.896	0.015			
	0.879	0.894	0.015			
	0.881	0.899	0.018			
4	0.881	0.896	0.015	881 ± 2	896 ± 2	15 ± 1
	0.856	0.931	0.075			
	0.855	0.933	0.078			
	0.859	0.933	0.074			
	0.851	0.936	0.085			
10	0.858	0.932	0.074	856 ± 3	933 ± 2	77 ± 1
	0.879	0.887	0.008			
	0.879	0.887	0.008			
	0.882	0.890	0.008			
	0.884	0.887	0.003			
20	0.881	0.886	0.005	881 ± 2	887 ± 2	6 ± 2

Table C3: Results for measured E_n and E_p values, the calculated ΔE values and standard deviation for copper (250 mg/L) and cobalt (250 mg/L) evaluated.

Impurity (250 mg/L)	$-E_n$ (V)	$-E_p$ (V)	ΔE (V)	Average $-E_n$ (mV)	Average $-E_p$ (mV)	Average ΔE (mV)
	0.707	0.686	−0.021			
	0.706	0.685	−0.021			
	0.701	0.689	−0.012			
	0.705	0.684	−0.021			
Co	0.708	0.683	−0.025	705 ± 3	685 ± 2	−20 ± 5
	0.699	0.689	−0.010			
	0.698	0.686	−0.012			
	0.704	0.691	−0.013			
	0.701	0.690	−0.011			
Cu	0.702	0.684	−0.018	701 ± 2	688 ± 3	−13 ± 3

Table C4: Results for measured E_n and E_p values, the calculated ΔE values and standard deviation for three selenite concentrations evaluated.

[Se(IV)] (mg/L)	$-E_n$ (V)	$-E_p$ (V)	ΔE (V)	Average $-E_n$ (mV)	Average $-E_p$ (mV)	Average ΔE (mV)
	0.719	0.699	−0.020			
	0.718	0.702	−0.016			
	0.722	0.699	−0.023			
	0.722	0.696	−0.026			
5	0.720	0.699	−0.021	720 ± 2	699 ± 2	−15 ± 1
	0.704	0.688	−0.016			
	0.704	0.689	−0.015			
	0.710	0.686	−0.024			
	0.699	0.686	−0.013			
8	0.704	0.682	−0.022	704 ± 4	686 ± 3	−18 ± 5
	0.719	0.676	−0.043			
	0.718	0.678	−0.040			
	0.724	0.671	−0.053			
	0.726	0.675	−0.051			
10	0.722	0.676	−0.046	722 ± 3	675 ± 3	−47 ± 5

Table C5: ICP-OES analysis of a typical reference electrolyte from RBMR.

Element	Deionised water (Merck) (mg/L)	Reference electrolyte RBMR concentration (mg/L)
Al	<0.0118	<0.0009
Ca	Not detected	<0.0023
Cr	Not detected	<0.0013
Cu	Not detected	<0.0003
Co	Not detected	<0.0011
Cd	<0.0137	<0.0038
Fe	Not detected	<0.0027
Mn	<0.0119	<0.0018
Pb	<0.0484	<0.0004